UNIVERSITÀ
DEGLI STUDI
DI PADOVA

Sede Amministrativa: Università degli Studi di Padova

Dipartimento di Medicina Molecolare

CORSO DI DOTTORATO DI RICERCA IN: Medicina Molecolare

CURRICOLO: Biomedicina

CICLO XXXI

TITOLO TESI

Inhibition of HCMV replication by small molecules interfering with the dimerization of the DNA polymerase processivity factor UL44

Coordinatore: Ch.mo Prof. Stefano Piccolo

Supervisore: Dr. Gualtiero Alvisi

Dottorando: Martina Timmoneri

Index

Abstract

Human cytomegalovirus (HCMV) is a leading cause of severe disease in immunocompromised individuals, including AIDS and transplanted patients, and in congenitally infected newborns. Despite the availability of several drugs, pharmacological treatment of HCMV infections is associated with poor bioavailability, toxicity and the emergence of resistant strains. Furthermore, no vaccine is available and no drugs are approved to prevent vertical transmission during pregnancy, therefore, it is essential to identify new potential targets of therapeutic intervention.

HCMV DNA polymerase accessory protein UL44 plays an essential role in viral replication, conferring processivity to the DNA polymerase catalytic subunit UL54 by tethering it to the DNA. Binding of UL44 to dsDNA occurs in the absence of ATP and clamp loaders, and depends on UL44 homodimerization. Indeed, our research group previously demonstrated that the protein can dimerize in cells and point mutations disrupting protein self-interaction also prevent DNA binding and abolish viral Ori*Lyt*-dependent DNA replication in transcomplementation assay. Therefore, disruption of UL44 homodimerization represents an attractive target for the development of new antivirals. Based on these observations, using the recently published crystal structure of UL44 hodimers our research group previously performed a virtual screening with the Glide software in combination with a library of 1.3 x 10^6 small molecules (SMs) to identify SMs potentially interfering with UL44 homodimerization. After three rounds of screening (HTVS: high-throughput virtual screening, SP: standard precision, XP: extra precision), followed by an in depth analysis of compounds chemical properties, 18 SMs were selected for further analysis. Selected compounds were obtained from a commercial supplier, to be tested in a variety of assays for their ability to inhibit UL44 homodimerization both in cell and *in vitro*, as well as on HCMV replication.

For this purpose, we applied two *in vitro* methods to monitor the effect of our candidates on UL44 dimerization such GST-pulldown Assay and Thermal Shift Assay (TSA). Furthermore, Plaque Reduction Assay (PRA) and Fluorescence Reduction Assay (FRA) were performed to study their inhibitory effects on viral replication.

Initially we validated that GST-pulldown assay was suitable to study UL44 dimerization and its perturbation caused by SMs. Therefore, we performed a first screening to test the effect of the 18 SMs on UL44 dimerization, and we identified 3 of these which reproducibly inhibited the dimerization. Prompted by these results, we selected such SMs to investigate a possible dose-response relationship between the dimerization inhibition and the compounds concentration. Unfortunately, data analysis revealed a high variability, and lack of correlation between the inhibition and the concentration of SMs used in the assays. In parallel, PRAs were performed to validate the effect of selected SMs, but these were unable to inhibit viral replication with high potency.

Subsequently, two recombinant HCMV viruses (TB4-IE2-EYFP and TB4-UL83-EYFP) were obtained from Michael Winkler (Leibniz-Institut für Primatenforschung Goettingen, Germany) in order to study the effect of our molecules on HCMV replication by FRAs. Therefore, after a screening of the 18 SMs, 4 of these were identified as possible inhibitors of viral replication and were selected to further studies. We investigated their and 50% effective dose (ED50) and 50% cytotoxic concentration (CC50) values and their effects on the viral gene expression. Only 2 SMs reproducibly inhibited expression of Early and Late genes.

Then we evaluated an alternative *in vitro* assay and among the various possibilities, we have chosen TSA that is able to inform whether a SM induce the disruption of constitutive oligomeric interfaces. In a first moment we validated that the assay allow the discrimination between monomeric and dimeric forms of UL44, suggesting its potential for the screening of our SMs. As result of the SMs screening by TSA, one molecule revealed a possible inhibition of dimerization.

Riassunto

Cytomegalovirus (CMV) è un importante patogeno di interesse umano. Al momento gli antivirali disponibili ed utilizzati per la terapia contro l'infezione da CMV presentano una serie di problematica quali l'alto costo, bassa biodisponibilità, alta tossicità ed il presentarsi di ceppi virali resistenti. Inoltre non è disponibile un vaccino ed ancora non è stato approvato alcun farmaco per prevenire la trasmissione verticale durante la gravidanza. Per questi motivi, sono necessari nuovi efficaci farmaci antivirali.

La proteina accessoria UL44 della DNA polimerasi di CMV, svolge un ruolo essenziale nella replicazione virale, conferendo processività alla subunità catalitica UL54 ancorando il complesso oloenzimatico al DNA.

Il legame di UL44 al dsDNA avviene in assenza di ATP e dei clamp loaders, e dipende dalla omodimerizzazione di UL44. Il nostro gruppo di ricerca, infatti ha recentemente dimostrato che la proteina può dimerizzare in cellule e che mutazioni puntiformi in grado di inficiare tale dimerizzazione prevengono il legame con il DNA ed aboliscono la replicazione del DNA virale oriLyt-dipendente in saggi di transcomplementazione transiente.

Perciò, la distruzione dell'omodimerizzazione UL44 rappresenta un potenziale ed allettante target per lo sviluppo di nuovi antivirali. Partendo da queste osservazioni ed usando la struttura cristallografica degli omodimeri UL44 che è stata recentemente pubblicata, il nostro gruppo di ricerca ha eseguito un virtual screening con il software Glide in combinazione con una libreria di 1.3 x 10^6 piccole molecole (SMs) per identificare SMs che potenzialmente potessero interferire con l'omodimerizzazione di UL44. Dopo tre rounds di screening (HTVS: high-throughput virtual screening, SP: standard precision, XP: extra precision), seguiti da un'analisi delle proprietà

chimiche dei composti, sono state selezione 18 SM per ulteriori analisi. I composti selezionati sono stati acquistati presso un fornitore commerciale, per essere testati in diversi saggi per valutare le loro abilità di inibire l'omodimerizzazione di UL44 *in vitro*, sia la replicazione virale.

Con questo scopo, abbiamo utilizzato due metodi *in vitro* per monitorare l'effetto dei nostri candidati sulla dimerizzazione di UL44, quali GST-pulldown assay e Thermal Shift Assay (TSA). Inoltre per studiare l'inibizione sulla replicazione virale sono stati eseguiti saggi di Plaque Reduction Assay (PRA) e Fluorescence Reduction Assay (FRA).

Inizialmente abbiamo confermato che il GST-pulldown assay fosse idoneo per studiare la dimerizzazione di UL44 e la sua perturbazione causata dalle SMs. Pertanto abbiamo eseguito un primo screening per saggiare l'effetto delle 18 SMs sulla dimerizzazione di UL44, ed abbiamo identificato 3 molecole che inibivano la dimerizzazione in modo riproducibile. Incoraggiati da questi risultati, abbiamo selezionato queste SMs per valutare una possibile relazione dose-risposta tra l'inibizione della dimerizzazione e la concentrazione dei composti. Sfortunatamente, l'analisi dei dati hanno rivelato alta variabilità, e perdita di correlazione tra l'inibizione e la concentrazione delle SMs utilizzate nei saggi.
In parallelo, abbiamo eseguito PRAs per validare l'effetto delle SMs precedentemente selezionate, ma queste si sono presentati incapaci di inibire la replicazione virale in modo consistente.

Successivamente abbiamo ottenuto due virus CMV ricombinanti (TB4-IE2-EYFP and TB4-UL83-EYFP) da Michael Winkler (Leibniz-Institut für Primatenforschung Goettingen, Germany) per studiare l'effetto delle nostre molecole sulla replicazione di CMV mediante FRAs. Pertanto, dopo uno screening delle 18 SMs, 4 di queste sono state identificate come possibili inibitori della replicazione virale e sono state selezionate per essere ulteriormente studiate. Abbiamo valutato la loro dose effettiva

50% (ED50) e la loro concentrazione citotossica 50% (CC50) e gli effetti relativi all'espressione genica. Solo due SMs in modo riproducibile inibivano l'espressione dei geni Early e Late.

Poi abbiamo valutato un saggio *in vitro* alternativo e tra le varie possibilità, abbiamo scelto il TSA che è un saggio in grado di informare se una SM induce la distruzione delle interfacce di un oligomero costitutivo. In un primo momento abbiamo confermato che il saggio permettesse la discriminazione tra le forme monomeriche e dimeriche di UL44, suggerendo il suo potenziale per lo screening delle nostre SMs. Come risultato di questo screening, una molecola ha rivelato possibile inibizione della dimerizzazione.

1. Introduction

1.1 Human Cytomegalovirus (HCMV)

Human Cytomegalovirus (HCMV), also known as Human Herpesvirus-5 (HHV-5), is a member of the *Herpesviridae* family, subfamily *Betaherpesvirinae*. CMVs from other mammals also belong to this subfamily. HCMV is a species-specific ubiquitous virus, which only rarely causes diseases in immunocompetent individuals, but it is responsible for a variety of pathologies in immunocompromised patients. It is also one of the major causes of congenital defects in newborns.

Its name stems from its ability to cause enlargement of the infected cells (cytomegaly), inducing the formation of inclusion bodies in the nucleus and in the cytoplasm, which lysosomes along with newly assembled viruses. HCMV shares several characteristics with other members of the *Herpesviridae* family, including viral particle and genome structure, the ability to induce acute infections associated with a highly productive lytic cycle, persistent infections with low replicative levels, or latent infections without production of viral particles [1]. In addition to infectious virions, HCMV infected cell cultures also produce the Non-Infective Enveloped Particles (NIEPS) and Dense Bodies (DB). NIEPS differ from the infective virions because they lack the viral genome; the DB, instead, are completely devoid of both capsid and genome [2]. The relative presence of the three forms depends on the cell culture passages and on the viral strain [3].

1.2 Epidemiology and Pathogenesis

HCMV is a ubiquitous pathogen, widely distributed worldwide, with a seroprevalence raging from 50 to 90% according to the geographic area and socio-economic factors [4].

HCMV comes in contact with the body through mucous membranes or parenterally (blood, or stem cell, organ transplants) and can lead to general infection with involvement of the whole organism, causing a wide range of symptoms such as encephalitis, retinitis, hepatitis and splenomegaly.

HCMV can cause dangerous consequences in four cases: i) in congenital infections; ii) in immunocompromised individuals; iii) in primary infection; iv) in reinfection; v) in reactivation.

In the congenital infections, the virus is vertically transmitted from the mother. The frequency of vertical transmission is of about 0.5-1%, and can occur either transplacentally from the mother to the fetus/child, or via cervical/vaginal secretions, as wells as via breast milk. Vertically transmitted CMV infections represent the major cause of congenital defects in newborns. Congenital CMV infection is symptomatic in about 10 percent of the infected neonates and is associated with clinically significant neurologic *sequelae* in almost half of them. In addition, neurologic defects will eventually develop in 8 to 13 percent of neonates with asymptomatic infection [5, 6]. Among women with a primary infection during pregnancy, the rate of fetal infection is approximately 40% [6, 7].

HMCV can also be transmitted horizontally by direct contact (sexual or oral transmission), trough urine or after solid organ or hematopoietic stem cells transplant [8]. In immunocompetent individuals, most HCMV infections are asymptomatic, even though the levels of viremia are very high. During primary infection, CMV engages the innate and the adaptive immunity, thus leading to development of neutralizing antibodies, and generation of CMV-specific T cells that play critical roles in effectively controlling infection [9-11]. As a result, the natural outcome of primary CMV infection is the establishment of lifelong subclinical latent infection in humans. Latent CMV can be detected in several cell types including monocytes, macrophages, lymphocytes, endothelial cells, and bone marrow progenitor cells. Reactivation of latent CMV in these cells occurs periodically throughout life in response to inflammation, stress, and immunosuppression. Such periodic reactivation of latent CMV is controlled by a healthy immune system, which responds by progressive expansion of CMV-specific CD8 + T cells and, to a lesser extent, CD4 + T cells [12, 13]. The immune fitness in healthy individuals limits the ability of CMV to cause significant clinical disease in immunocompetent hosts. However, viral reactivation and primary infections can lead to life-threatening complications in individuals, which are not immunocompetent. For example,

CMV is a common infectious agent that causes significant morbidity and mortality in case of AIDS, solid organ transplantation (SOT) and allogeneic hematopoietic stem cell transplantation (HSCT) [14]. In particular, in patients with AIDS, progressive loss of cell-mediated immunity, allows CMV reactivation. Clinical disease due to CMV has been recognized in up to 40% of patients with advanced HIV disease. The most common clinical manifestation is retinitis, although colitis, esophagitis, pneumonitis and neurological disorders are also reported frequently. The gastrointestinal tract (mainly esophagus and colon) are the most common extraocular sites of CMV infection in AIDS patients [15].

On the other hand, in both SOT and HSCT patients the "CMV disease" is associated with the involvement of several organs such as lungs, digestive tract, liver, retina, central nervous system and the bone marrow, as well as with indirect effects on the immune system, which may increase the risk of infections caused by other pathogens, acute graft rejection, and graft versus host reaction (in HSCs transplant recipients) [4, 16, 17].

1.3 HCMV structure

HCMV viral particle is composed by a host cell membranes-derived viral envelope, in which several glycoproteins are embedded, an icosahedral nucleocapsid and, between them, the so-called tegument which is a phosphoprotein layer [18] (Figure 1.1).

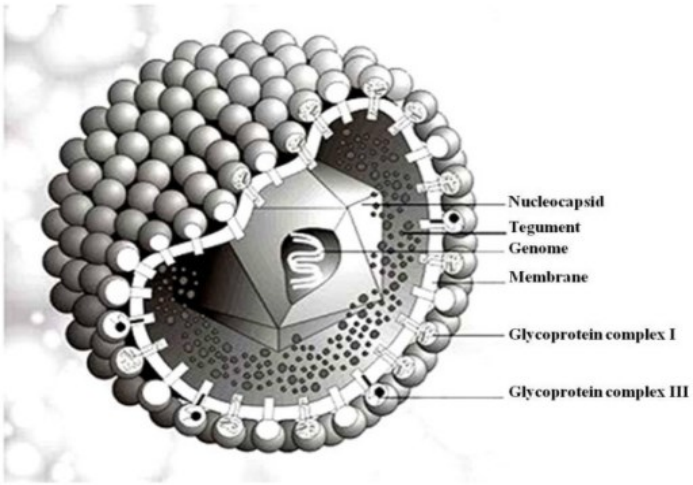

Figure 1.1: HCMV viral particle structure. From: http://www.virology.net/big_virology/bvdnaherpes.html website.

The viral capsid is made up of 162 capsomers subdivided into 12 pentons and 150 exons which are composed by four main proteins: UL86 (major capsid protein), UL48-49, UL85 (minor capsid protein), and UL46 (minor capsid binding protein). The envelope contains six viral encoded glycoproteins, which are essential for the virus entry into the host cell, cell-to-cell diffusion as well as for virus maturation: gpUL55 (gB), gpUL73 (gN), gpUL74 (gO), gpUL75 (gH), gpUL100 (gM), and gpUL115 (gL). The tegument contains the majority of viral proteins, most of which are phosphorylated and able to interact with the cytoplasmatic portions of envelope and capsid proteins, thus bridging the two viral elements [19]. When the virus is released into the cytoplasm, the tegument proteins become functionally active and play an important role in all the phases of the viral cycle, including virus entry, gene expression, evasion from the host immune response, assembly, maturation and release [20]. Many tegument proteins are of particular interest for the role they play in the HCMV replication cycle. The most abundant of them are pp150 (ppUL32, or basic phosphoprotein), and UL83 which encodes for pp65. pp65 is the major tegument phosphoprotein

and, being the main virion constituent, it is also used as a marker of infection in diagnostic tests [21]. Despite being in involved in immune system evasion, antagonizing a pathway that affects NF-kB and preventing the accumulation of mRNAs encoded by numerous cellular antiviral genes [22], its importance during HCMV infection in cell culture is unclear at the moment. Indeed the protein appears fully dispensable for HCMV replication in HFF and endothelial cells, whereas its deletion appears detrimental in monocyte-derived macrophages [23, 24].

1.4 Genome structure

HCMV is a double stranded non-segmented DNA virus with a very large linear genome of about 235 kbp. HCMV genome is the largest among the *Herpesviridae* members and has the highest amount of G-C content. Its genome can be divided into two main regions: a unique long (UL) one, and a unique short (US one), which are flanked by terminal (TRL and TRS) and internal (IRL and IRS) inverted repeats (Figure 1.2). UL and US can be oriented in both directions, so the viral progeny can present any of the four possible isomers of the genome. In the terminal part of the genome and in the junction between the UL and US, there is a direct repeated sequence, responsible for the inversion of the two regions, and, through cis elements called pac-1 and pac-2, for the cleavage and packaging of the DNA [25].

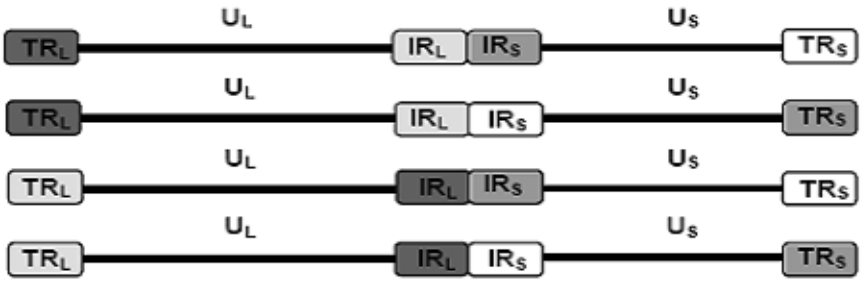

Figure 1.2 The 4 isomers of the HCMV genome with the UL region and US region flanked by terminal and internal repeats. From: [20].

The HCMV genome contains around 200 canonical protein coding genes, whose transcription is driven by a series of open reading frames (ORFs), which are named by the region and the numerical order in which they occur [26]. HCMVs ORFs encode 11 proteins absolutely required for viral DNA synthesis [27] and 54 membrane proteins, including at least 25 membrane glycoproteins found in the virion envelope. The gene products of more than 40 ORFs are very similar to proteins encoded by α- and γ-herpesviruses [28], and of these ORFs, also called "core genes", ca 25% encode for functions relative to metabolism and replication of the viral DNA, while ca 75% are involved in maturation and structural organization of virions. The products of more than 50 ORFs, instead, are specific for HCMV or for β-Herpesviruses, and the function of many of them has not been characterized yet. Importantly, a recent study investigated the importance of all HCMV ORFs in viral propagation in cell culture using the viral reference strain Towne and HFF as model systems. The authors discovered that 41 genes were required for viral replication in cell culture. More than 90% of such ORFs are core genes conserved amongst all herpesviruses, whereas more than 70% of the genes which were dispensable for viral replication are HCMV-specific, and possibly play a role during *in vivo* infection, with important implications for immune evasion and pathogenesis [29].

In addition to protein-coding genes, HCMV genome also bears genes for polyadenylated non-coding RNAs and non-polyadenylated RNAs such as micro-RNAs, which play a regulatory role during infection [26].

1.5 Viral life cycle

1.5.1 HCMV strains

The study of HCV life cycle is crucial for the understating of the pathophysiological mechanisms underlying HCMV disease, and for the development of HCMV antivirals. Such studies heavily relied on the propagation of HCMV in cell culture. HCMV clinical strains, however, are very difficult to be propagated in cell culture, in that they are highly cell-associated, with low viral

amounts being released in the supernatants of cultured infected cells [30]. However such viruses can efficiently infect several cell types, including human fibroblast (HF), epithelial, and endothelial cells [31]. Several laboratory-adapted strains have been developed to allow the propagation of HCMV in cell culture and obtain high titer viral stocks from HF. These include the AD169 [32], Davis [33] and Towne strains [34] obtained by passage of infected fibroblasts for a high number of times. Such viruses lost the ability to infect endothelial cells but are endowed with the ability to be released in the supernatants of infected cultures to high titers. These properties are the consequences of the accumulation of a series of mutations which led to the loss the functionality of gene RL13 (responsible for an enhancement of viral release in cellular supernatants) and subsequently of the UL128 locus, which includes genes UL128, UL130 and UL131A, restricting the tropism to HF [35]. Propagation of clinical isolates on endothelial cells led to the isolation of strains which are not highly cell-associated but which retained the ability of infect both HF and endothelial cells, such as the TB40 strain [30].

It should be therefore noted that most of our knowledge regarding HCMV life cycle has been obtained using such laboratory strains and therefore important differences might be present as compared to clinical isolates.

1.5.2 Cellular permissiveness and *in vitro* growth

During HCMV natural infection, the virus replicates productively in a large number of cell types including epithelial cells, endothelial cells, smooth muscle cells, mesenchymal cells, hepatocytes, granulocytes and monocytes-macrophages [36]. In latent form the DNA can be found in the progenitors of macrophages and granulocytes in bone marrow and in peripheral blood monocytes [37]. In contrast, *in vitro*, the only completely permissive replication cells for laboratory strains are human cutaneous or pulmonary fibroblasts, whereas clinical viral isolates preferentially replicate in endothelial cells and macrophages. Also some transformed cell lines derived from glioblastoma, such as U373MG, and primary smooth artery muscle cells allow productive infection, although at lower levels than fibroblasts [38, 39].

1.5.3 Adhesion and entry

HCMV entry is regarded as a two-step process promoted by interaction of viral glycoprotein complexes present on the viral envelope and host factors [40]. The first step is viral attachment and involves the viral glycoprotein gB and the gH/gL complex. It is believed that initially gB promotes virus adsorption on cell membrane by interacting with heparan sulfate glycosaminoglycans (GAGs). Subsequently, the gH/gL complex interacts with cellular receptors such as the epidermal grow factor receptor (EGFR), platelet-derived grow factor receptor-α (PDGFRα), integrins [41-43] to promote the second step which consists in the fusion of the viral envelope with cellular membranes to allow access to the cytosol. Such fusion is believed to be mediated by the viral glycoprotein gB and involves membranes of different origins accordingly to the cell type infected [44, 45]. Indeed, infection of fibroblasts, the sole cell type efficiently infectable *in vitro* by laboratory strains such as AD169, Towne and Toledo, is a pH-independent event and occurs by fusion of the viral envelope with the plasma membrane [44]. On the other hand, infection of epithelial and endothelial cells with clinical strains results in viral uptake by endocytosis and low pH-dependent fusion [45]. Such differences are believed to depend on the ability of proteins encoded by HCMV US128-130 (lacking in the above mentioned laboratory strains (§1.5.1) to form a complex with gH/gL, thus enabling interaction with a still unknown receptor expressed on epithelial and endothelial cells, and promote endocytosis [45]. The entry is followed by the nucleocapsid tegument proteins access into the cytoplasm and their rapid translocation into the nucleus, where pp65 can be visualized demonstrated less than 1 h later. The interaction of viral glycoproteins with the respective cell receptors would generate pathways of intracellular signaling and consequent alterations of gene expression, mostly similar to those observed after interaction of Interferons with their receptors [46-48]. The specific viral ligand that triggers this response is likely to be responsible for the main mechanism by which HCMV modifies the cellular gene expression profile at the earliest stages of infection [49, 50]. Furthermore, the recruitment of gB and gH glycoproteins with receptors is sufficient to induce the activity of nuclear transcription factors nuclear factor-kB (NF-kB) and Sp1

[51]. Nevertheless, viral tegument proteins and viral genomes are translocated into the nucleus where viral transcription and replication begins [19].

1.5.4 Regulation and expression of viral genes

During productive infection, the viral genome is a temporal coordinated transcriptional cascade, leading to the synthesis of three categories of viral proteins, defined as immediate-early (IE or α), early (E or β), and late (L or γ) (Figure 1.3). The HCMV genes are transcribed from cellular RNA polymerase II with the intervention of cellular transcription factors, whose activity can be stimulated by viral trans activators [52].

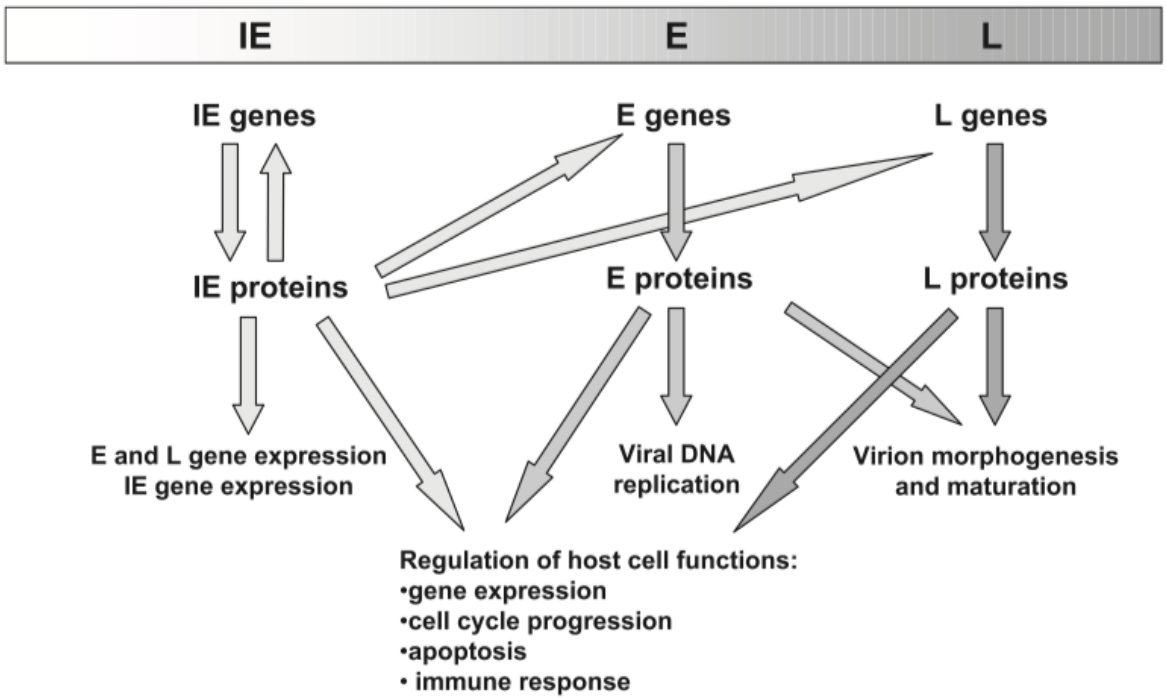

Figure 1.3. Expression of HCMV genes and viral gene products functions during productive infection (from [53]).

1.5.5 Characteristics of IE proteins

The expression of the HCMV genes starts from some IE proteins after 1 h without a *de novo* protein synthesis. The IE genes include the most important genes IEUL122/123 (IE1 and IE2) and auxiliary genes, such as UL36-UL38, UL115-UL119, IRS1/TRS1, and US3. The major proteins, alone or in synergy, are required for subsequent gene expression by acting as transactivators of viral and cellular gene expression [52]. The expression of the major IE genes is regulated by a complex enhancer element, which works in a specific way according to the tissue, the type of cell and its level of differentiation, and which exerts its strong transcriptional activity interacting with different transcription factors. The major IE region encodes 4 proteins, of which the most abundant is the nuclear phosphoprotein pp72 (IE1-72), whose function is required for viral replication at low multiplicity of infection. It cooperates with another IE protein, IE2-86, to regulate the expression of viral genes belonging to the following categories. IE1-72, which also possess kinase activity, may also have effects on cell cycle regulation interacting with the p107 protein of the Retinoblastoma family and with E2F1 [54]. IE2-86 is a nuclear phosphoprotein whose function is critical for viral replication, in fact it is a powerful transcriptional regulator that can both stimulate and suppress the expression of HCMV and cellular genes [52, 55]. IE2-86 is believed to be the key regulator of viral transcription transition from the IE to E gene expression phase. IE2-86 is also responsible modulating host cell metabolism to promote viral replication, by blocking the former in early S phase and inhibiting cellular DNA synthesis [56-58].

1.5.6 Characteristics of E proteins

The expression of the E or β genes relies on the expression IE proteins, being stimulated by IE2-86 alone or in cooperation with IE1-72. E genes mostly encode non-structural proteins, including viral DNA replication factors, repair enzymes, and proteins involved in immune response evasion. Through analysis of the viral gene expression profile it was possible to draw the temporal map of expression of the genes IE, E, and L of the entire viral genome. Expression of 36% of HCMVs

ORFs is not affected by treatment with Ganciclovir (GCV), which blocks the replication of viral DNA [59].

1.5.7 Characteristic of L proteins

The L proteins, which are mainly structural proteins, are the last class of HCMV gene products expressed during its replication and whose transcription begins more than 24 hours p.i. and requires the successful replication of viral DNA.

1.5.8 Gene expression and the late stages of viral life cycle

Replication and packaging of HCMV genome occurs in host cell nucleus. Viral DNA synthesis begins 16 hours p.i and it requires the activity a plethora of viral and cellular proteins. Since HCMV, unlike other herpetic viruses, does not encode enzymes for the synthesis of deoxyribonucleotides, it hijacks host cell metabolism, stimulating, rather than inhibiting gene transcription and translation. Being blocked in a S-phase-like state, infected cells, do not undergo DNA replication/division thus making available a large quantity of DNA precursors for viral genome replication. The replication of the viral DNA continues through an initial circularization of the genome within 4 hours p.i, followed by DNA synthesis through a bidirectional mechanism θ starting from a single replication origin (ori*Lyt*), which then turns into a late phase DNA replication in the form of a rolling circle.

HCMV genome replication is a complex process requiring the activity of several proteins endowed with different enzymatic activities. Pioneeristic studies demonstrated that 11 viral genomic loci are required to transcomplement *ori*Lyt dependent DNA replication in transient transfection based assays [27]. Six of them encode for replication fork proteins, as identified by similarity to homologous proteins in Herpes Simplex Virus type 1 (HSV-1). Such proteins are the DNA polymerase catalytic subunit UL54 and its putative processivity factor UL44, a ssDNA binding protein UL57 as well as heterotrimeric a trimeric helicase-primase complex, whose function is to unwind dsDNA and synthesize a RNA primer, composed by the helicase UL105, the primase UL70 and a cofactor UL102. During viral DNA replication, the trimeric helicase-primase complex

unwinds dsDNA and synthesize RNA primers [60]. Subsequently, UL57 binds and stabilizes the ssDNA strand released by the helicase primase complex, while the DNA polymerase holoenzyme mediates DNA synthesis. The remaining 5 loci do not have obvious homologous proteins in other herpesviruses and comprise 3 IE regulatory regions such as UL122-123, UL36-38 and Internal Repeated Sequence 1/Terminal Repeated Sequence 1 (IRS1/TRS1), as well as two E proteins such as UL112-113 and UL84. The UL122-123 regions are localized under the control of the extremely strong Major Immediate Early (MIE) promoter/enhancer, containing several binding sites for cellular transcription factors (TFs). It primarily encodes the IE-72 and IE-86 proteins. The UL36-38 region generates several different transcripts, based on the activation of different promoters and the use of a number of splicing sites [61]. Such genes encode for a number of proteins endowed with anti-apoptotic function such as viral Inhibitor of Caspase-8-Induced Apoptosis (vICA), encoded by UL36, a protein able to bind to pro-caspase 8 preventing its auto-proteolytic activation, and subsequently Fas-binding and apoptosis [62]. UL37 encodes proteins gpUL37 e pUL37x1 (pUL37exon1). gpUL37 is a glycoprotein also known as viral Mitochondria-localized Inhibitor of Apoptosis, (vMIA), which inhibits Fas-mediated apoptosis by localizing to mitochondria and preventing cytochrome c release. pUL37x1 prevents cytochrome c release by interacting with mitochondrial Adenosine Nucleoside Transporter (ANT) [63]. In addition, the UL38 gene product encodes an anti-apoptotic factor blocking caspase-mediated apoptosis [64]. The two highly homologous proteins IRS1/TRS1 cooperate with other IE proteins in viral mediated transactivation of viral and cellular promoters [65]: for example, they can activate expression of β genes together with IE1-72 and IE2-86 and increase the activity of the MIE promoter cooperating with UL69 [65]. Genes UL112-113 can generate four different phosphoproteins as a consequence of alterative splicing events. Such proteins have different molecular weights (34, 43, 50 e 84 kDa), and are differently expressed and localized at different stages of the viral life cycle. Such proteins bind to dsDNA and recruit UL44 to replication sites [66, 67]. Furthermore, the 84 kDa protein appears to regulate nuclear transport of the other UL112-113 proteins [68]. Finally, the UL84 protein is a

nucleocytoplasmic shuttling protein, with structural and functional homology to DExD/H box helicases, a family of nucleocytoplasmic shuttling RNA helicases with transcriptional regulation activities [69]. Its transcriptional properties are exemplified by its ability to bind IE2, inhibiting its activity, while such complex activates a bidirectional promoter present at the *ori*Lyt, most likely starting the replication process. UL84 is also capable of binding RNA and possess UTPase activity [70-73]. Its role as origin binding protein is supported by the interaction in vivo with HCMV *ori*Lyt, in a region containing RNA/DNA hybrid structures and stem-loops, with in vitro studies suggesting it can change the structure of such stem loop structures possibly priming the assembly of the replication complex [70]. Furthermore, UL84 is able to bind both UL44 and UL57 [74].

During the late stages of infection, large units of concatamer replication, without terminal fragments, are then cut into fragments of such length and to be packaged. The DNA packaging that starts when the pac-sequence, is recognized on concatemeric DNA by the viral terminase complex. The functional packaging holocomplex, a hetero-oligomer composed of proteins pUL56, pUL89 and pUL51, makes a first specific cut, thus generating a free end at which further packaging is initiated. The DNA/terminase complex then binds to an empty preformed procapsid at its unique portal vertex, across which the DNA is translocated. A second site-specific cleavage step terminates packaging when a unit length genome has been translocated.

The formation of viral capsids and the viral DNA packaging take place in the nucleus. Subsequently, the nucleocapsids acquire a first envelope budding from the nuclear membrane, then mature through loss and reacquisition of the envelope passing through the cytoplasm, from where they are released outside the cell through a mechanism similar to exocytosis [75].

1.6 Herpetic DNA polymerase holoenzyme general characteristics

All known *Herpesviridae* members encode their own DNA polymerase holoenzymes, essential for viral DNA replication. Sequence alignments shown that all herpetic DNA polymerases have conserved structures and functional domains. Furthermore, such polymerases are composed by two distinct subunits, a catalytic and an accessory protein, whose physical interaction is essential for replication of viral DNA (Table 1.1).

Virus	Catalytic Subunit	Accessory Subunit	Reference
HSV-1	UL30	UL42	[76]
HSV-2	POL	ICSP34, 35	[77]
VZV	POL	ORF16	[78]
HCMV	UL54	UL44	[60]
HHV-6	Pol6	p41	[79]
HHV-7	U38	U27	[80]
HHV-8	Pol-8	PF-8	[81]

Table 1.1: Human *Herpesvridae* members DNA holoenzyme subunits.

For all known *Herpesviridae* members, the catalytic subunit is of the DNA Polymerase holoenzyme is a large protein (110-140 kDa), constituted by six conserved functional domains: a pre NH2 domain, with 6 highly conserved residues, most likely involved in the interaction with the helicase/primase complex; a NH2 domain, probably endowed with RNA binding ability and hypothesized to be involved in RNAse activity; a domain possessing 3'-5' esonuclease activity; a palm domain involved in catalytic activity; a fingers domain responsible for nucleotide binding; a thumb domain, binding dsDNA. Such catalytic subunit thus possesses a 5'-3' DNA polymerase activity, being able to extend DNA templates as well as RNA primers. It also possesses an intrinsic 3'-5' proofreading activity as well as 3'-5' and 5'-3' esonuclease activities. However, the catalytic DNA polymerase has a much lower activity as compared to the holoenzyme (therefore defined basal activity). Binding to the smaller accessory subunit, results in increased holoenzyme DNA polymerase and DNA binding activities, as well as in higher nucleotides incorporation rates and processivity, thus making the holoenzyme capable of replicating the entire viral genome. The essential role of the association between the two subunits has been proved by the fact that mutations

impairing such intermolecular association also prevent viral replication [61, 76]. The current biochemical model, universally accepted for all known *Herpesviridae* DNA polymerase holoenzymes, is mainly based on studies on the HSV-1 holoenzyme, formed by the catalytic subunit UL30 and the processivity factor UL42. UL42 is known to be able to simultaneously bind to dsDNA and UL30 using different protein domains, thus tethering it to dsDNA [61, 76].

1.7 HCMV DNA Polymerase Catalytic subunit

DNA polymerases are classified in seven different families. Herpetic DNA polymerases belong to the B family. Such family comprises several viral and cellular DNA polymerases, all containing 7 conserved regions, designed I, II, III, IV, V, VI and VII. Such regions play an important role in enzyme catalytic activity. Regions I to V, along with an additional region called region C, shared by all *Herpesviridae* DNA polymerase catalytic subunits, are involved in binding to substrates and antiviral nucleoside analogs. The N-terminal domain possesses RNAse H activity and interacts with several viral proteins, while the intrinsic exonuclease 3'-5' activity has been mapped to region IV and the C region [82]. In the catalytic site, three highly conserved regions (Exo I, II and III) possess 5'-3' exonuclease activity.

The N-terminal region is the most conserved one, with regions I, II and III being extremely conserved in all known DNA polymerases (from bacteriophages to mammals), thus suggesting they could fulfil all catalytic functions. Region I in involved in substrate recognition, including dNTPs and PPi, since several mutants mapping in this region exhibit resistance to nucleoside and pyrophosphate analogues, or affect its catalytic activity. Furthermore, several mutations affecting sensibility to nucleoside or pyrophosphate analogues map to regions II and II, suggesting a direct role in dNTPs binding and pyrophosphate hydrolysis [83]. Finally, regions V and VII are the less conserved and characterized, and their role has still to be defined. The HCMV DNA polymerase is called UL54 and it is a 140 kDa protein of 1242 amino acids. Regions I to VII are located within residues 379-1100 [84], so that the catalytic core is located in the central part of the protein. On the

other hand, the N-terminal part of the protein contains the three regions (Exo I, II, III) responsible for the 5' -3' exonuclease activity [85], while the C-terminal domain is responsible for binding to UL44 and nuclear transport of the protein. Indeed, UL54 C-terminal 22 residues are necessary and sufficient to mediate binding to its accessory subunit UL44 [86]. In addition, UL54 C-terminal domain contains two NLSs. The first to be discovered was an atypical, poorly characterized hydrophobic NLS (hNLS), which lies within the protein UL44 binding domain (PRRLHL-1127), and thus appears to be active only when UL54 is not associated with UL44 [86, 87]. UL54 also contains a classical NLS (cNLS), located upstream of the UL44 binding domain (PAKKRAR-1159). Such NLS is active also when UL54 comlpexed with UL44 and has been shown to confer energy- and Ran-dependent nuclear targeting to reporter proteins, as well as recognition by the IMPα/β heterodimer through direct interaction with IMPα [86, 88].

1.8 HCMV DNA polymerase accessory subunit UL44

HCMV DNA polymerase accessory subunit, UL44 is a 52 kDa phosphoprotein essential for HCMV genome replication [89]. UL44 has been shown dimerize, thus being able to bind to dsDNA in the absence of clamp loaders and ATP, and to directly interact with UL54, and stimulating its holoenzyme activity [60, 90]. UL44 can be functionally and structurally divided in an N-terminal domain (residues 1-290), and a C-terminal domain (residues 291-433). The N-terminal domain retains all known UL44 biochemical properties, including the ability to bind to dsDNA and UL54 and to stimulate to latter activity [90]. The C-terminal domain is largely unstructured, containing five stretches of glycine, which confer extreme flexibility. Its main function described so far appears that of regulating the nuclear import process of UL44 thanks to a C-terminally located functional cNLS (PNTKKQK-431) interacting with IMPα/β [91]. In addition, UL44 C-terminus (residues 409-433) is the target of extensive post-translational modifications. These include multiple phosphorylation sites (S413, S415, S418 and T42T) and a sumoylation site (K410), which regulate UL44 subcellular localization by controlling its ability to interact with host cell proteins [88, 91-94],

although the exact role of UL44 sumoylation is still unknown [93]. UL44 N-terminal portion (residues 1-290) has been recently crystallized [95]. UL44 forms heat to head dimers, and each monomer shares a very similar structure to that of other processivity factors such as proliferating nuclear antigen (PCNA) monomers, and the monomeric HSV-1 UL42 (Figure 1.4), despite lacking high sequence homology [96, 97].

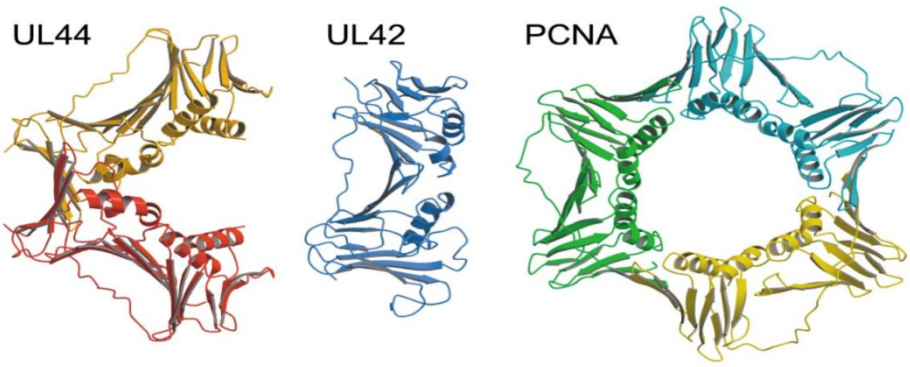

Figure 1.4 Comparison of the UL44 dimer, the UL42 monomer, and the PCNA trimer. Adapted from [98].

Each monomer forms two topologically similar domains. They share a central β-sheet and are connected by a long connector loop running along the front face of the molecule, which is important for binding to other protein partners, including UL54 [98]. (Figure 1.5).

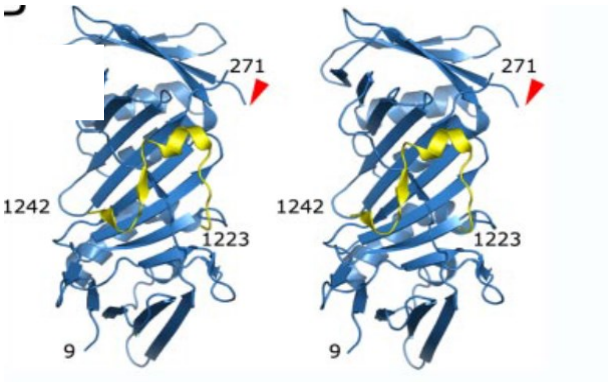

Figure 1.5: Representation of the UL44-UL54 complex (*blue* and *yellow*, respectively). From: [98].

The back face of UL44 is flanked by four helices and is rich in basic residues involved in DNA binding [99]. Dimerization relies on the interaction between the two most N-terminal B-sheets of each monomer, with six main chain hydrogen bonds formed. The interaction involves also

extensive packing of hydrophobic side chains at the interface, with F121, M123 and L93 of each monomer is being packed against L86 and L87 of the opposite monomer (Figure 1.6).

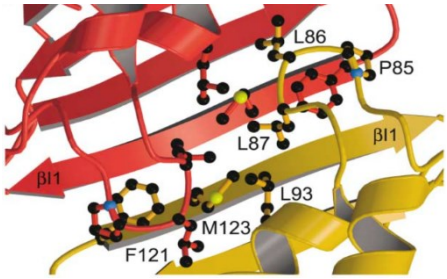

Figure 1.6. Structural representation of UL44 dimerization interface with crucial residues depicted in ball and stick. Adapted from [98].

Intriguingly, dimerization appears a prerequisite for DNA binding by UL44. Upon dimerization, the basic face of each monomer contributes to the formation of a positively charged central cavity which is involved in DNA binding via electrostatic interaction [99]. Accordingly, point mutations impairing dimerization – such as the L86A/L87A double mutant, strongly impair binding to dsDNA. Also, the F121A mutant is impaired for DNA binding - although to a lesser extent as compared to the L86A/L87A double mutant- and it has been speculated that it could possess weak DNA binding upon dimerization. Importantly, the L86A/L87A double substitution prevented viral DNA replication as shown by the failure of such mutants to sustain *ori*Lyt dependent DNA replication in transient trans-complementation assays, suggesting that UL44 homodimerization is essential for viral genome replication [100]. Therefore, UL44 dimerization can be considered a potential target of therapeutic intervention to interfere with HCMV replication.

Furthermore, each UL44 monomer possesses a basic face containing several basic lysine residues which, upon dimerization, forma a basic cavity binding to dsDNA via electrostatic interactions. In addition, each UL44 monomer has a 13 aa long flexible loop (FL), not visible in the electron density map [PHTRVKRNVKKAP-172], which has been modelled as protruding towards the back face and potentially contacting dsDNA. *In vitro* modelling and mutagenic studies have shown that basic residues within the back face and the FL of UL44 are important for DNA binding: their substitution to alanine strongly impaired DNA binding [99]. The importance of UL44-FL in cells

has been recently demonstrated: substitution of UL44-FL basic residues with hydrophobic ones impaired DNA binding, and its ability to form nuclear speckles, simultaneously increasing its intranuclear mobility upon transfection in Mammalian cells. Such mutation also abolished HCMV *ori*Lyt-dependent DNA replication in transient transcomplementation assays, implying that the UL44-FL is important for DNA binding during viral replication [101]. Furthermore, overexpression of such UL44 mutant (called UL44Δloop) in the presence of wild-type UL44 abolished HCMV *ori*Lyt-dependent DNA replication in transient transcomplementation assays, suggesting a transdominant negative phenotype [101]. Indeed, transient relocalization assays suggested that UL44Δloop could still interact both with UL54 and to interact with UL44, implying that the formation of DNA defective UL54/UL44 and UL44/UL44 complexes could be detrimental for viral replication [101]. Other single aa substitutions in UL44 are known to severely affect its biochemical properties such as the interaction between UL44-UL44 homodimers, the formation of UL54-UL44 complex, as well as its ability to bind dsDNA. In particular, UL44-F121A and UL44-L86/L87A mutants possess amino acid substitutions that interfere with the dimerization of UL44, without affecting binding to UL54 neither *in vitro* nor in living cells [98, 100]. Importantly such mutants exhibit reduced DNA binding ability in filter binding assays [95], and are not compatible with viral DNA replication in *ori*Lyt replication assays, suggesting that UL44 homodimerization is essential for viral life cycle [100]. The UL44-I135A mutant, instead, has an amino acid substitution in the connector loop of UL44. Such mutation does not affect UL44 DNA binding ability or dimerization ability [95, 100] but completely disrupts the UL54-UL44 interaction preventing DNA replication [101]. On the other hand, UL44Δloop, containing hydrophobic substitutions in place of basic residues within UL44-FL (see above), retains the ability to dimerize and bind to UL54 in cells but is defective for DNA binding, as shown by cellular sub-fractionating experiments and by subcellular localization assays [101]. Such mutant, intriguingly, does not support HCMV *ori*Lyt-dependent HCMV DNA replication, where it behaves as a trans-dominant-negative mutant [101]. Finally, the

UL44ΔNLS mutant bears point mutations within UL44-NLS (PNTKKQK-431), impairing its nuclear localization, without affecting its ability to bind to UL54 and self-interact [88, 91].

1.9 Treatment of HCMV infection

Management of HCMV infections in transplant patients can be achieved by different strategies using a number of antivirals, however, although prenatal diagnosis of congenital infection is possible, no prenatal therapy is currently available [7]. Different trials aimed to study the effect of CMV-specific hyperimmune globulin in pregnant women with primary CMV infection were performed. CMV hyperimmune globulin (Cytotect Biotest) has a half-life of approximately 22 days, has been safely used in other studies, and has antiviral and immunomodulatory effects [102-106]. A nonrandomized study [107], showed that when CMV-specific hyperimmune globulins were administered to pregnant women with primary infection, the rate of mother-to-fetus transmission decreased significantly, from 40% to 16% ($P = 0.04$), and the risk of congenital disease also decreased significantly, from 50% to 3% ($P<0.001$). In this study, hyperimmune globulin appeared less effective for the prevention of fetal infection than for the treatment of fetuses already infected. In fact, for the prevention of fetal infection, hyperimmune globulin presumably reduced maternal systemic or placental viral loads, thus decreasing the likelihood of fetal infection. But for this study, once the fetus is infected, however, hyperimmune globulin presumably reduced placental or fetal inflammation, or both, resulting in increased fetal blood flow with enhanced fetal nutrition and oxygenation. In contrast, another study [108], a not significant reduction in the rate of transmission of CMV infection to the fetus among women receiving hyperimmune globulin as compared with women receiving placebo was detected. Moreover, this study showed no effect of hyperimmune globulin on the activity of neutralizing antibodies and no clearance of maternal levels of DNA in the blood was annotated. In addition, a higher number of serious adverse events were detected among women who received hyperimmune globulin and among their newborns than

among women who received placebo and their newborns. In conclusion, the opinions about the administration hyperimmune globulin in pregnant woman are still very contrasting.

As alluded to above, in contrast, a variety of therapeutic options are available for the treatment of HCMV infections in transplant patients, which include either a prophylactic or a preventive approach. The prophylactic treatment starts immediately after an organ or stem cells transplant and continues for the next 90-100 days to prevent the appearance of the virus [109]. Even though the prophylactic therapy doesn't exclude the possibility of infections, without it 20-30% of transplanted patients are infected in the subsequent 90 days post transplantation. The preventive treatment, instead, starts when in asymptomatic patients is diagnosed the presence of the virus, also at very low levels (sign of primary infection or viral reactivation). Antivirals are administered to prevent the progression of the asymptomatic viremia. A number of drugs have been approved for the management of CMV infections by the Food and drug Administration (FDA).

1.10 FDA approved anti-HCMV drugs

Ganciclovir, (GCV) [9-(1,3-dihydroxy-2-propoxy- methyl) guanine], was the first antiviral agent approved for the treatment of CMV disease and remains the first-line treatment for CMV infection and CMV disease in SOT recipients [110]. GCV is a guanosine nucleoside analogue, and can be considered an inhibitor of the viral DNA polymerase. GCV is structurally similar to acyclovir, a widely used anti HSV therapeutic, but has a hydroxymethyl group at the 3′ position of the acyclic side chain (Figure 1.7). This relatively minor structural modification accounts for enhanced activity of GCV against CMV as well as for its greater toxicity.

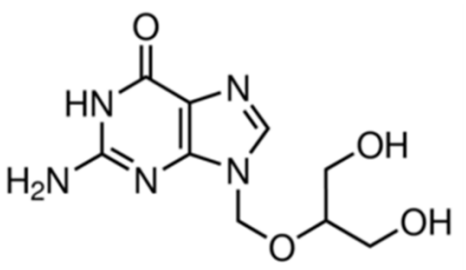

Ganciclovir

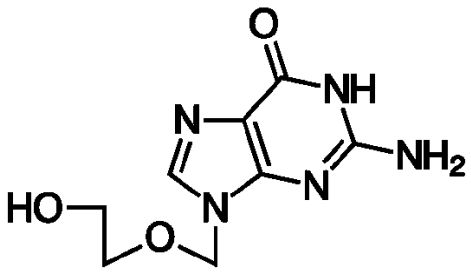

Aciclovir

Figure 1.7. Chemical structures of Ganciclovir and Aciclovir.

The selectivity of GCV selectivity mainly relies on its higher affinity for the CMV DNA polymerase as compared to the cellular one, and on the fact that GCV initial phosphorylation is mediated exclusively by a viral-encoded protein kinase, encoded by the viral gene UL97 [111]. Indeed, only after this first phosphorylation, GCV can be converted to GCV triphosphate (GCV-3P) by cellular kinases, such as the guanylate kinase and the nucleoside diphosphate kinase. At this point, the drug competitively inhibits DNA synthesis catalyzed by the viral DNA polymerase holoenzyme, leading to incomplete genome amplification due to GCV-3P incorporation of in place of dGTP into the growing viral DNA chain [112]. Indeed, GCV incorporation causes the generation of abortive, incomplete viral DNA genomes [113], which are believed to be the result of slower DNA synthesis rather than of an absolute DNA synthesis termination [114]. FDA initially approved GCV in 1989 for intravenous (IV) use [112, 115, 116]. This drug has been shown to reduce the severity of HCMV retinitis, gastrointestinal disease, and pneumonia (to a lesser extent) in SOT, HSCT, and AIDS patients as well as neurological *sequalae* in case of symptomatic congenital infection [53, 115-117]. Despite its therapeutic efficacy, GCV use is strongly limited by several drawbacks. These include the occurrence of side effects, drug resistance and its poor bioavailability. As far as side effects are concerned, the main toxicity of GCV is hematological (primarily neutropenia, anemia, and thrombocytopenia), while the other potential toxicities are marginal (fever, rash, hepatic toxicity). Such toxicity is mainly due to the fact that, although GCV-3P preferentially targets CMV DNA polymerase, it also has some activity against cellular DNA

polymerases. The second potential cause of treatment failure with GCV is represented by the occurrence drug-resistant strains [118-121]. This is more common upon prolonged exposure to GCV and/or with suboptimal GCV plasma concentrations [121-123]. Treatment of transplanted patients with GCV results in the occurrence of viral resistant strains in 1.5% to 9.5% of cases. Most commonly, resistance emerges as a consequence of mutations in the UL97 gene [118, 124, 125]. Such mutations are responsible for viral kinase instability or reduced ability to phosphorylate GCV and do not confer cross-resistance to other drugs active against CMV (see below). More rarely, mutations of the UL54 gene, encoding for the viral DNA polymerase, are responsible for viral resistance to GCV. Unlike mutations of the UL97 gene, UL54 gene mutations can confer cross-resistance to other antiviral drugs such as Foscarnet (FOS) and Cidofovir (CDF) [112]. However, they are only observed in 5% to 22.2% of GCV-resistant viruses, and they are most often combined with mutations of the UL97 gene [118]. Finally, the use of GCV is limited by its poor bioavailability, in fact oral GCV capsules have a low bioavailability (6%) and limit the drug concentration in serum.

GCV poor oral bioavailability led to the development of *Valganciclovir (VGCV)* (see Figure 1.8), a L-valyl ester prodrug, which is rapidly metabolized in the liver and intestinal wall after oral administration [112, 116, 126, 127, 128].

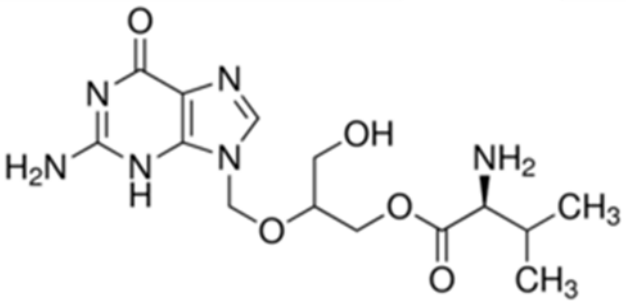

Valganciclovir

Figure 1.8. Chemical structures of Valganciclovir.

The adverse effects of VGCV are similar to those of GCV; however, VGCV has a much better oral bioavailability (60%) and allows treatment without hospitalization [112, 127, 128]. Thus, VGCV

tends to be widely used among transplant recipients, not only for prophylaxis, but also for preemptive, curative, and maintenance therapy hospitalization [112, 127, 128]. VGCV was approved in 2000 for treatment of CMV retinitis in AIDS patients [128] and was later approved for prophylactic treatment of CMV in certain SOT recipients.

Foscarnet (FOS) is an organic analogue of inorganic pyrophosphate (see Figure 1.9) that reversibly and noncompetitively (in contrast to GCV-3P and cidofovir) inhibits the activity of the viral DNA polymerase.

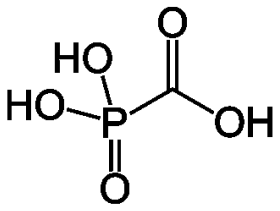

Foscarnet

Figure 1.9. Chemical structure of Foscarnet.

This non-competitive inhibitor reversibly blocks the pyrophosphate-binding site of pUL54 and inhibits the cleavage of pyrophosphate from deoxynucleoside triphosphates [112, 129, 130]. Point mutations conferring resistance to FOS have been mapped in the UL54 gene. Moreover, cross-resistance has been observed between GCV and FOS in several laboratory and clinical isolates. FOS was FDA approved in 1991, and despite its utility, it has been associated with nephrotoxicity and metabolic toxicity as well as renal failure, hypocalcaemia, hypomagnesemia, and hypophosphatemia [112, 117, 129]. Due to its nephrotoxic potential, its administration requires slow infusion, extensive prehydration and dose adjustment based on creatinine clearance. Because of its side effects, FOS is considered as a second-line therapy. However, it is widely used, especially in patients with myelosuppression or weak graft after HSCT, AIDS patients with HCMV retinitis who fail GCV therapy because of viral resistance, or patients who cannot be treated with GCV because of dose-limiting neutropenia or leukopenia [126, 131, 132, 133].

Cidofovir [(S)-1-(3-hydroxy-2-phosphonylmethoxypropyl)cytosine; Vistide1, Gilead] is an acyclic nucleoside phosphonate analogue of dCMP (see Figure 1.10).

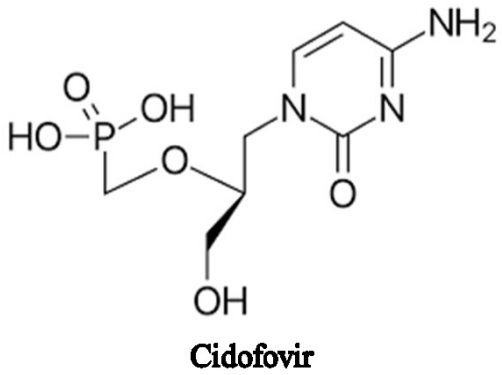

Cidofovir

Figure 1.10. Chemical structure of Foscarnet.

It has a mechanism of action similar to that of other nucleoside analogues, but as an acyclic nucleoside phosphonate, is not dependent on activation by a virus-encoded enzyme for activity. It is converted to the di and triphosphoryl forms by cellular kinases, and then acts as an inhibitor of the viral DNA polymerase, causing premature chain termination in viral DNA synthesis. CDV is a broad-spectrum antiviral agent, which is active against herpesviruses and other DNA viruses [116]. CDV is available only as an intravenous formulation and possesses low bioavailability. Its major limitation is its severe renal toxicity, thus rendering it a second-line therapy. Patients receiving IV CDV must be given oral probenecid (that reduces elevated blood uric acid levels), to protect against kidney failure and must be prehydrated before infusion. Neutropenia is another toxicity associated with CDV, and this drug was shown to be both carcinogenic and teratogenic in preclinical toxicological studies. Its use is therefore currently very limited.

The three main HCMV compounds available until 2017, GCV, FOS and CDV, all target the CMV polymerase pUL54 (Figure 1.11), and have too high levels of toxicity to be used for prophylaxis of bone-marrow transplanted patients. Indeed, the use of CDV/FOS and GCV, is strongly limited by nephrotoxicity, and bone-marrow suppression, respectively (see above).

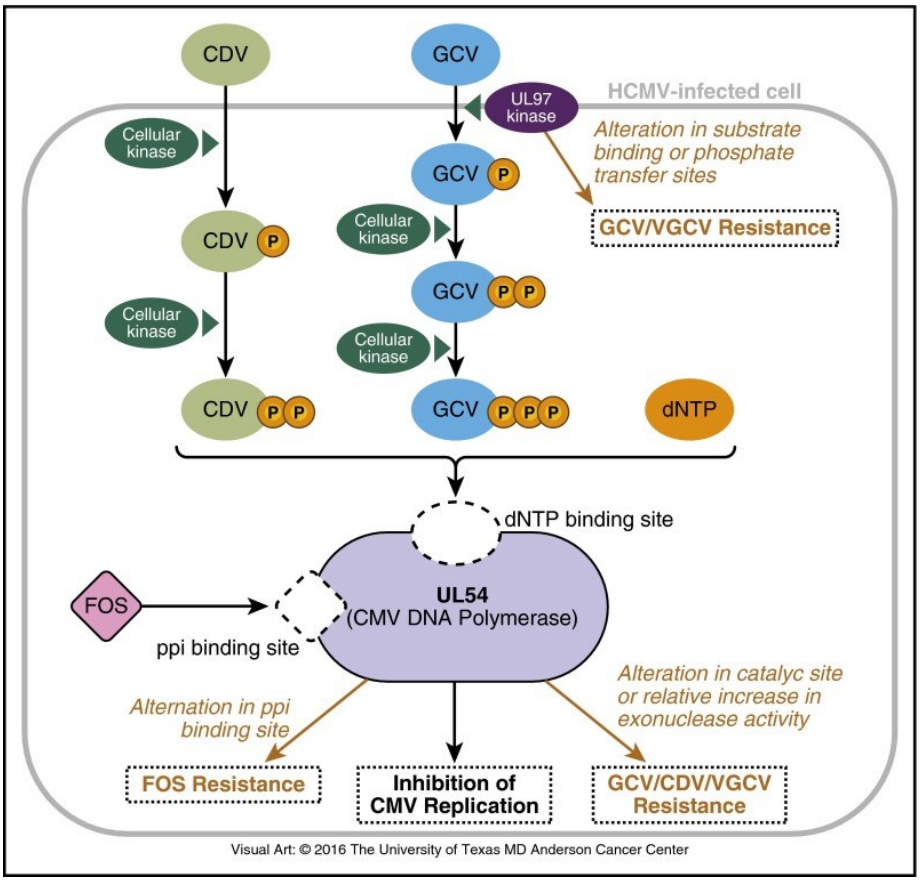

Figure 1.11 Mechanism of action of anti-HCMV drugs targeting the DNA polymerase. In the CMV-infected cell, GCV and VGCV undergo phosphorylation by UL97 kinase (pUL97) and cellular kinases. CDV phosphorylation is independent of pUL97; cellular kinases add an additional phosphate. GCV, VGCV, and CDV compete with deoxynucleotide triphosphate (dNTP) for the binding site on pUL54. FOS does not require phosphorylation. Once inside the CMV-infected cell, FOS directly inhibits CMV DNA replication by binding to the pyrophosphate (ppi) site of pUL54. Alterations in the substrate binding or phosphate transfer sites of pUL97 confer *UL97* resistance to GCV and VGCV. Alterations in the catalytic site or relative increases in the exonuclease activity of pUL54 confer *UL54* resistance to GCV, VGCV, and CDV. Alterations of the ppi binding site of pUL54 confer *UL54* resistance to FOS.

Recent attempts to develop new anti-HCMV compounds have focused mainly on novel targets such as the viral terminase complex involved in viral DNA cleavage/packaging, that could be used in prophylaxis. *Letermovir (AIC246; LMV)* is derived from a new chemical class of antiviral drugs, the quinazolines [134] (see Figure 1.12), and exerts its anti-CMV activity by inhibiting the CMV DNA terminase complex (encoded by UL51, UL56, and UL89, see section 1.5.8). This terminase complex is required for neo-synthesized CMV DNA processing and packaging. By inhibiting the terminase, LMV prevents the cleavage of long DNA concatamers into individual viral units, thereby impairing the production of infectious particles, without affecting viral DNA replication [134-136]. Its pre-clinical profile indicated that it was highly selective in its antiviral activity for CMV,

demonstrating little activity against other human or rodent herpesviruses, and minimal activity against other human pathogenic viruses, hepadnavirus, adenovirus, retroviruses, orthomyxoviruses, and flaviviruses [137]. The selectivity index (SI), which is the ED_{50} (amount of drug needed to cause 50% inhibition of viral replication) divided by the CC_{50} (amount of drug required to kill 50% of uninfected cells), is greater than 15,000 for LMV, therefore demonstrating not only excellent overall antiviral activity but also a remarkable lack of cellular toxicity [134]. It is a potent antiviral drug with *in vitro* activity surpassing the current gold standard, GCV, by over 400-fold for the 50% effective concentration (ED50; 4.5 nM versus 2μM) and over 2000-fold the EC90 (6.1 nM versus 14.5μM), without significant cytotoxic effects [134, 137, 138].

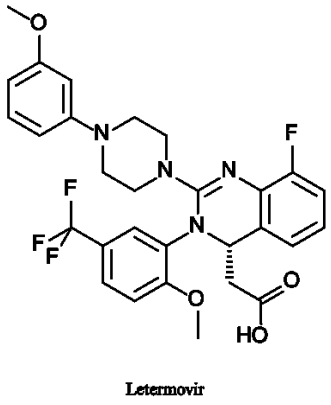

Letermovir

Figure 1.12. Chemical structures of Letermovir.

Importantly, in August 2017, LMV has been approved by the US Food and Drug Administration as a new molecular entity for prophylaxis of cytomegalovirus infection and disease in adult CMV-seropositive recipients of an allogeneic hematopoietic stem cell transplant, under the name of Prevymis (www.accessdata.fda.gov, Reference ID 4179078). Furthermore, LMV can be orally or intravenously administered and it is absorbed rapidly after oral administration. Its bioavailability is increased from 35 to 85% in the presence of cyclosporine [139]; the increased bioavailability is due to cyclosporine inhibition of hepatic transporters, including ATP-binding cassette transporters and soluble transporters [139]. Several recent studies of CMV strains isolated from immunocompromised patients who have never received LMV suggest that primary resistance to this molecule is rare to inexistent [140, 141]. A large number of LMV resistance mutations in UL56 that

have been identified *in vitro* or in clinical studies, clustered at UL56 codons 231–369. Thus, these mutations were located outside the functional domains of pUL56 involved in DNA-packaging and do not impact viral replicative capacity [138, 140]. The most common adverse effects of LMV are nausea, vomiting, diarrhea, abdominal pain, peripheral edema, cough, and fatigue.

Fomivirsen (Vitravene®; developed by Isis Pharmaceuticals, licensed to Novartis Ophthalmics) is a 21-nucleotide anti-sense RNA (5'-GCG TTT GCT CTT CTT CTT GCG-3'), specifically targeted against the mRNA from the major immediate early transcriptional unit of CMV. Fomivirsen is administered by intraocular injection, and was approved by FDA in 1998 as a second-line therapy for local treatment of CMV retinitis in AIDS patients [112]. Novartis withdrew the marketing authorization in the EU in 2002 *("Public Statement on Vitravene (fomiversen): Withdrawal of the Marketing Authorization in the European Union". EMA. August 6, 2002) and in the US in 2006 (Initiating Coverage: Rexahn Pharmaceuticals (RNN)". LifeSci Capital. May 23, 2016.).* The drug was withdrawn because while there was a high unmet need for drugs to treat CMV when the drug was initially discovered and developed due to the CMV arising in people with AIDS, the development of HAART dramatically reduced the number of cases of CMV.

1.11 Investigational agents

Maribavir (*MBV*) is an antiviral drug that inhibits the UL97 viral protein kinase of human CMV and causes inhibition of viral encapsidation and nuclear egress of viral particles from infected cells [112, 142] (see Figure 1.13).

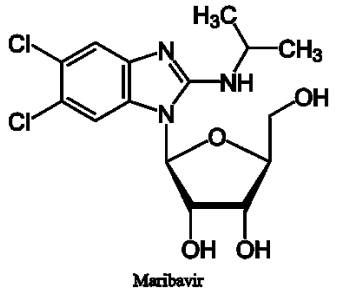

Figure 1.13. Chemical structures of Maribavir.

No intracellular phosphorylation is required, and its mechanism of action is independent from the UL54 DNA polymerase. MBV has an *in vitro* activity against some CMV strains resistant to ganciclovir or cidofovir [143]. Indeed, although many mutations have been identified *in vitro* as conferring resistance to MBV by changing the binding site of ATP to UL97 [144], MBV-resistant CMV viruses usually remain susceptible to GCV and vice versa. MBV has good oral bioavailability. Prophylactic MBV is safe and well-tolerated and effectively reduce CMV infection after allogeneic stem cell transplantation. MBV significantly decrease CMV antigenemia and DNAemia, resulting in less use of preemptive therapy with GCV [143].

Brincidofovir (CMX-001; BCV) is a new broad-spectrum antiviral molecule with an in vitro activity against herpes viruses, polyomaviruses, adenoviruses, papillomaviruses, and the smallpox virus [145] (see Figure 1.14). BCV is a lipid-conjugated analogue of CDV with a high oral bioavailability and a long half-life. It can thus be administered twice a week.

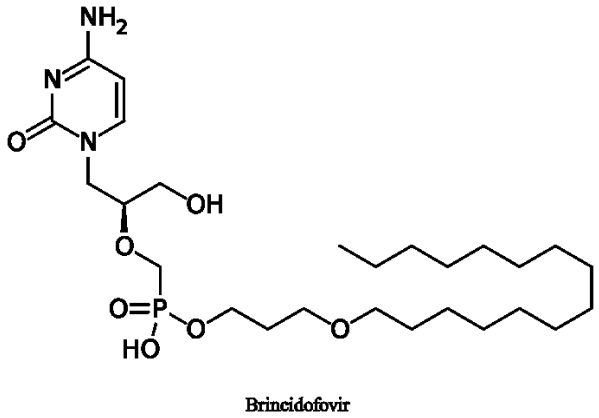

Figure 1.14. Chemical structure of Brincidofovir.

Unlike CDV, BCV is not a substrate for organic anion transporters and, therefore, has significantly reduced potential for renal toxicity [146]. BCV is still active *in vitro* against many isolates carrying resistance mutations on UL97 and/or UL54 genes. Although the same resistance mutations of the UL54 gene can reduce susceptibility to CDV and BCV, a recent *in vitro* study suggests that BCV could have a unique resistance profile associated with a reduced replicative capacity of CMV and a preserved susceptibility to FOS and GCV [147].

As of 2014, BCV was in Phase III clinical trials for use in humans against HCMV and adenovirus, after testing for safety in over 1,000 human subjects (*"Brincidofovor for Ebola". NCT02271347),* and has received FDA Fast Track Designation for treatment of HCMV, adenovirus, and smallpox (*Chimerix Announces Emergency Investigational New Drug Applications for Brincidofovir Authorized by FDA for Patients With Ebola Virus Disease". Archived from the original on 6 October 2014. Retrieved 8 October 2014.).* Chimerix announced in December 2015 that the Phase III trials for use of the drug in preventing HCMV infection in stem cell transplant patients (NCT01769170) had failed, and in February 2016 shut down two other late-stage trials for use of the drug in preventing infection after kidney transplants (NCT02439970).

There are no active clinical trials evaluating BCV for CMV prevention, as the manufacturer is evaluating a better formulation. Nonetheless, a prospective registry database (NCT02167685) is

ongoing to evaluate the potential impact of prior treatment with BCV on long-term outcomes, including late CMV disease and survival [148].

1.12 Other treatments (non-specific to HCMV): leflunomide and artesunate

Leflunomide, mainly used for the treatment of adult rheumatoid arthritis, has a documented antiviral activity against several viruses, including CMV and the BK virus [149]. Leflunomide has been used, alone or in combination, for the rescue treatment of severe HCMV or HCMV diseases caused by GCV-resistant viruses, and showed mixed results [150, 151-153]. However, Lefunomide is not been approved clinically as HCMV treatment, and there are no large randomized clinical trials planned to assess its efficacy and safety. Artesunate is an antimalarial drug with a broad spectrum of activity in vitro, including against herpes viruses [154], because of its ability to repress NFkB and Sp1 pathways [155]. Its use, either alone or in combination, for the treatment of severe CMV infections and/or multidrug-resistant CMV infections was the focus of several studies reporting conflicting results [156-158]. Just like leflunomide, randomized prospective studies are required to assess the efficacy and tolerability of artesunate in this indication. Recently, the disruption of protein-protein interaction has been proposed as a potential alternative strategy for the development of new, highly needed, anti-viral drugs [159].

1.13 Protein-protein interaction (PPI) as druggable targets in human disease

Protein–protein interactions (PPIs) play a pivotal role in various mechanisms of cellular growth and differentiation, and in the replication of pathogen organisms in host cells. Thus, inhibition of these interactions represents a promising novel approach for rational drug design against a wide number of cellular and microbial targets. PPIs play a key role in virtually every cellular process. The dynamic processes of living organisms depend on the coordinated formation of such PPIs; for example, they occur during DNA replication, gene regulation, transcription and splicing of mRNA, protein synthesis and secretion, formation of intracellular structures and oligomeric enzymes, and in

the many pathways associated with cell signaling [160]. Aberrant PPIs can also be responsible for the development of pathological processes, like Alzheimer's and prion diseases [161, 162], and several types of human cancer. In addition, PPIs between virus-encoded components or between viral proteins and cellular factors occur during the replication and assembly of human viruses in host cells [163]. Many of these interactions could become pharmaceutical targets. In fact, the ubiquitous nature of protein–protein interactions in essential processes suggests the possibility of developing a novel strategy for drug discovery based on selective disruption of protein assemblies. They take place as a result of stereochemical cognate interaction between the surfaces of homologous or heterologous protein subunits during assembly of quaternary structures and macromolecular complexes [164].

The past 20 years have seen many advances in understanding of PPIs and how to target them with small-molecule therapeutics. Surprisingly, many of these PPI clinical candidates have efficiency metrics typical of ‘‘drug-like’’ or ‘‘lead-like’’ molecules. Successful discovery efforts have integrated multiple disciplines and make use of all the modern tools of target-based discovery structure, computation, screening, and biomarkers. PPIs become progressively more challenging as the interfaces become more complex, as binding epitopes are displayed on primary, secondary, or tertiary structures. PPIs represent a vast class of therapeutic targets both inside and outside the cell. PPIs are extremely diverse in the size and shapes of the interfaces and the binding affinities and dynamics of assembly.

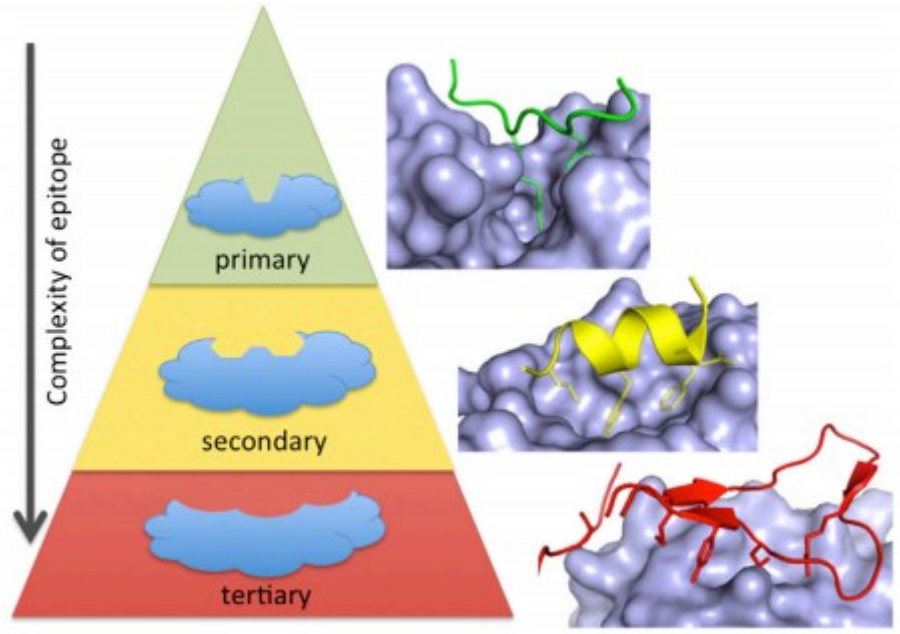

Figure 1.15. The Complexity of the PPI Interface Affects druggability PPIs. On side of the interface can be represented by a primary protein sequence (green), by a region of secondary structure, like an alpha helix (yellow), or by a tertiary structure (red). As the interface become more complex (from primary to tertiary structure), as fewer examples of SMs inhibitors. From [165].

Given that are (conservatively) 100,000 PPIs [166], the current database of PPI inhibitors is small and biased. Twenty years ago, PPIs were considered ‘‘intractable.’’ High-resolution structures in the 1980s to 1990s showed that PPI interfaces are generally flat and large (roughly 1,000–2,000 A^2 per side) [167], in stark contrast to the deep cavities that typically bind small molecules (about 300–500 A^2) [168]. Between 1995 and 2005, hopeful signs were emerging. A clinically approved integrin antagonist (tirofiban) and natural products like taxanes, rapamycin, and cyclosporine inspired confidence that PPIs could be modulated by small molecules. Mutational analysis of protein interfaces showed that not all residues at the PPI interface were critical, but rather that small ‘‘hot spots’’ conferred most of the binding energy [165]. Hot spots tended to cluster at the center of the interface, to cover an area comparable to the size of a small molecule, to be hydrophobic, and to show conformational adaptivity. These features suggested that at least some PPIs might have small-molecule-sized patches that could dynamically adjust to bind a drug-like molecule. The last decade has seen amazing progress in tackling challenging PPI targets with synthetic molecules. More than 40 PPIs have now been targeted [169-171], and several inhibitors have reached clinical trials.

Analyses of PPIs in which crystal structures a of PP and protein-small-molecule were available show some suggestive themes [172-174]. First of all, PPI target proteins tend to have extended binding channels that may be divided into subpockets [168]. Hot-spot residues are center in or around these pockets and are complementary on both sides of the interface. Second, small conformational alteration in the binding site present a deeper pocket to small molecules than to the partner protein. These pockets are also more readily formed at the PPI interfaces than somewhere else on the protein surfaces [172]. The consensus is that ligand-binding surfaces (including PPIs) have a higher propensity for binding (to cognate ligands, solvent molecules, inhibitors) than the rest of the protein surface. Third, PPIs with small-molecule inhibitors tend to have small, high-affinity interfaces and include a hot segment that can summarize the binding of the partner protein. The observation that high-affinity complexes have more small-molecule ligands [173] could imply that they are inherently ‘‘sticky.’’ PPI inhibitors bind at the hot spot and tend to mimic the types of binding interactions (e.g., hydrophobic) made by the partner. However, they generally use different functional groups and approach the binding site from different orientations than in the PPI. To date, more traction has been gained through virtual screening and the use of non-traditional libraries, including larger, more natural-product-like macrocycles on the one hand and fragment-based lead discovery on the other. Fragment screening has been a particularly successful, perhaps because the pocket sizes at PPIs are close to fragment size and the bias in chemical composition is lower. Experimental and virtual fragment screens have even been used to define the druggability of a PPI [175, 176]. Inhibitors of PPI have several favor features over other classes of drugs. For example, the very high specificity of these cognate interactions provide the possibility of interfering with them in a specific manner, making them attractive targets, in particular against microbial pathogens. The great structural variability of PP interface may provide a possibility for the effective differentiation between the host and the pathogen [177]. In contrast to the design of inhibitors binding to active site of enzyme of pathogen organism can be limited by high structural similarity between the human and the pathogen enzyme. Secondly, in targeting cellular or microbial enzymes,

dissociative inhibitors could be less likely to promote the development of drug resistance than are inhibitors that bind the enzyme active site. In fact, a single mutation in one subunit of PP interfaces needs the complementary mutation in the other subunit to maintain intact the protein complex. As the simultaneous coupled double mutation in different subunits is rather improbable, it is unlikely that the target protein complex can acquire resistance for such an inhibitor. In contrast, since active site directed inhibitors usually form a few high-affinity interactions with the enzyme, a single change of residues in the active site frequently leads to drug resistance. Another topic is the affinity of PP binding that is overemphasized when considering the potential of small molecules to inhibit such interactions. In fact, even proteins that bind with high affinity will be successfully out-competed by a weakly binding small molecule, if the concentration of the target protein is quite low and the small molecule concentration is enough high [178]. Moreover, at least in some cases, the simple alteration of a binding equilibrium will be sufficient to cause a significant biological effect without the requirement to entirely inhibit the target PP interaction. Nonetheless, it is clear that PP interfaces vary largely in nature and some are likely to be more appropriate targets than others for drug discovery. The first example in literature of successful disruption of protein–protein interactions concerns a viral enzyme, the ribonucleotide reductase (RR) of herpes simplex virus type 1 (HSV-1) [179]. The results obtained with HSV-1 RR inhibitors encouraged further efforts in this direction. Screening of small molecules libraries brought to the identification of an inhibitor of the interaction between HSV-1 catalytic subunit (UL30) and accessory protein (UL42) leading to the inhibition of viral replication [180]. Other examples of successfully disrupted viral PPI include dimerization of HIV protease, reverse transcriptase, or integrase by peptides and small molecules [181-183], as well the Influenza A virus RNA polymerase subunits PB1-PB2 and PB1-PA interaction by small molecules [184, 185]. Notably, a high throughput screening approach recently identified AL18, a small molecule capable of interfering with the UL54-UL44 interaction, thus inhibiting HCMV replication in cells in the low micromolar range. This small molecule is able to inhibit in a dose dependent manner the of UL54-UL44 interaction, with an IC50 of 9-30 μM (as

assessed by ELISA or fluorescence polarization assays, respectively), and HCMV replication with a selectivity index above 100 (as defined by the ratio between the CC50 - compound concentration causing death in 50% of cells, and the ED50, compound concentration causing a reduction of 50% in viral replication) [186]. Clearly, disruption of protein-protein interaction holds promises for the development of anti-HCMV drugs.

1.14 Methods to detect protein-protein interaction (PPI)

The investigation of these PPIs requires different experimental techniques designed to characterize protein complexes and PPI network. There are two main approaches for the investigation: *in vitro* methods and *in* cells methods. *In vitro* methods comprise a broad range of techniques adopted for both interaction discovery and confirmation. These methods rely on the natural affinity of binding partners for each other (see Table 1.3).

In vitro method	*Description*
Co-immunoprecipitation	An immunoprecipitation (IP) experiment designed to affinity-purify a bait protein antigen together with its binding partner using a specific antibody against the bait.
Pull-down Assays	An affinity chromatography method that involves using a tagged or labelled bait to create a specific affinity matrix that will enable binding and purification of a prey protein from a lysate sample or other protein-containing mixture.
Crosslinking Reagents	Strategies involve chemical crosslinking which may or may not be reversed. Nearest neighbors (suspected to interact) *in vivo* or *in vitro* can be trapped in their complexes for further study.
Protein Interaction Mapping	Uses an "artificial protease" on a bait protein to initiate contact-dependent cleavages in the prey protein in the presence of specific reactants. contact sites or interface of a known protein-protein interaction.
Surface Plasmon Resonance	Relates binding information to small changes in refractive indices of laser light reflected from gold surfaces to which a bait protein has been attached.
Mass Spectroscopy	Used in concert with affinity-based methods (such as co-IPs) to isolate binding partners and complexes and to identify the component proteins using standard mass spectral methods.
Thermal Shift Assay (TSA)	Monitors protein thermal denaturation by using an extrinsic, environmentally sensitive probe, for which the fluorescence increases upon binding to the unfolded protein.

Table 1.2. *In cells* methods for PPIs analysis [Adapted from Thermo Scientific Pierce Protein Interaction Technical Handbook. Version 2, Thermo Scientific, 2010].

In cells methods, instead, are a more restricted number and can be found listed in the Table below.

In cells methods	*Description*
Yeast Two-Hybrid System	Monitor complex formation through transcriptional activation of reporter genes.
Crosslinking Reagents	Incorporating functional groups into proteins which can react, trapping a protein complex.
Immunofluorescence/FRET/BRET	Detect co-localized signal from two different proteins or monitor complex formation thought fluorescent/bioluminescent resonance energy transfer.
Proximity Ligation Assay	Two primary antibodies recognize the target antigens of interest. Secondary antibodies (PLA), each with a unique short DNA strand attached, bind to the primary antibodies. When the PLA probes are in close proximity, the DNA strands can interact forming DNA oligonucleotides. After their joining, oligonucleotides are amplified using a polymerase, and labelled complementary oligonucleotide probes highlight the product.
Biomolecular Fluorescence Complementation (BiFC)	Based on the association of fluorescent protein fragments that are attached to components of the same macromolecular complex.

Table 1.3: In cells methods for PPIs analysis [Adapted Thermo Scientific Pierce Protein Interaction Technical Handbook. Version 2, Thermo Scientific, 2010].

Each method has its own advantages and disadvantages. In vitro methods allow great sensitivity, but often rely on the use of non-physiological systems, such as bacterial cells, to produce proteins largely, so that their conformation might result different from what expected. Furthermore, *in vitro* methods, detect interactions occurring outside their physiological context, i.e. the cell. On the other hand, in cells methods, overcome these issues. The proteins of interest are directly expressed in their preferred cell type, and localization is readily detectable. However, such methods, are more limited, offer reduced flexibility, and are less sensitive as compared to *in vitro* ones.

1.14.1 Pulldown Assays

The pull-down assay is an *in vitro* method used to determine a physical interaction between two or more proteins. Pull-down assays are useful for confirming the existence of a protein–protein interaction predicted by other research techniques (e.g., co-immunoprecipitation) or to study che PPI inhibition by SMs. The affinity system consists of a glutathione S-transferase (GST)–, polyHis-

or streptavidin-tagged protein or binding domain that is captured by glutathione-, metal chelate (cobalt or nickel) – or biotin-coated agarose beads, respectively. The immobilized fusion-tagged protein acts as the "bait" to capture a putative binding partner (i.e., the "prey"). In a typical pull-down assay, the immobilized bait protein is incubated with a cell lysate, and after the prescribed washing steps, the complexes are selectively eluted using competitive analytes or low pH or reducing buffers for in-gel or western blot analysis.

1.14.2 Thermal Shift Assays (TSA)

Thermal Shift Assay is an *in vitro* technique which monitors protein thermal denaturation by using an extrinsic, environmentally sensitive probe, for which the fluorescence rises upon binding to the unfolded protein [187, 188]. As a protein is incrementally heated, it unfolds and display its hydrophobic core. Unfolded protein shows more nonpolar regions for protein-dye interaction, causing a rise in the fluorescence intensity (Figure 1.16). Fragments that bind to and stabilize or destabilize the protein will increase or lower the melting temperature (Tm), respectively. TSA allows to evaluate the effects of PPI inhibitor: whether small molecules that induced the disruption of constitutive oligomeric interfaces would produce thermal destabilization, corresponding to a loss of stabilizing subunit interactions.

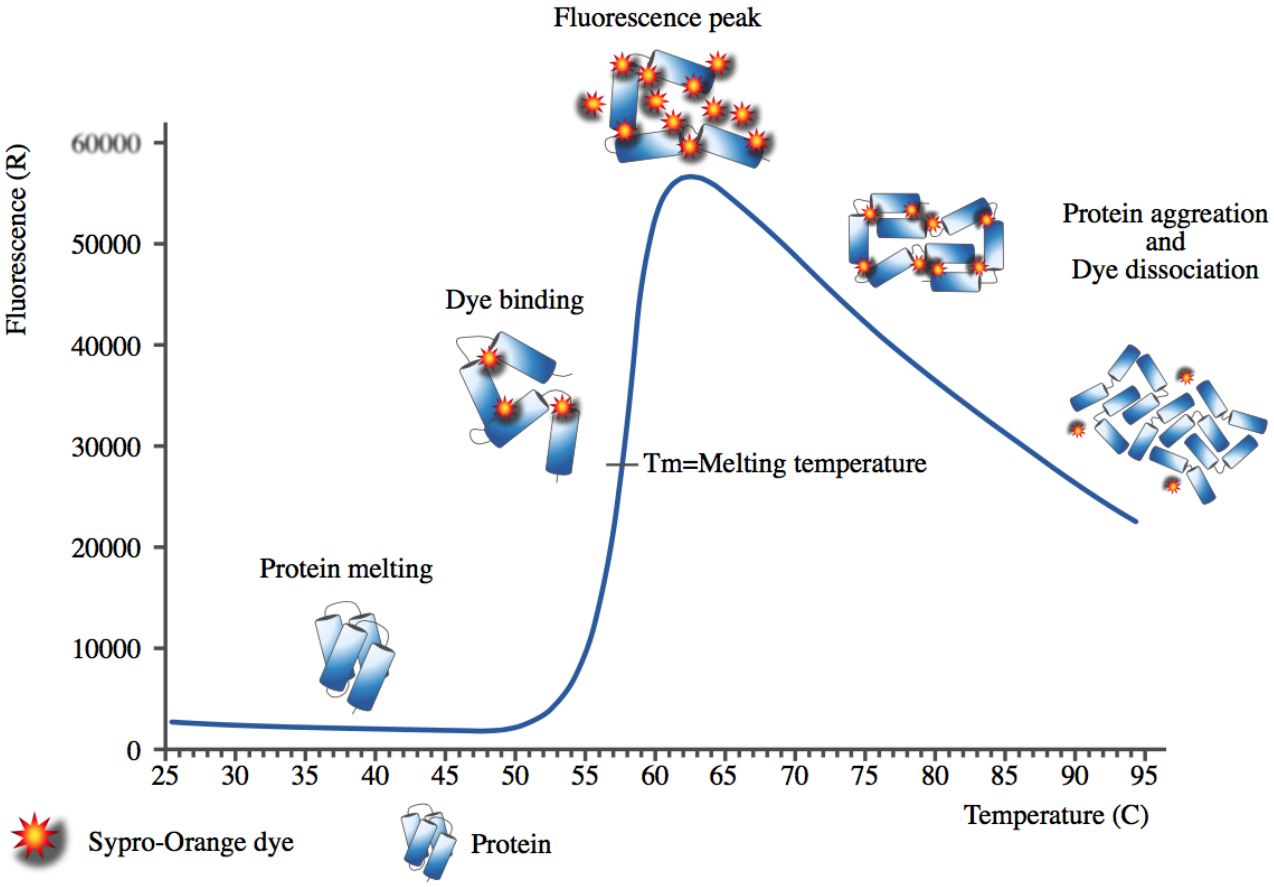

Figure 1.16. SYPRO Orange binds non-specifically to hydrophobic surfaces. When the protein unfolds, the exposed hydrophobic surfaces bind the dye, resulting in an increase in fluorescence. As the T decrease as decrease the fluorescence - we started focused (Argonne National Laboratory).

1.15 Previous Results – Homodimerization in vivo and screening SMs

Our group initially confirmed that UL44 dimerization occurs in a cellular context by Fluorescence and Bioluminescence Transfer (FRET and BRET, respectively). Further experiments suggested that the affinity of UL44 homodimerization in living cells is very similar to that of the UL54-UL44 interaction that can be disrupted by Small Molecules (SMs; DiAntonio et al., unpublished).

Based on these observations, we recently performed a structure-based virtual screening of commercially available databases, with the aim of identifying SM inhibitors of the HCMV UL44 homodimerization (DiAntonio et al., unpublished). The Glide software (Schrödinger, NY, USA) was employed to dock molecules to the interface of the two monomers. Three rounds of screening by docking were performed using the High throughput virtual screening (HTVS), Standard Precision (SP) and Extra Precision (XP) docking settings. After each docking round only the top-

ranked molecules in term of docking score were selected for the following round. The resulting 500 molecules were further reduced by visual inspection, cluster analysis and on the basis of their commercial availability, 18 compounds were purchased and tested for their ability to disrupt UL44 dimerization (see Figure 1.17).

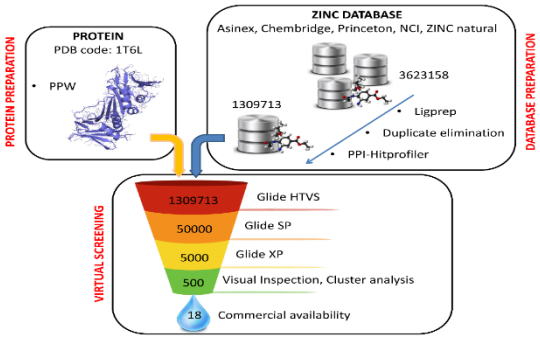

Figure 1.17. Use of Virtual screening to identify SMs potentially interfering with UL44 homodimerization. [DiAntonio et al., unpublished].

2. Aim

Antiviral agents currently used for the treatment of HCMV infection present several problems: induction of resistant viral strains, toxic side effects causing significant morbidity and mortality in immunocompromised individuals.

Furthermore, HCMV is the leading cause of congenital viral infection and there are no drugs available to prevent vertical transmission during pregnancy. These problems have stimulated the search for new compounds that are less toxic, more active and more specific against HCVM. That is why we propose to inhibit viral replication through the dissociation of UL44 homodimeric complex using compounds that bind to homodimerization interface.

This strategy has two possible advantages. The first one is represented by the fact that a protein-protein interaction – in this case, the dimerization of UL44 – is highly specific and therefore this paves the way for virus-specific inhibition. Secondly, whereas a single point mutation in the catalytic site of an enzyme is sufficient to give rise to drug resistance, the homodimerization of UL44 would be restored by two different mutations, thus reducing the possibility of drug resistance onset.

3. Materials and Methods

3.1 Preparation of Small Molecules (SMs) and Ganciclovir (GCV) stocks

Small Molecules (SMs) were purchased from Vitas-M. SMs were diluted in appropriate amounts of DMSO 100% to obtain 20 mM stocks, aliquoted and stored in foil-covered eppendorfs (20 µl/vials) at -20°C until required.

Ganciclovir (GCV; Selleckchem, S1878) was resuspended in DMSO 100% to generate a 50 mM stock. Additional 10 mM dilutions of original stocks were prepared in DMSO 100%. Aliquots were stored in foil-covered eppendorfs (20 µl/vials) at -20°C until required.

3.2 Protein Purification

Recombinant GST-UL44(1-290) fusion protein and GST were purified from Escherichia coli BL21(DE3)/pLysS harboring the respective plasmids pDEST15-UL44(1-290) and pDEST15, as described in [189]. Typically, 2 liters of cells was grown in 2YT (see Appendix § 8.1) medium containing 100 µg of ampicillin/ml. The cells were grown until the A_{600} was between 0.6 and 0.8 and then induced by the addition of 0.3 mM isopropyl-β-D-thiogalactopyranoside (ICN) for 40 h at 16°C. The pelleted cells were resuspended in 50 mM Tris-HCl (pH 7.5), 500 mM NaCl, 10 mM EDTA, 2 mM dithiothreitol (DTT), 20% glycerol, and complete protease inhibitors (Roche Molecular Biochemicals) and then stored at -80°C until needed. The cells were thawed and lysed by three passes through an Emulsiflex-C5 apparatus (Avestin). The lysate was centrifuged at 43,000 X g for 1 h, applied to a 5-ml glutathione-Sepharose 4 FastFlow column (Amersham Pharmacia Biotech) that had been equilibrated in buffer A (see Appendix § 8.1), and then washed extensively with buffer A. To remove E. coli DnaK protein [190], the column was equilibrated with buffer B (buffer A minus EDTA) and then washed with buffer B plus 10 mM ATP (Sigma). Finally, GST-

UL44ΔC290 was eluted with buffer A containing 15 mM glutathione. Purified proteins were stored in 20 mM Tris- HCl (pH 7.5), 150 mM NaCl, 30% glycerol, 0.1 mM EDTA, and 2 mM DTT.

3.3 GST-pulldown assays

Aliquots of SMs stocks as well as of recombinant 6His-UL44(1-290) and GST-UL44(1-290) fusion proteins (see sections §3.1 and §3.2, respectively), GST and the dimerization impaired point mutant 6His-UL44(1-290)-L86/L87A, were thawed on ice and briefly centrifugated at 4°C.

In the preliminary experiments, 0.03 nmol either GST or GST-UL44(1-290) were incubated with 0.12 nmol of 6His-UL44(1-290) and 6His-UL44-L86/87A for 2 hours at 4°C in Binding Buffer (see Appendix § 8.1.) with gentle shaking in order to allow the formation of the GST/His6-UL44, GST-UL44/His6-UL44 and GST-UL44/His6-UL44L86-87A complexes.

For test the SMs effects on the UL44 dimerization 0.03 nmol of GST-UL44(1-290) were incubated for 30 min at 4°C in Binding Buffer (see Appendix § 8.1) containing DMSO 0.25% (v/v), either in the presence or in the absence of different concentrations of SMs. Subsequently, 0.12 nmol of 6His-UL44(1-290) were added, and the mixtures further incubated for 1.30 hours at 4°C with gentle shaking in order to allow the formation of the GST-UL44(1-290)/His6-UL44(1-290) complexes. To this end, SM stocks were serially diluted in Binding Buffer and DMSO in order to obtain 100x aliquots containing different SM concentrations, in DMSO 25%. Such dilutions, or DMSO 25% as a control were then diluted 1:100 in Binding Buffer containing GST-UL44(1-290) (13 μM), before addition of His6-UL44(1-290) (40 μM), according to the volumes specified in Table 3.1.

Sample	GST-UL44 (1-290) x µM	His6-UL44 (1-290) x µM	SM in DMSO 25%	DMSO 25%	Binding Buffer
Negative control	2.3 µl	3 µl	/	1 µl	93.4 µl
Reaction	2.3 µl	3 µl	1 µl	/	93.4 µl

Table 3.1. Formation of GST-UL44(1-290) and His6-UL44(1-290) complexes

Towards the end of the incubation, 100 µl of Glutathione Sepharose 4 Fast Flow (GE Healthcare, GE17-5132-01) were packed onto Poly-Prep chromatography columns (Biorad, #731-1550). The resin was activated by addition of 500 µl of Binding Buffer for 3 times and not let to dry. Samples were subsequently loaded onto the columns for three times. At the end of the three binding steps the flowthrough fractions, containing the material that did not bind to the resin, were collected for subsequent analysis (Flowthrough, FT; see Figure 3.1). Columns then were washed with 400 µl of NETN buffer (see Appendix § 8.1) for 15 times. The last wash fractions were collected for subsequent analysis (Wash, W; see below). Bound complexes were eluted by addition of 100 µl of elution buffer [NETN buffer plus 19.5 mM Glutathione (SIGMA-ALDRICH, PHR1359), see Appendix § 8.1] for 4 times. Each elution was individually collected (E1, E2, E3, E4) and singly stored, or 30 µl of each elution were added together to obtain a representative mixture of the elutions. This mixture or each elution collected were analyzed by SDS-PAGE Western-Blotting as described in section 3.11§. A schematic representation of the procedure is shown in Figure 3.1

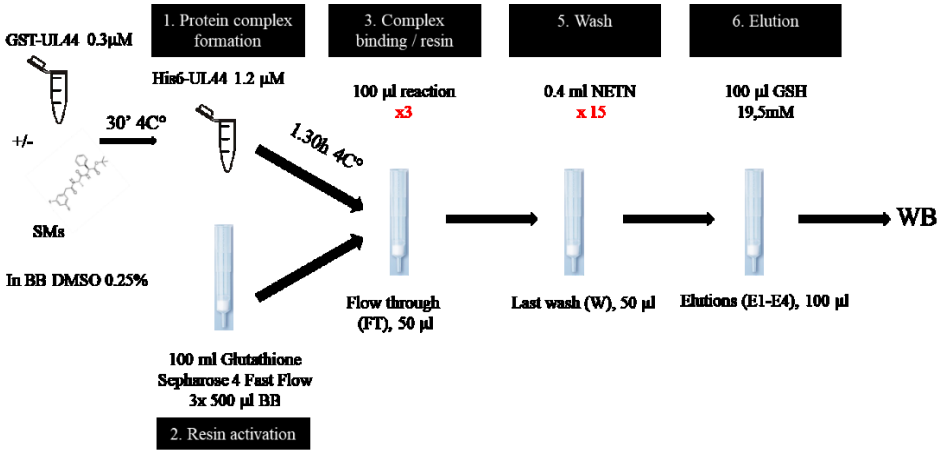

Figure 3.1 Schematic representation of the GST-pulldown approach used in this study.

3.3.1 GST-pulldown assays Image Analysis and evaluation criteria

Data obtained by Western Blot analysis were used to evaluate the effect of SMs inhibition on the GST-UL44/6His-UL44 interaction. Digital images were analyzed using Image J software. The total signal relative to each band was calculated by multiplying the band area per the average band signal after background subtraction. Signals were expressed as a percentage of those obtained in the presence of DMSO 0.25% (negative controls, always run at least in duplicate).

Only samples whose total band signal relative to the 6His-UL44 band differed by at least 2 standard deviation of the mean (S.D.) from the average percentage of signals relative to negative controls were considered different (++, --). Samples whose total band signal relative to the 6His-UL44 differed from the average percentage of negative controls in a range between 2 and 0.5 S.D. were considered slightly different (+,-), and finally samples whose total band signal relative to the 6His-UL44 differed less of 0.5 S.D. from the average percentage of negative controls were considered equal to the controls (=).

3.4 Viruses and Cells

Human cytomegalovirus (HCMV) strain AD169 was purchased from ATCC (VR-538). HCMV recombinant viruses TB4-IE2-EYFP and TB4-UL83-EYFP [191] were a generous gift from Micheal Winkler (Leibniz-Institut für Primatenforschung Goettingen, Germany).

Human foreskin fibrobalsts (HFFs) were a generous gift from Arianna Loregian, University of Padua [192]. The human diploid fibroblast cell line MRC5, were obtained from American Type Culture Collection (ATCC; CCL 171). All cells were grown in Dulbecco's Modified Eagle's Medium (DMEM), which was supplemented (cpt DMEM) with 10% Fetal Bovine Serum (FBS), non-essential aminoacids, L-glutamine (2 mM), Penicillin and Streptomycin (100U/mL) at 37 °C ad 5% CO_2 in a humidified incubator.

Cells were passaged when reached > 90% confluence. To this end, cells were briefly washed with Dulbecco's phosphate-buffered saline (D-PBS) and incubated with 0.05% trypsin-EDTA until they started detaching from the flask. Cells where then resuspended in an appropriate volume of cpt DMEM, and centrifuged for 5 minutes at 700 rpm to eliminate residual trypsin. Finally, cells were resuspended in cpt DMEM an appropriate volume of cells was transferred to a new flask containing required amount of cpt DMEM. For all experiments, MRC5 cells were used between passages 19 and 26, whereas HFFs were used between passages 4-20. All cell culture reagents were purchased from Gibco, Thermofisher Scientific. PBS, Trypsin and DMEM volumes varied according to the format of the flasks and plates used (See Table 3.2).

Flask format	DMEM	PBS 1X	Trypsin
T25	6 ml	2 ml	0.5 ml
T75	14 ml	5 ml	1 ml
T150	30 ml	8 ml	2 ml

Table 3.2: Volumes of DMEM, PBS and trypsin used for each flask format.

3.4.1 Cells Freezing

Cells grown in a T150 flask, at a 90% confluence cells were washed with PBS before being treated for few seconds with trypsin before being resuspended in cpt DMEM. Cells were gently resuspended in 12 ml of DMEM cpt. Subsequently 2 ml of cells were plated in a new T150 flask for subculturing, while the remaining 10 ml were centrifuged 5' at 700 rpm at 4°C. Supernatans were removed and pellets resuspended in ice 10.5 ml of ice cold 10% DMSO/FBS (v/v). 1.8 ml of cells were aliquoted in pre-chilled cryovials, and incubated 10' on ice, 2 hours at -20°C, and ON at -80°C before being transferred to liquid nitrogen for long term storage.

3.4.2 Cells thawing

Cryovials were quickly transferred from liquid nitrogen to cell culture hood. Cells were then gently resuspended in a small volume of cpt DMEM and transferred into a Falcon tube containing 7 ml of cpt DMEM. Tubes were centrifuged for 5' at 700 rpm, supernatants were discarded and the pellets were in 6 ml of cpt DMEM, before being seeded on a T25 flask. Cells were subsequently incubated at 37°C, 5% CO2 and 95% of humidity. The following day cells were observed by optical microscope for their conditions, and medium was replaced with fresh cpt DMEM.

3.4.3 Preparation of viral stocks

One day before infection, $3x10^6$ MRC5 cells were seeded in a T150 flask. Viral stocks were thawed at 37°C and diluted in 10 ml of DMEM. Cells were infected at low multiplicity of infection (MOI; 0.002-0.01) to allow ample time for the spread of propagating virus. Flasks were gently shaken every 15 minutes at 37°C during the infection to allow even distribution of the virus on the cell monolayer. The inoculation media was removed after 2 hours post-infection (p.i) and replaced with 30 ml of cpt DMEM. Every day p.i cells were observed and refed every 3 days with 30 ml of cpt DMEM. When the monolayers displayed approximately 80% cytopathic effect (CPE), cells were refed with 20 ml of cpt DMEM in preparation for the harvest. After 3-4 days supernatans were collected from the flasks and the cells were refed with 20 ml of cpt DMEM. When possible another harvest was made 2-3 days after.

Supernatants were cleared from cell debris by centrifugation at 1500 rpm for 5 min at 4°C. As a cryopreservative, a mixture of DMEM/DMSO 10% was added dropwise while gently swirling the tube to the supernatants at 1:10 ratio, in order to reach a final 1% DMSO concentration. Viral aliquots were subsequently stored at -80°C until required.

3.4.4 Titration of Viral Stocks

The day before beginning the titration process, $1.5x10^4$ MRC5 cells/well were seeded into clear flat bottom 96 wells tissue culture plates with low evaporation lids (Falcon, #353072). The day after, an aliquot of frozen virus stock was quickly thawed and was serially diluted in DMEM, and 100 µl or each dilution were added to each well in triplicate. Infection were carried out for 1 hour at 37°C and 5% CO_2 in a humidified incubator, and cells were subsequently refeed with 200 µl of fresh media. One day later, cells were washed three times with 200 µl of PBS/well. After the final wash the monolayer was fixed with 96% ethanol for 15 min at room temperature (RT; 200 µl/well). Subsequently, the ethanol was removed, the plate was washed twice with PBS (200 µl/well) and finally aspecific binding sites were blocked by incubating the cells with 50 µl/well of PBS-FBS 5% either for 1 hour at 37°C or overnight at 4°C. Subsequently, cells were incubated with 50 µl/well of the primary monoclonal anti-CMV IE1&2 antibody (P1215 – Virusys Corporation) 1:100 (10 µg/ml, in PBS-FBS 5%) for 1 hour at 37°C. Following this incubation, the wells were washed four times with PBS (200 µl/well). Cells were then incubated with 50 µl/well of appropriate secondary antibodies [Alexa Fluor 555 Goat Anti-mouse IgG (A21424-Life Technologies), or Alexa Fluor 488 Goat Anti-mouse IgG (A11001)] 1:1000 (2 µg/ml) for 1 hour at 37°C. The secondary antibody was removed by washing four times with 200 µl of PBS.

Occasionally, for recombinant HCMV viruses TB4-IE2-EYFP and TB4-UL83-EYFP encoding for spontaneously fluorescent viral proteins, the immunostaining procedure was avoided, and infected plates analyzed either 24 (TB4-IE2-EYFP) or 48-72 (TB4-UL83-EYFP) hours p.i. Infected cells were counted using an inverted fluorescence microscope (Leica, DFC420 C) equipped with a 20x

objective and appropriate fluorescence filters. Each plate was initially scanned to identify wells containing a number between 50 and 100 positive cells. The titer of the sample was calculated using the following formula:

$$\textbf{infectious units/ml} = \frac{number\ of\ positive\ cells\ x\ 10}{dilution\ of\ inoculum}$$

3.5 Plaque reduction assays

HFF cells were seeded at 2 × 10^5 cells per well in 24-well plates. The following day, cells were infected with HCMV (strain AD169) at 80 PFU per well in DMEM containing 5% FBS at 37°C. Two hours p.i the inocula were removed and cells were washed twice with 1 ml of PBS. Subsequently, media containing 5% FBS, 0.6% methylcellulose and various concentrations of SMs was added. All drug concentrations were tested at least in duplicate. GCV was used as a positive control for viral replication inhibition. After incubation at 37°C for 10–11 days, cell monolayers were stained with crystal violet and plaques were counted. The final concentration of compound-derived DMSO was maintained at 0.1% or 0.5% (v/v) in all samples.

3.6 Fluorescent reduction assays

3.6.1 Cell seeding and infection.

To set up the Fluorescent Reduction Assays enabling rapid quantification of the inhibition of SMs and to evaluate the DMSO effects on viral replication, initial experiments were performed to establish the proper assay conditions in terms of plate format, infection time, MOI and DMSO concentration. To this end, either 1,5 x10^4 or 7,5x10^4 MRC5 cells were seeded in 96 well special optics black microplates (Corning, CLS3614) or in clear flat bottom 24 wells tissue culture plates with low evaporation lids (Falcon, #353047), respectively. One day later, cells were infected at different MOIs of either TB4-UL83-EYFP or TB4-IE2-EYFP in DMEM for 1 hour at 37 °C and treated with 2 different DMSO concentrations. Every day p.i plates were observed under an optical

microscope to evaluate cells confluence and CPE, and the fluorescence signals were visualized on an inverted fluorescent microscope (Leica, DFC420 C). At different time points, cells were processed for fluorometric measurement using a plate Fluorimeter (Victor X2, Perkin Elmer). Plates were processed as described in section § 3.6.4, and data analyzed as described in § 3.6.5

3.6.2 Small scale screening for the identification of SMs interfering with HCMV replication.

For identification of SMs active on HCMV replication, 1.5 x 10^4 MRC5 cells were seeded in 96 well special optics black microplates (Corning, CLS3614) and incubated ON at 37°C, 5% CO_2 and 95% humidity. The day after cells were infected for 1 hour at 37 °C in 100 µl/well of DMEM containing a MOI of 0.3 - 0.03 with TB4-UL83-EYFP. Subsequently, cells were washed, and media containing either DMSO 0.5% or two different concentrations (100 e 10 µM) of each SMs with a 0.5% DMSO final concentration were added. GCV (50 µM) was included as positive control of viral replication inhibition. All drugs were tested at least in duplicate. Mock infected cells served as a reference for calculation of background fluorescence After addition of SMs the plates were incubated again at 37°C, 5% CO2 and 95% humidity. Every day plates were observed under optical microscope to evaluate cells confluence and morphology as well as CPE and the presence of precipitates. Fluorescence signals were visualized on an inverted fluorescent microscope (Leica, DFC420 C). Plates were processed as described in section § 3.6.4, and data analyzed as described in § 3.6.5. Each experiment was performed three times, and each plate comprised at least two wells treated under the same condition. The layouts of the plates are reported in the Appendix (see Appendix § Table 8.2.1).

3.6.3 Dose-response fluorescent reduction assays.

MRC5 cells (1,5 x 10^4) were seeded in 96 well special optical plate (Corning, 3614). The day after cells were infected in 100 µl/well of DMEM containing TB4-UL83-EYFP with MOI 0.03-0.3 at 37 °C. One hour p.i, cells were washed and media containing either DMSO 0.5% or various concentrations of each SMs with 0.5% DMSO final concentration was added. GCV was included as

reference compound. All drug concentrations were tested at least in duplicate. Mock infected cells served as a reference for calculation of background fluorescence. Every day plates were observed under optical microscope to evaluate cells confluence and CPE, and the fluorescence signals were visualized on inverted fluorescent microscope (Leica, DFC420 C). After 7 days cells were lysed and processed as described in § 3.6.4 and § 3.6.5. Each experiment was performed five times.

3.6.4 Fluorimetric quantification of viral replication.

Cells grown in 96 well plates (Corning, CLS3614) were washed once with PBS (200 µl/well) and lysed in luciferase lysis buffer (100 µl/well) (see Appendix § 8.1). Plates were immediately frozen at -20°C until directly analyzed. Cells grown in 24 well plates were washed once with PBS (1ml/well) and lysed in 290 µl/well of luciferase lysis buffer (see Appendix § 8.1). Plates were immediately frozen at -20°C until analyzed. After thawing, 100 µl /well of cells grown in 24 well plates were transferred to 96 well flat bottom black plates (Costar #3916) in duplicate.

Fluorescent signals were acquired using a fluorimetric plate reader (VICTOR X2 Multilabel Plate Reader, Perkin), using a fluorimetric excitation filter (band pass 485 ± 14 nm) and a fluorimetric emission filter (band pass 535 ± 25 nm). Instruments settings are reported in the Table § 8.2.2 (see Appendix).

3.6.5 Fluorimetric data analysis.

Data were exported to excel and analyzed to calculate the mean fluorescence relative to each condition. To this end the average signal relative to the mock infected samples was subtracted to the signal relative to every well. When comparing the effect of drug treatments on HCMV replication, values relative to each condition were also expressed as a percentage of the untreated infected corresponding control. For calculation of 50% effective dose (ED50), defined as the concentration of compound required to decrease viral replication, data were exported to Graphpad Prism, *x* data transformed to logarithmic and fitted to a linear regression or 4 Parameter Logistic Equation (Sigmoidal).

3.7 Analysis of HCMV gene expression by Western blot assays

MRC5 cells were seeded on 6 well flat bottom plates with low evaporation lid (Falcon, 353046) according to the conditions reported in Table 3.3. The following day, cells were infected with HCMV (strain AD169) at MOI 0.1 in DMEM at 37°C. One hour p.i SMs were added at concentration at subtoxic concentration (B1 100 μM, B3 20 μM, B6 5 μM, C6 40 μM, GCV 5 μM). After two washes with PBS, cells were lysed in ice with 250 μl of RIPA Buffer containing protease inhibitors (see Appendix § 8.1) to prevent protein degradation. Cell lysates were frozen and the protein content was quantified using Micro BCA Protein Kit assay (Thermo Scientific). The presence of specific proteins was detected by SDS-Page Western Blotting at the different time points as reported in Table 3.4.

Lysis p.i (hours)	Cell number for 6 well plate
8	/
12	60 x 10^4
24	60 x 10^4
47	37.5 x 10^4
72	37.5 x 10^4
96	37.5 x 10^4

Table 3.3: number of MRC5 cells seeded for processing by Western blotting at the indicated time points p.i.

Viral genes		Hours pi
IE	IE1&2	12
E	UL44	24 - 48 – 72 - 96
	Pp65	48 – 72 - 96
Late	Pp28	72 - 96

Table 3.4: evaluation of genes expression at different time points.

3.8 Western-blot assays

Relevant fractions derived from GST-pulldown assay, or 30 µg of infected cell lysates were diluted in Laemni loading buffer (1x final concentration) and boiled 5 minutes at 95°C. Samples were loaded on 8.5% or 8% bis-tris polyacrylamide gels, respectively, before being electrophoretically separated using a Biorad vertical gel system apparatus for 2 hours at 100 V in Running Buffer (See Appendix § 8.1). Separated proteins were blotted on polyvinylidene fluoride (PVDF) membranes (GE Healthcare Life Sciences, RPN303F), for 1 hour in Transfer Buffer (See Appendix § 8.1) at 350 mV. Membranes were saturated for 1 hour with PBS containing 0.2% tween and 5% milk (w/v), and incubated over night at 4°C with the appropriate primary antibodies diluted in PBS containing 0.2% tween and 5% milk (w/v). The day after, membranes were washed 3 times with PBS containing 0.2% tween (w/v) for 3 minutes and washed 3 times with PBS containing tween 0.1%. Then the membranes were incubated 1 hour with the appropriate secondary antibodies diluted in PBS containing 0.2% tween and 5% milk (w/v). After the incubation, membranes were washed 3 times with PBS 0.2% tween (w/v) for 10 minutes and 3 times with PBS for 5 minutes.

For analysis of GST-pulldown assays, fusion proteins of interest were visualized by enhanced chemiluminescence (LiteAblot Extend Long Lasting Chemiluminescent Substrate Kit, Euroclone) and signal acquired using an imaging system (Versadoc, Biorad). Digital images were analyzed with Image J (NIH). For analysis of cell lysates, membranes were incubated for 5 minutes either with a commercial (ECL Prime Western Blotting Detection Reagent, RPN2236, GE Healthcare) or with an homemade ECL substrate (see Appendix § 8.1). Membranes were incubated for different times with an autoradiography film (Carestream Kodak Biomax Light Film, Sigma Aldrich, Z370371-50EA) inside an autoradiography film cassette in the dark before being developed with a film developer (Hyper Processor, GE Healthcare Amersham). Digital images were acquired with an imaging station (Gel Doc EZ System) and processed using Image J (NIH).

The antibodies, diluted in PBS containing 0.2% tween and 5% milk (w/v), were used:

- Anti-6His tag mAb, Mouse, 1:2500 (Sigma, H-1029)
- GST Antibody [HRP-conjugated], mAb, Mouse 1:1000 (Genscript, A00866)
- Anti-IE1&2 of Citomegalovirus mAb, 1:10000 (Virusys Corporation, CA003-1)
- AntiICP36 of Citomegalovirus mAb, 1:100 (Virusys Corporation, P1202-1)
- Anti-CMVpp65 mAb, 1:2000 (Virusys Corporation, P1251)
- Anti-Cytomegalovirus mAb, pp28 1:10000 (abcam, ab6502)
- Anti-GADPH Rabbit, 1:5000 (Santa Cruz Biotech, sc-25778)
- Goat Anti-mouse immunoglobulin Ab conjugated to horseradish peroxidase (sc-2055, Santa Cruz Biotech) 1:2000, for acquisition with Versadoc
- Goat Anti-mouse immunoglobulin Ab conjugated to horseradish peroxidase (Santa Cruz Biotech, sc-2055) 1:20000 to 1:2000 for acquisition by autoradiography
- Goat Anti-RABBIT immunoglobulin Ab conjugated to horseradish peroxidase (Sigma Aldrich, A 6154) 1:20000 for acquisition by autoradiography

3.9 Cytotoxicity assays

Cells were seeded clear flat bottom 96 wells tissue culture plates with low evaporation lids (Falcon, #353072) in duplicate in a final volume of 200 µl/well. Twenty-four hours later cells were treated with different concentrations of drugs and SMs, or solvent only, in a final volume of 100 µl. A number of wells containing only cpt DMEM and no cells were also included for background correction. At the desired time point post treatment, cells were processed for measurement of cell metabolic activity using 3-(4,5-Dimethyl-2-thiazolyl)-2,5-diphenyl-2H-tetrazoliumbromid (MTT; Applichem, A2231,0001). To this end, 10 µl of MTT (5 mg/ml, in PBS; see Appendix § 8.1) were added to each well, and cells place back at 37°C 5% CO_2. Two hours later, cells were lysed by gently pipetting in 100 µl of Lysis Buffer (SDS 10%, HCl 0,01M in MQ H_20). Plates were further incubated ON at 37°C. The day after absorbance was determined with a spectrophotometer plate reader at 620 nm (Sunrise, Tecan). Data were exported to excel and background signal relative to the average of cpt DMEM only containing wells were subtracted from each well. For calculation of 50% cytotoxic concentration (CC50), defined as the concentration of compound required to

decrease cell viability by 50%, data were exported to Graphpad Prism, *x* data transformed to logarithmic and fitted to a linear regression or to a 4 Parameter Logisitic Equation (Sigmoidal).

The ideal experimental conditions relative to HFF were established previously, whereas for MRC5 cells they have been empirically determined in set up assays (see Table 3.5).

Lysis post treatment (hours)	MRC5	HFF
24	1 x 10^4	/
72	0.4 x 10^4	/
120	/	10^3
140	0.1 x 10^4	/
168	1.5 x 10^4	/

Table 3.5: cell number seeded MTT assays at the indicated time points post treatment.

3.10 Thermal Shift Assays (TSA)

Thermal Shift Assays (TSA) were performed on three different platforms: an ABI PRISM 7000 Sequence Detection Systems, a LightCycler 480 Real-Time PCR System (Roche), and a ViiA 7 Real-Time PCR System.

3.10.1 TSA on ABI PRISM 7000 Sequence Detection Systems

Lysozyme (1.25-350 μM final concentration) and Sypro orange (0.5-10x final concentration) were diluted either in Potassium Phosphate or in Citrate Phosphate buffers (see Appendix § 8.1), and 25 μl of such mixtures were loaded on 96-well white plates (Microamp Optical 96-well Reaction Plate with Barcode, 4306737, Applied Biosystems), in duplicate.

Alternatively, lysozyme, 6His-UL44 (1.25-20 μM final concentration), UL44L86 /87A dimerization impaired mutant (5 μM final concentration) and Sypro orange were diluted in Dilution Buffer (see Appendix § 8.1) and each different 5x TSA buffers (see Figure 3.2) were added. Twenty μl of such

mixture were loaded on the plates. Subsequently SMs (5mM) were added to each well to obtain a final concentration of 1 mM.

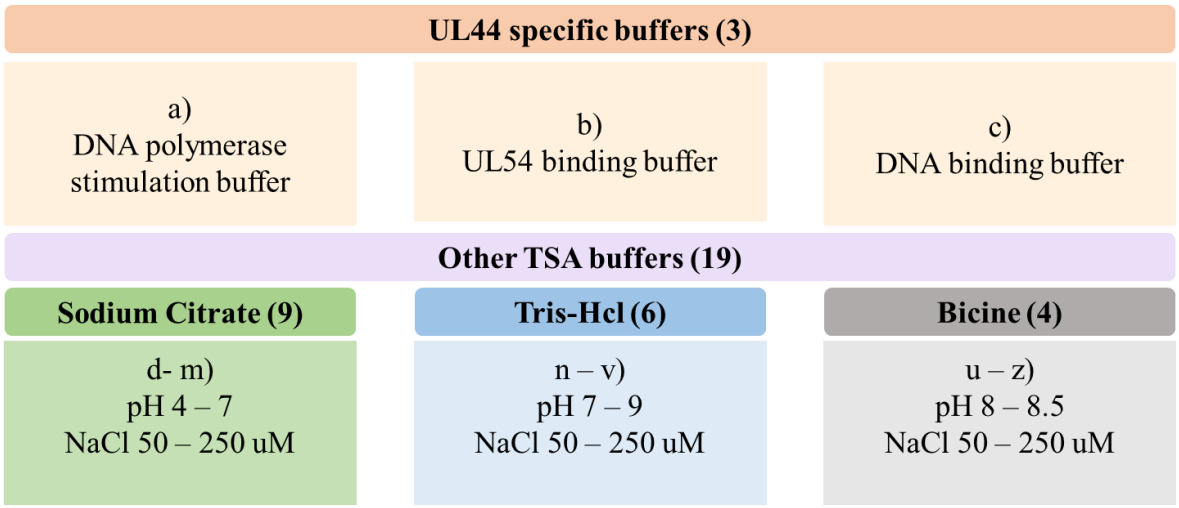

Figure 3.2 Schematic representation of the 22 TSA Buffers used in this study.

Plates were sealed with film (MicroAmp Optical Adhesive film, 4311971, Applied Biosystems) and centrifuged for 1 minute at 700 rpm. Plates were heated from 22-95 °C at approximately 1°C/ min. Fluorescence data were acquired with ROX and SYBR emission filers. Instrument was set up as described in [193] and reported in the Appendix § 8.3.1.

3.10.2 TSA on a LightCycler 480 Real-Time PCR System

Fifteen µl of mixtures prepared as described above, were loaded on 480 Multiwell Plate 384, white (Roche, 04729749001) in duplicate. The plate was sealed with film (MicroAmp Optical Adhesive film, 4311971, Applied Biosystems) and centrifuged for 1 minute at 700 rpm. The plate was heated from 20 to 85 °C in Melting mode with an acquisition mode of continuous and 10 acquisitions per degree C. Samples were excited at 460 nm and fluorescence detected at 560 nm. Instrument was set up as reported in the Appendix § 8.3.2.

3.10.3 TSA on a ViiA 7 Real-Time PCR System

Lysozime and 6His-UL44 (5 μM final concentrations) and Sypro orange (10x final concentration) were diluted in Dilution Buffer (see Appendix § 8.1) and Buffer I 5x (see Appendix § 8.1) was added. Twenty μl of such mixture or only Buffer I 5x were loaded on MicroAmp™ Fast Optical 96-Well Reaction Plate (ThermoFischer Scientific, 4346907). Subsequently 4 SMs (B1, B3, B6, and C6) were added to each well to obtain various final concentrations (25, 50, 100 and 200 μM). The plate was sealed with film (MicroAmp Optical Adhesive film, 4311971, Applied Biosystems) and centrifuged for 1 minute at 700 rpm. The plate was heated from 25 °C ramping up in increments of 1 °C to a final temperature of 95 °C. Multiple wavelengths were selected for samples excitation (470, 520 and 580 nm) and fluorescence detection (520, 586, 623 and 682 nm). Instrument was set up as reported in the Appendix § 8.3.3.

3.10.4 TSA data analysis

Data from TSA experiments were exported to Excel and analyzed to quantify the following parameters: Maximum Fluorescence, Maximum/Baseline fluorescence, dF/dT and T of Melting (Tm). Tm were calculated using software GraphPad Prism (Graphpad Software Inc.) as described in [194]. Briefly, fluorescent values relative to each temperature were imported. Post-peak fluorescence values were deleted, and Tm were calculated using the Boltzman Sigmoidal Fit Function.

4. Results

4.1 Study of UL44 dimerization by GST-pull down

We aimed at developing an *in vitro* assay suitable to monitor UL44 dimerization and its disruption by SMs. Among the several available methods to study protein-proteins interactions (PPi) *in vitro*, we chose the GST-pulldown assay, a popular method used to determine the physical interaction between two or more proteins. To evaluate if this assay is suitable to study UL44 dimerization, we performed GST-pulldown assays with the recombinant proteins 6His-UL44(1-290) and GST-UL44(1-290). The assay was performed also for 6His-UL44(1-290) with GST as negative control and for GST-UL44(1-290) with the dimerization impaired point mutant 6His-UL44(1-290)-L86/L87A to assess the sensitivity of the system to the impairment of ULL-44 dimerization [185]. Importantly, we could detect a band of the expected molecular weight corresponding to 6His-UL44(1-290) relative to the GST-UL44(1-290)/6His-UL44(1-290) complex, but not relative to the GST/6His-UL44(1-290) complex, indicative of the specificity of the assay. Intriguingly, the 6His-UL44(1-290)-L86/L87A band, relative to the GST-UL44(1-290)/6His-UL44(1-290)L86/L87A complex was much less intense as compared to the 6His-UL44 band, indicating that the assay can highlight differences in UL44 dimerization (Figure 4.1).

These results suggest that GST-pulldown is suitable to monitor UL44 dimerization in vitro and test its perturbation caused by SMs.

4.2 A small scale screening to evaluate the ability of SMs to inhibit UL44 dimerization in GST-pulldown assays

We subsequently decided to test the effect of the 18 SMs identified as potentially able to disrupt UL44 dimerization (§ 1.15), on the ability of 6His-UL44(1-290) to interact with GST-UL44(1-290) by GST-pull down assays. Therefore we performed GST-pulldown assays between GST-UL44(1-

290) and 6HisUL44(1-290) in the presence or in the absence of the 18 selected SMs (50 μM) and analysed the extent of GST- and 6His-UL44(1-290) eluted, by means of SDS/PAGE Western blotting (Figure 4.2, Figure Appendix A1-4). After two repetitions of such assays, digital images were analyzed using Image J software (§3.3.1). We could identify 3 SMs (B5, B7 and C4) which reproducibly decreased the amount of 6His-UL44(1-290) eluted. In fact, in both repetitions after incubation with B7 and B5 the total band signal relative to the 6His-UL44 band differed by at least 2 standard deviation of the mean (S.D.) from the average percentage of signals relative to negative controls (--). Regarding C4 the 6His-UL44 band differed from the average percentage of negative controls in a range between 2 and 0.5 S.D. (-) and at 2 S.D (--) in the two different experiments respectively (Figure 4.3).

For such SMs, the GST-pulldown assay was repeated two additional times, and two SMs (A2 and C2) which did not cause a decrease the amount of 6His-UL44(1-290) eluted, were also included as negative controls (Figure 4.4A). Quantitative analysis of the eluted fractions revealed that none of the SMs tested affected the extent of GST-UL44(1-290) eluted, whereas the inhibitory effect of the elution of 6His-UL44(1-290) relative to C4 and B5 could be confirmed (Figure 4.4B). Surprisingly, in such experiments also A2 and C2 also reduced the elution of 6His-UL44(1-290).

4.3 Study of dose-response effects by GST-pulldown assays

Prompted by these results, we selected such SMs to investigate a possible dose-response relationship between the inhibition of 6His-UL44 (1-290) elution and the concentration of SM used. To this end, protein complexes were incubated with the selected SMs at 50, 12.5 and 3 μM, or in DMSO 0.25%, before being processed by GST-pulldown/SDS-page/Western blotting as above (Figure 4.5A). Surprisingly, data analysis revealed a high variability, and most-importantly lack of correlation between the inhibition of the 6His-UL44 eluted band and the concentration of SMs used in the assays (Figure 4.5B).

4.4 Validation of GST-pulldown hits for HCMV replication inhibition by Plaque Reduction Assays

We decided to investigate if the SMs capable of inhibiting UL44 self-interaction identified from the small-scale GST-pulldown based screening could affect HCMV replication. To this end, we performed plaque reduction assays (PRAs) using HCMV laboratory strain AD169 in the presence and in the absence of the identified SMs or of GCV as a positive control for viral replication inhibition. As expected, GCV exhibited a 50% effective dose (ED50) of 2.5 μM [195]. None of the 5 tested SMs inhibited plaque formation by HCMV AD169, with a ED50 values lower than 100 μM (see Figure 4.6A).

In parallel, we determined the 50% cytotoxic concentration (CC50) relative to each molecule. To this end, HFF cells were seeded on 96 well plates, treated with the desired compounds, and cell metabolic activity was evaluated 120 h post treatment by means of MTT assays.

As expected, GCV exhibited a CC50 value of around 1000 μM. Among the tested compounds, B5 and C4 SMs exhibited significant cytotoxicity in this assay with a CC50 around 6 and 24 μM respectively, while the remaining molecules were less toxic with CC50 values between 125 and 287 μM Figure 4.6B). Overall, our GST-pulldown based approach to identify SMs able to interfere with HCMV replication by interfering with UL44 dimerization did not prove successful, leading to the identification of SMs unable to inhibit viral replication with high potency.

4.5 Assessment of selected SMs cytotoxicity

Initially the toxicity and solubility of our compounds were analyzed on MRC5 cells. Solubility was visually evaluated using an inverted microscope by analyzing cells for the presence of precipitates, whereas cells viability was estimated both using an inverted microscope and through a MTT colorimetric assay (PanReac Applichem).

An initial experiment was performed to establish the proper assay conditions for MTT assays using MRC5 cells. Variables included number of cells seeded, as well as time of cell growth and of incubation with the chromogenic substrate (Fig. 4.7A). To this end, a different amount of MRC5 cells was seeded in 96 well-plates. The following day DMEM/DMSO 1% was added to the cells and the plates processed for MTT assays (§3.9). At the desired time point post treatment chromogenic substrate was incubated with cells for different periods of time in order to identify the optimal assay conditions. Data were acquired and the absorbance at 620 nm relative to each condition was plotted against the seeded cell number, and a linear regression calculated. Our results showed that increasing the incubation with the chromogenic substrate (1, 2 or 4h) increased the intensity of the signal. However, the signal to noise ratio appeared optimal already after incubation for 2h (Fig. 4.7B). We were furthermore able to identify the optimal cell number to be seeded at specific time points, to warrant linearity between cell number and absorbance. Indeed when we performed a linear regression between cell seeded and absorbance we found very good correlation ($R > 0.98$) when the maximum number of seeded cells considered was $1x10^4$, $4x10^3$ and $1x10^3$cells/well for analysis at 24, 72 and 140 hours post treatment, respectively, with a 2 hours incubation time with the chromogenic substrate (Figure 4.7C).

Subsequently, the optimal cells number was seeded in 96 well-plates and the day after SMs were added at different concentrations (range 1.56 – 100 μM) in DMSO 1%. At 24, 72 and 140 h post treatment, cells were observed using an inverted microscope and each well was scored for the presence of precipitates -indicative of poor solubility- and to evaluate cell morphology/viability. Plates were then processed for MTT assays, and data analyzed to calculate cell culture 50 (CC50) values (§3.9). Our results indicate that 3 SMs exhibited poor solubility, and formed precipitates in the low micromolar range (12.5 – 25 μM), while 13 of them caused toxicity to some degree, resulting in alteration morphology alterations (3.1 – 100 μM). It was also evident that 1 SM interfered with absorbance at 620 nm, resulting in very high absorbance values despite noticeable

cell death observed by inverted microscope (Table 4.1). CC50 values calculated varied from 7.4 to more than 100 μM, depending on the SM and the condition tested, indicating a high degree of variability among the different SMs. (Table 4.1 and Figure Appendix C1-8).

4.6 Use of YFP reporter recombinant HCMVs for antiviral screening

Our results highlighted the issues related to the identification of SMs interfering with UL44 dimerization, due to the lack of a quick and robust assay to assess their functionality. In order to develop a high throughput test to study the effect of SMs on HCMV replication, and to develop alternative assay to the above described, time consuming PRA, two recombinant HCMV viruses were obtained from Micheal Winkler (Leibniz-Institut für Primatenforschung Goettingen, Germany). In particular, TB4-IE2-EYFP and TB4-UL83-EYFP, recombinant HCMV viruses carrying the enhanced yellow fluorescent protein (EYFP) fused with the viral proteins IE-2, and ppUL83 (pp65) respectively (Figure 4.8). Such viruses allow to directly visualize infection kinetics using an inverted epifluorescent microscope, offer the possibility to quantify viral replication by fluorimetric measurements using a plate reader, and they have already successfully used for the identification of anti-HCMV active compounds [191].

4.7 Kinetics of Intracellular Localization of Recombinant Viruses

We started to produce viral stocks of recombinant viruses TB4-UL83-YFP and TB4-IE2-YFP in MRC5 cells (§3.4.3). Viral stocks were used to infect MRC5 cells and investigate the subcellular localization of the fusion proteins at different time points p.i using an inverted epifluorescent microscope. For TB4-IE2-EYFP a nuclear localization was observed at all time points (Figure 4.9). IE2-EYFP showed a diffuse nuclear staining at 18 h p.i, and at later time points accumulated to replication compartments, which continued to enlarge as the infection progressed, resulting in very bright IE2-YFP foci (Figure 4.9). On the other hand, TB4-UL83 EYFP was very faintly detectable

in the nucleus of infected cells starting from 18 h p.i, but strongly accumulated in the cytoplasm where viral assembly takes place at later time points (Figure 4.9).

4.8 Setup of Fluorescent Reduction Assays (FRAs) to monitor HCMV replication

With the ultimate goal of using such viruses for testing the effect on HCMV replication of the 18 previously identified SMs, we performed preliminary experiments to determine the optimal conditions for Fluorescence Reduction Assays (FRAs). Therefore, as reported in the Materials and Methods section §3.6.1, cells were seeded either in 96 well-plate imaging or in 24 well-plates, infected at different MOIs (0.062-4) and monitored daily for the presence of cytopathic effect (CPE) as well as of specific spontaneous fluorescent signals relative to the expression of YFP fusion proteins. Cells were finally lysed at different time points before being processed for the quantification of viral replication using a plate fluorimeter (4, 7 and 10 days p.i) (Figure 4.10A).

As expected, our microscopic analysis revealed that already from day 1 p.i infected cells exhibited CPE, and fluorescent signals relative to the specific fusion proteins were detectable in cells infected with both viruses, proportionally to the MOI used, regardless of the format used (24 or 96 well plates). Additionally, while IE2-EYFP were was readily detectable using a fluorescent microscope from d1 p.i in infected cell nuclei, UL83-EYFP signal was very faint at the same time pi (Figure 4.10B, *left panels*). At day 2 p.i., IE2-YFP signal slightly increased, whereas a few UL83-YFP positive cells started to be clearly detectable. Fluorescent signals for both viruses appeared sensibly higher at day 7 p.i. In particular, the UL83-EYFP relative signal appear very particularly strong, consistently with pp65 being the most abundant HCMV structural protein (Fig. 4.10B). As the infection progressed, The UL83-EYFP subcellular localization was predominantly nuclear, indicative the beginning of a new viral life cycle (Figure 4.11B). At high MOIs of infection (MOI =1), fluorescent signals relative to each virus appeared very similar to those observed at 7 days p.i (Figure 4.11B, *right panels*). Furthermore, at even higher MOIs of infection (MOI = 4), viral

replication resulted in cell death making difficult to evaluate the extent of viral replication (not shown).

Our fluorometric analysis showed that the 24 well plate format is not ideal for such kind of studies, in that resulted in very high well to well variations (Figure 4.10C, and Figures Appendix D1-2). Additionally, infection of cells with high MOIs did not prove useful for the study of viral replication. In fact, infection with MOIs of 4, resulted in a stable YFP signal over time, which did not appear to increase with viral infection progression (Figure 4.10C, *top panels* and Figure Appendix D1-2), furthermore at every time p.i. considered the difference between fluorescent signals acquired relative to cells infected with a MOI of 4 or 1 appeared very similar (Figure 4.10C, *bottom panels*). On the other hand, lower MOIs of infection (0.25 and 0.06) were associated with a linear increase of the YFP signal over time (Figure 4.10C, *top* panels, and Figure Appendix D1-2) and with clearly proportionally different signals at every time point until 7 days p.i.

Finally, infection with TB4-UL83-YFP resulted in stronger YFP signals as compared to with TB4-IE2-YFP (Fig. 4.10C).

Based on such results, the screening of the effect of SMs on viral replication was performed, infecting MRC5 cells in 96 well black optical plates with TB4 -UL83-YFP at low MOI (0.3 - 0.03) for 7 days, before processing plates for FRAs (§3.6.4).

4.9 Evaluation of the effect of DMSO on viral replication by FRAs

Since the SMs are resuspended in DMSO, and such solvent has been proposed to have an effect on HCMV replication [196, 197], we performed specific experiments to evaluate how it could affect our experimental setup. To this end, MRC5 cells were seeded in 24 well-plates, infected at different MOIs (0.0075 – 0.5) with either TB4-IE2-YFP or TB4 -UL83-YFP recombinant viruses, and treated with different concentrations of DMSO immediately after infection. CPE and fluorescence were monitored daily using a fluorescent microscope and, at 4 and 7 days p.i. plates were lysed and viral replication was estimated by fluorimetric analysis (Figure 4.11A). All conditions tested

resulted in a measurable level of YFP signal as a consequence of viral replication. Importantly, at 4 and 7 days p.i cells treated with DMSO 1% exhibited a higher CPE as compared to cells treated with plain medium or with DMSO 0.5% (Figure 4.11B). Consistently with the literature [196, 197], the enhancing effect of DMSO on viral replication was also evident by microscopic evaluation (Figure 4.11C) and fluorimetric analysis (Figure 4.11D) of YFP fusion proteins expression. In fact, both at 4 and 7 days p.i DMSO 1% clearly increased the YFP expression after infection with either virus. Importantly, such increase was not observed after treatment with DMSO 0.5% (Figure 11CD). Therefore, we decided not to exceed a DMSO 0.5% final concentration in subsequent experiments.

4.10 Evaluation of the effect of GCV on viral replication by FRAs

In order to verify if our experimental setup allowed to monitor the inhibitory effect of antivirals on HCMV life cycle, MRC5 cells were seeded in 24-well plate, infected with TB4-IE2-EYFP and TB4-UL83-EYFP and subsequently treated with GCV (50 μM), a well know anti-CMV drug. Cells were monitored daily and scored for CPE, and fluorescent cells visualized using an inverted fluorescent microscope. Moreover at 4 and 7 days p.i cells were analyzed and processed for measurement of viral replication by FRA (Figure 4.12A). As expected, GCV treatment strongly reduced HCMV induced CPE both at 4 and 7 days p.i. with a reduction of ca 50% and 80%, respectively (Figure 4.12B). Such differences were also evident in the YFP signal observation deriving from the expression of the recombinant viral proteins (Figure 4.12C). Fluorimetric evaluation of the levels of viral replication confirmed that the effect of GCV did not show MOI-dependence effect, inhibiting viral replication even at higher MOI, and exerted its inhibition in the same way on both viruses (Figure 4.12D). Our results thus suggest that FRAs are suitable to study the possible inhibitory effects on viral replication of the 18 SMs.

4.11 A small scale screening identifies 4 SMs capable of inhibiting HCMV replication

Having established proper conditions to detection inhibition of HCMV replication, we decided to screen the previously identified SMs (§1.15) for their ability to interfere with viral infection. Each SMs was tested at two different concentrations (10 and 100 μM), and GCV (50 μM) was included as a positive control for inhibition of viral replication. To this end, MRC5 cells were seeded in 96 well special optics black microplates and were infected with TB4-UL83-EYFP (§3.6.2). One h p.i, media containing either DMSO 0.5% or two different concentrations (100 e 10 μM) of each SMs with a 0.5% DMSO final concentration was added. Cells were microscopically monitored daily for 7 days p.i to evaluate CPE, presence of precipitates, and viral replication. Seven days p.i cells were lysed and the plates processed for fluorimetric quantification of the levels of viral replication relative to each condition (Figure 4.13A). In parallel, MTT assays were performed on non-infected cells (§3,9: Figure 4.13B). Several of the 18 SMs at 100 μM formed visible precipitates or caused cell death, indicating poor solubility and toxicity (Figure 4.13D). In particular A1, B4 and B6 cytotoxic effects were evident already from 1 day p.i. Only one compound (A4) caused evident cytotoxicity at 10 μM (Figure 4.13C). Importantly, our data showed that four SMs reduced viral replication in the absence of precipitates and evident cell cytotoxicity, to levels similar to those observed after GCV treatment (Fig. 4.13D). Such inhibition was confirmed by microscopic analysis of infected cells, with a noticeable decrease in CPE and number and intensity of YFP-positive cells, to similar levels as GCV treated cells.

4.12 Identification of 4 SMs capable of inhibiting CMV replication in a dose-dependent fashion

We decided to calculate ED50 and CC50 of each of the 4 SMs identified in our small-scale FRA-based screening. To this end, we performed dose-response FRAs and MTT assays, respectively (§ 3.6.4 – 3.9). For FRAs, MRC5 cells were seeded in 96 well special optics black microplates and were infected with TB4-UL83-EYFP (§3.6.3). One h p.i media containing either DMSO 0.5% or

increasing concentrations (0.2-200 μM) of each SMs with a 0.5% DMSO final concentration was added. Cells were microscopically monitored daily for 7 days p.i to evaluate CPE, presence of precipitates, and viral replication. Seven days p.i cells were lysed and the plates processed for fluorimetric quantification of the levels of viral replication relative to each condition (Figure 4.14A). In parallel, MTT assays were performed on noninfected cells (§3.9: Figure 4.14B).

Importantly, all tested SMs reproducibly inhibited viral replication in a dose-dependent fashion, with ED_{50} values in the low micromolar range (Figure 4.14C). In such experimental setup GCV efficiently inhibited HCMV replication with a ED_{50} of 2.3 μM and did not cause detectable cytotoxic effects at any concentration tested, thus resulting in a selective index (SI) greater than 43 (Figure 4.14C). Among the SMs tested B6 was the most active compound and exhibited a ED_{50} slightly lower that that calculated for GCV (2.3 vs 2.1 μM, respectively). However, it also was endowed with considerable cytotoxicity (CC50 of ca 10 μM) resulting in a SI of around 5. On the other hand, B3, the second most active compound (ED_{50} of 4.7 μM), did not cause evident cytotoxicity up to 200 μM, and therefore has a SI greater than 20. C6 also exhibited low cytotoxicity, but was significantly less efficient in inhibiting HCMV replication than the other two SMs (ED_{50} of 16.5 μM). Finally, the effect of B1 on HCMV life cycle was evident only at high concentrations (ED_{50} of 86.5 μM), suggesting the possibility of an unspecific effect.

4.13 Analysis of HCMV gene expression by Western blot assays

In order to gain insights in the SMs mode of action, we analyzed their effect on HCMV life cycle by Western blotting. To this end, MRC5 cells were seeded on 6 well flat bottom plates and infected with HCMV (strain AD169) at a MOI of 0.1. One h p.i SMs were added at sub-toxic concentration (B1 100 μM, B3 20 and 10 μM, B6 5 μM, C6 40 μM, GCV 5 μM). Cell lysates collected at different time points p.i (12, 24, 48, 72 and 96 h) were subjected to SDS-Page Western Blotting to detect specific viral antigens and GAPDH as loading control (Figure 4.15A, Table 3.4) .

As expected, at 12-24 h p.i neither any of tested SMs nor GCV affected the expression of the IE1/2 proteins, indicating that the selected SMs did not interfere with IE gene expression or viral entry (Figure 4.15B, *top two panels*). By 48 h p.i however, treatment with either B6 or C6 reduced the expression of HCMV UL44, similarly to treatment to GCV, suggesting a possible effect on viral DNA replication (Figure 4.15B, *third panel*). Such inhibitory effect was even more pronounced when expression of the pp65 structural protein was analysed at 72 h p.i, whereby treatment with either B6 or C6 abolished viral protein expression to a comparable extent to GCV, strongly suggesting inhibition of viral DNA replication (Figure 4.15B, *fourth panel*). By 96 h p.i, however, only treatment of C6 prevented expression of the late protein pp28 (Figure 4.15B *bottom panel*). Surprisingly, no effect on viral gene expression was observed after treatment of infected cells with SM B3, even when it was added at a concentration of 20 μM, corresponding to around 4 times the ED50, and no effect on pp28 expression was detected after treatment of infected cells with SM B6 (Figure 4.15B and Figure Appendix E1-3).

4.14 Study of B3 and B6 antiviral effects by Plaque Reduction Assay

In order to further investigate the antiviral properties of SMs B3 and B6, we performed PRA on HFF cells using HCMV laboratory strain AD169 and MTT assay as described above. GCV was included in these experiments as a control for inhibition. As expected, GCV exhibited a ED_{50} of 2.5 μM (Figure 4.16), which is compatible with the ED_{50} calculated by FRAs (see Figure 4.14C). Surprisingly, neither B6 nor B3 inhibited plaque formation with high efficacy, with ED_{50} values of around 50 μM (Figure 4.16).

4.15 Analysis of UL44 thermal stability by Thermal Shift Assay (TSA)

Since the GST-Pulldown Assay was not suitable to study the effect of SMs on UL44 dimerization *in vitro*, we decided to develop a Fluorescence-based Thermal Shift Assay (TSA). Indeed TSA has been recently used is able to inform whether a SM induce the disruption of constitutive oligomeric interfaces [198]. TSA assays were setup up using the ABI PRISM 7000 thermal cycler as described in [194]. To validate the experimental conditions, Wheat Germ Lysozyme, was used. Indeed Lysozyme melting properties have already been extensively characterized, and it is use as in TSAs is extremely widespread, due to its commercial availability [199]. In particular, different concentrations of protein and Sypro Orange (1.25-350 μM and 0.5-10x final concentrations respectively, see Figure 4.17A) in two very common TSA buffers such as the Potassium Phosphate and the Citrate Phosphate ones (§ 8.1). Fluorescence data were acquired with ROX and SYBR emission filers (§3.10.1). Analysis of the ratio between the Maximum Fluorescence over the Baseline Fluorescence (defined as the fluorescence detected at the beginning of the experiment, i.e. at 22 °C) relative to each condition, revealed that best signal to noise ratios were obtained using the citrate buffer and acquiring data using the ROX emission filter (Figure 4.17B). Overall, optimal Maximum/Baseline Fluorescence ratios were obtained using Lysozyme 50 μM and Sypro orange 10x (Figure 4.17B). In particular Sypro orange concentrations lower than 10x did not allow to generate sufficiently strong fluorescent signals at any Lysozyme concentration tested (Figure 4.17B), resulting in suboptimal Tm and -dF/dT curves, and not enabling the accurate T melting measurement (Figure Appendix F1-4). On the other hand, very similar Tm were calculated for each Lysozyme concentration tested in the presence of Sypro 10x, with very reliable Tm and -dF/dT curves (Figure 4.17C). Overall, Lysozyme appeared relatively stable, with a Tm of ca 73 °C, consistent with previous reports [200].

Subsequently we decided to investigate the thermal stability of UL44 by means of TSA. In order to identify the optimal UL44 concentration for such experiments, we used a Roche Lightcycler 480, which allows the use of very small reaction volumes, and consequently reduce

reagents requirement. 6His-UL44(1-290) was therefore mixed with Sypro 10x final concentration in Citrate and Potassium Phosphate buffers, using Lysozyme 50 μM as positive control (Figure 4.18A). Our results indicated that usage of 6His-UL44(1-290) at both 20 and 5 μM was compatible with thermal profiling, and resulted in high Maximum/Baseline Fluorescence ratios, similar to that obtained for Lysozyme 50 μM, whereas signal relative to UL44 1.25 μM was too low to enable further analysis (Figure 4.18B). Tm curve analysis showed that 6His-UL44(1-290) is considerably less stable than Lysozyme under the tested conditions resulting in a Tm comprised between 57 and 62 °C depending on the buffer and the protein concentration tested (Figure 4.18C).

4.16 Analysis of UL44 thermal stability in different buffers

We therefore decided to screen a several buffers to identify the best conditions to investigate the effect of SMs on protein stability by TSA. To this end, we used an ABI PRISM 7000 and the ROX acquisition filter to perform TSAs with 6His-UL44(1-290) (5 μM) in the presence of 22 different buffers (§3.10.1-§8.1). Three of the latter were selected as previously used to characterize UL44 biochemical properties. In particular, Buffer A has been used to test the ability of UL44 to stimulate UL54 DNA polymerase activity, buffer B to study the UL44-UL54 interaction, and buffer C for UL44-DNA binding assays [201-203]. The other 19 buffers were chosen among those suggested by Huynh et al., [194] for the optimization of TSA protocols (Figure 4.19A). In particular, different salt concentrations (NaCl 50 and 250 mM) were tested across specific pH ranges for three different TSA buffers, based on Citrate (pH4-7), Tris-HCl (pH7-9) and Bicine (pH8-8.5). Analysis of the Tm and the -dF/dT curves revealed that UL44 stability was extremely variable under the different buffers tested, with Tm ranging from ca 39 to 52 °C. The lowest stability was exhibited in a Citrate buffer containing low salt concentration at pH4 (Tm = 38.8°C), whereas the protein was most stable (Tm = 52.2°C) in a citrate buffer containing high salt concentration at pH 6 (Figure 4.19B). Overall, UL44 was less stable in Bicine buffer as compared to Tris-HCl, and Citrate buffer (Figure 4.19C).

Such differences appear to mainly depend on the different pH range allowed by each TSA buffer. Indeed, UL44 Tm appeared to be highly dependent on the pH used for the assay (Figure 4.19D). This is exemplified by the behavior of the protein in Citrate buffer containing high salt concentrations: the stability was lowest at pH 4 (Tm = 39.3°C), considerably higher at pH5 (Tm = 47.1°C), and reached a peak at pH 6 (Tm = 52.2°C). A further increase to pH 7 slightly destabilized the protein (Tm = 51.4°C). On the other hand, the salt concentrations tested in this study did not appear to strongly affect UL44 stability, as shown by the identical Tm calculated in Citrate buffer at pH 7 (Figure 4.19E). Such pH dependence is likely the reason for the relative low stability of 6His-UL44(1-290) in its specific DNA polymerase stimulation buffer (buffer A, pH 8: Tm = 47.2°C) as compared to in the DNA binding (buffer C, pH 7.5: Tm = 49.2 °C) and UL54 binding (buffer B, pH 7.5: Tm = 51.0 °C) buffers (Figure 4.19F). Based on these results, we decided to use three different buffers for follow up experiments (UL54 binding, Citrate pH 6, high salt and Citrate pH 7, low salt buffers; Figure 4.19G).

4.17 TSA-based discrimination between monomeric and dimeric 6His-UL44(1-290)

TSA has been recently used for the identification of compounds capable of disrupting the CK2β kinase constitutive homodimer, based on their ability to cause a negative shift in Tm. Indeed, protein dimers are believed to be more stable than monomers, and therefore endowed with higher Tm [198]. We therefore aimed at investigating if such principle could also be applied to UL44. To this end, we performed TSAs to compare the thermal stability profiles of 6His-UL44(1-290) and of its dimerization-defective derivative 6His-UL44(1-290)L86A/L87A (Figure 4.20A). Our results indicated that, during thermal denaturation in presence of SYPRO Orange 10x, the UL44 dimerization impaired mutant was emitted a lower fluorescent signal as compared to the wild-type protein, under each buffer condition tested (Figure 4.20B, *left panels*). Remarkably, it also exhibited a ΔTm of c – 10°C as compared to the *wild type* protein, thus confirming that UL44 monomers are much less stable than the dimeric form of the protein (Figure 4.20B, *right panels*). The difference if

Tm was maximal in Citrate pH7, low salt (ΔTm = 10.6°C) and minimal in UL54 binding buffer (ΔTm = 8.4°C). These results strongly suggest that TSAs allow discrimination of UL44 monomeric and dimeric forms and imply their potential for the screening of SMs disrupting UL44 homodimerization.

4.18 Evaluation of DMSO effect on TSAs

Since the SMs are resuspended in DMSO, we performed specific experiments to evaluate how it could affect our experimental setup. We therefore decided to evaluate different DMSO concentration using an UL44-specific buffer to identify the best conditions that allows to investigate the effect of SMs on protein stability by TSA. To this end, we decide to study we used an ABI PRISM 7000 and the ROX acquisition filter to perform TSAs with either 6His-UL44(1-290) and Lysozime (5 μM), and SYPRO Orange 10x diluted in buffer B with increased DMSO concentrations (0.25%, 1%, 5%) (Figure 4.21A). In the study with 6-His-UL44(1-290) our results suggest that each DMSO concentrations did not affect the assay in a detectable way, in presence of DMSO the fluorescence curves with lower values than the control were highlighted. In particular, it is important to underline that each concentration did not alter the assay, and the greatest differences relative to the fluorescence curves compared to the untreated derive from the 0.25% DMSO. The comparison of Tm instead showed a dose-dependent effect, with the maximum Tm relative to the untreated (Tm = 72.2 ° C) and the minor detected with the DMSO 5% treatment (Tm = 50.6 ° C) (Figure 4.21 *upper panel*).

As shown in figure 4.21 *bottom panel* the UL54 biding buffer is not suitable for study the Lysozime thermal profile.

4.19 Screening of the 18 SMs by TSAs

Having established proper conditions to detection UL44 thermal profile, we decided to screen the previously identified SMs (§1.15) with Lysozyme to evaluate their possible interaction with the SYPRO Orange with consequent alteration of the protein thermal profile. To this end, we performed TSAs to compare the thermal and fluorescence profile of Lysozyme (5 μM) in presence and in the absence of SMs (1mM with DMSO 5% final concentration) either in buffer B and in buffer I (Figure 4.22A). From the observation of both fluorescence and the -dF/dT curves it was possible highlight a substantial difference between the curves relative to the treatment of several SMs and the untreated (Figure 4.22B), suggesting that these molecules affect the thermal and fluorescence profile of the protein. As shown in the Figure, an important ΔTm was detected between the protein in the presence and in the absence of SMs.

Noteworthy, several molecules in the absence of Lysozyme showed curves similar to those related to the protein, suggesting their possible interaction with SYPRO ORANGE or direct excitation, interfering with the assay (Figure 4.22C).

4.20 Evaluation of the 4 selected SMs effect by ViiA7 Instrument

Considering that SYPRO Orange is excited at 490 nm and emits at 610 nm, to avoid the possible SMs excitation, we decided to perform the TSAa with Viia7 Real Time PCR-System, that allows to select the excitation and emission spectrum specifically at 470 nm and 586 nm respectively.

To this end, we tested the fourth SMs (B1, B3, B6 and C6) selected by FRA as potential inhibitor of viral replication. In particular, Lysozyme (5 μM) and SYPRO orange (10x) were diluted in buffer I with increased concentrations (25, 50, 100 and 200 μM with DMSO 2% final concentration) of the molecules. Multiple wavelengths were selected for samples excitation (470, 520 and 580 nm) and fluorescence detection (520, 586, 623 and 682 nm). Data were exported to Excel and the values relative to the combination of 470 nm and 623 nm excitation and emission filters respectively were analyzed (Figure 4.23A).

From the observation of the fluorescence curves it was evident that the signal levels in the presence of B1 and B3 were similar to that of the control (untreated), whereas a significantly higher signal was detected with the addition of B6 and C6, suggesting an interference of the thermal profile of the protein (Figures 4.23B). Consistent with this hypothesis is the observation of the fluorescence and -dF/dT curves relative to SMs in the absence of the protein. In fact it is possible to underline that B1, B6 and C6 at 200 μM, revealed a specific thermal profile comparable to that of a protein (Figure 4.23C). To assess whether fluorescence signal relative to SMs alone derived from an interaction with SYPRO Orange, our candidates were evaluated in the absence of both protein and SYPRO Orange. As result, an intrinsic interaction between C6 with SYP Orange has been detected in the absence of the Lysozyme, indicating that this compound presented a fluorescence independent from the protein, therefore it was not suitable for this assay (Figure 4.23D). In conclusion, our results suggest that only B3 200 μM and B1 100 μM (not shown) did not interfere with the protein or exhibited a specific interaction with the SYPRO Orange.

4.21 Evaluation of B1 and B3 on UL44 dimerization by TSAs

As describe above, B1 and B3 were suitable for the TSAs, and for this reason, these candidates were selected to evaluate their inhibition effects on UL44 dimerization. To this end, 6His-UL44(1-290) (5μM) and SYPRO Orange were diluted in buffer I with either B1 (100μM) and B3 (200μM) with DMSO 2% final concentration. Data were exported to Excel and the values relative to the combination of 470 nm and 623 nm excitation and emission filters respectively were analyzed (Figure 4.24A). As expected neither B1 nor B3 affected the Lysozyme fluorescence profile, confirming that these SMs did not interfere with the fluorescence profile of the protein. The Tm resulted higher (ca 1 degree) in the presence of B1 (Figure 4.24B).

As result, 6His-UL44 thermal profile resulted slightly altered by the 2 molecules. In particular, as shown in Figure 4.24C, B1 increased the UL44 Tm of ca 1 degree, whereas in the presence of B3 a Tm decrease was detected. This may be the result of an effective *in vitro* inhibition of dimerization. Certainly, in the next future we will perform the assay again to confirm this result.

5. Discussion

HCMV is a major human pathogen, whose genome is replicated via a rolling circle mechanism in the nucleus of infected cells by a number of cellular and viral proteins. Among them, the DNA polymerase holoenzyme is strictly required for viral genome replication. Such enzyme is composed by a catalytic subunit, UL54 and a processivity factor UL44, which tethers the holoenzyme to dsDNA [60]. The latter protein function as a dimer, and importantly, the L86A/L87A double substitution prevented viral DNA replication as shown by the failure of such mutants to sustain *ori*Lyt dependent DNA replication in transient trans-complementation assays, suggesting that UL44 homodimerization is essential for viral genome replication [100]. Therefore, UL44 dimerization can be considered a potential target of therapeutic intervention to interfere with HCMV replication.

Since more than 40 PPIs have now been targeted, and several inhibitors have reached clinical trials [169-171], we reasoned that is might be possible to identify compounds hindering viral replication by targeting the UL44 dimerization. This idea was fostered by the recent crystallization of UL44 N-termal dimeric structure, which revealed a surface potentially amenable to drug targeting [95, Di Antonio et al, unpublished]. Before the start of this thesis, our research group confirmed UL44 dimerization in living cells by FRET and BRET approaches, validating the published crystal structure by substitution of key aa at the dimerization interface. Using the recently published crystal structure of UL44 in combination with the software Glide, we also performed a virtual screening to identify 137 SMs potentially targeting UL44 dimerization and selected the 18 ideal candidates by means visual inspection [Di Antonio et al, unpublished].

In the current study, we concentrated in validating the ability of such SMs to interfere with UL44 dimerization *in vitro* and with HCMV replication in cell culture. First of all, we confirmed that the dimerization occurred in an *in vitro* context using both GST-pulldown Assay [185] and Thermal Shift Assay (TSA) [198], then we screened the 18 SMs potentially interfering with the UL44

dimerization. We performed GST-pulldown assays with the recombinant proteins 6His-UL44(1-290), GST-UL44(1-290) and with the dimerization impaired point mutant 6His-UL44(1-290)-L86/L87A to assess the sensitivity of the system to the impairment of ULL44 dimerization [185]. Importantly, we could detect the formation of GST-UL44(1-290)/6His-UL44(1-290) complex, but the 6His-UL44(1-290)-L86/L87A band, relative to the GST-UL44(1-290)/6His-UL44(1-290)L86/L87A complex was much less intense, indicating that the assay can highlight differences in UL44 dimerization, consistent with precedent studies [95, 100, Di Antonio et al, unpublished] (Figure 4.1). Unfortunately, GST-pulldown did not prove suitable to test the ability to disrupting UL44 dimers in that surprisingly revealed a high variability, and most-importantly lack of correlation between the inhibition of dimerization and the concentration of SMs used (Figure 4.5). Consistent with the non-reliability of the assay were ED50 values >100 μM obtained by Plaque Reduction Assay of the SMs initially selected as potential inhibitors of the dimerization by GST-pulldown (Figure 4.6). For this reason, we started focused on the development of a TSA similar to one been recently used for the identification of compounds capable of disrupting the CK2β kinase constitutive homodimer, based on their ability to cause a negative shift in Tm. Indeed, protein dimers are believed to be more stable than monomers, and therefore endowed with higher Tm [198]. We therefore aimed at investigating if such principle could also be applied to UL44. To this end, we performed TSAs to compare the thermal stability profiles of 6His-UL44(1-290) and of its dimerization-defective derivative 6His-UL44(1-290)L86A/L87A. As result the mutant exhibited a ΔTm of c – 10°C as compared to the wild type protein, thus confirming that UL44 monomers are much less stable than the dimeric form of the protein (Figure 4.20B). These results strongly suggest that TSAs allow discrimination of UL44 monomeric and dimeric forms and imply their potential for the screening of SMs disrupting UL44 homodimerization. Several problems have been found also relative to TSAs, such as the difficulty in resuspending some SMs in the dilution Buffer -indicative of poor solubility-, as well as that some molecules emitted in the presence or absence of SYPRO

Orange interfering with the thermal profile of the protein. Before proceeding to the study on viral replication, the cytotoxicity of our compounds was evaluated through MTT assay. Several SMs exhibited cytotoxic effect and precipitates under microscopic observation, further confirming the poor solubility. In parallel we obtained two recombinant HCMV viruses (TB4-IE2-EYFP and TB4-UL83-EYFP) from Michael Winkler, that allow to directly visualize infection kinetics, quantify viral replication and identify anti-HCMV active compounds [191]. We performed preliminary experiments to determine the optimal conditions for Fluorescence Reduction Assays (FRAs), confirming the enhancing DMSO effect on HCMV replication [196, 197] (Figure 4.11). Therefore, the ability to interfere with viral infection of our molecules was investigated, and 4 of these (B1, B3, B6 and C6) reproducibly inhibited viral replication. Among these 4 candidates B6 was the most active compound and exhibited a ED50 value of 2.3 μM but with a considerable cytotoxicity (CC50 of ca 10 μM) resulting in a SI of around 5. On the other hand B3, the second most active compound (ED50 of 4.7 μM), did not cause evident cytotoxicity up to 200 μM, and therefore has a SI greater than 20. C6 also exhibited low cytotoxicity, but was significantly less efficient in inhibiting HCMV replication than the other two SMs with an ED50 value of 16.5 μM. Finally, the effect of B1 on HCMV life cycle was evident only at high concentrations (ED50 of 86.5 μM), suggesting the possibility of an unspecific effect (Figure 4.14).

Since we speculate the SMs selected affect the UL44 dimerization hindering viral replication, we compared expression of viral gene in the presence of the 4 SMs to those in presence of GCV (Table 3.4). As expected, at 12-24 h p.i neither any of tested SMs nor GCV affected the expression of the IE1/2 proteins, indicating that the selected SMs did not interfere with IE gene expression or viral entry. By 48 h p.i however, treatment with either B6 or C6 reduced the expression of HCMV UL44, similarly to treatment to GCV, suggesting a possible effect on viral DNA replication. Such inhibitory effect was even more pronounced when expression of the pp65 structural protein was analyzed at 72 h p.i, whereby treatment with either B6 or C6 abolished viral protein expression to a

comparable extent to GCV, strongly suggesting inhibition of viral DNA replication. By 96 h p.i, however, only treatment of C6 prevented expression of the late protein pp28 (Figure 4.15B). Surprisingly, no effect on viral gene expression was observed in cells infected with HCMV AD169 after treatment with SM B3, even when it was added at a concentration of 20 μM, corresponding to around 4 times the ED50, and no effect on pp28 expression was detected after treatment of infected cells with SM B6. These results could be explained either with the fact that such compounds could inhibit more efficiently HCMV strain TB40, from which TB4-UL83-YFP was generated [191] or with some issues relative to the resuspension and aliquoting process of the compounds. Indeed, such hypothesis are being investigated in our laboratories. In the next future to validate that our candidates inhibit viral replication by disrupting UL44 dimerization, we will test their ability to inhibit GCV resistant strains. Indeed, molecules disrupting UL44 dimerization should be also effective on such viral mutants. To this end, we will test HCMV AD169 GFP and AD169-GCV R-GFP fluorescent viruses and FRA. The expected result is the inhibition of viral replication in both viruses in equal way. We will produce resistant viral strains to our SMs to allow its viral DNA extraction and evaluate the mutation responsible for the resistance by sequencing of the UL44 gene, possibly identifying mutations responsible for the phenotype. Given the observed problems relative to the detection of the disruption of UL44 dimerization *in vitro* by GST-pulldown assay and TSA, we will test our SMs focus on the development of alternative approaches, such as Gel Filtration assays, which allow monitoring macromolecular complexes and do not require fluorescent-based approaches.

6. Tables and figures

Figure 4.1

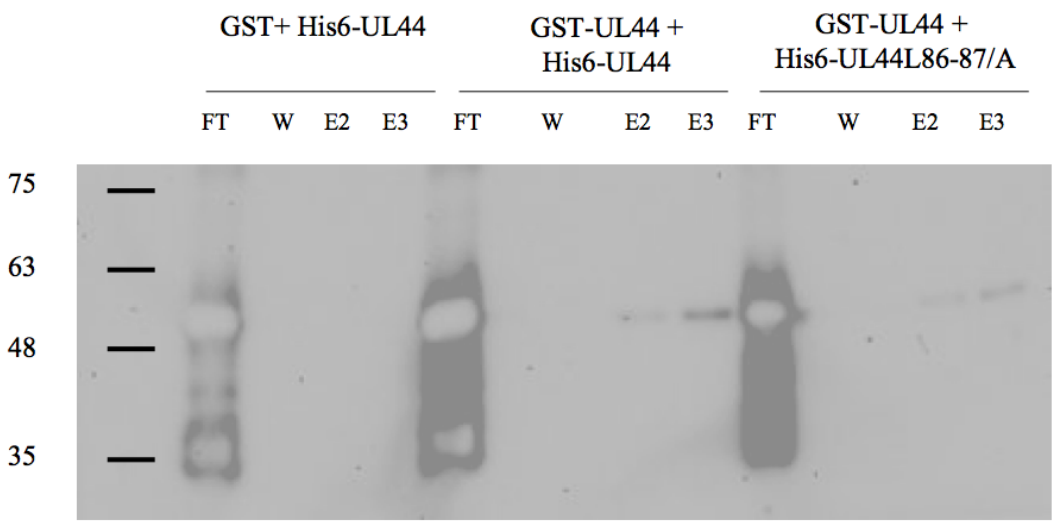
GST+ His6-UL44
GST-UL44 +
His6-UL44
GST-UL44 +
His6-UL44L86-87/A
FT W E2 E3 FT W E2 E3 FT W E2 E3
75
63
48
35

Figure 4.2

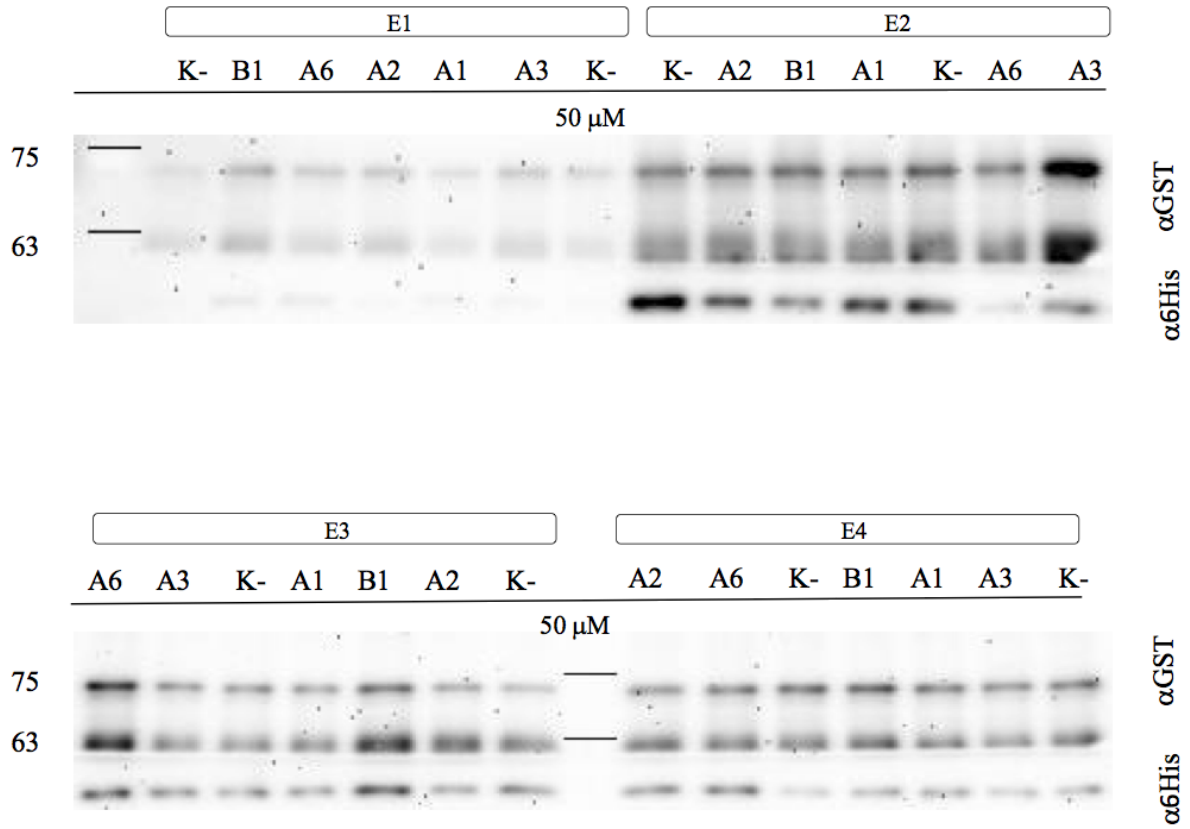
E1
E2
K- B1 A6 A2 A1 A3 K- K- A2 B1 A1 K- A6 A3
50 µM
75
63
αGST
α6His
E3
E4
A6 A3 K- A1 B1 A2 K- A2 A6 K- B1 A1 A3 K-
50 µM
75
63
αGST
α6His

Figure 4.3

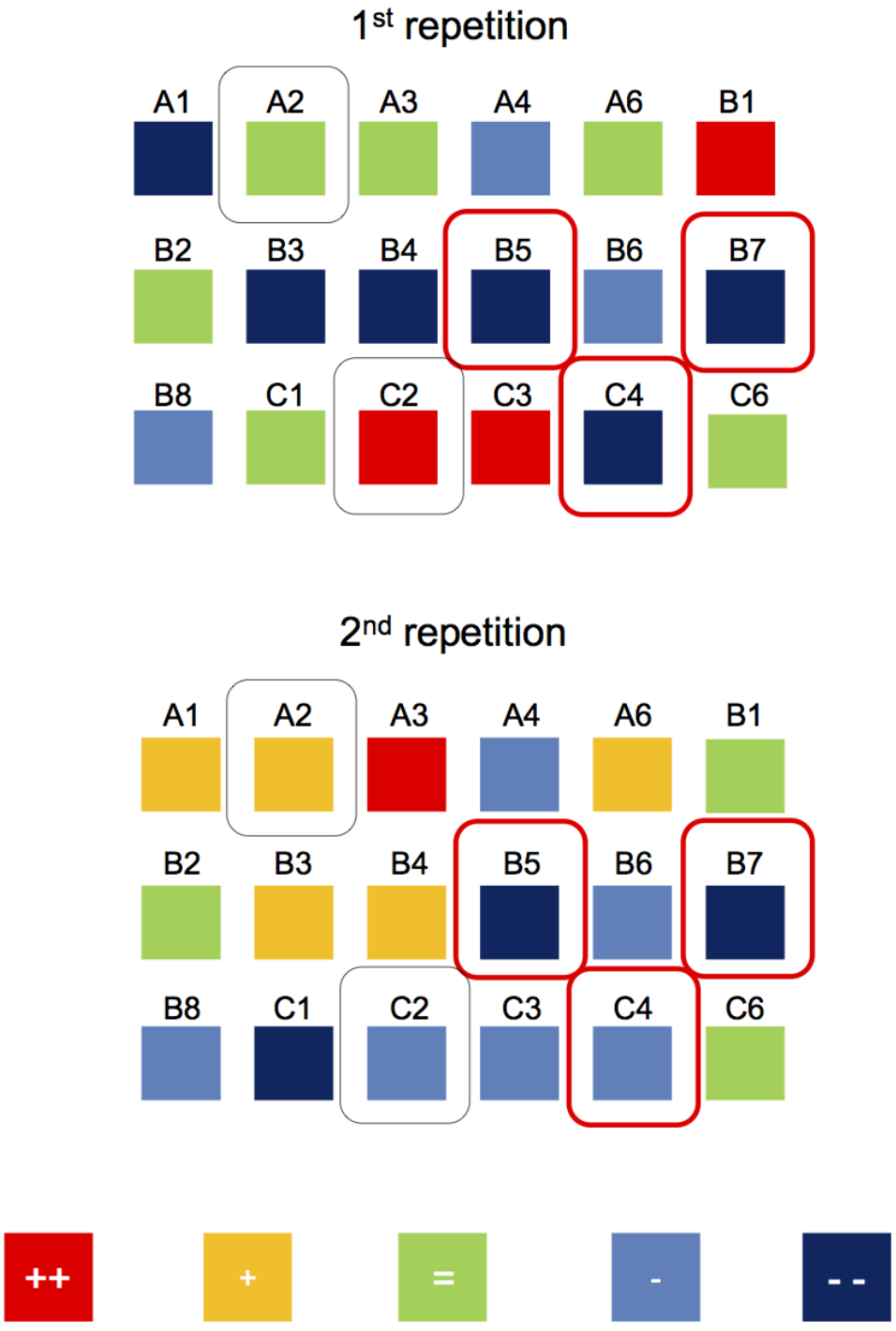
1st repetition
A1
A2
A3
A4
A6
B1
B2
B3
B4
B5
B6
B7
B8
C1
C2
C3
C4
C6
2nd repetition
A1
A2
A3
A4
A6
B1
B2
B3
B4
B5
B6
B7
B8
C1
C2
C3
C4
C6
++
+
=
-
- -

Figure 4.4

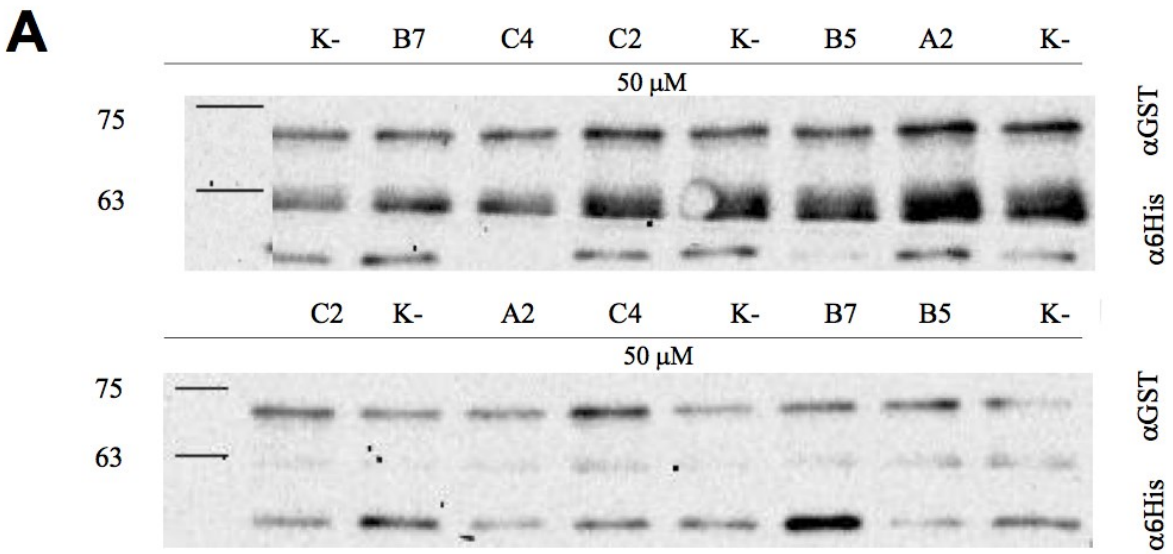
A
K-
B7
C4
C2
K-
B5
A2
K-
50 µM
75
63
αGST
α6His
C2
K-
A2
C4
K-
B7
B5
K-
50 µM
75
63
αGST
α6His

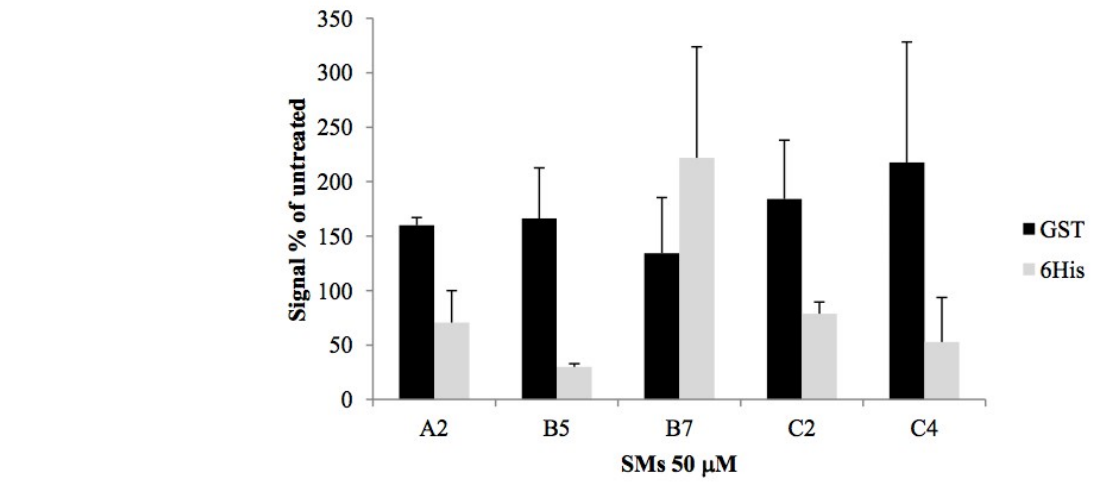
B
Signal % of untreated
350
300
250
200
150
100
50
0
A2
B5
B7
C2
C4
SMs 50 µM
GST
6His

Figure 4.5

A

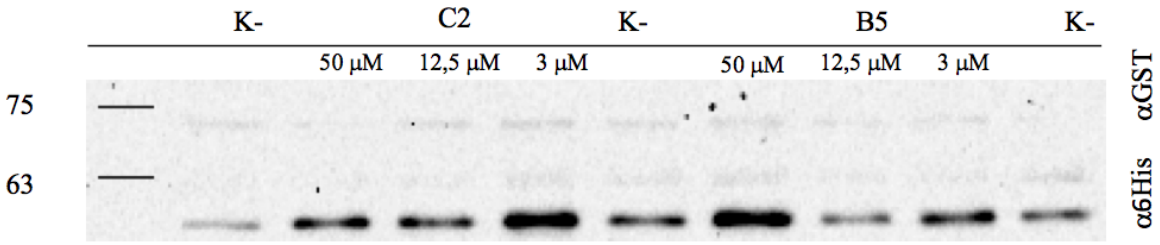
K-
C2
K-
B5
K-
50 µM
12,5 µM
3 µM
50 µM
12,5 µM
3 µM
75
63
αGST
α6His

B

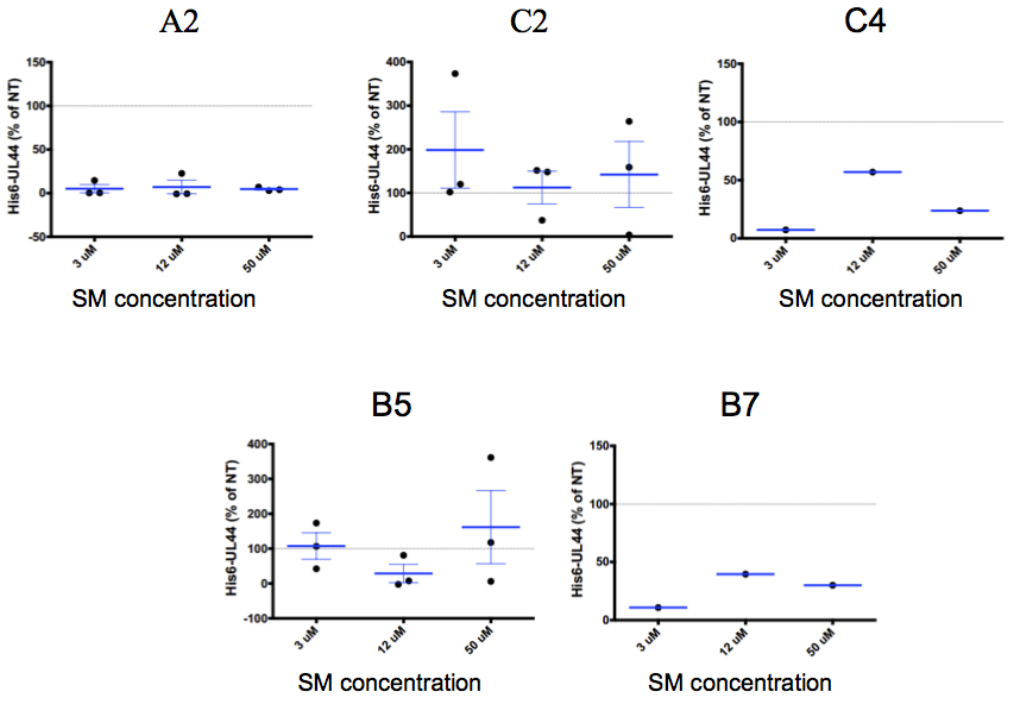
A2
C2
C4
B5
B7
His6-UL44 (% of NT)
SM concentration
3 uM
12 uM
50 uM

Figure 4.6

A

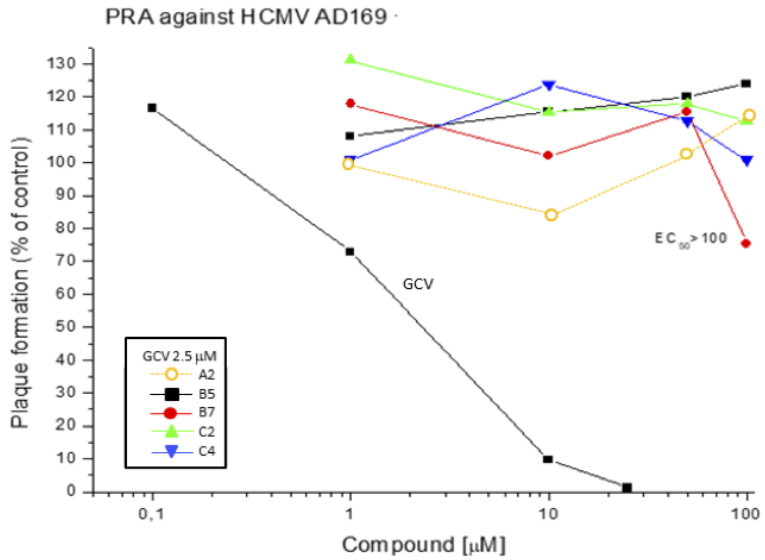

B

SMs	CC50	ED50
GCV	>1000 µM	2,5 µM
B5	6 µM	>100 µM
B7	286,7 µM	>100 µM
C2	125 µM	>100 µM
C4	24,4 µM	>100 µM
A2	>100 µM	>100 µM

Figure 4.7

A

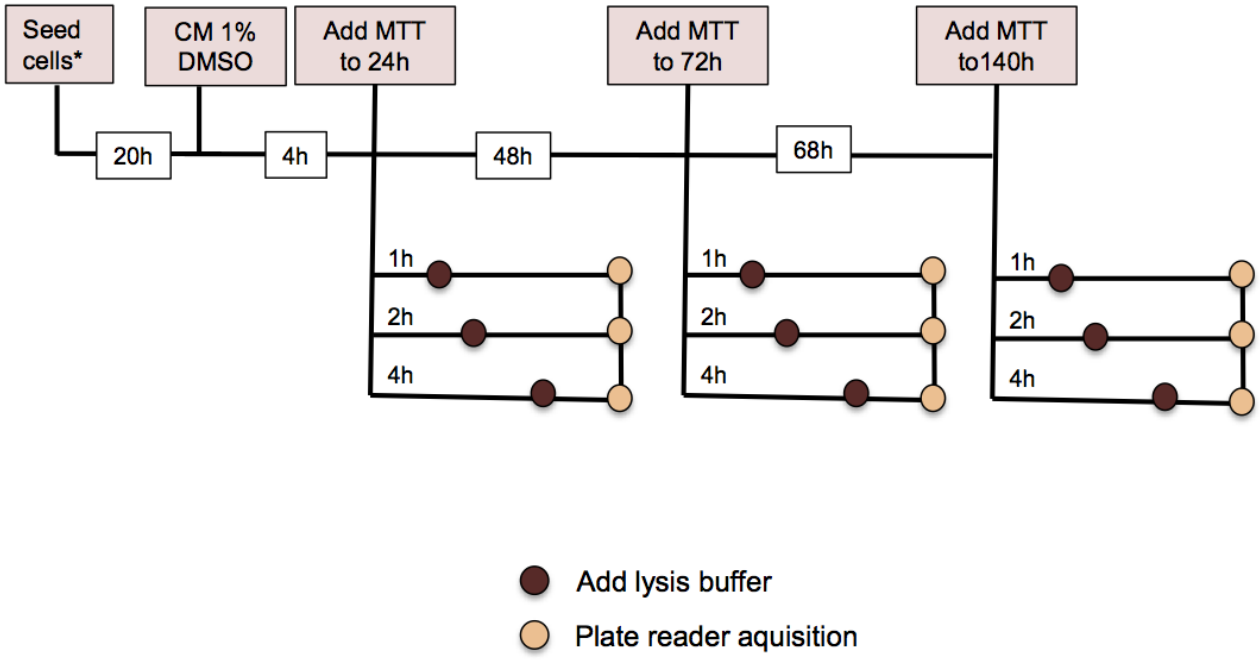

- Seed 1 96-well plate for each time point.
- Each time point well plate was incubated for 1, 2 or 4 hour with MTT.

*Cell range
24h (6.5×10^2 - 8×10^4)
72h (2.5×10^2 - 3.2×10^4)
140h (6.5×10 - 8×10^3)

Figure 4.7

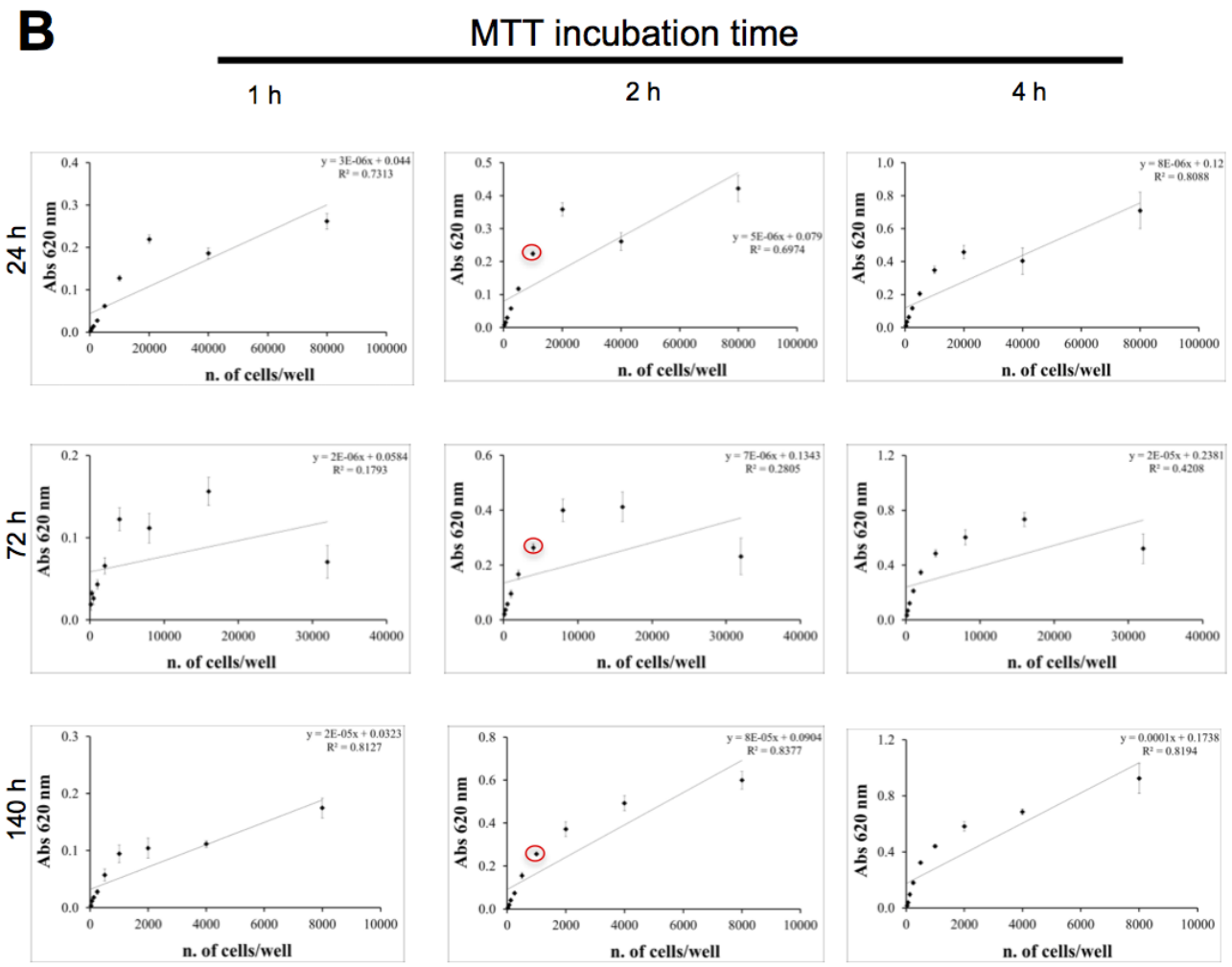
B
MTT incubation time
1 h
2 h
4 h
24 h
72 h
140 h
Abs 620 nm
n. of cells/well
y = 3E-06x + 0.044
R² = 0.7313
y = 5E-06x + 0.079
R² = 0.6974
y = 8E-06x + 0.12
R² = 0.8088
y = 2E-06x + 0.0584
R² = 0.1793
y = 7E-06x + 0.1343
R² = 0.2805
y = 2E-05x + 0.2381
R² = 0.4208
y = 2E-05x + 0.0323
R² = 0.8127
y = 8E-05x + 0.0904
R² = 0.8377
y = 0.0001x + 0.1738
R² = 0.8194

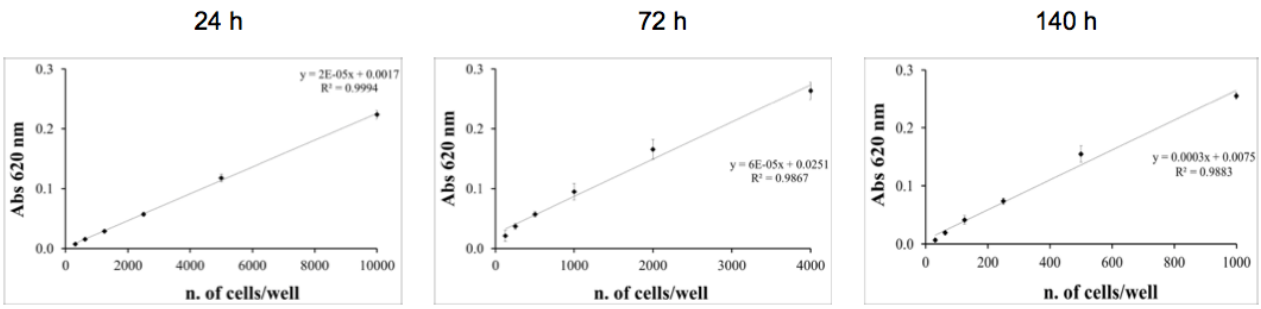
C
24 h
72 h
140 h
Abs 620 nm
n. of cells/well
y = 2E-05x + 0.0017
R² = 0.9994
y = 6E-05x + 0.0251
R² = 0.9867
y = 0.0003x + 0.0075
R² = 0.9883

Figure 4.8

Recombinat virus TB4-IE2-EYFP

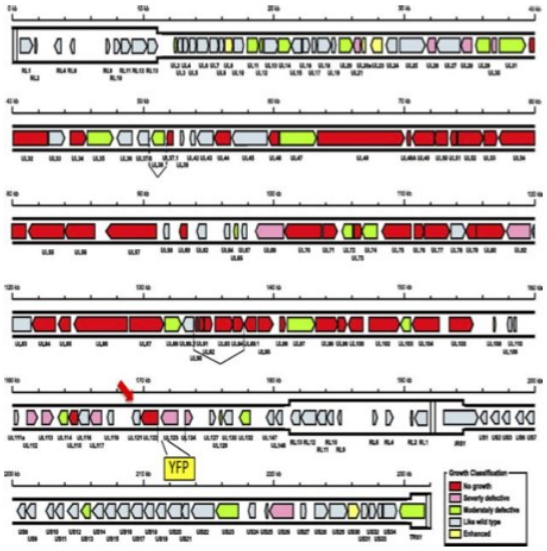

Recombinat virus TB4-UL83-EYFP

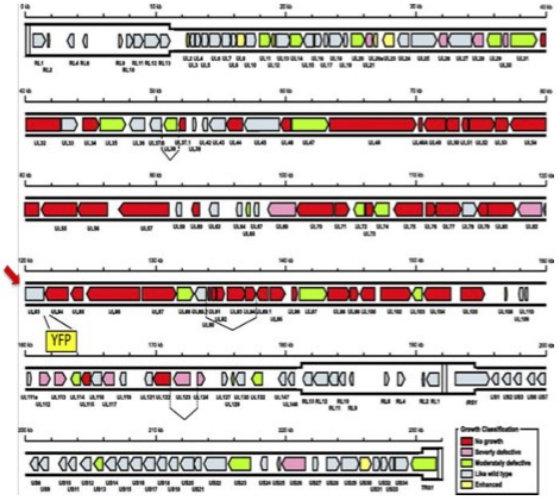

Figure 4.9

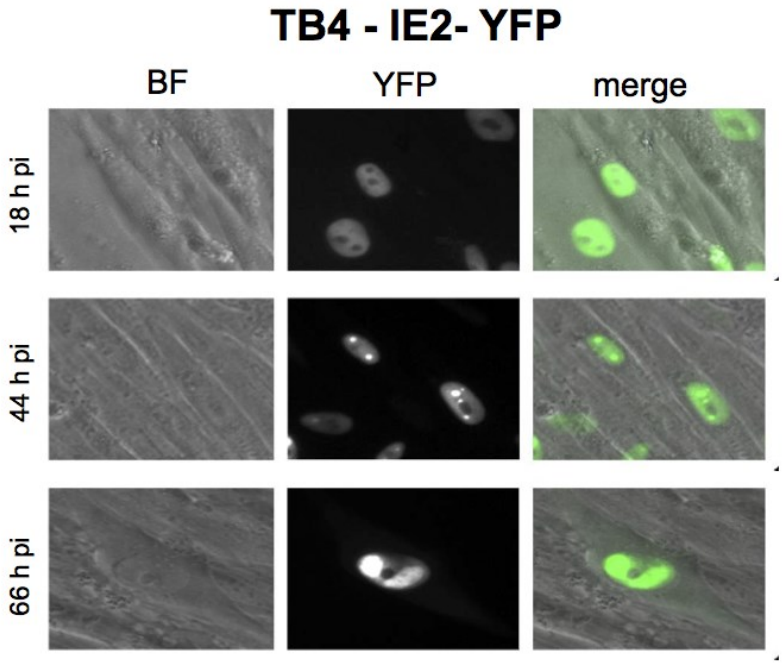
TB4 - IE2- YFP
BF
YFP
merge
18 h pi
44 h pi
66 h pi

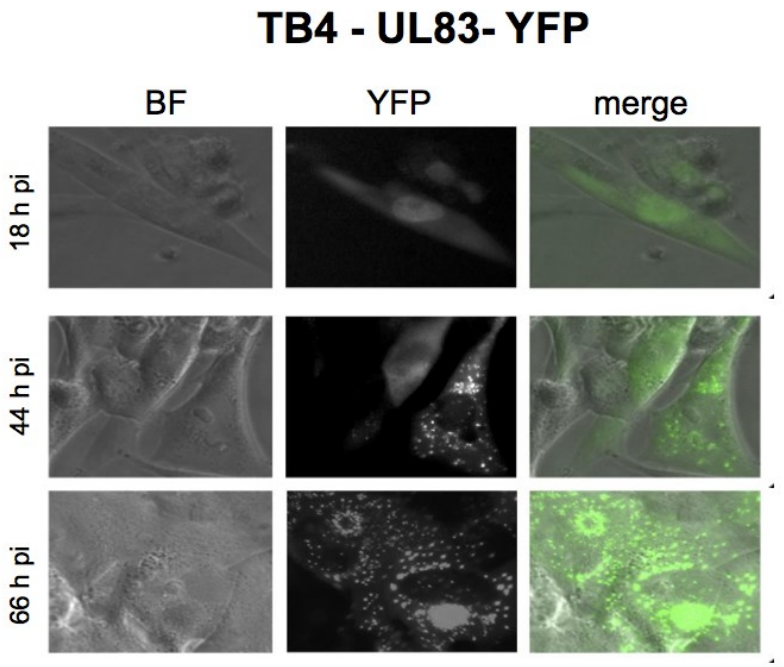
TB4 - UL83- YFP
BF
YFP
merge
18 h pi
44 h pi
66 h pi

Figure 4.10

A

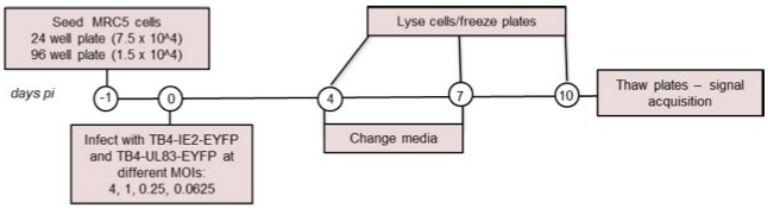

B

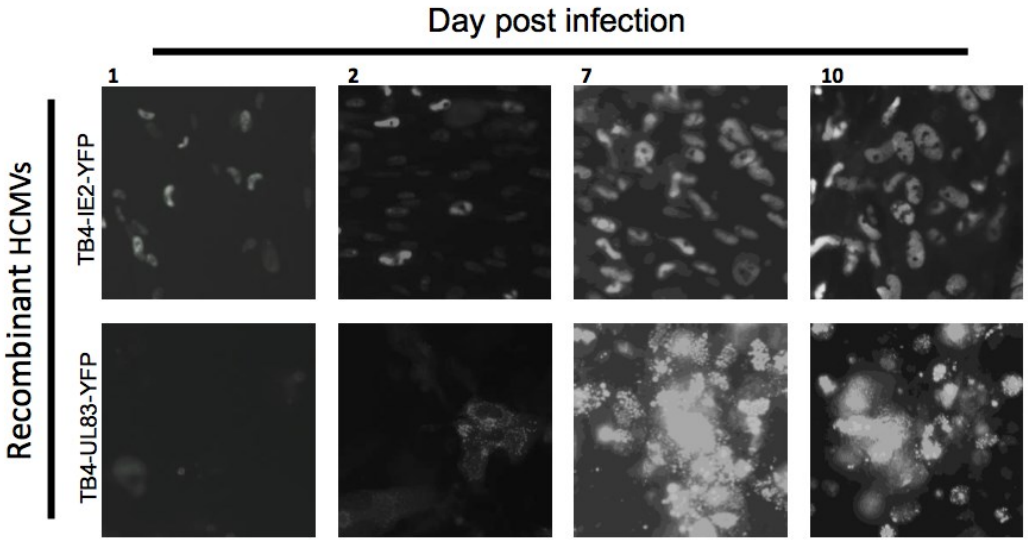

C

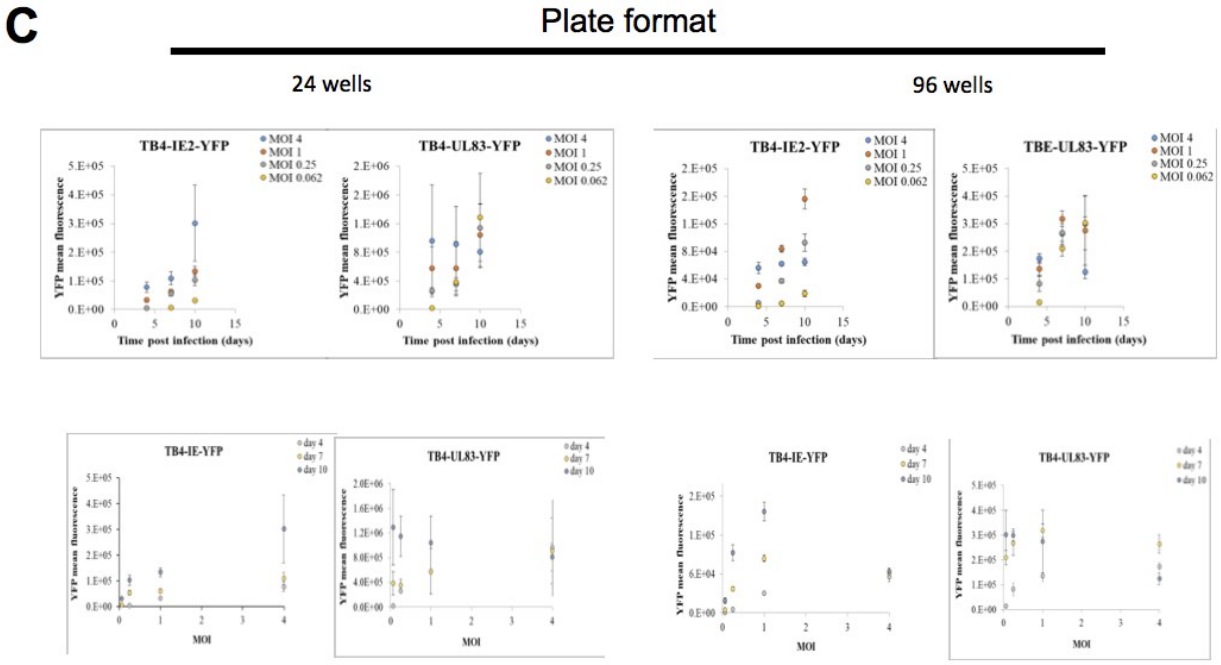

Figure 4.11

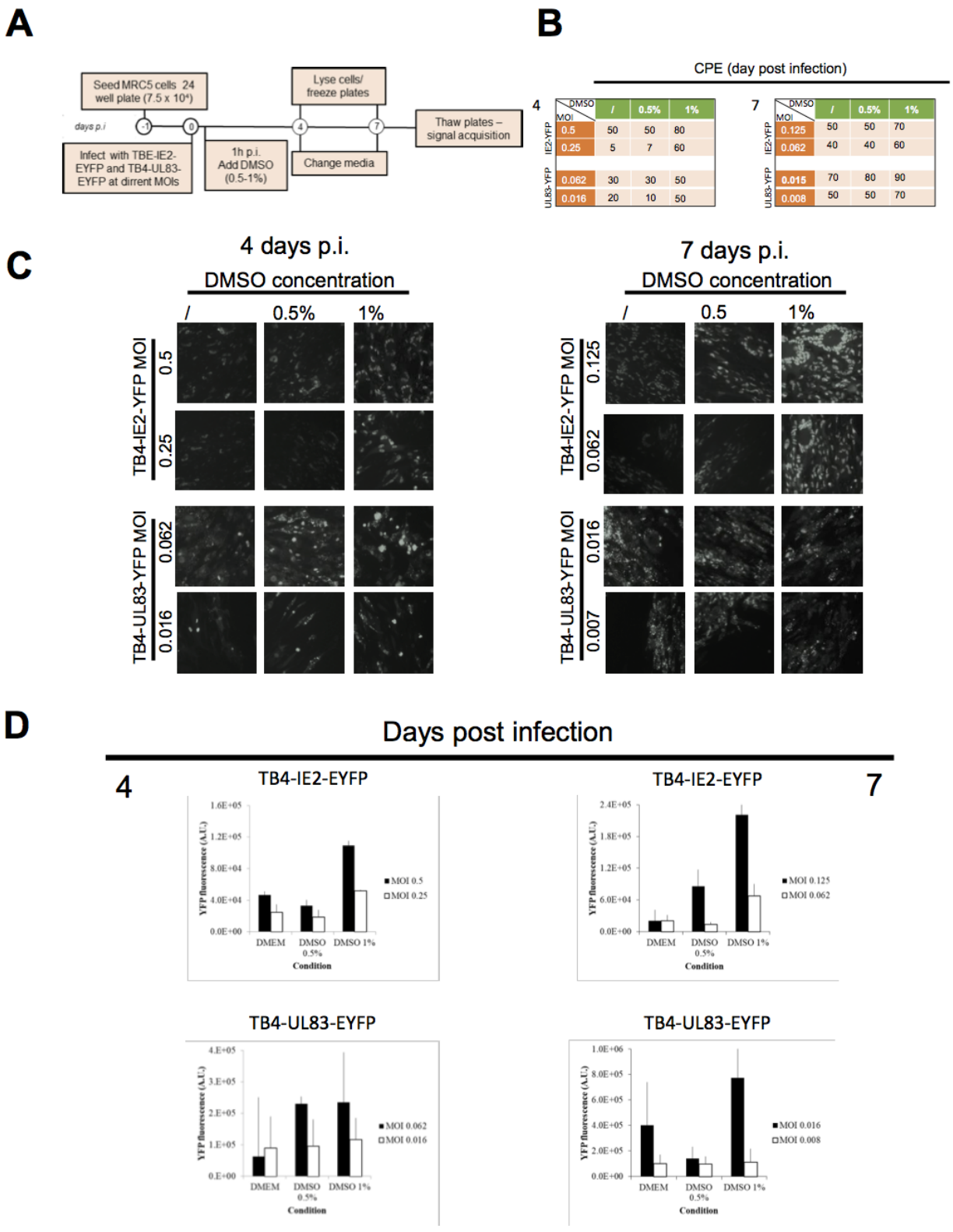
A
Seed MRC5 cells 24 well plate (7.5 x 10⁴)
Lyse cells/ freeze plates
Thaw plates – signal acquisition
days p.i
-1
0
4
7
Infect with TBE-IE2-EYFP and TB4-UL83-EYFP at dirrent MOIs
1h p.i. Add DMSO (0.5-1%)
Change media
B
CPE (day post infection)
4
DMSO
MOI
/
0.5%
1%
IE2-YFP
0.5
50
50
80
0.25
5
7
60
UL83-YFP
0.062
30
30
50
0.016
20
10
50
7
DMSO
MOI
/
0.5%
1%
IE2-YFP
0.125
50
50
70
0.062
40
40
60
UL83-YFP
0.015
70
80
90
0.008
50
50
70
C
4 days p.i.
DMSO concentration
/
0.5%
1%
TB4-IE2-YFP MOI
0.5
0.25
TB4-UL83-YFP MOI
0.062
0.016
7 days p.i.
DMSO concentration
/
0.5
1%
TB4-IE2-YFP MOI
0.125
0.062
TB4-UL83-YFP MOI
0.016
0.007
D
Days post infection
4
TB4-IE2-EYFP
YFP fluorescence (A.U.)
1.6E+05
1.2E+05
8.0E+04
4.0E+04
0.0E+00
DMEM
DMSO 0.5%
DMSO 1%
Condition
MOI 0.5
MOI 0.25
TB4-IE2-EYFP
7
YFP fluorescence (A.U.)
2.4E+05
1.8E+05
1.2E+05
6.0E+04
0.0E+00
DMEM
DMSO 0.5%
DMSO 1%
Condition
MOI 0.125
MOI 0.062
TB4-UL83-EYFP
YFP fluorescence (A.U.)
4.E+05
3.E+05
2.E+05
1.E+05
0.E+00
DMEM
DMSO 0.5%
DMSO 1%
Condition
MOI 0.062
MOI 0.016
TB4-UL83-EYFP
YFP fluorescence (A.U.)
1.0E+06
8.0E+05
6.0E+05
4.0E+05
2.0E+05
0.0E+00
DMEM
DMSO 0.5%
DMSO 1%
Condition
MOI 0.016
MOI 0.008

Figure 4.12

A

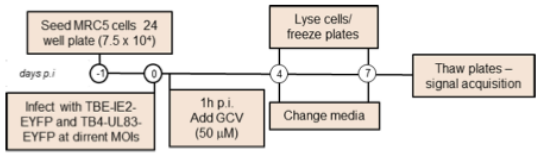

B

CPE (day post infection)

4

	MOI \ GCV	/	50µM
IE2-YFP	0.5	35	20
	0.25	25	15
UL83-YFP	0.062	50	25
	0.016	40	20

7

	MOI \ GCV	/	50µM
IE2-YFP	0.125	60	10
	0.062	40	5
UL83-YFP	0.015	70	20
	0.008	50	20

C

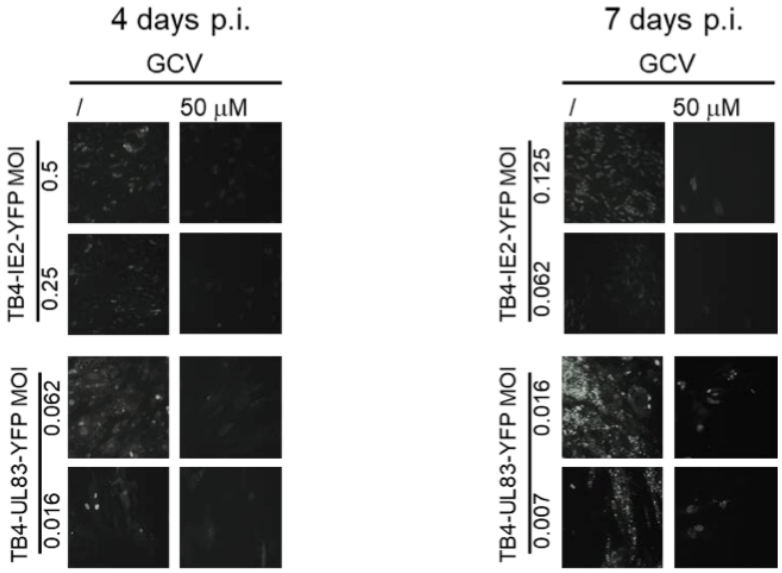

D

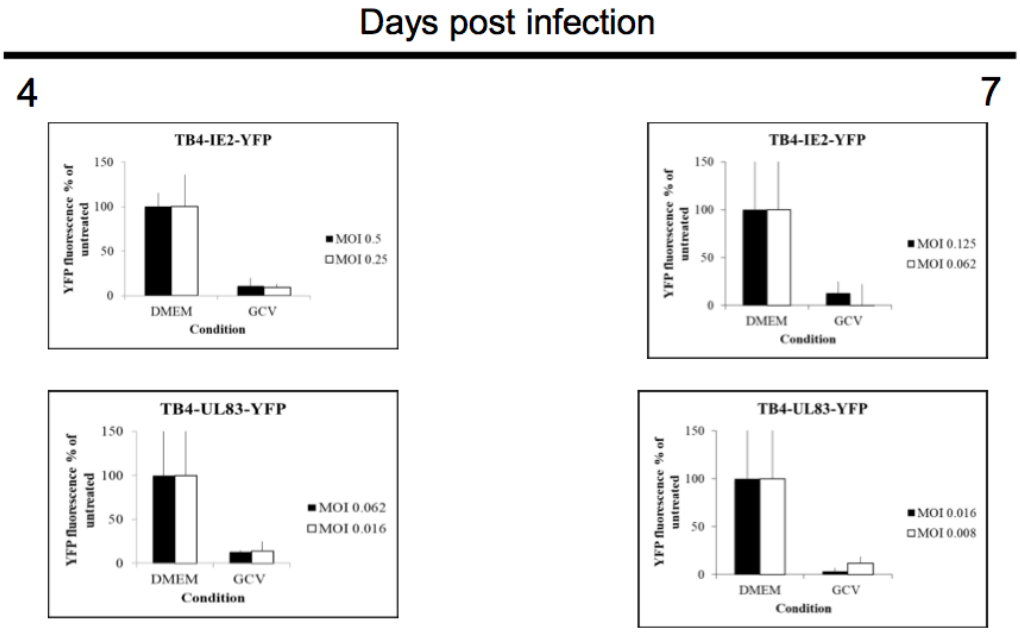

Figure 4.13

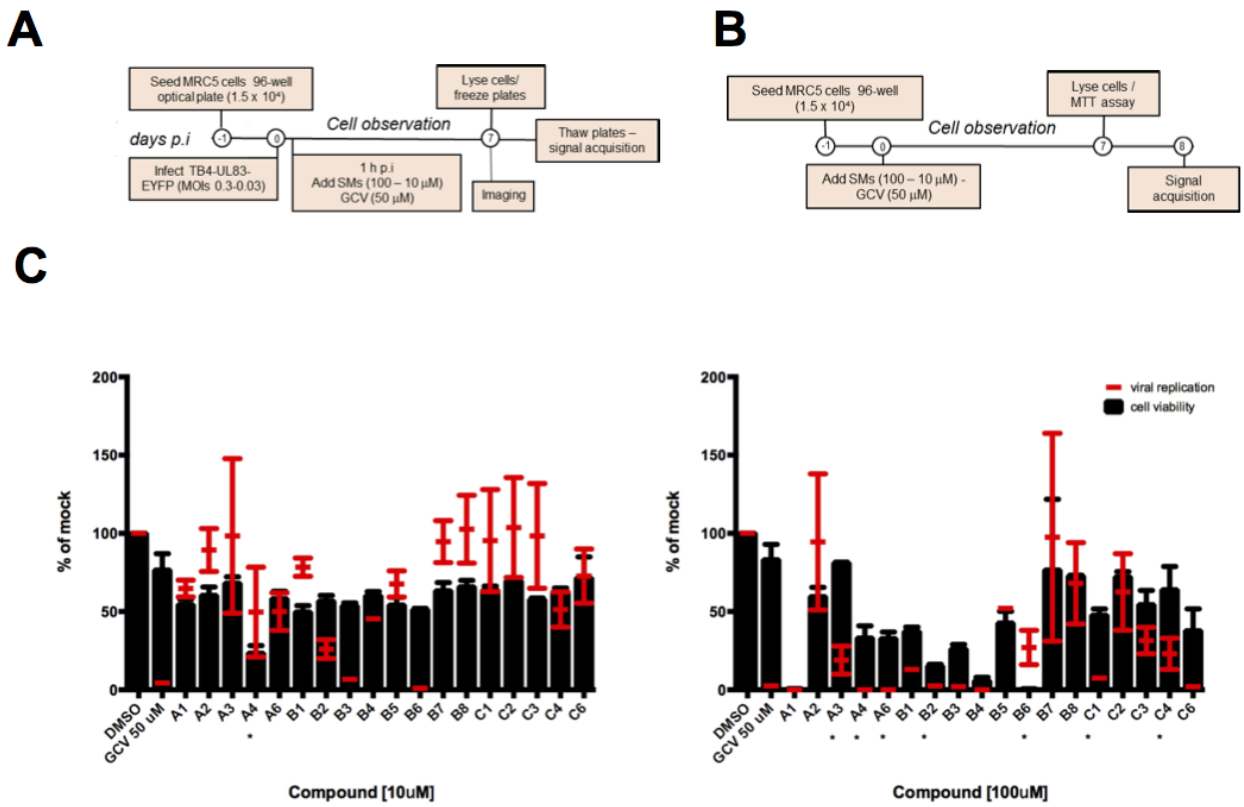
A
Seed MRC5 cells 96-well optical plate (1.5 x 10⁴)
Lyse cells/ freeze plates
Cell observation
days p.i
-1
0
7
Thaw plates – signal acquisition
Infect TB4-UL83-EYFP (MOIs 0.3-0.03)
1 h p.i Add SMs (100 – 10 µM) GCV (50 µM)
Imaging
B
Seed MRC5 cells 96-well (1.5 x 10⁴)
Lyse cells / MTT assay
Cell observation
-1
0
7
8
Add SMs (100 – 10 µM) - GCV (50 µM)
Signal acquisition
C
% of mock
200
150
100
50
0
DMSO
GCV 50 uM
A1 A2 A3 A4 A6 B1 B2 B3 B4 B5 B6 B7 B8 C1 C2 C3 C4 C6
Compound [10uM]
viral replication
cell viability
Compound [100uM]
D
TB4-UL83-YFP
DMSO 0.5%
GCV 50 µM
B3 10 µM
B6 10 µM
DMSO 0.5%
GCV 50 µM
B1 100 µM
C6 100 µM

Figure 4.14

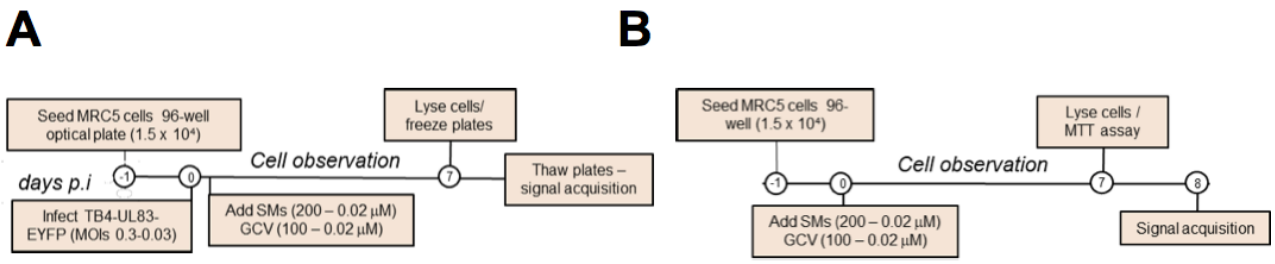
A
Seed MRC5 cells 96-well optical plate (1.5 x 10⁴)
Lyse cells/ freeze plates
Cell observation
days p.i
-1
0
7
Thaw plates – signal acquisition
Infect TB4-UL83-EYFP (MOIs 0.3-0.03)
Add SMs (200 – 0.02 µM) GCV (100 – 0.02 µM)
B
Seed MRC5 cells 96-well (1.5 x 10⁴)
Lyse cells / MTT assay
Cell observation
-1
0
7
8
Add SMs (200 – 0.02 µM) GCV (100 – 0.02 µM)
Signal acquisition

C

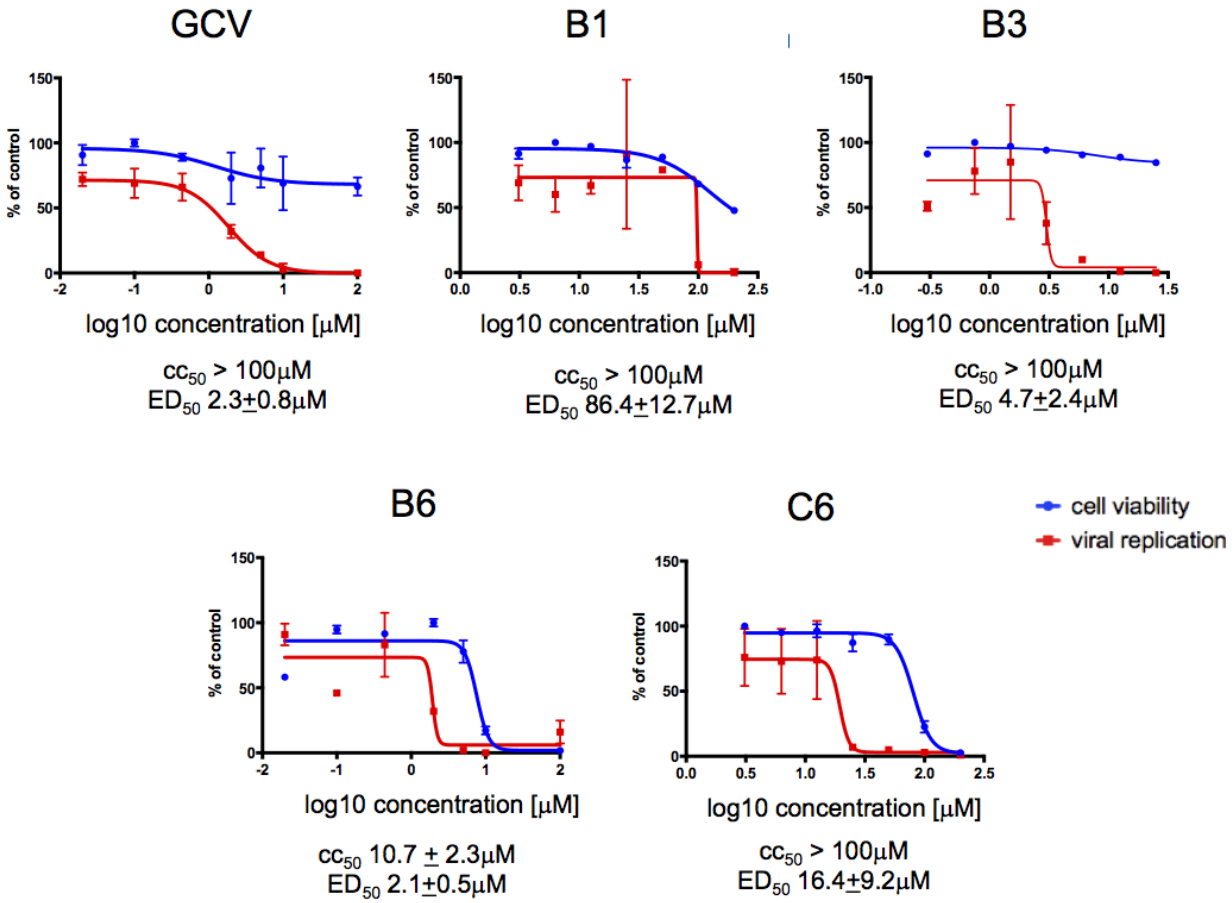
GCV
B1
B3
% of control
log10 concentration [µM]
cc50 > 100µM
ED50 2.3±0.8µM
cc50 > 100µM
ED50 86.4±12.7µM
cc50 > 100µM
ED50 4.7±2.4µM
B6
C6
cell viability
viral replication
cc50 10.7 ± 2.3µM
ED50 2.1±0.5µM
cc50 > 100µM
ED50 16.4±9.2µM

Figure 4.15

A

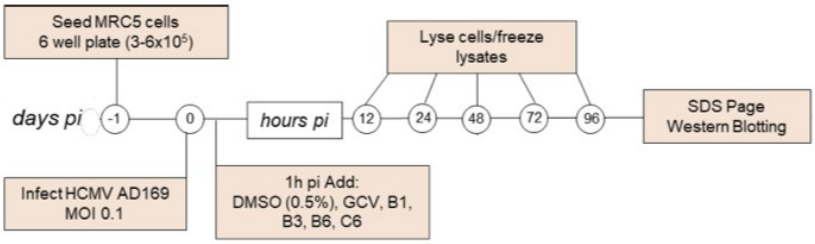

B

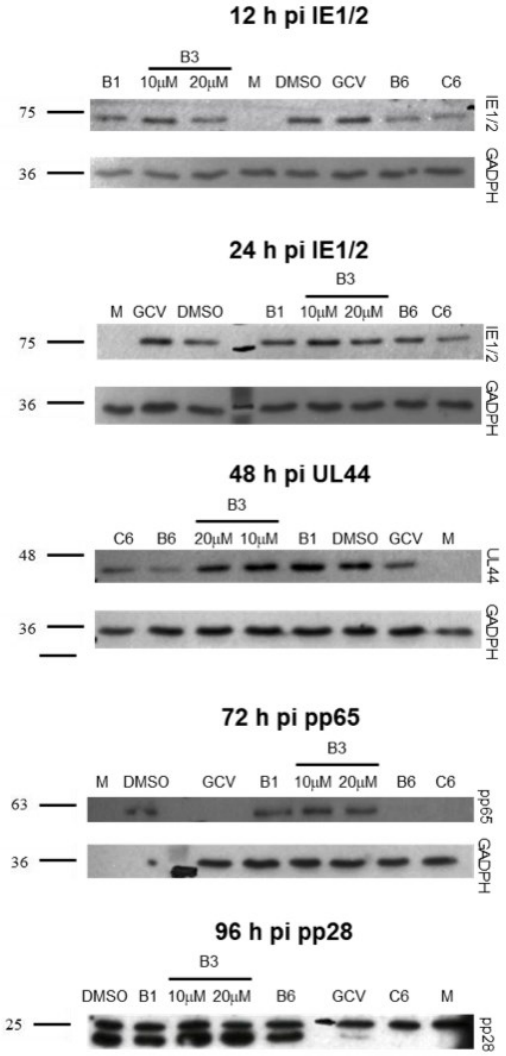

Figure 4.16

A

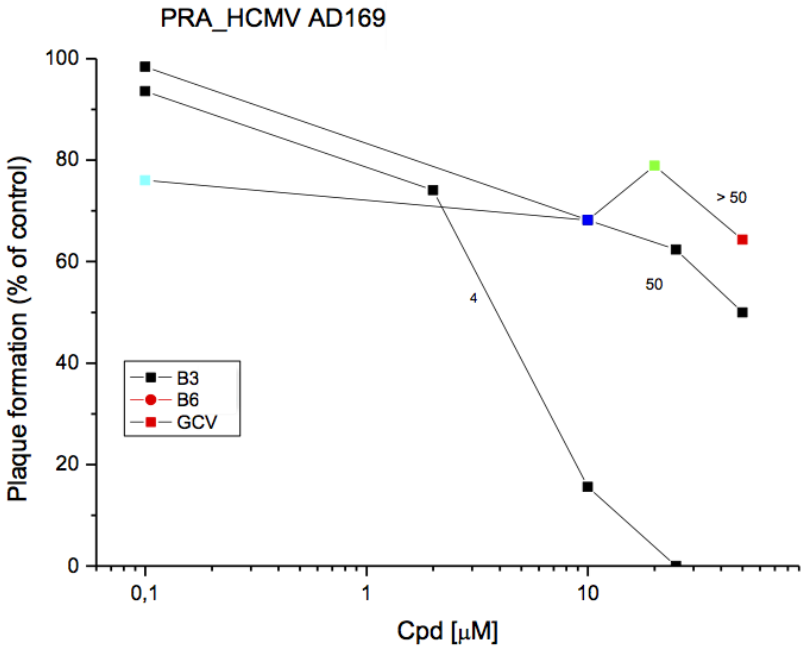

B

SMs	ED50
GCV	3 µM
B3	50 µM
B6	40 µM

Figure 4.17

A

Instrument	Filters	SYPRO Orange	Protein	Buffers
• ABI PRISM7000	• ROX • Sybr	• 0.5x • 2x • 10x	• Lysozime 5 µM • Lysozime 50 µM • Lysozime 350 µM	• KPO4 • Citrate

B

Emission filters

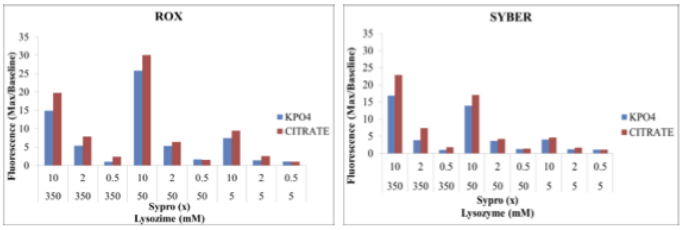

C

ROX emission filter, Citrate buffer

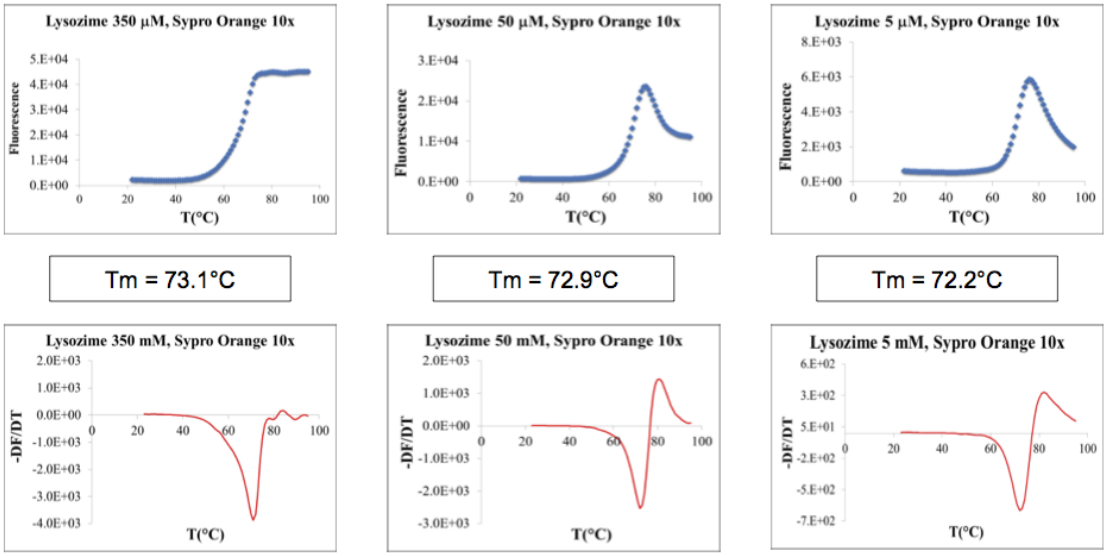

Figure 4.18

A

Instrument	Filters	SYPRO Orange	Protein	Buffers
• ABI PRISM7000	• ROX • Sybr	• 10x	• Lysozime 50 µM • 6His-UL44 1.25 µM • 6His-UL44 5 µM • 6His-UL44 20 µM	• KPO4 • Citrate

B

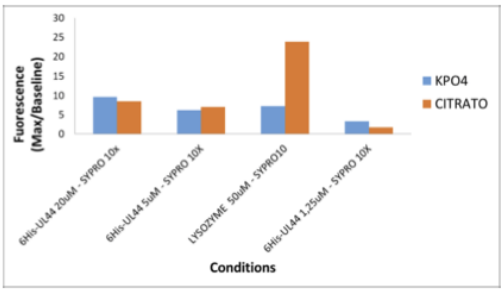

C

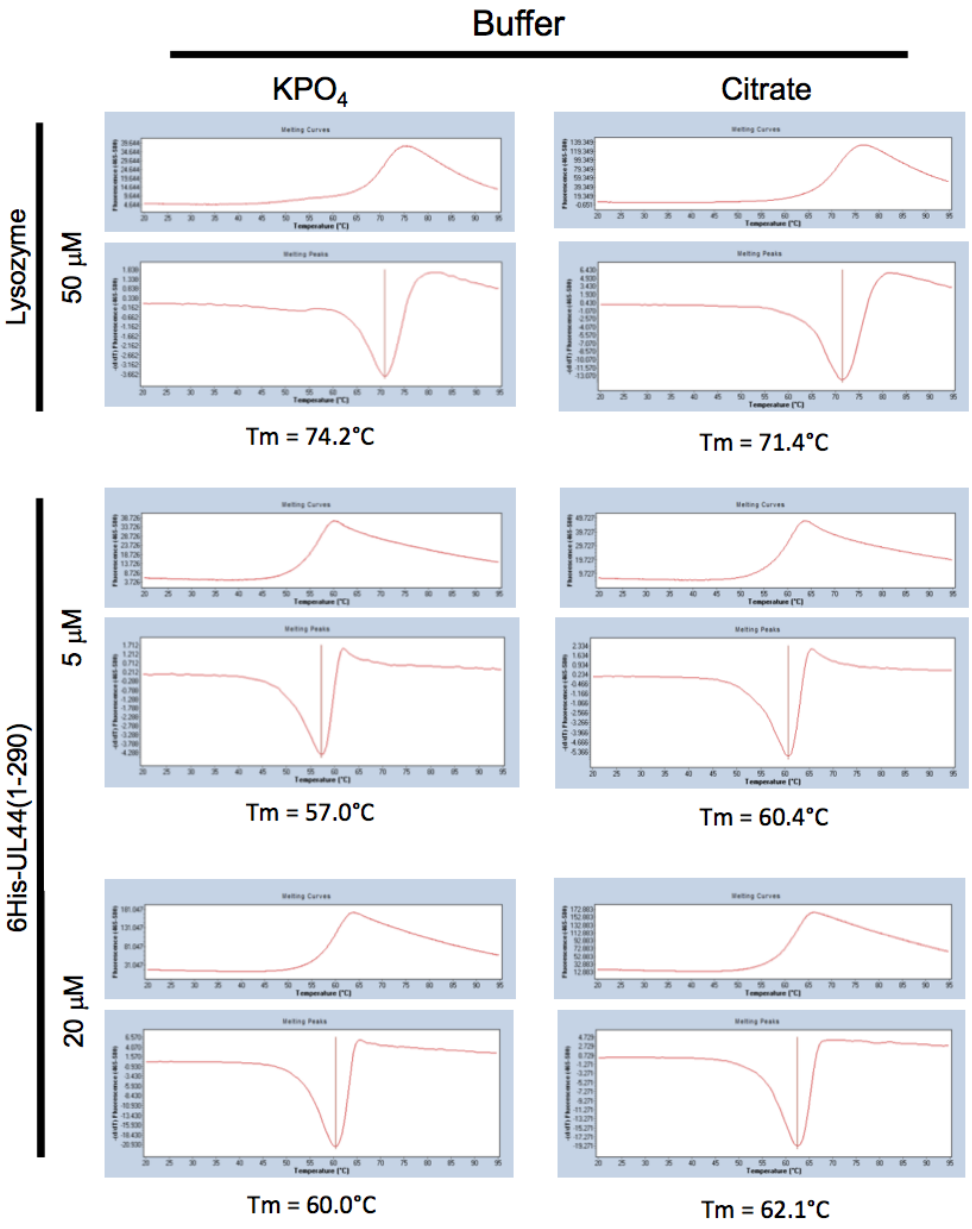

Figure 4.19

A

Instrument	Filters	SYPRO Orange	Protein	Buffers
• ABI PRISM 7000	• ROX	• 10x	• Lysozime 5 µM • 6His-UL44 5 µM	• 22 TSA Buffers

UL44 specific buffers (3)		
a) DNA polymerase stimulation buffer	b) UL54 binding buffer	c) DNA binding buffer
Other TSA buffers (19)		
Sodium Citrate (9)	**Tris-Hcl (6)**	**Bicine (4)**
d- m) pH 4 – 7 NaCl 50 – 250 uM	n – v) pH 7 – 9 NaCl 50 – 250 uM	u – z) pH 8 – 8.5 NaCl 50 – 250 uM

B

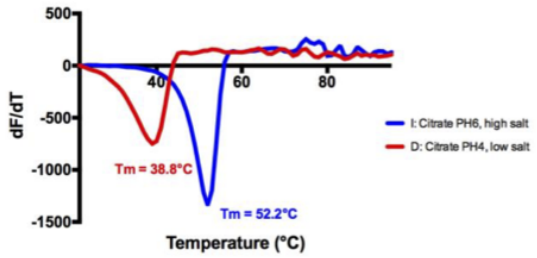

C

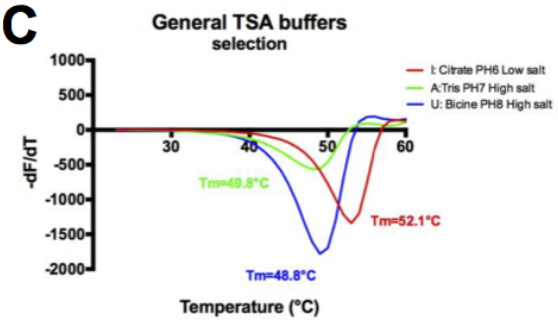

D

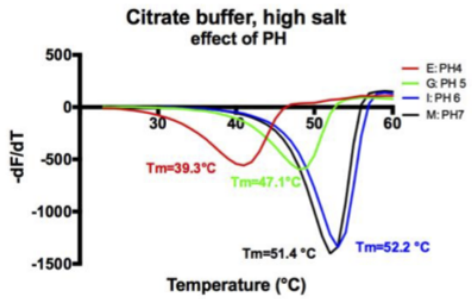

E

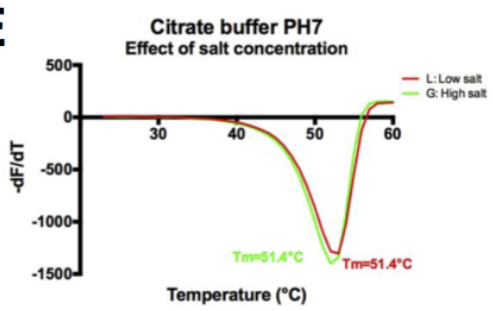

F

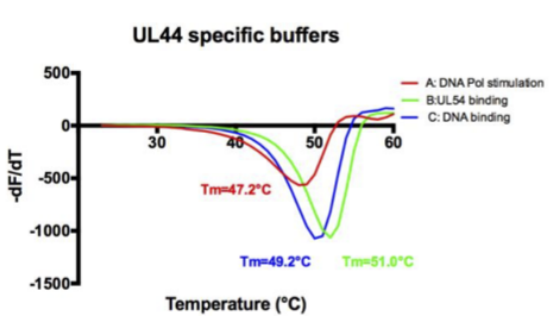

G

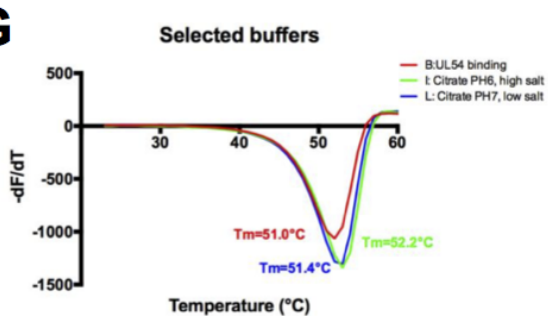

Figure 4.20

A

Instrument	Filters	SYPRO Orange	Protein	Buffers
• ABI PRISM 7000	• ROX	• 10x	• Lysozime 5 µM • 6His-UL44 WT 5 µM • UL44L86 /87A mutant 5 µM	• B • I • L

B

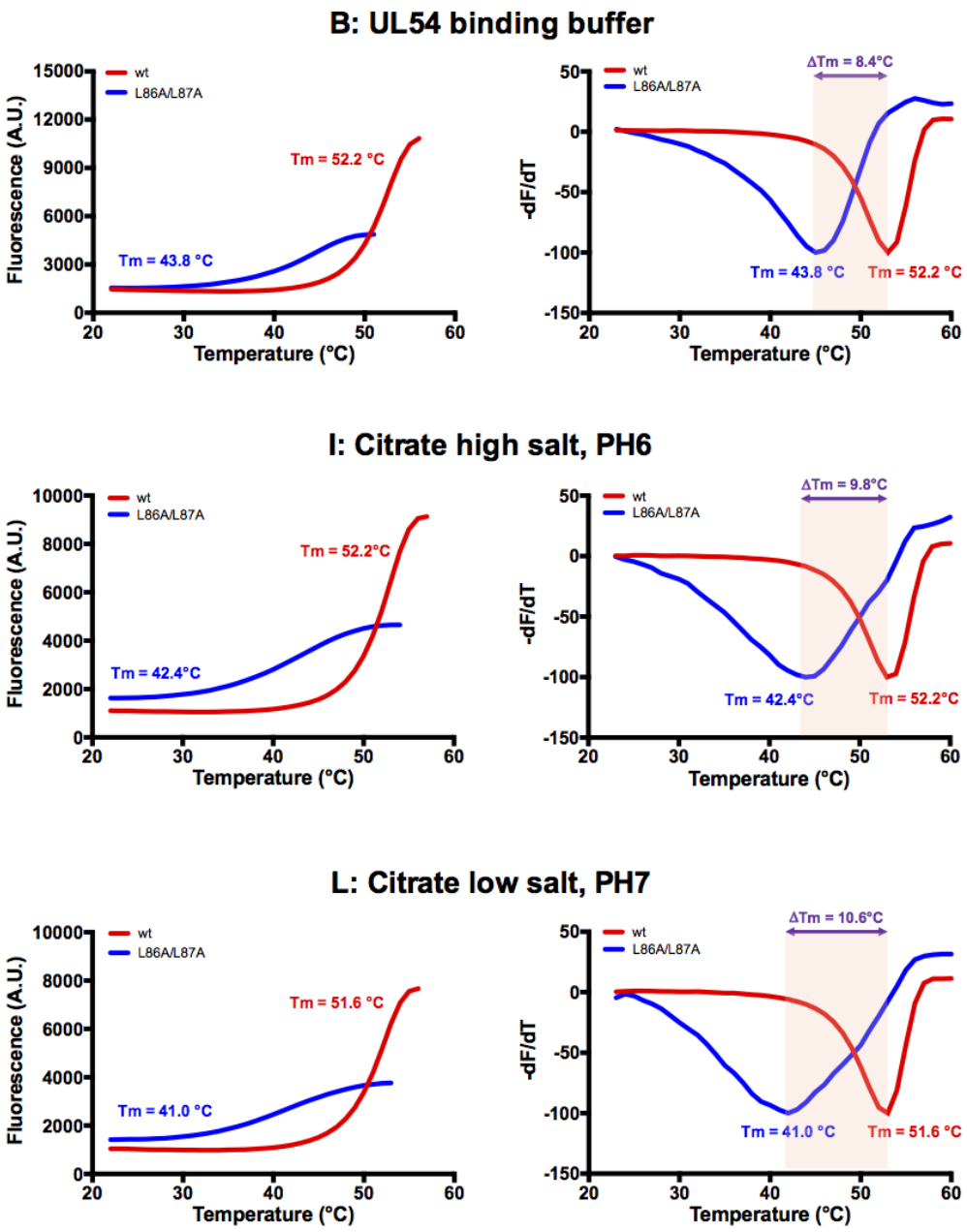

Figure 4.21

A

Instrument	Filters	SYPRO Orange	Protein	Buffers	DMSO
• ABI PRISM 7000	• ROX	• 10x	• Lysozime 5 µM • 6His-UL44 5 µM	• B • I • L	• 0.25% • 1% • 5%

B

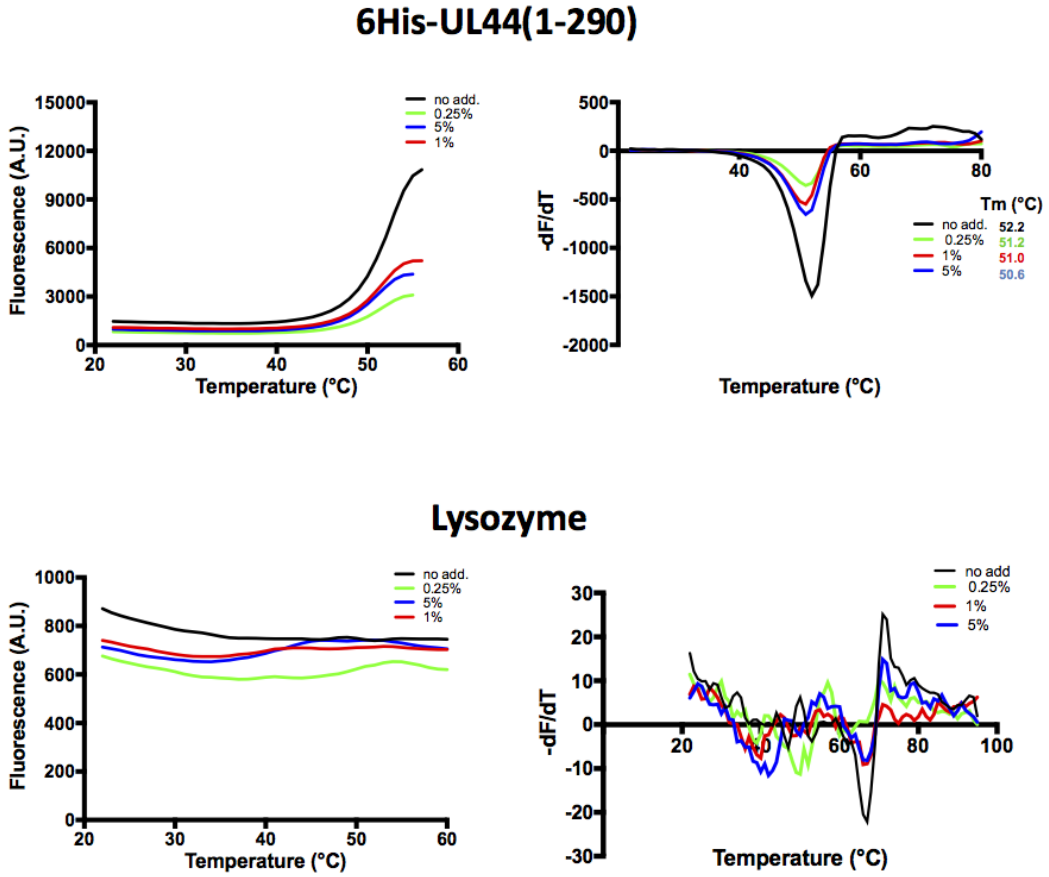

Figure 4.22

A

Instrument	Filters	SYPRO Orange	Protein	Buffers	DMSO	18 SMs
• ABI PRISM 7000	• ROX	• 10x	• Lysozime 5 µM	• B • I	• 5%	• 1 mM

B

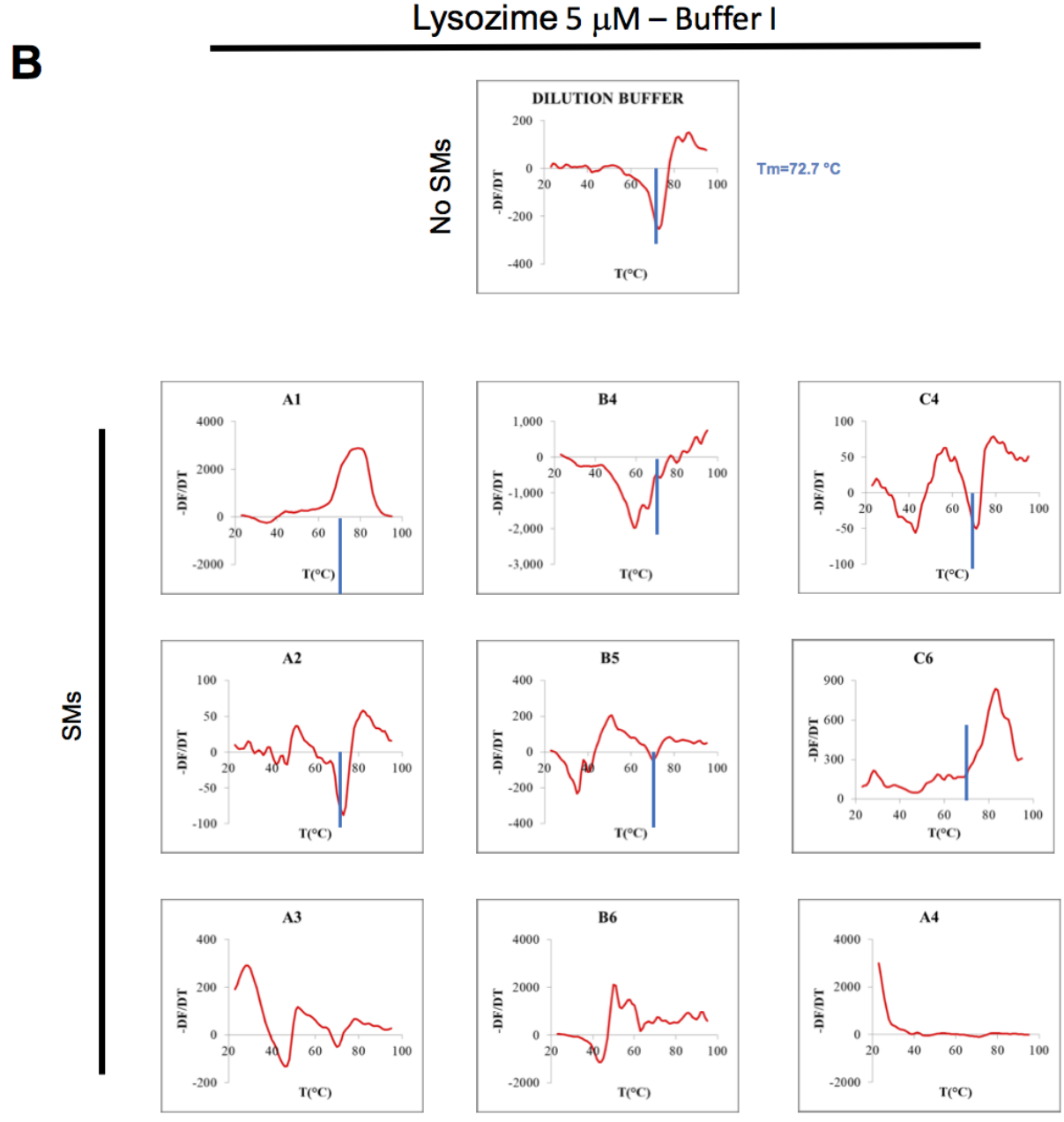

Figure 4.22

B

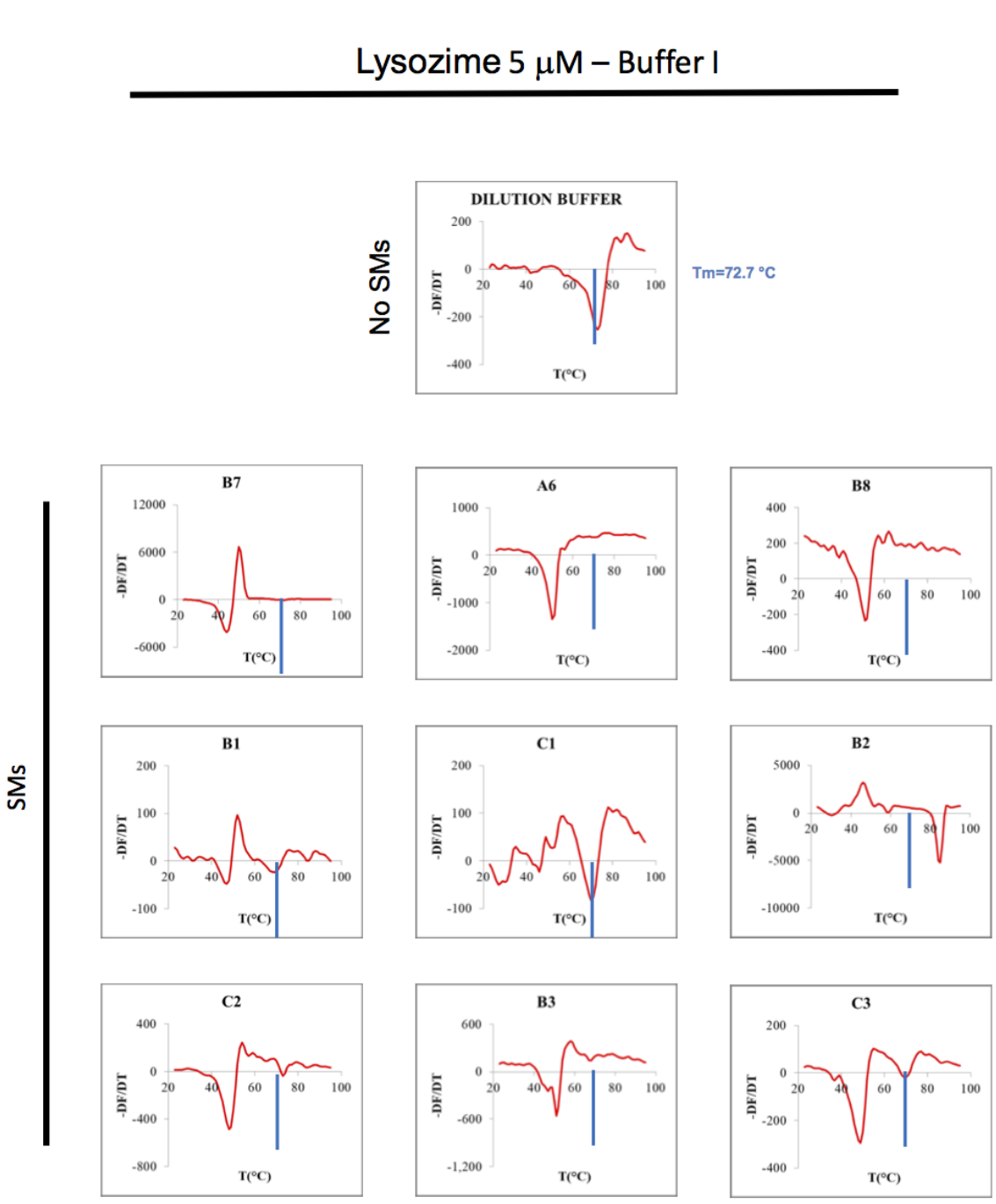
Lysozime 5 µM – Buffer I
No SMs
DILUTION BUFFER
Tm=72.7 °C
SMs
B7
A6
B8
B1
C1
B2
C2
B3
C3
-DF/DT
T(°C)

Figure 4.22

C

Lysozime 5 μM – Buffer I

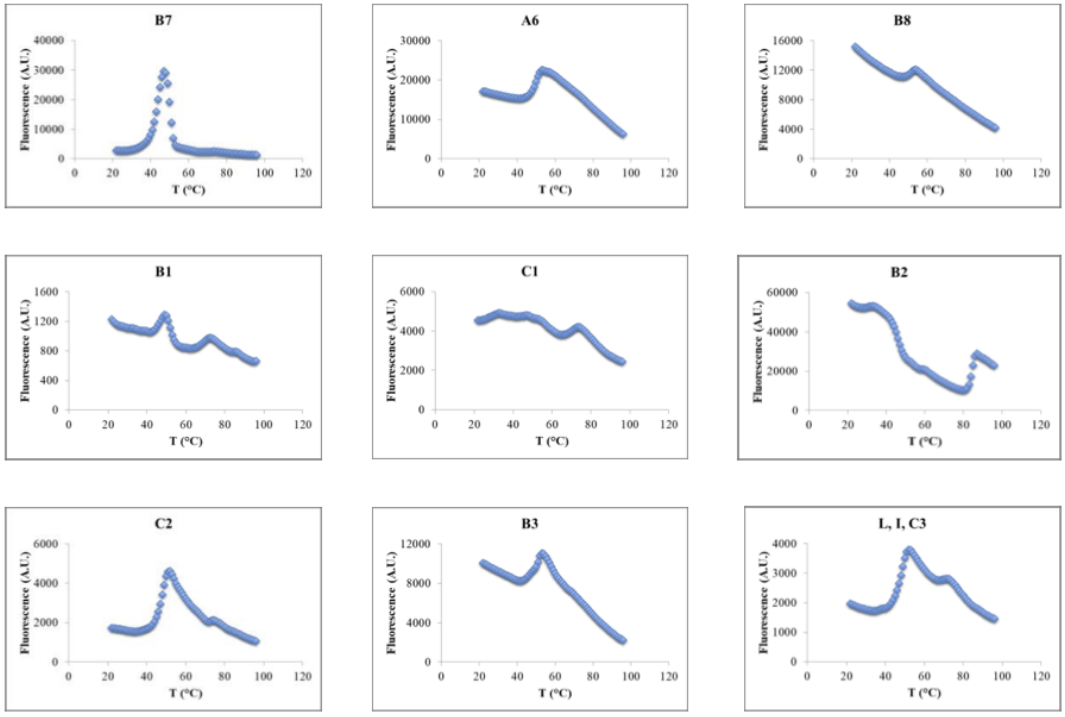

No SMs

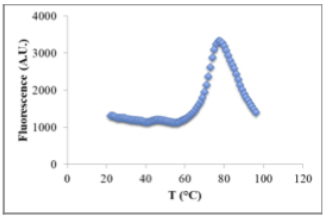

Figure 4.22

C

Lysozime 5 μM – Buffer I

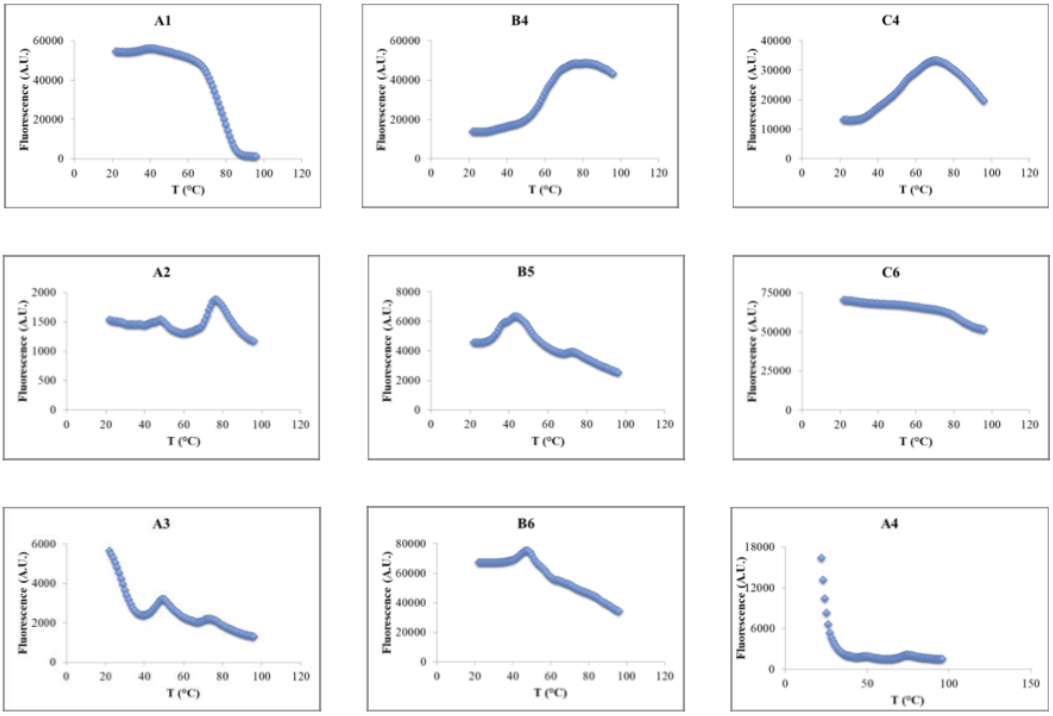

No SMs

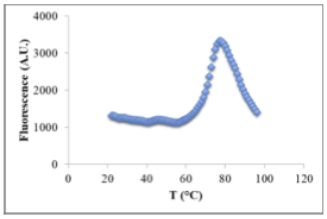

Figure 4.22

D

No Lysozime

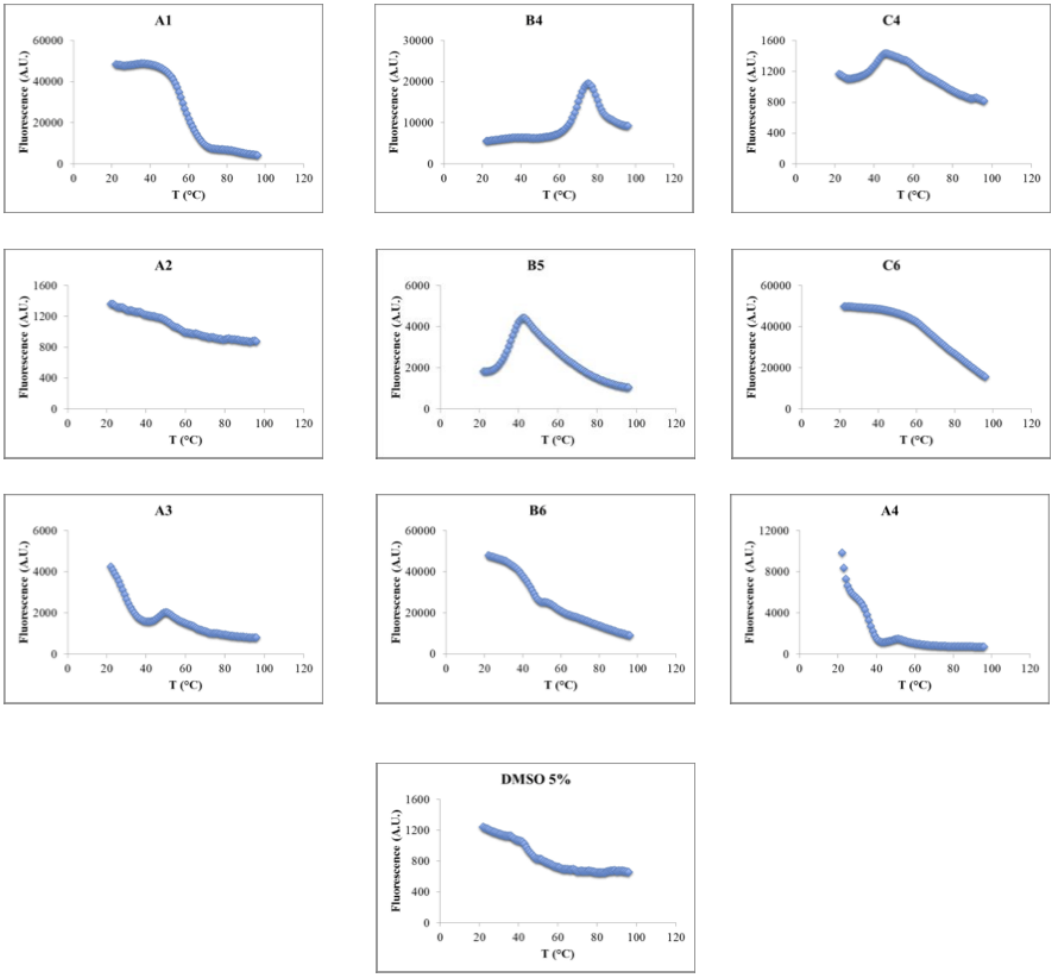

Figure 4.23

A

Instrument	Filters	SYPRO Orange	Protein	Buffers	DMSO	4 SMs
• ViiA 7	• Excitation: 470,520,580 nm • Emission: • 520,586,623,682 nm	• 10x	• Lysozime 5 µM	• I	• 2%	• 200 µM • 100 µM • 50 µM • 25 µM

B

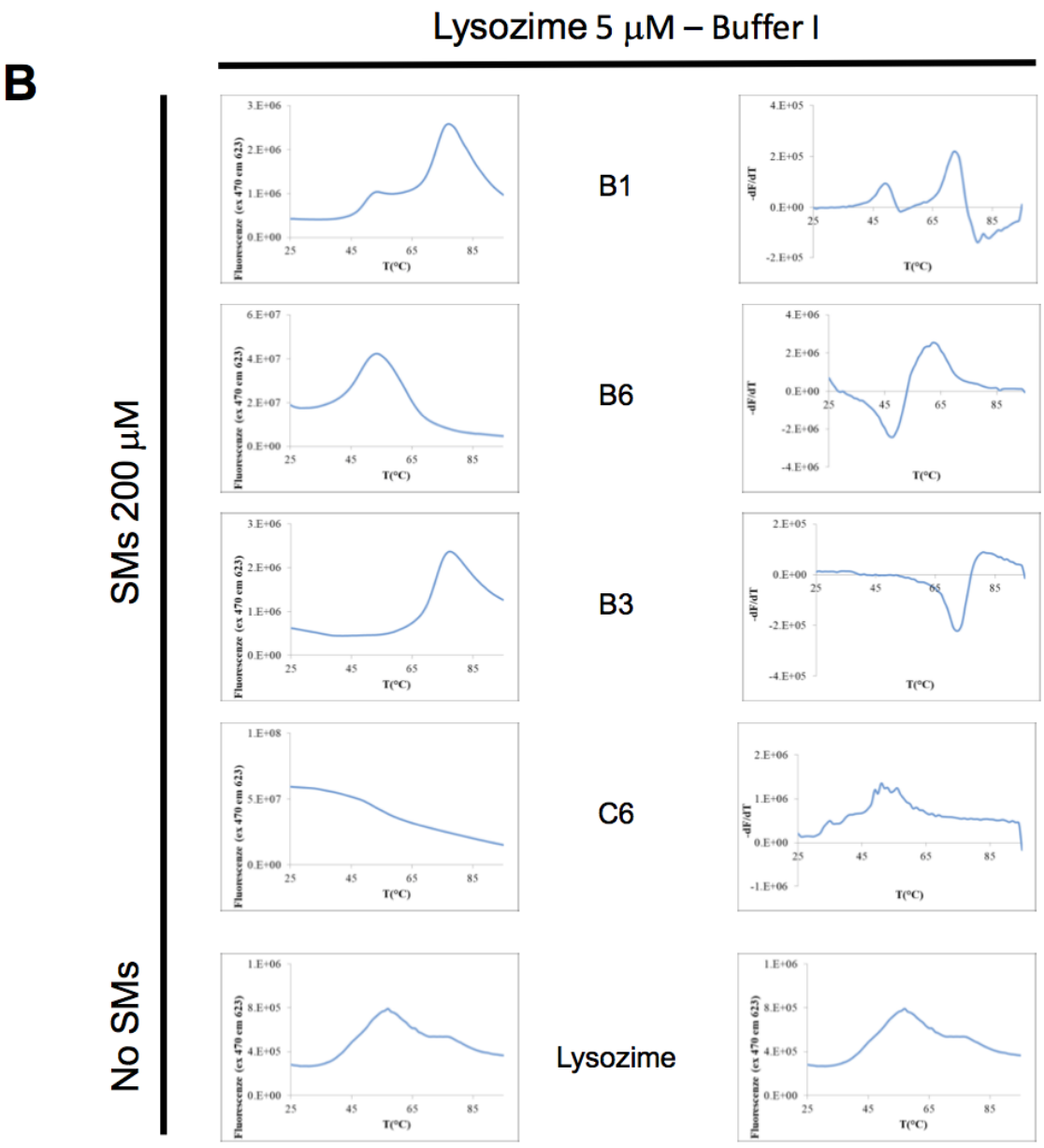

Figure 4.23

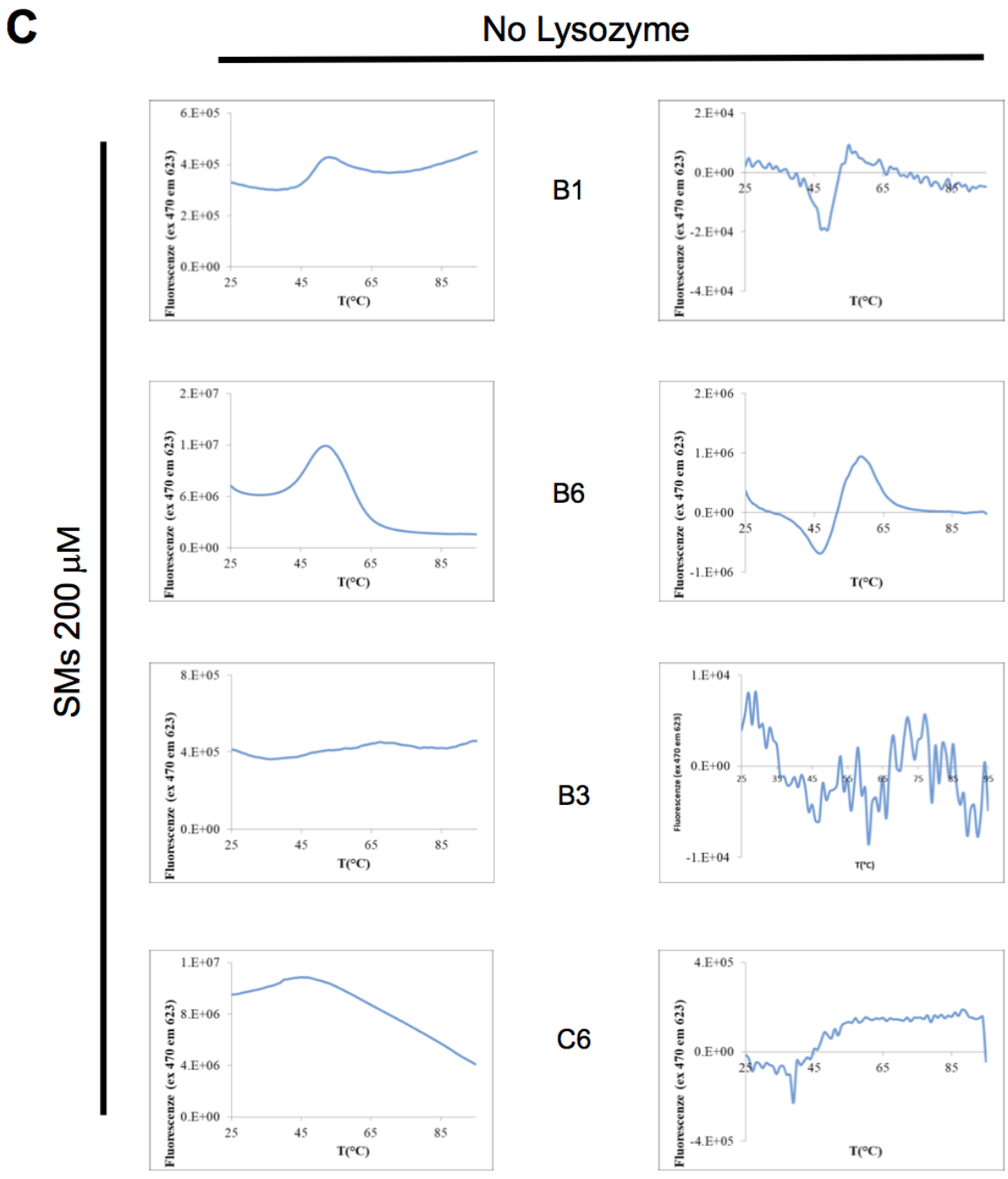
C
No Lysozyme
SMs 200 µM
B1
B6
B3
C6
Fluorescenze (ex 470 em 623)
T(°C)

Figure 4.23

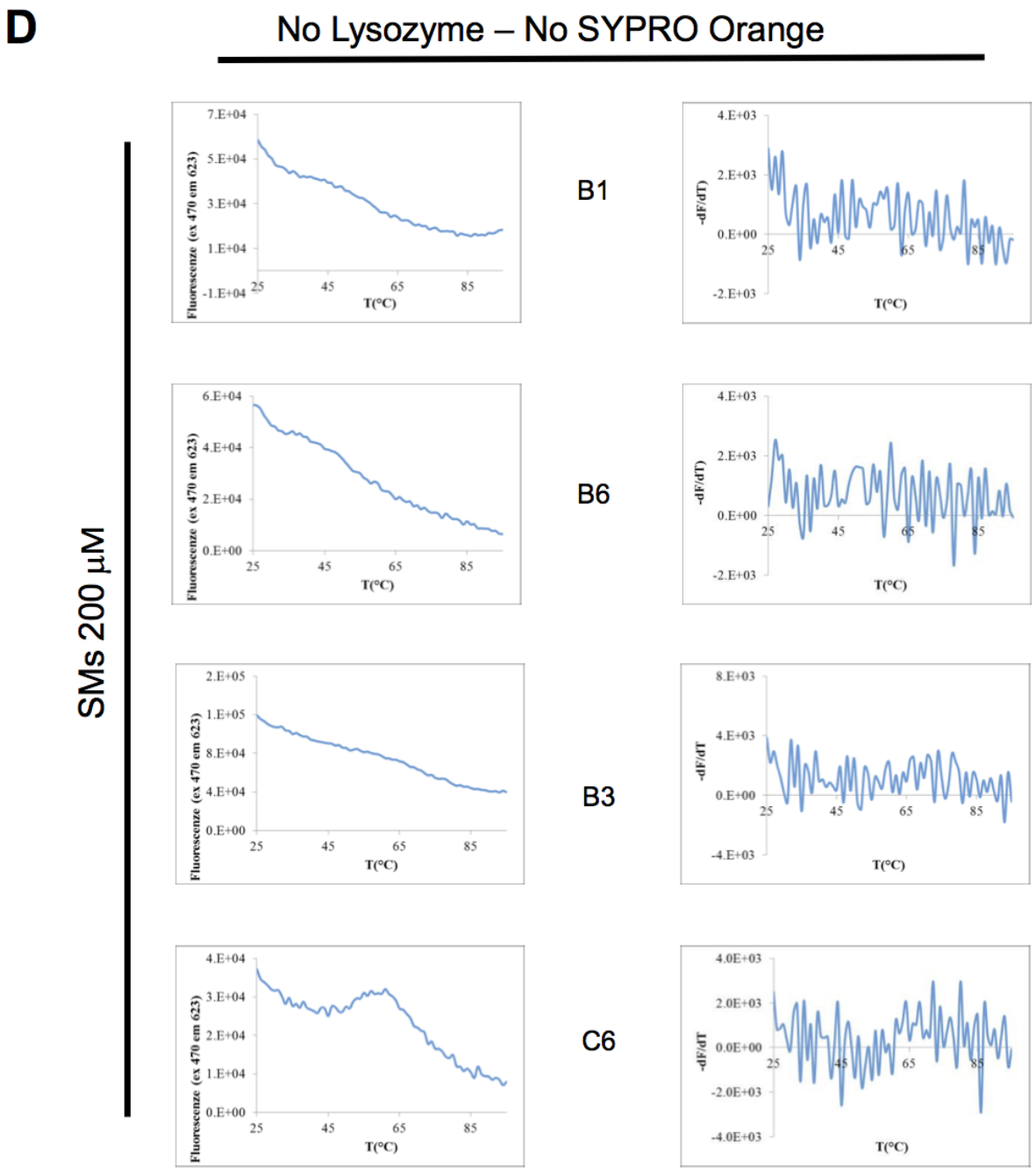
D
No Lysozyme – No SYPRO Orange
SMs 200 µM
B1
B6
B3
C6
Fluorescenze (ex 470 em 623)
-dF/dT
T(°C)

Figure 4.24

A

Instrument	Filters	SYPRO Orange	Protein	Buffers	DMSO	2 SMs
• ViiA 7	• Excitation: 470,520,580 nm • Emission: 520,586,623,682 nm	• 10x	• Lysozime 5 µM • 6His-UL44	• I	• 2%	• 200 µM • 100 µM

B

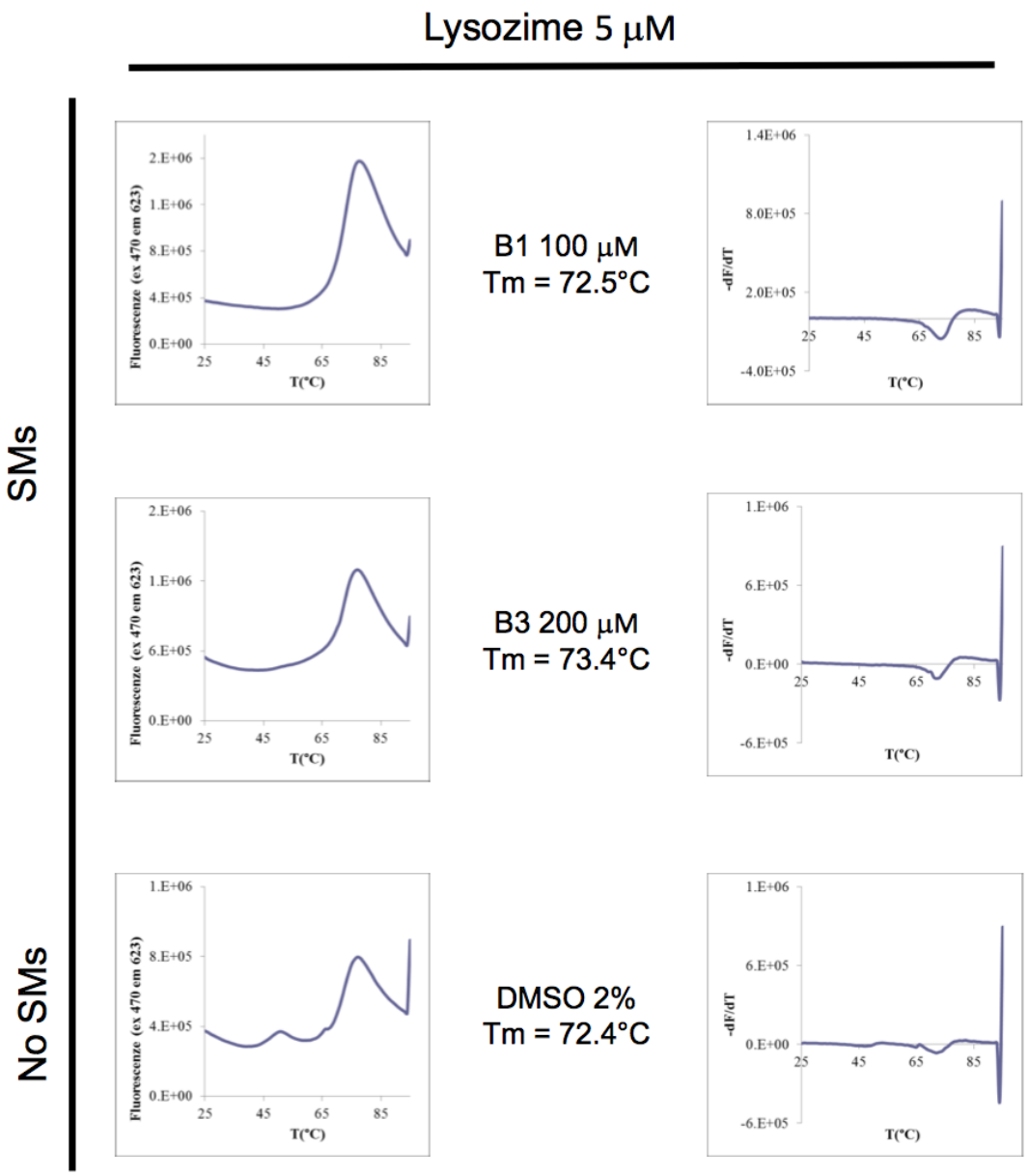

Figure 4.24

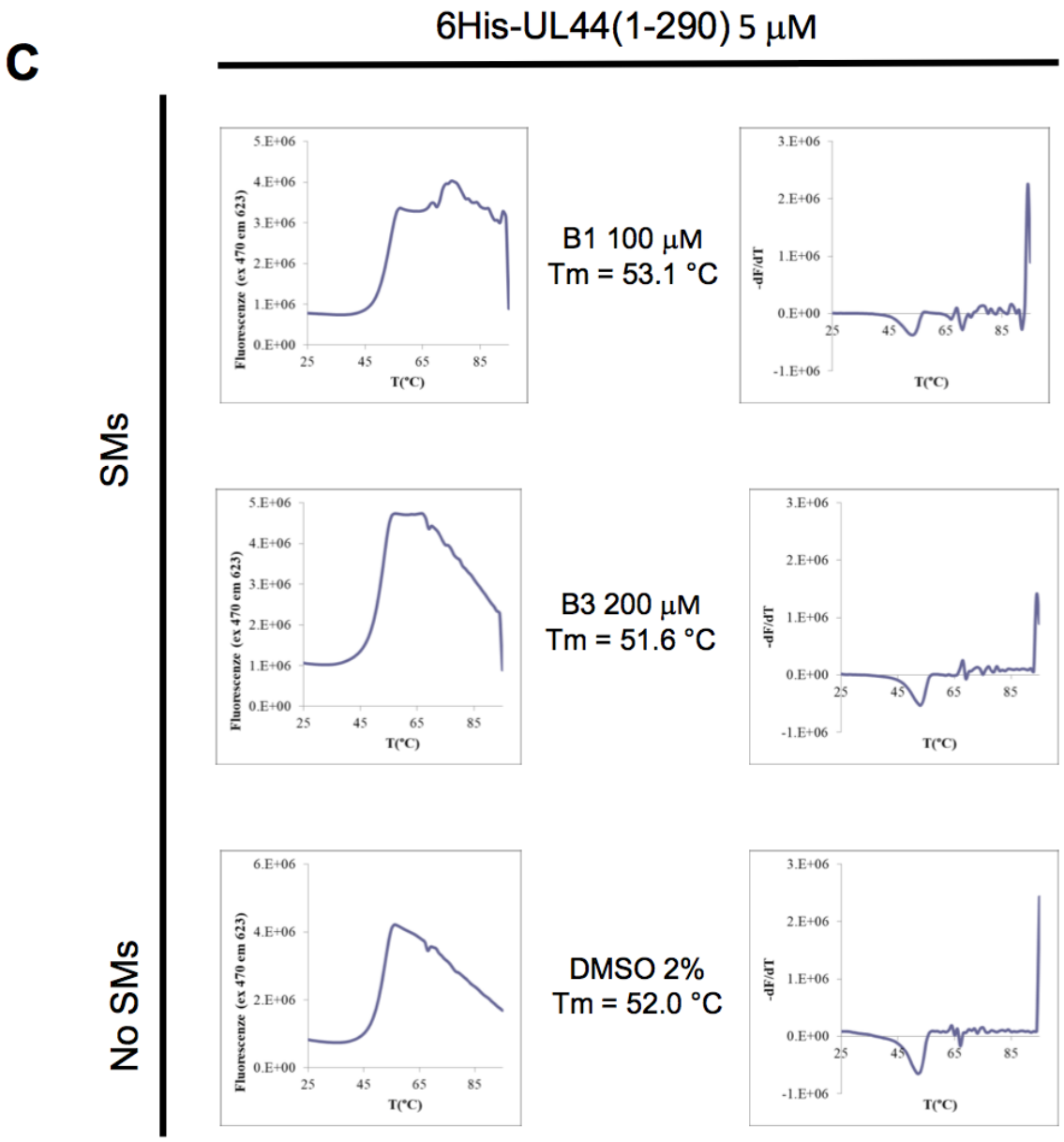
C
6His-UL44(1-290) 5 µM
SMs
No SMs
Fluorescenze (ex 470 em 623)
T(°C)
-dF/dT
B1 100 µM
Tm = 53.1 °C
B3 200 µM
Tm = 51.6 °C
DMSO 2%
Tm = 52.0 °C

Table 4.1

24H	CELL VIABILITY visual analysis	CELL VIABILITY CC50	PRECIPITATES visual analysis
A1	25 µM	52.1 µM	
A2	100 µM	>100 µM	
A3	50 µM	76.5 µM	
A4	1.56 µM	NA	
A6	50 µM	>100 µM	
B1	100 µM	>100 µM	
B2	6.25 µM	20.3 µM	6.25 µM
B3	100 µM	>100 µM	
B4*	6.25 µM	NA	
B5	100 µM	>100 µM	
B6	12.5 µM	16.3 µM	
B7	12.5 µM	NA	
B8	50 µM	>100 µM	
C1	12.5 µM	NA	12.5 µM
C2	100 µM	>100 µM	
C3	50 µM	>100 µM	
C4	100 µM	>100 µM	6.25 µM
C6	100 µM	>100 µM	

72H	CELL VIABILITY visual analysis	CELL VIABILITY CC50	PRECIPITATES visual analysis
A1	12.5 µM	47.5 µM	
A2	100 µM	NA	
A3	12.5 µM	15.2 µM	
A4	3.12 µM	7.4 µM	
A6	25 µM	62.5 µM	
B1	25 µM	43.7 µM	
B2	25 µM	50 µM	25 µM
B3	100 µM	>100 µM	
B4*	12.5 µM	NA	
B5	25 µM	NA	
B6	12.5 µM	25.2 µM	
B7	12.5 µM	NA	
B8	25 µM	>100 µM	
C1	25 µM	33.2 µM	12.5 µM
C2	100 µM	NA	
C3	100 µM	>100 µM	
C4	100 µM	NA	6.25 µM
C6	25 µM	>100 µM	

140H	CELL VIABILITY visual analysis	CELL VIABILITY CC50	PRECIPITATES visual analysis
A1	12.5 µM	28.5 µM	
A2	25 µM	43.27 µM	
A3	12.5 µM	29.2 µM	
A4	6.25 µM	8.9 µM	
A6	25 µM	73.3 µM	
B1	100 µM	43.7 µM	
B2	12.5 µM	25.4 µM	25 µM
B3	50 µM	68.3 µM	
B4*	12.5 µM	NA	
B5	100 µM	38.9 µM	
B6	12.5 µM	22.6 µM	
B7	12.5 µM	41.8 µM	
B8	50 µM	100 µM	
C1	25 µM	30.3 µM	12.5 µM
C2	100 µM	37.45 µM	
C3	50 µM	>100 µM	
C4	100 µM	30.2 µM	6.25 µM
C6	50 µM	49 µM	

7. Table and figures legends

Figure 4.1. Study of UL44 dimerization by GST-pull down. The indicated recombinant proteins were used for GST-pull down assays as described in the Materials and Methods section. A proportional amount of the indicated fractions (FT, flowthrough; W, last wash; E, elutions) was loaded on tris Acrylammide gels and processed by SDS-PAGE/western blotting to reveal the presence of 6His-UL44(1-290) fusions.

Figure 4.2. Study of effect of the 18 SMs on UL44-dimerization by GST-pulldown assays. . GST-UL44(1-290) and 6His-UL44(1-290) were incubated in the presence (50 μM) or in the absence of the 18 SMs, in DMSO 0.25% and subjected to GST-pulldown assays. Each elutions (E1, E2, E3, E4) were evaluated by SDS page/Western blotting. A representative Western blot image relative to incubation of the membranes with αGST or α6His antibodies is shown. K- = control mixture incubated in the absence of SMs, loaded in duplicate to allow estimation of lane to lane variations. All Western Blot images are shown in Appendix (A1-3).

Figure 4.3. Schematic representation of the effect of the 18 SMs on UL44-dimerazation obtained in two repetitions of GST-pulldown assay. Images such as those shown in Figure 4.2 or in A1-4 were analysed with Image analysis to compare the extent of eluted 6His-UL44 in the presence or in the absence of the SMs, based on the criteria reported in the Materials and Methods section. Each box represents the outcome of one repetition, relative to the 6His-UL44 band. Red boxes, (++); yellow boxes (+); green boxes, (=); pale blue boxes (-); dark blue boxes (- -).

Figure 4.4 Only SMs B5 and C4 inhibit the formation of the complex. GST-UL44(1-290) and 6His-UL44(1-290) were incubated in the presence (50 μM) or in the absence of the indicated SMs, in DMSO 0.25% and subjected to GST-pulldown assays and SDS page/Western blotting. (A) Western blot image relative to incubation of the membranes with αGST or α6His antibodies is shown. K- = control mixture incubated in the absence of SMs, loaded in triplicate to allow estimation of lane to lane variations. (B) Digital images such as shown in (A) were quantified as described §3.3.1. Data shown represent the mean of two independent experiments relative to the detection of the GST (black boxes) or 6His (gray boxes) UL44(1-290) fusion proteins.

Figure 4.5. Lack of dose-response relationship between the inhibition of 6His-UL44 elution and the concentration of SM used. GST-UL44(1-290) and 6His-UL44(1-290) were incubated in the presence or in the absence of increasing concentrations of the indicated SMs, in DMSO 0.25% and subjected to GST-pulldown assays and SDS page/Western blotting. (A) Representative Western blot images relative to incubation of the membranes with α6His and αGST antibodies are shown. K- = control mixture incubated in the absence of SMs, loaded in triplicate to allow estimation of lane to lane variations. (B) Digital images such as shown in (A) were quantified as described §3.3.1. Data shown represent the mean of three independent experiments relative to the detection of the 6His-UL44 fusion protein for each of the indicated SMs.

Figure 4.6. Preliminary assessment of the antiviral and cytotoxic effects of 5 SMs selected on HCMV replication. (A) HFF cells were infected with AD169 for 2h. Subsequently the indicated compounds were added at different concentrations, and PRA assays performed (§3.5). The number of plaques counted relative to each condition, expressed as a percentage of those counted relative to the untreated, is shown. (B) ED50 and CC50 values of each SMs tested by PRA and MTT assay

that were performed in parallel. CC50 values derived from the mean of three repetitions. ED50 derived from the mean of two repetitions.

Figure 4.7. Optimization of MTT assays conditions. (A) MRC5 cells were seeded in 96-well plates, and incubated for 24, 72 and 140 h before being processed for MTT assays. A specific number of cells was seeded in the first column, and then serially diluted 1:2 in DMEM in order to ensure a twofold dilution of the seeded cell number in each column of the plate, resulting in a different cell range for plates to be processed at the different time points. Each plate was then incubated for 1, 2 or 4 h with the chromogenic substrate, before being processed for MTT assays as described in the Materials and Methods section. (B) The absorbance at 620 nm relative to each condition was plotted against the seeded cell number and linear regression calculated. The cell number resulting in the highest signal which still assured linearity between the two parameters was chosen for subsequent assays and is circled in red. (C) Data relative to the 2h incubation time with the chromogenic substrate were plotted as in *panel B*, after exclusion of values relative to cell numbers higher than those selected for further experiments. Linear regression values are shown.

Figure 4.8. Schematic representation of reporter viruses used in this study. The genetic organization of the TB4-IE2-EYFP (A) and TB4-UL83-EYFP (B) recombinant fluorescent viruses and the presence of the YFP fusion tag located at the C-terminus of the respective fusion proteins are shown.

Figure 4.9. Live cell imaging of MRC5 cells infected with TB4-IE2-EYFP and TB4-UL83-EYFP. MRC5 cells were infected with TB4-IE2-EYFP (MOI 0.25-0.06) and TB4-UL83-EYFP (MOI 1-0.4) and were observed using an epifluorescence inverted microscope equipped with a 40x objective as described in the Materials and Methods section at the indicated time point p.i.

Figure 4.10. Optimization of Fluorescence Reduction Assay (FRA) conditions. (A) Different number of MRC5 cells were seeded either in 96 well special optical plates or in 24-well plates and infected with TB4-IE2-EYFP and TB4-UL83-EYFP at different MOIs. At the indicated time points cells were processed for either microscopic analysis or fluorimetric quantification, as indicated. (B) Digital images representative of cells infected with the indicated recombinant HCMVs are shown. Images were acquired using a 20x objective and either 8s or 2s acquisition times for the 1-2 or 7-10 days p.i samples, respectively. (C) YFP signals relative to HCMV infected cells were quantified using a plate reader. Data were exported to excel and analyzed to calculate the mean fluorescence relative to each condition. To this end, the average signal relative to the mock infected samples was subtracted to the signal relative to every well. Data shown are mean $\pm$ standard deviation of the mean relative to a single experiment performed in triplicate, whereby the YFP mean fluorescence is plotted against the time post infection (*top panels*) or the MOI (*bottom panels*).

Figure 4.11 Effect of DMSO on viral replication. (A) 7.5 x 10^4/well MRC5 cells were seeded in a 24-wells plate and infected with TB4-IE2-EYFP and TB4-UL83-EYFP at different MOIs. At the indicated time points CPE was evaluated, and cells were processed for either microscopic analysis or fluorimetric quantification, as indicated. (B) The percentage of cells with morphological alterations caused by viral replication for the indicated conditions are shown. (C) Digital images representative of cells infected with the indicated recombinant HCMVs are shown. Images were acquired using a 20x objective and an acquisition time of the 3 sec (D). YFP signals relative to HCMV infected cells were quantified using a plate reader. Data were exported to excel and analyzed to calculate the mean fluorescence relative to each condition. To this end, the average signal relative to the mock infected samples was subtracted to the signal relative to every well. Data shown are mean $\pm$ standard deviation of the mean relative to a single experiment performed in triplicate.

Figure 4.12 Assessment of the antiviral effect of GCV on HCMV replication by FRA. (A) 7.5 x 10^4/well MRC5 cells were seeded in a 24-wells plate and infected with TB4-IE2-EYFP and TB4-UL83-EYFP at different MOIs. One h p.i viral incula were removed and either cpt DMEM of DMEM containing GCV (50 μM) was added to infected cells. At the indicated time points CPE was evaluated, and cells were processed for either microscopic analysis or fluorimetric quantification, as indicated. (B) The percentage of cells with morphological alterations caused by viral replication for the indicated conditions are shown. (C) Digital images representative of cells infected with the indicated recombinant HCMVs are shown. Images were acquired using a 20x objective and an acquisition time of 3 sec. (D). YFP signals relative to HCMV infected cells were quantified using a plate reader. Data were exported to excel and analyzed to calculate the mean fluorescence relative to each condition. To this end, the average signal relative to the mock infected samples was subtracted to the signal relative to every well. Data shown are mean ± standard deviation of the mean relative to a single experiment performed in triplicate.

Figure 4.13. Identification of SMs inhibiting HCMV replication. (A) 1.5 x 10^4 MRC5 cells were seeded in 96 well special optics black microplates in duplicate, and infected with TB4-UL83-EYFP at a moi of 0.03-0.003. One h p.i DMEM containing either DMSO 0.5% or two different concentrations (100 and 10 μM) of each SMs with a 0.5% DMSO final concentration was added. GCV (50 μM) was included as control. Cells were monitored daily using an inverted fluorescent microscope for development of CPE, formation of precipitates and presence of fluorescent signal. Seven days p.i cells were lysed and plates processed for fluorimetric analysis using a plate reader. (B) 1.5 x 10^4 MRC5 cells were seeded in clear flat bottom 96 wells tissue culture plates in duplicate. The day after cells were treated with either DMSO 0.5% or with two different concentrations (100 and 10 μM) of each SMs with a 0.5% DMSO final concentration. GCV (50 μM) was included as control. (C) YFP signals relative to HCMV infected cells were quantified using a plate reader. Data were exported to excel and analyzed to calculate the mean fluorescence relative to each condition. To this end, the average signal relative to the mock infected samples was subtracted to the signal relative to every well. Mean values relative to each condition were expressed as a percentage of DMSO treated cells are shown as *black bars*. Cell viability was assessed by MTT assays, and data expressed as a percentage of DMSO treated cells are shown as *red bars*. The mean ± S.E.M relative to 3 independent experiments is shown. * = presences of precipitates. (D) Digital images representative of cells infected with the TB4-UL83-YFP HCMV and treated as indicated are shown. Images were acquired using a 20x objective and an acquisition time of 3 sec.

Figure 4.14. Evaluation of ED50 and CC50 of 4 SMs by FRA and MTT assay. (A) 1.5 x 10^4 MRC5 cells were seeded in 96 well special optics black microplates in duplicate, and infected with TB4-UL83-EYFP at a moi of 0.03-0.003. One h p.i DMEM containing either DMSO 0.5% or increasing concentrations (0.02-200 μM) of the indicated compounds in 0.5% DMSO final concentration was added. Cells were monitored daily using an inverted fluorescent microscope for development of CPE, formation of precipitates and presence of fluorescent signal. Seven days p.i cells were lysed and plates processed for fluorimetric analysis using a plate reader. (B) 1.5 x 10^4 MRC5 cells were seeded in clear flat bottom 96 wells tissue culture plates in duplicate. The day after cells were treated with either DMSO 0.5% or with increasing concentrations (0.02-200 μM) of each SMs with a 0.5% DMSO final concentration. (C) YFP signals relative to HCMV infected cells were quantified using a plate reader. Data were exported to excel and analyzed to calculate the mean fluorescence relative to each condition. To this end, the average signal relative to the mock infected samples was subtracted to the signal relative to every well. Mean values, expressed as a percentage of DMSO treated cells are shown as *red squares*. Cell viability was assessed by MTT

assays, and data expressed as a percentage of DMSO treated cells are shown as *blue circles*. For calculation of ED50 and CC50, data were exported to Graphpad Prism, compounds concentration data transformed to logarithmic and fitted to a 4 Parameter Logistic Equation (Sigmoidal).

Figure 4.15. Evaluation of HCMV gene expression by Western Blot assays. (A) MRC5 cells were seeded on 6-well plates. The following day, cells were infected with HCMV (strain AD169) at MOI 0.1 in DMEM at 37°C. One h p.i cells were incubated with the indicated SMs. At the indicated time points cells were lysed and 30 μg separated by SDS-Page Western Blotting to allow detection of the indicated fusion proteins. (B) Representative Western blot images relative to incubation with the indicated antibodies. Compounds were added at the following concentrations: B1 100 μM, B3 20 μM, B6 5 μM, C6 40 μM, GCV 5 μM.

Figure 4.16. Assessment of the antiviral and cytotoxic effects of B3 and B6 on HCMV replication. (A) HFF cells were infected with AD169 for 2h. Subsequently the indicated compounds were added at different concentrations, and PRA assays performed as described in the Material and Methods section. The number of plaques counted relative to each condition, expressed as a percentage of those counted relative to the untreated, is shown. (B) ED50 derived from the mean of two repetitions.

Figure 4.17. Development of a TSA protein stability using ABI PRISM 7000. (A) Lysozyme and SYPRO Orange were diluted to the indicated final concentrations, either in Potassium Phosphate (KPO_4) or in Citrate Phosphate (Citrate) buffers. Mixtures were loaded on 96-well white plates, before being loaded on a ABI PRISM7000 thermal cycler. Plates were heated from 22 to 95 °C at approximately 1°C/min, and fluorescence data were acquired either with ROX or SYBR emission filters. (B) Data were exported to Excel and analyzed to calculate the Maximum (Max)/Baseline Fluorescence ratios relative to each of the indicated conditions. (C). Fluorescence data (*top panels*) or -dF/dT ratios (*bottom panels*) relative to the indicated conditions were plotted as a function of the temperature. Data were analyzed with GraphPad Prism to calculate the Tm after deletion of post-peak fluorescence using the Boltzman Sigmoidal Fit Function.

Figure 4.18. Optimization of 6His-UL44 concentration for TSAs. (A) Lysozyme and 6His-UL44(1-290) were diluted to the indicated final concentrations in SYPRO Orange 10x, either in Potassium Phosphate (KPO_4) or in Citrate Phosphate (Citrate) buffers. Mixtures were loaded on 384-well white plates, before being loaded on a Roche 480 lightcycler. Plates were heated from 22 to 95 °C using the *Protein Melting* program, and fluorescence emitted at 560 nm was acquired following excitation at 460 nm. (B) Data were exported to Excel and analyzed to calculate the Maximum (Max)/Baseline Fluorescence ratios relative to each of the indicated conditions. (C). Fluorescence data (*top panels*) or -dF/dT ratios (*bottom panels*) relative to the indicated conditions were plotted as a function of the temperature. Data were analyzed with GraphPad Prism to calculate the Tm after deletion of post-peak fluorescence using the Boltzman Sigmoidal Fit Function.

Figure 4.19. Optimization of TSA buffers for 6His-UL44(1-290). (A) The indicated buffers were used to dilute 6His-UL44(1-290) to a 5 μM final concentration in SYPRO Orange 10x. Mixtures were loaded on 96-well white plates, before being loaded on a ABI PRISM7000 thermal cycler. Plates were heated from 22 to 95 °C at approximately 1°C/min, and fluorescence data were acquired with a ROX emission filter. Data were exported to Excel, analyzed to calculate the -dF/dT relative to each condition and GraphPad Prism was used to calculate the Tm relative to each condition, after deletion of post-peak fluorescence using the Boltzman Sigmoidal Fit Function. (B) Melting curves relative to the two buffers in which 6His-UL44(1-290) proved most and less stable, are shown. (C) Melting curves relative to the buffer of each class in which 6His-UL44(1-290)

proved most stable, are shown. (D) A comparison of melting curves relative to 6His-UL44(1-290) in Citrate buffer, high salt at different pHs is shown. (E) A comparison of melting curves relative to 6His-UL44(1-290) in Citrate buffer, pH7 at different salt concentrations is shown. (F) A comparison of melting curves relative to 6His-UL44(1-290) in the three UL44 specific buffers in shown. (G) A comparison of melting curves relative to 6His-UL44(1-290) in the three specific buffers selected for further experiments in shown. *High salt*, NaCl 250 mM; *low salt*, NaCl 50 mM.

Figure 4.20. TSA is suitable to monitor UL44 dimerization in vitro. (A) Lysozyme, 6His-UL44(1-290) and were diluted to the indicated final concentrations in SYPRO Orange 10x, either in Potassium Phosphate (KPO_4) or in Citrate Phosphate (Citrate) buffers. Mixtures were loaded on 96-well white plates, before being loaded on a ABI PRISM7000 thermal cycler. Plates were heated from 22-95 °C at approximately 1°C/min. Fluorescence data were acquired with a ROX excitation filter. Data were exported to Excel, analyzed to calculate the -dF/dT relative to each condition and GraphPad Prism was used to calculate the Tm relative to each condition, after deletion of post-peak fluorescence using the Boltzman Sigmoidal Fit Function. (B) The mean fluorescence and the -dT/dT relative to 6His-UL44(1-290; *red lines*) and 6His-UL44(1-290);L86A/L87A (*blue lines*) were plotted against the temperature. Data shown are representative from two duplicate wells. The ΔTm between 6His-UL44(1-290) and 6His-UL44(1-290)L86A/L87A relative to each buffer condition are shown in *purple*.

Figure 4.21. TSA tolerates high DMSO concentrations. (A) Lysozyme and 6His-UL44(1-290) were diluted in UL54 binding buffer to a 5 μM final concentrations in SYPRO Orange 10x, in the presence of increasing concentrations of DMSO. Mixtures were loaded on 96-well white plates, before being loaded on a ABI PRISM7000 thermal cycler. Plates were heated from 22-95 °C at approximately 1°C/min. Fluorescence data were acquired with a ROX excitation filter. Data were exported to Excel, analyzed to calculate the -dF/dT relative to each condition and GraphPad Prism was used to calculate the Tm relative to each condition, after deletion of post-peak fluorescence using the Boltzman Sigmoidal Fit Function. (B) The mean fluorescence and the -dT/dT relative to 6His-UL44(1-290; *top panels*) and Lysozyme (*bottom panels*) were plotted against the temperature. The Tm relative to each condition is shown.

Figure 4.22. Screening of 18 SMs by TSAs. (A) Lysozyme was diluted either in buffer B and buffer I to a (5 μM) final concentrations in SYPRO Orange 10x, in the presence of the 18 SMs (1mM DMSO 5% final concentration). Mixtures were loaded on 96-well white plates, before being loaded on a ABI PRISM7000 thermal cycler. Plates were heated from 22-95 °C at approximately 1°C/min. Fluorescence data were acquired with a ROX excitation filter. Data were exported to Excel, analyzed to calculate the -dF/dT relative to each condition. (B) The mean -dT/dT relative to Lysozyme in the presence of SMs were plotted against the temperature. (C) The mean fluorescence relative to Lysozyme in the presence of SMs were plotted against the temperature. (D) The mean fluorescence relative to each SMs in absence of Lysozyme were plotted against the temperature.

Figure 4.23. Evalutation of 4 SMs effect by ViiA 7 Real Time PCR-System. (A) Lysozyme was diluted either in buffer I to a 5 μM final concentrations in SYPRO Orange 10x, in the presence of increased concentration (25-200 μM) of the 4 SMs selected by FRA (B1, B3, B6 and C6) with DMSO 2% final concentration. Mixtures were loaded on 96-well white plates, before being loaded on a ViiA 7 Real Time PCR-System. Plates were heated from 22-95 °C at approximately 1°C/min. Multiple wavelengths were selected for samples excitation (470, 520 and 580 nm) and fluorescence detection (520, 586, 623 and 682 nm). Data were exported to Excel, analyzed to calculate the -dF/dT relative to each condition. (B) The mean fluorescence relative to Lysozyme in the presence

of SMs were plotted against the temperature. (C) The mean fluorescence relative to each SM in the absence of Lysozyme were plotted against the temperature. (D) The mean fluorescence relative to each SM either in the absence of Lysozyme and SYPRO Orange were plotted against the temperature.

Figure 4.24. Tm of 6His-UL44(1-290) decrease in the presence of B3. (A) Lysozyme and 6His-UL44 was diluted either in buffer I to a 5 μM final concentrations in SYPRO Orange 10x, in the presence B1 (100 μM) and B3 (200 μM), with DMSO 2% final concentration. Mixtures were loaded on 96-well white plates, before being loaded on a ViiA 7 Real Time PCR-System. Plates were heated from 22-95 °C at approximately 1°C/min. Multiple wavelengths were selected for samples excitation (470, 520 and 580 nm) and fluorescence detection (520, 586, 623 and 682 nm). Data were exported to Excel, the values relative to the combination of 470 nm and 623 nm excitation and emission filters respectively were analyzed to calculate the -dF/dT relative to each condition and GraphPad Prism was used to calculate the Tm relative to each condition, after deletion of post-peak fluorescence using the Boltzman Sigmoidal Fit Function. (B) The mean fluorescence relative to Lysozyme in the presence of SMs were plotted against the temperature. (C) The mean fluorescence relative to each SM in the absence of Lysozyme were plotted against the temperature.

Table 4.1. Analysis of solubility and toxicity of SMs. MRC5 Cells were seeded in 96 well plates, the day after were treated with increasing concentrations of SMs in DMEM/DMSO1%, and incubated for the indicated times, before being visually inspected for the presence of precipitates and of alterations of cell morphology and number, and processed for MTT assays. For visual analysis of the effect on cell viability, the highest SM concentration at which cells did not display any morphological or numerical alteration is shown. For visual analysis of the presence of precipitates, the highest SM concentration at which precipitates were not observable is shown. CC50 values relative to each compound are shown in black (4 Parameter Logistic Equation) or in red (linear regression). Orange cells, SMs forming precipitates; Green cells, SMs causing morphological or numerical cell alterations; *, SM that interfere with absorbance at 620 nm.

Figure A1

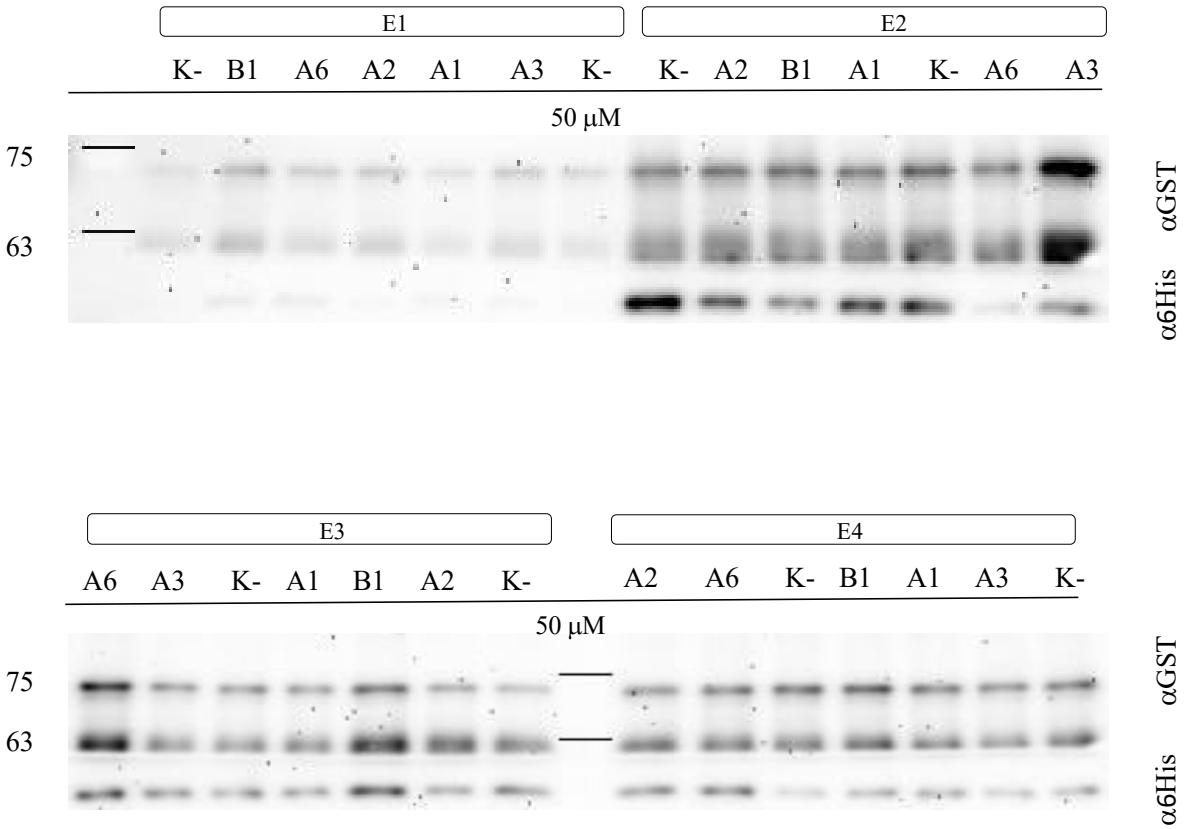
E1
E2
K- B1 A6 A2 A1 A3 K- K- A2 B1 A1 K- A6 A3
50 μM
75
63
αGST
α6His
E3
E4
A6 A3 K- A1 B1 A2 K- A2 A6 K- B1 A1 A3 K-
50 μM
75
63
αGST
α6His

Figure A2

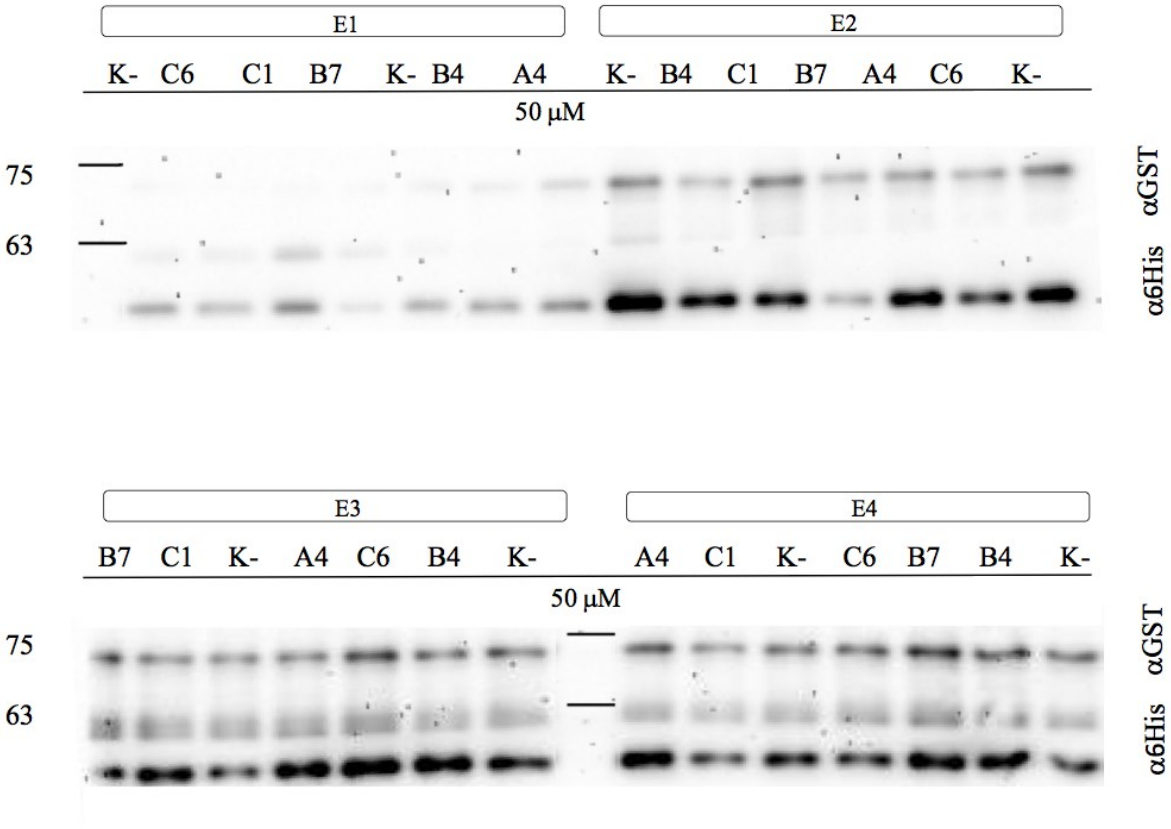
E1
E2
K- C6 C1 B7 K- B4 A4 K- B4 C1 B7 A4 C6 K-
50 µM
75
63
αGST
α6His
E3
E4
B7 C1 K- A4 C6 B4 K- A4 C1 K- C6 B7 B4 K-
50 µM
75
63
αGST
α6His

Figure A3

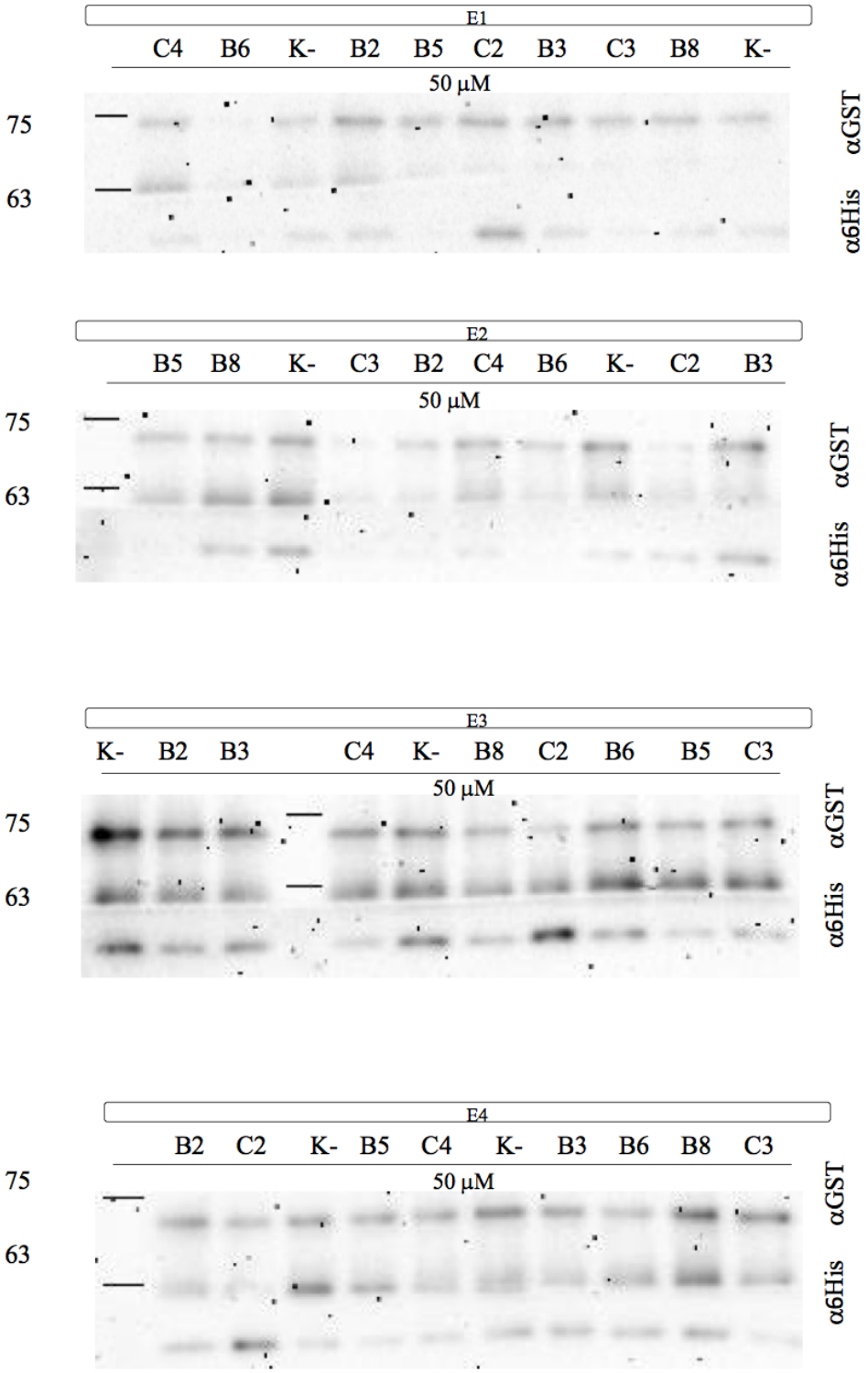
E1
C4 B6 K- B2 B5 C2 B3 C3 B8 K-
50 µM
75
63
αGST
α6His
E2
B5 B8 K- C3 B2 C4 B6 K- C2 B3
50 µM
75
63
αGST
α6His
E3
K- B2 B3 C4 K- B8 C2 B6 B5 C3
50 µM
75
63
αGST
α6His
E4
B2 C2 K- B5 C4 K- B3 B6 B8 C3
50 µM
75
63
αGST
α6His

Figure A4

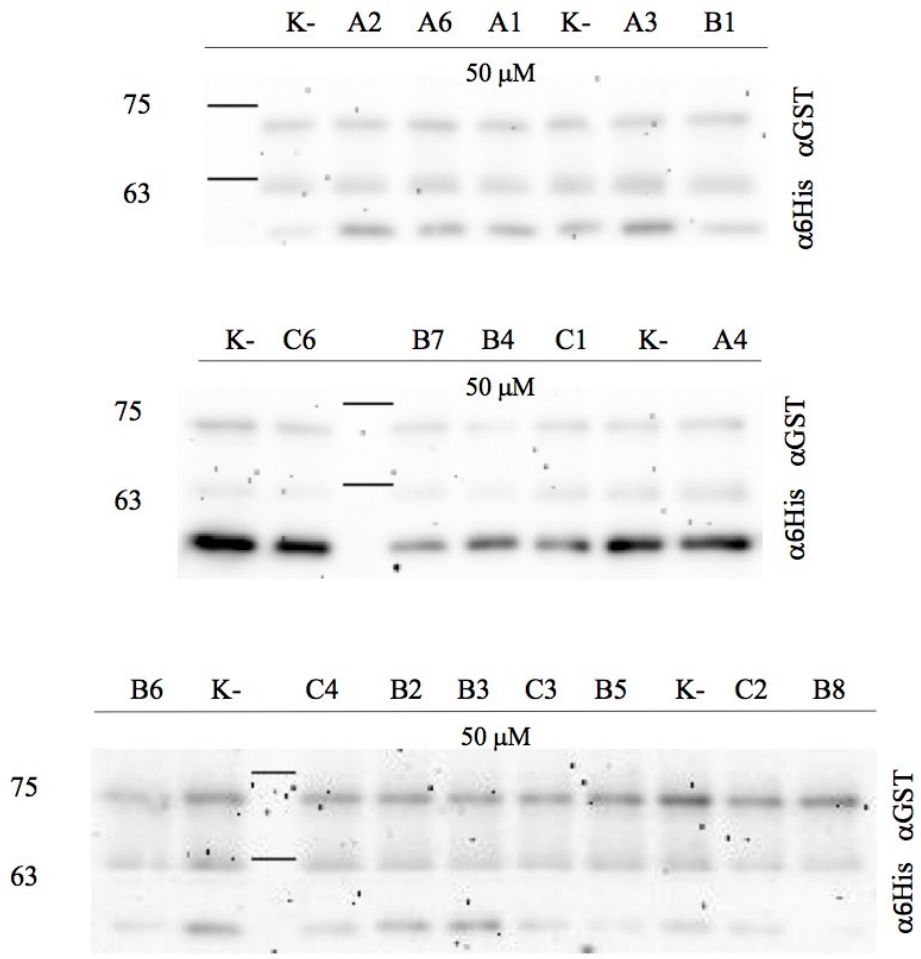
K- A2 A6 A1 K- A3 B1
50 µM
75
63
αGST
α6His
K- C6 B7 B4 C1 K- A4
50 µM
75
63
αGST
α6His
B6 K- C4 B2 B3 C3 B5 K- C2 B8
50 µM
75
63
αGST
α6His

Figure B1

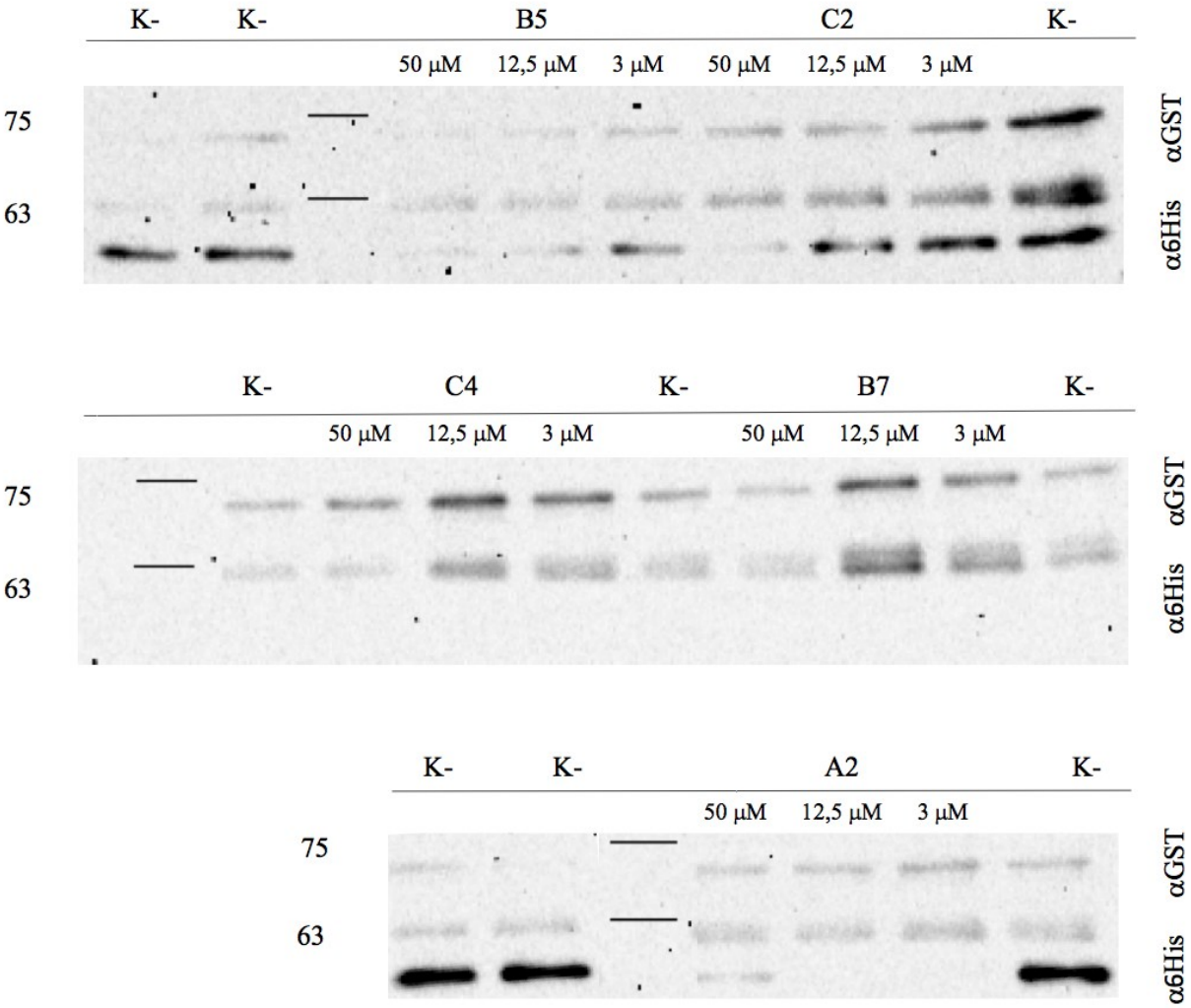
K-
K-
B5
C2
K-
50 µM
12,5 µM
3 µM
50 µM
12,5 µM
3 µM
75
63
αGST
α6His
K-
C4
K-
B7
K-
50 µM
12,5 µM
3 µM
50 µM
12,5 µM
3 µM
75
63
αGST
α6His
K-
K-
A2
K-
50 µM
12,5 µM
3 µM
75
63
αGST
α6His

Figure B2

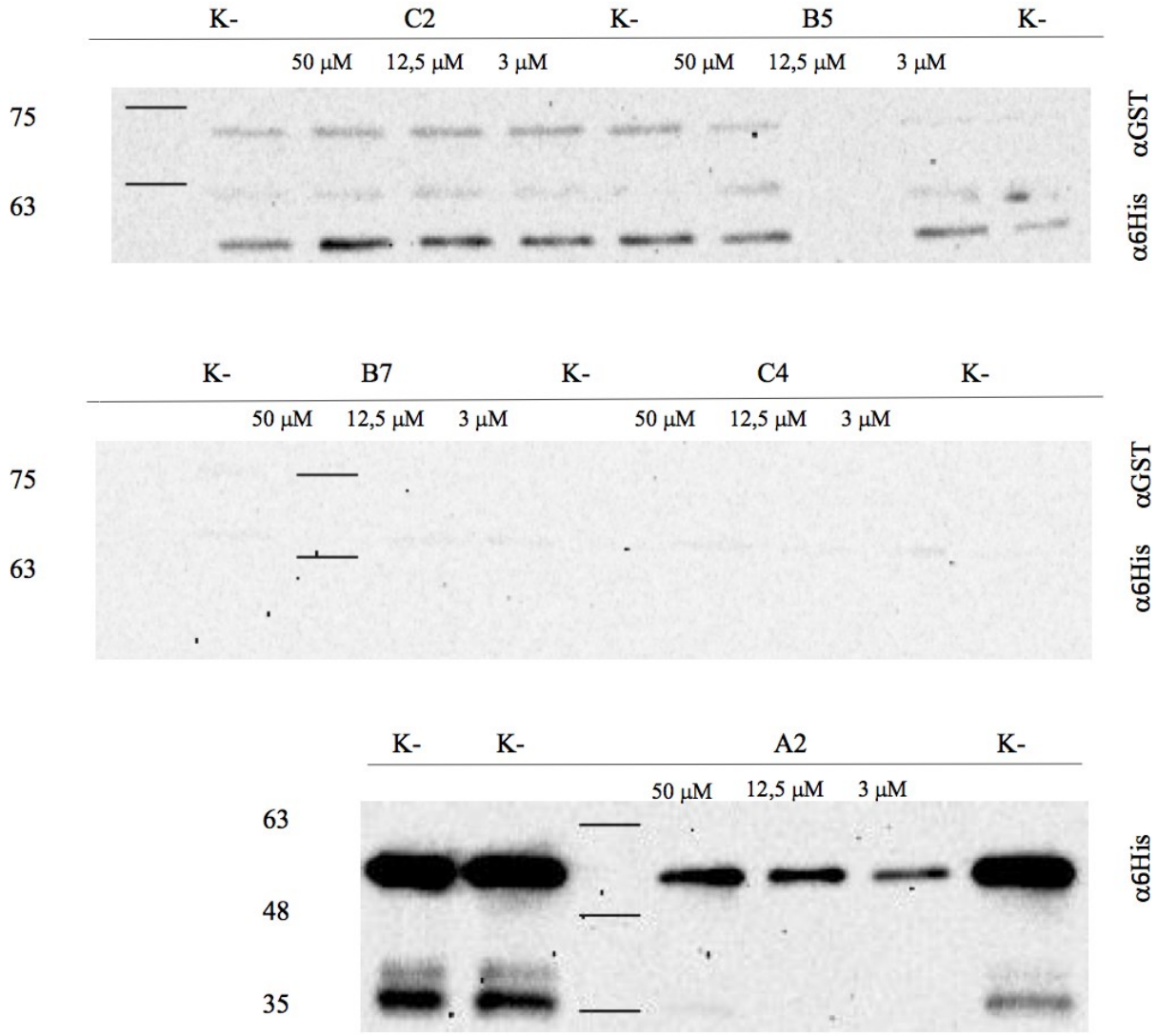
K-
C2
K-
B5
K-
50 µM
12,5 µM
3 µM
50 µM
12,5 µM
3 µM
75
63
αGST
α6His
K-
B7
K-
C4
K-
50 µM
12,5 µM
3 µM
50 µM
12,5 µM
3 µM
75
63
αGST
α6His
K-
K-
A2
K-
50 µM
12,5 µM
3 µM
63
48
35
α6His

Figure B3

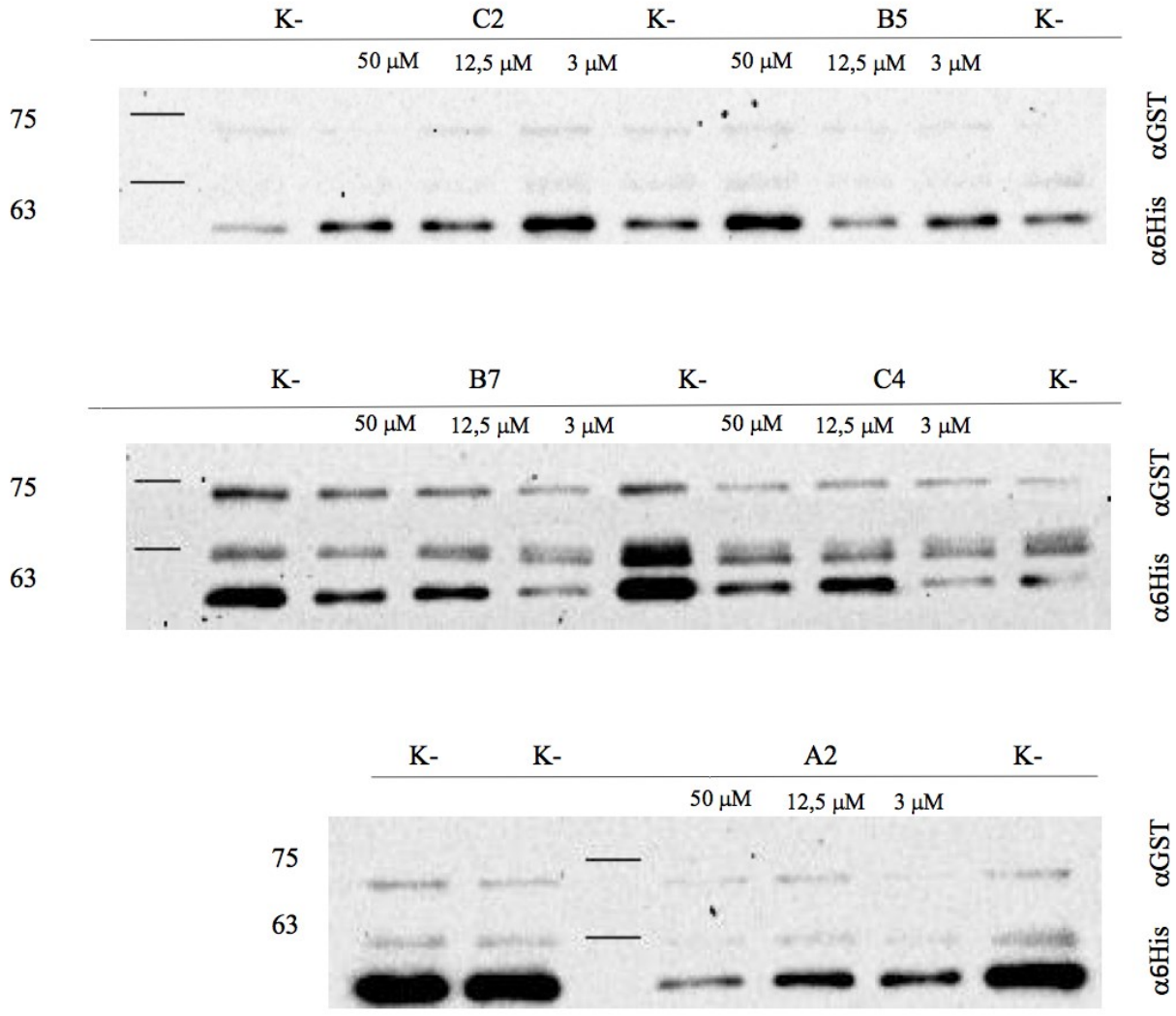
K-
C2
K-
B5
K-
50 µM
12,5 µM
3 µM
50 µM
12,5 µM
3 µM
75
63
αGST
α6His
K-
B7
K-
C4
K-
50 µM
12,5 µM
3 µM
50 µM
12,5 µM
3 µM
75
63
αGST
α6His
K-
K-
A2
K-
50 µM
12,5 µM
3 µM
75
63
αGST
α6His

Figure C1

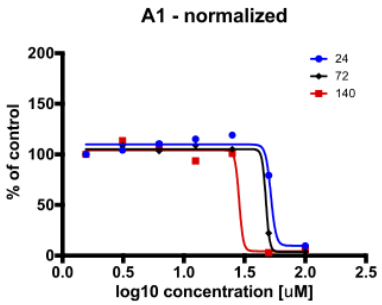
A1 - normalized
% of control
log10 concentration [uM]
24
72
140

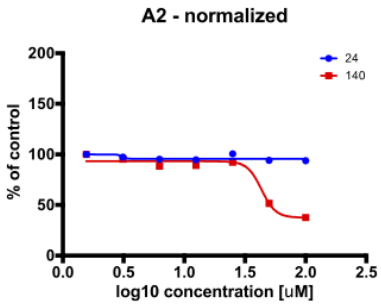
A2 - normalized
% of control
log10 concentration [uM]
24
140

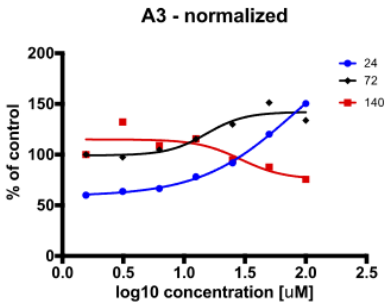
A3 - normalized
% of control
log10 concentration [uM]
24
72
140

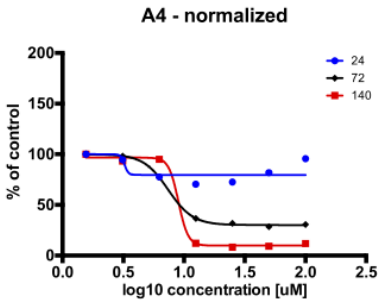
A4 - normalized
% of control
log10 concentration [uM]
24
72
140

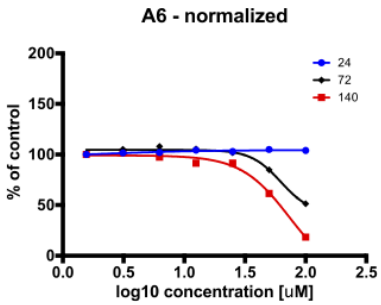
A6 - normalized
% of control
log10 concentration [uM]
24
72
140

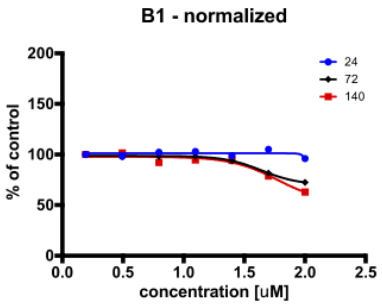
B1 - normalized
% of control
concentration [uM]
24
72
140

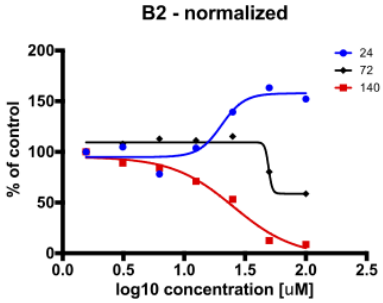
B2 - normalized
% of control
log10 concentration [uM]
24
72
140

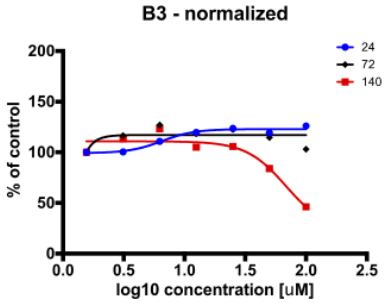
B3 - normalized
% of control
log10 concentration [uM]
24
72
140

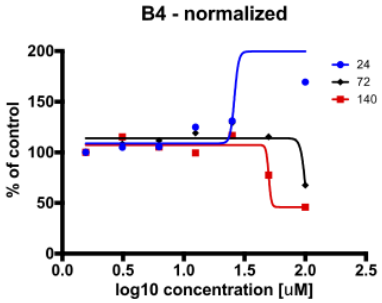
B4 - normalized
% of control
log10 concentration [uM]
24
72
140

Figure C2

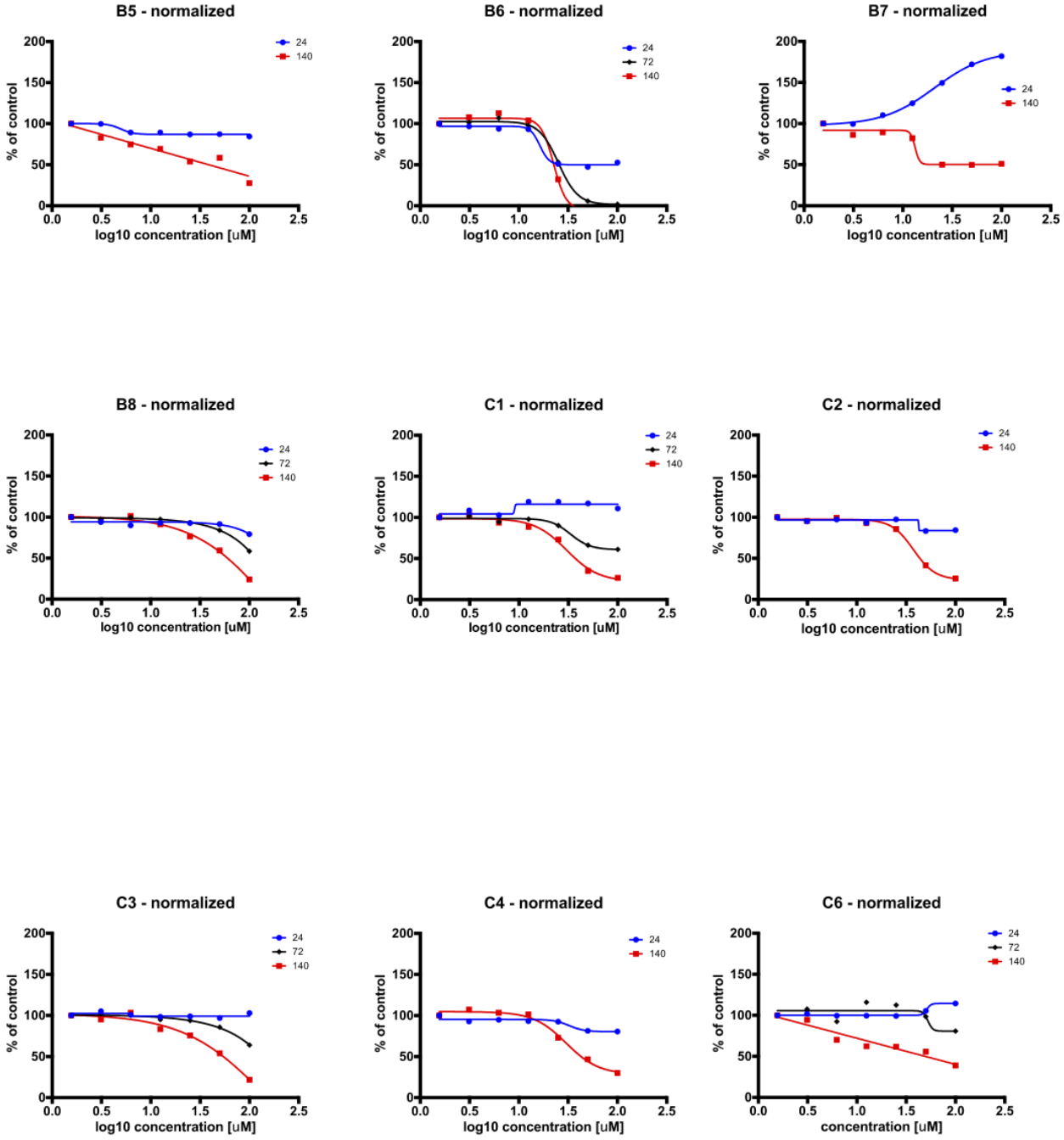
B5 - normalized
B6 - normalized
B7 - normalized
B8 - normalized
C1 - normalized
C2 - normalized
C3 - normalized
C4 - normalized
C6 - normalized
% of control
log10 concentration [uM]
concentration [uM]
24
72
140

Figure C3

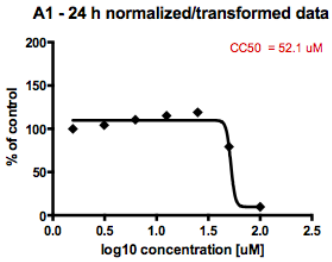
A1 - 24 h normalized/transformed data
CC50 = 52.1 uM
% of control
log10 concentration [uM]

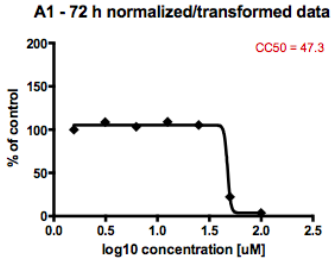
A1 - 72 h normalized/transformed data
CC50 = 47.3
% of control
log10 concentration [uM]

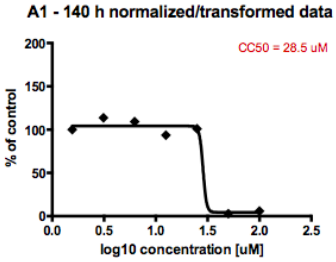
A1 - 140 h normalized/transformed data
CC50 = 28.5 uM
% of control
log10 concentration [uM]

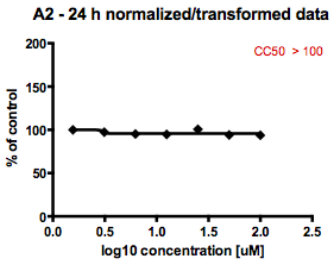
A2 - 24 h normalized/transformed data
CC50 > 100
% of control
log10 concentration [uM]

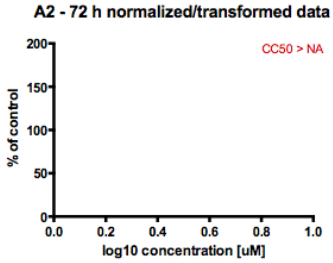
A2 - 72 h normalized/transformed data
CC50 > NA
% of control
log10 concentration [uM]

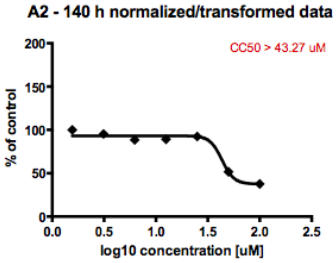
A2 - 140 h normalized/transformed data
CC50 > 43.27 uM
% of control
log10 concentration [uM]

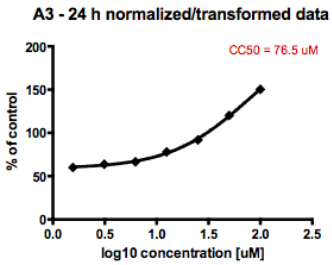
A3 - 24 h normalized/transformed data
CC50 = 76.5 uM
% of control
log10 concentration [uM]

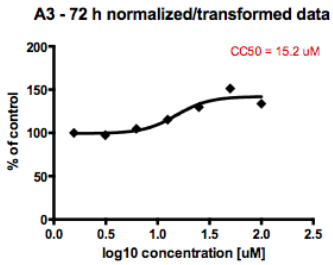
A3 - 72 h normalized/transformed data
CC50 = 15.2 uM
% of control
log10 concentration [uM]

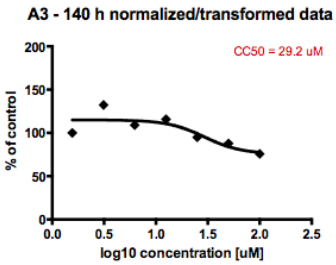
A3 - 140 h normalized/transformed data
CC50 = 29.2 uM
% of control
log10 concentration [uM]

Figure C4

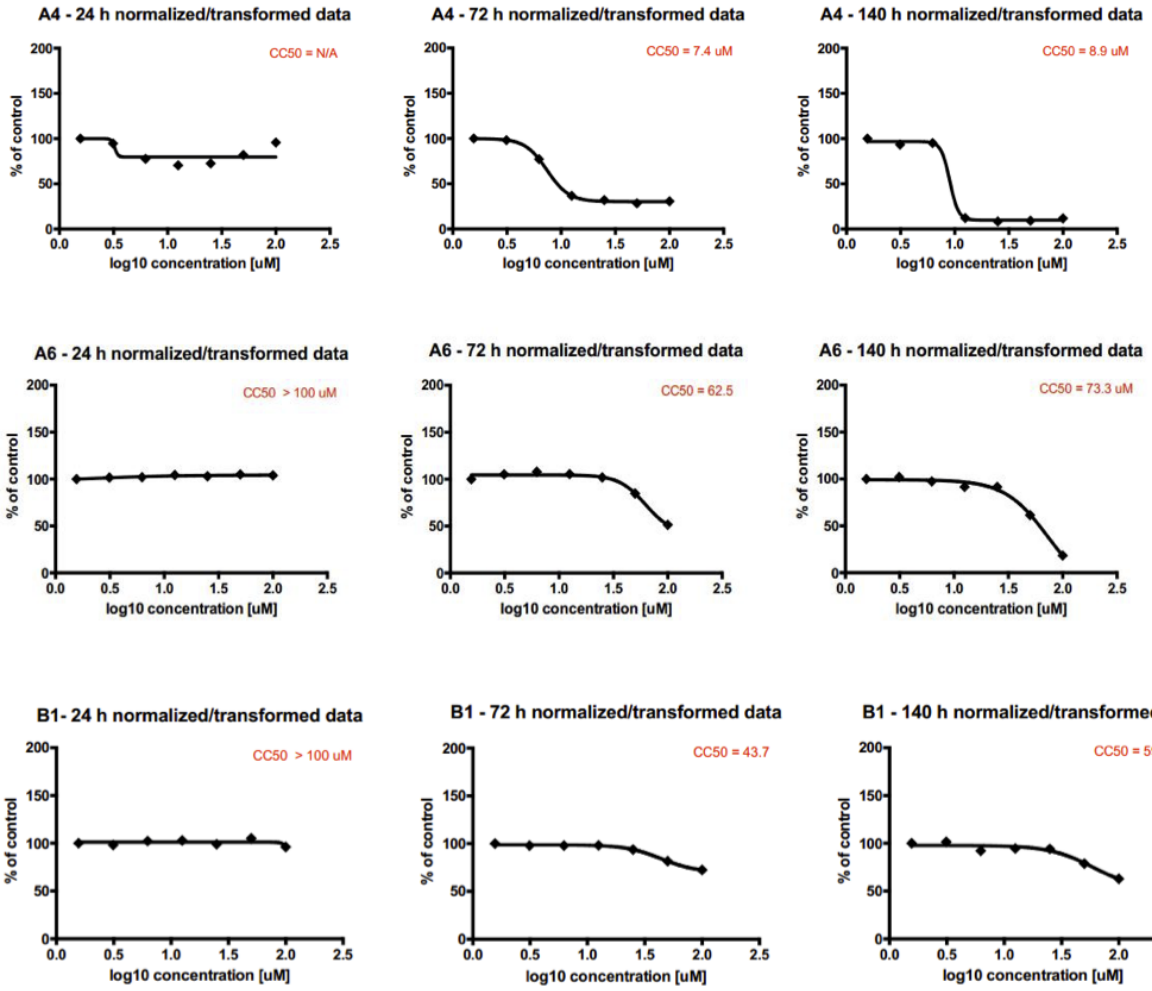
A4 - 24 h normalized/transformed data
CC50 = N/A
A4 - 72 h normalized/transformed data
CC50 = 7.4 uM
A4 - 140 h normalized/transformed data
CC50 = 8.9 uM
A6 - 24 h normalized/transformed data
CC50 > 100 uM
A6 - 72 h normalized/transformed data
CC50 = 62.5
A6 - 140 h normalized/transformed data
CC50 = 73.3 uM
B1- 24 h normalized/transformed data
CC50 > 100 uM
B1 - 72 h normalized/transformed data
CC50 = 43.7
B1 - 140 h normalized/transformed data
CC50 = 59.4 uM
% of control
log10 concentration [uM]

Figure C5

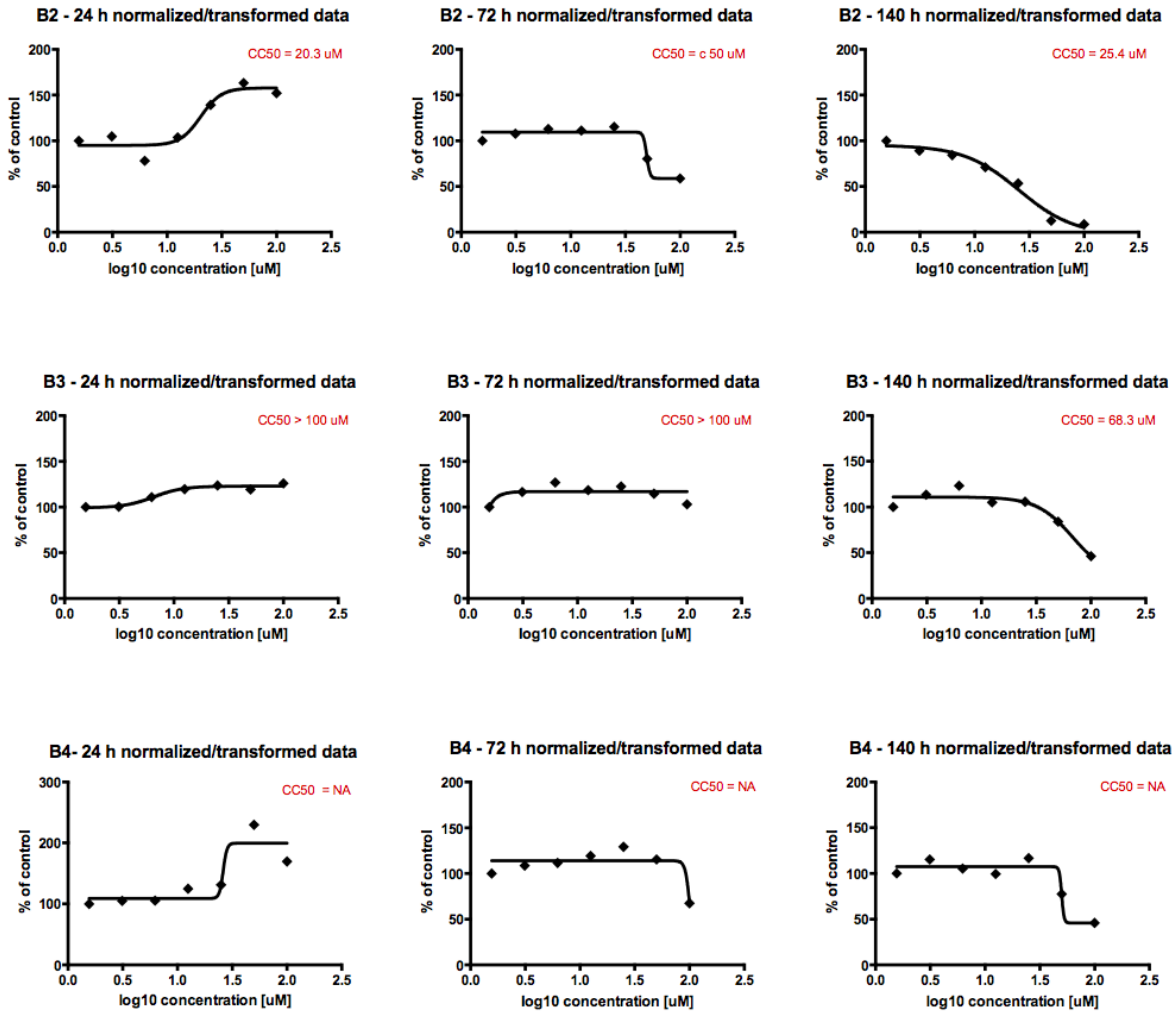
B2 - 24 h normalized/transformed data
CC50 = 20.3 uM
B2 - 72 h normalized/transformed data
CC50 = c 50 uM
B2 - 140 h normalized/transformed data
CC50 = 25.4 uM
B3 - 24 h normalized/transformed data
CC50 > 100 uM
B3 - 72 h normalized/transformed data
CC50 > 100 uM
B3 - 140 h normalized/transformed data
CC50 = 68.3 uM
B4- 24 h normalized/transformed data
CC50 = NA
B4 - 72 h normalized/transformed data
CC50 = NA
B4 - 140 h normalized/transformed data
CC50 = NA
% of control
log10 concentration [uM]

Figure C6

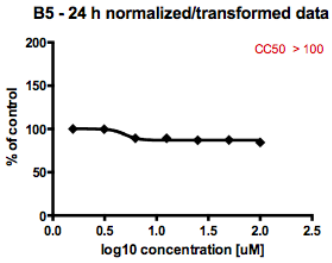
B5 - 24 h normalized/transformed data
CC50 > 100
% of control
log10 concentration [uM]

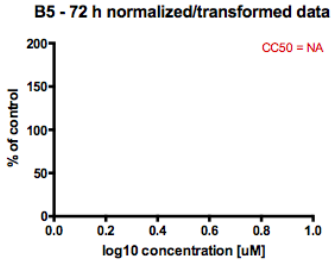
B5 - 72 h normalized/transformed data
CC50 = NA
% of control
log10 concentration [uM]

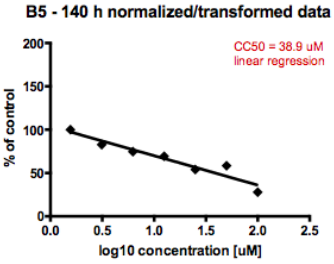
B5 - 140 h normalized/transformed data
CC50 = 38.9 uM
linear regression
% of control
log10 concentration [uM]

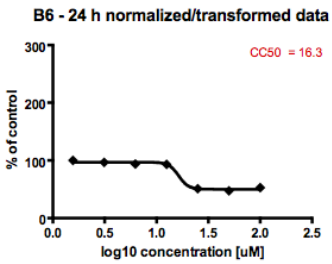
B6 - 24 h normalized/transformed data
CC50 = 16.3
% of control
log10 concentration [uM]

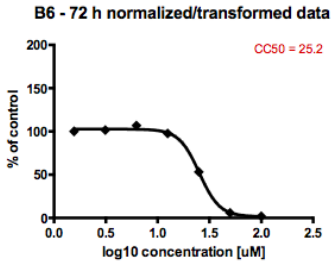
B6 - 72 h normalized/transformed data
CC50 = 25.2
% of control
log10 concentration [uM]

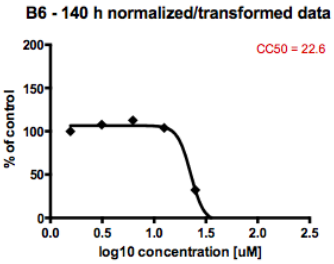
B6 - 140 h normalized/transformed data
CC50 = 22.6
% of control
log10 concentration [uM]

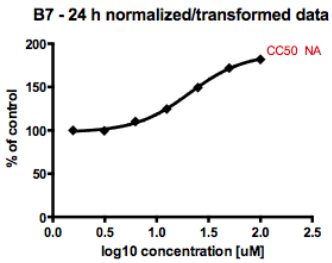
B7 - 24 h normalized/transformed data
CC50 NA
% of control
log10 concentration [uM]

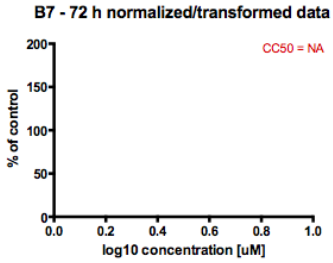
B7 - 72 h normalized/transformed data
CC50 = NA
% of control
log10 concentration [uM]

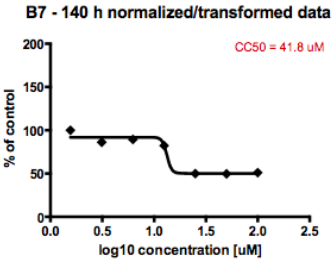
B7 - 140 h normalized/transformed data
CC50 = 41.8 uM
% of control
log10 concentration [uM]

Figure C7

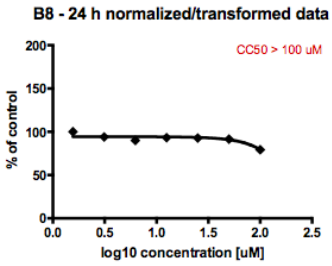
B8 - 24 h normalized/transformed data
CC50 > 100 uM
% of control
log10 concentration [uM]

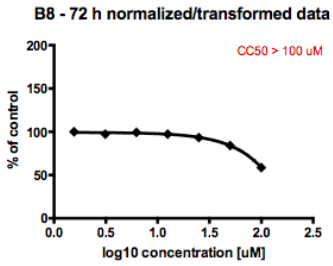
B8 - 72 h normalized/transformed data
CC50 > 100 uM
% of control
log10 concentration [uM]

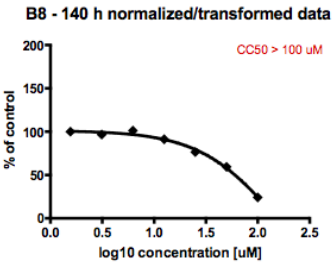
B8 - 140 h normalized/transformed data
CC50 > 100 uM
% of control
log10 concentration [uM]

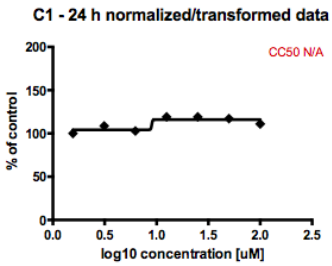
C1 - 24 h normalized/transformed data
CC50 N/A
% of control
log10 concentration [uM]

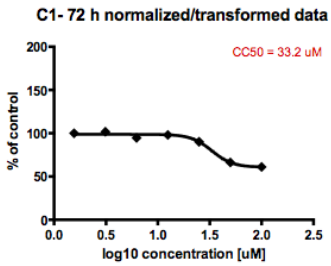
C1- 72 h normalized/transformed data
CC50 = 33.2 uM
% of control
log10 concentration [uM]

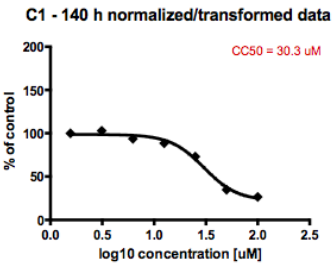
C1 - 140 h normalized/transformed data
CC50 = 30.3 uM
% of control
log10 concentration [uM]

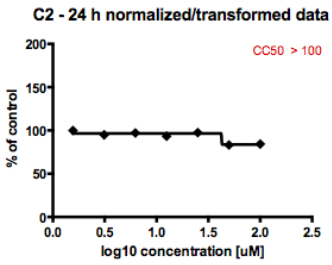
C2 - 24 h normalized/transformed data
CC50 > 100
% of control
log10 concentration [uM]

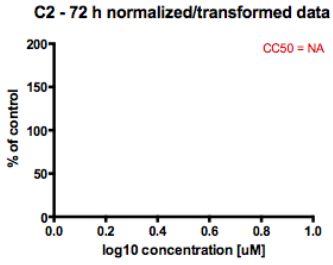
C2 - 72 h normalized/transformed data
CC50 = NA
% of control
log10 concentration [uM]

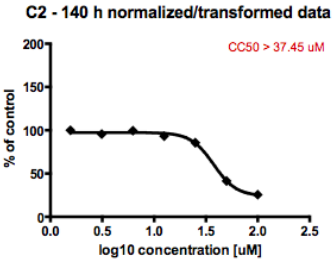
C2 - 140 h normalized/transformed data
CC50 > 37.45 uM
% of control
log10 concentration [uM]

Figure C8

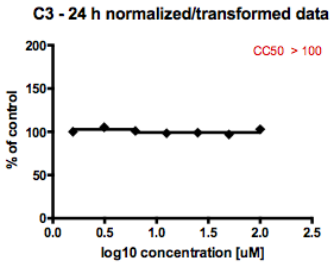
C3 - 24 h normalized/transformed data
CC50 > 100
% of control
log10 concentration [uM]

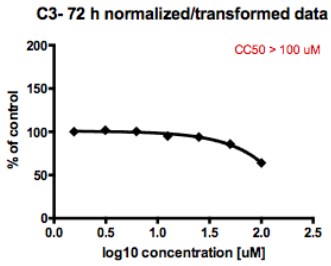
C3- 72 h normalized/transformed data
CC50 > 100 uM
% of control
log10 concentration [uM]

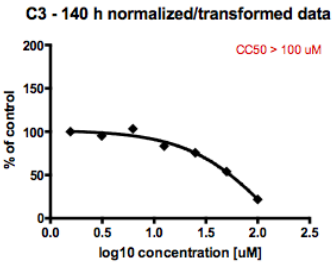
C3 - 140 h normalized/transformed data
CC50 > 100 uM
% of control
log10 concentration [uM]

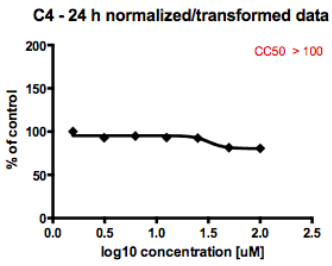
C4 - 24 h normalized/transformed data
CC50 > 100
% of control
log10 concentration [uM]

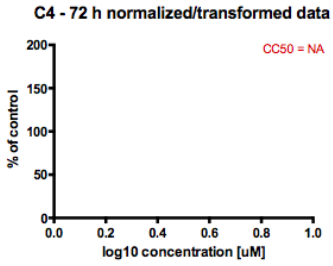
C4 - 72 h normalized/transformed data
CC50 = NA
% of control
log10 concentration [uM]

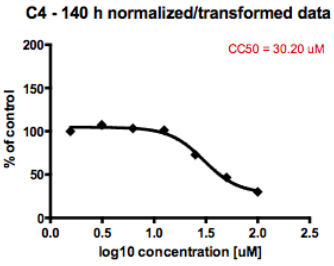
C4 - 140 h normalized/transformed data
CC50 = 30.20 uM
% of control
log10 concentration [uM]

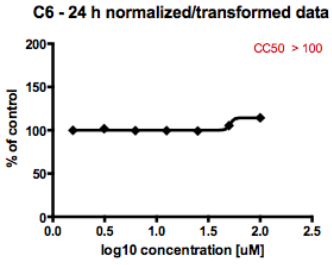
C6 - 24 h normalized/transformed data
CC50 > 100
% of control
log10 concentration [uM]

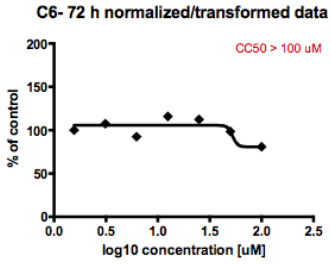
C6- 72 h normalized/transformed data
CC50 > 100 uM
% of control
log10 concentration [uM]

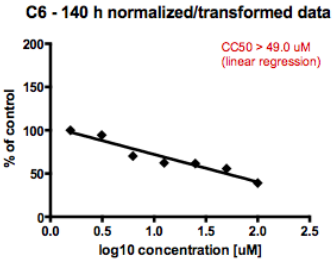
C6 - 140 h normalized/transformed data
CC50 > 49.0 uM
(linear regression)
% of control
log10 concentration [uM]

Figure D1

24 WELL-plate

Days post infection

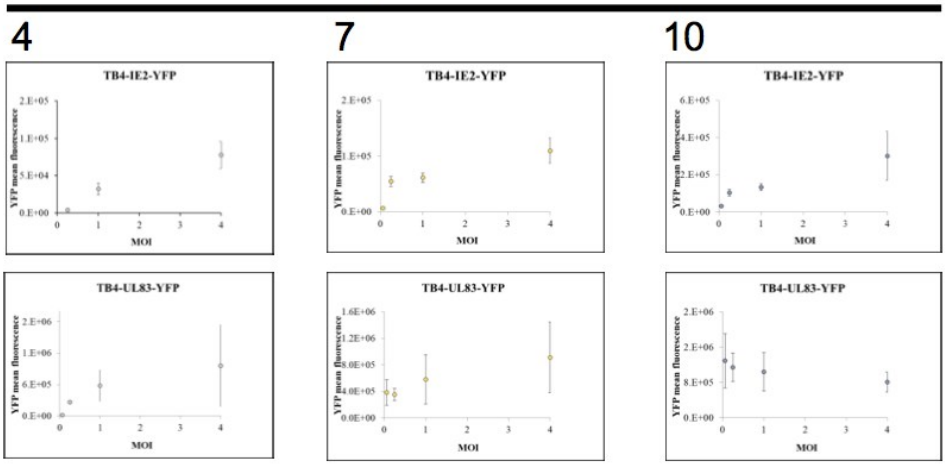

MOIs

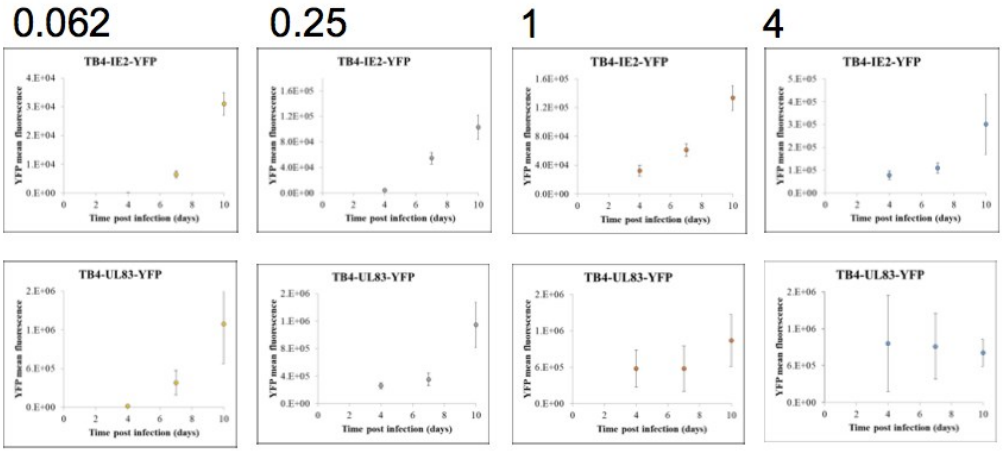

Figure D2

96 WELL-plate

Days post infection

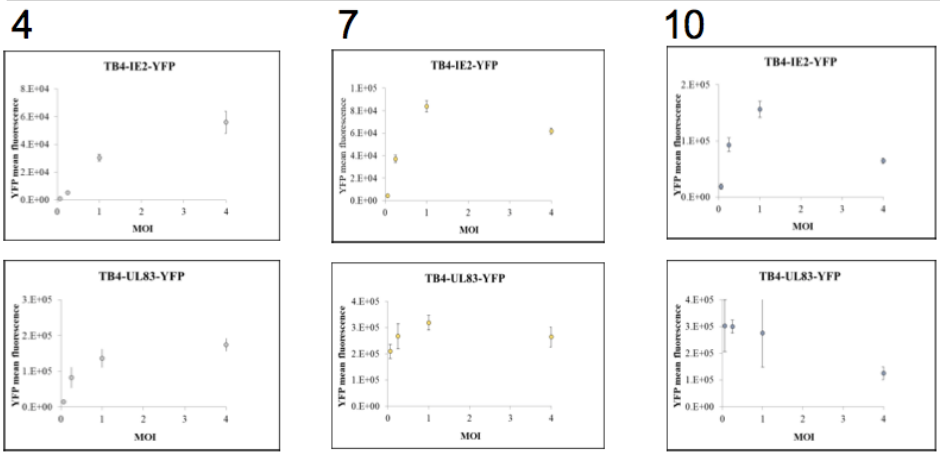

MOIs

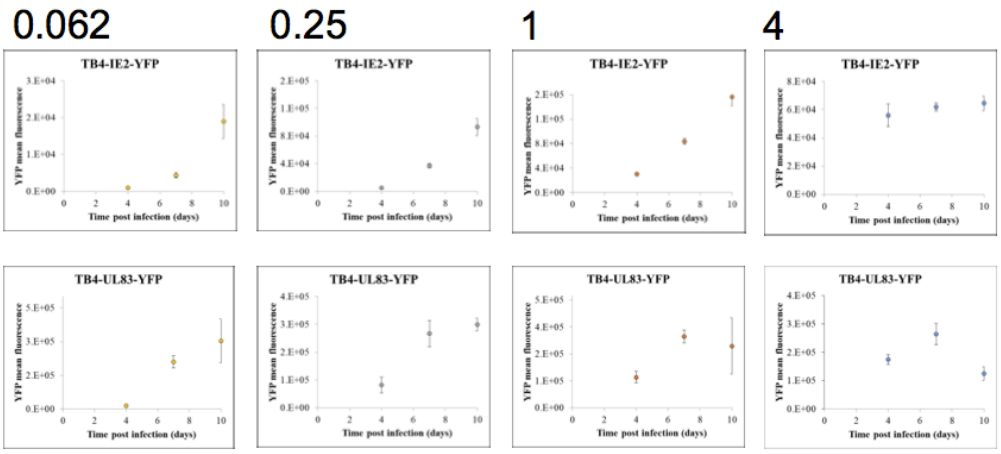

Figure E1

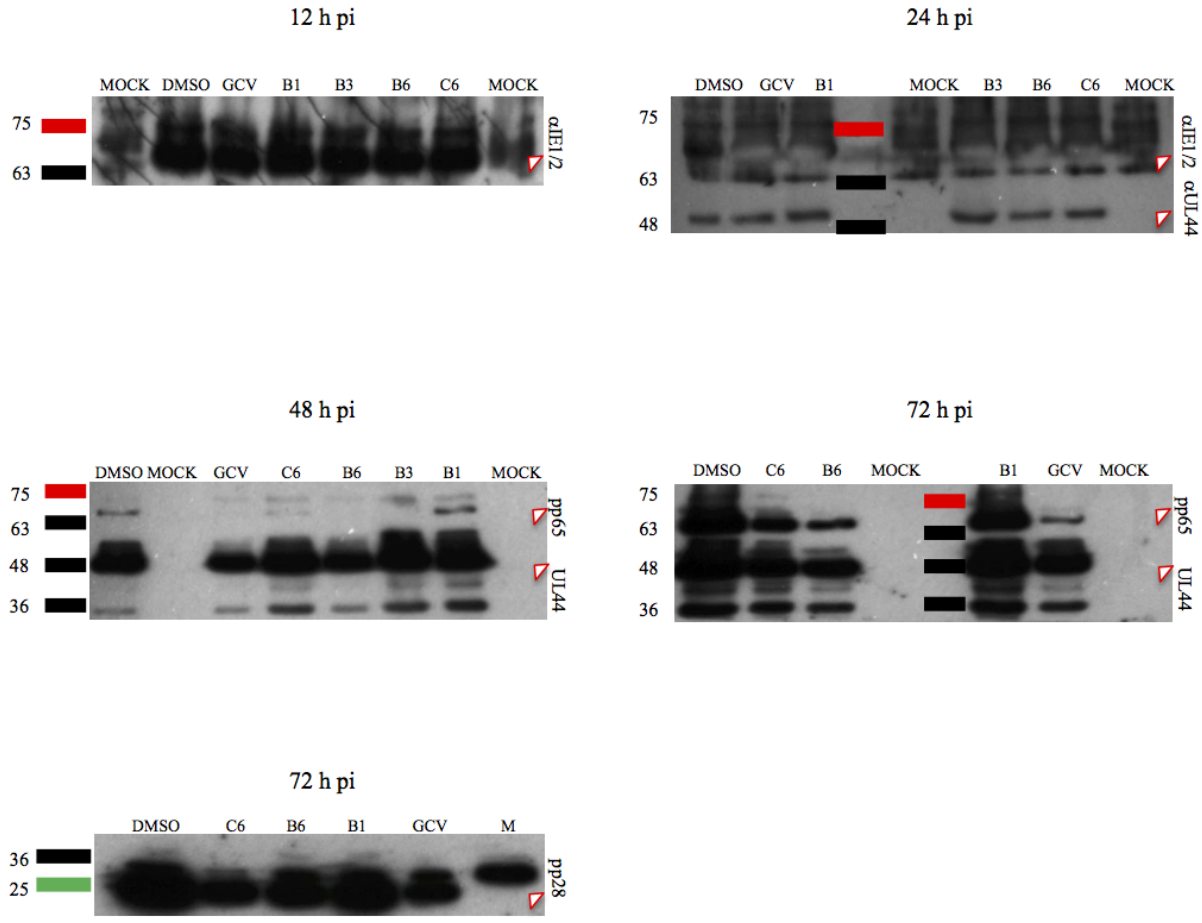
12 h pi
MOCK DMSO GCV B1 B3 B6 C6 MOCK
75
63
αIE1/2
24 h pi
DMSO GCV B1 MOCK B3 B6 C6 MOCK
75
63
48
αIE1/2 αUL44
48 h pi
DMSO MOCK GCV C6 B6 B3 B1 MOCK
75
63
48
36
pp65
UL44
72 h pi
DMSO C6 B6 MOCK B1 GCV MOCK
75
63
48
36
pp65
UL44
72 h pi
DMSO C6 B6 B1 GCV M
36
25
pp28

Figure E2

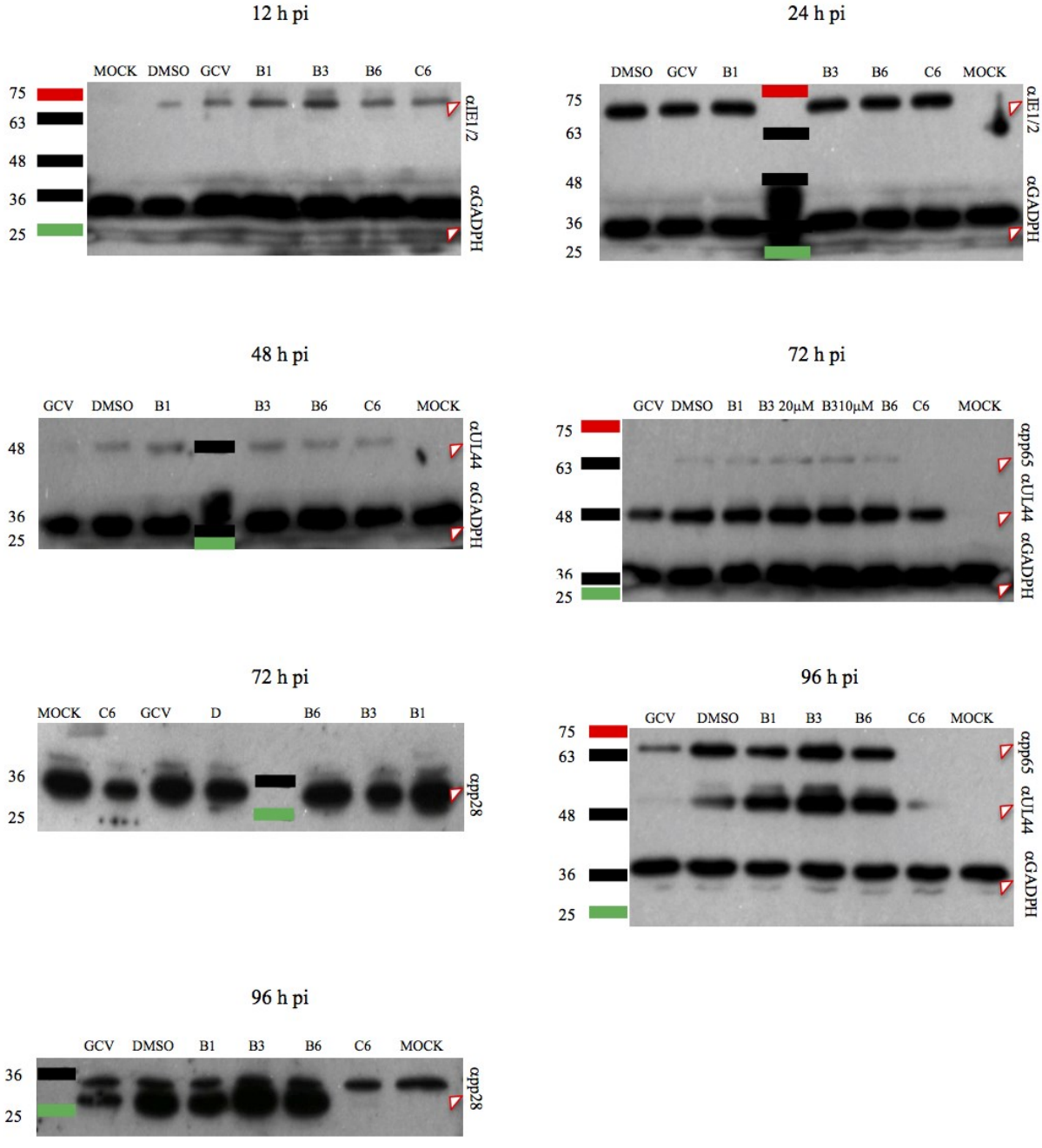
12 h pi
MOCK DMSO GCV B1 B3 B6 C6
75
63
48
36
25
αIE1/2
αGADPH
24 h pi
DMSO GCV B1 B3 B6 C6 MOCK
75
63
48
36
25
αIE1/2
αGADPH
48 h pi
GCV DMSO B1 B3 B6 C6 MOCK
48
36
25
αUL44
αGADPH
72 h pi
GCV DMSO B1 B3 20μM B310μM B6 C6 MOCK
75
63
48
36
25
αpp65 αUL44 αGADPH
72 h pi
MOCK C6 GCV D B6 B3 B1
36
25
αpp28
96 h pi
GCV DMSO B1 B3 B6 C6 MOCK
75
63
48
36
25
αpp65 αUL44 αGADPH
96 h pi
GCV DMSO B1 B3 B6 C6 MOCK
36
25
αpp28

Figure E3

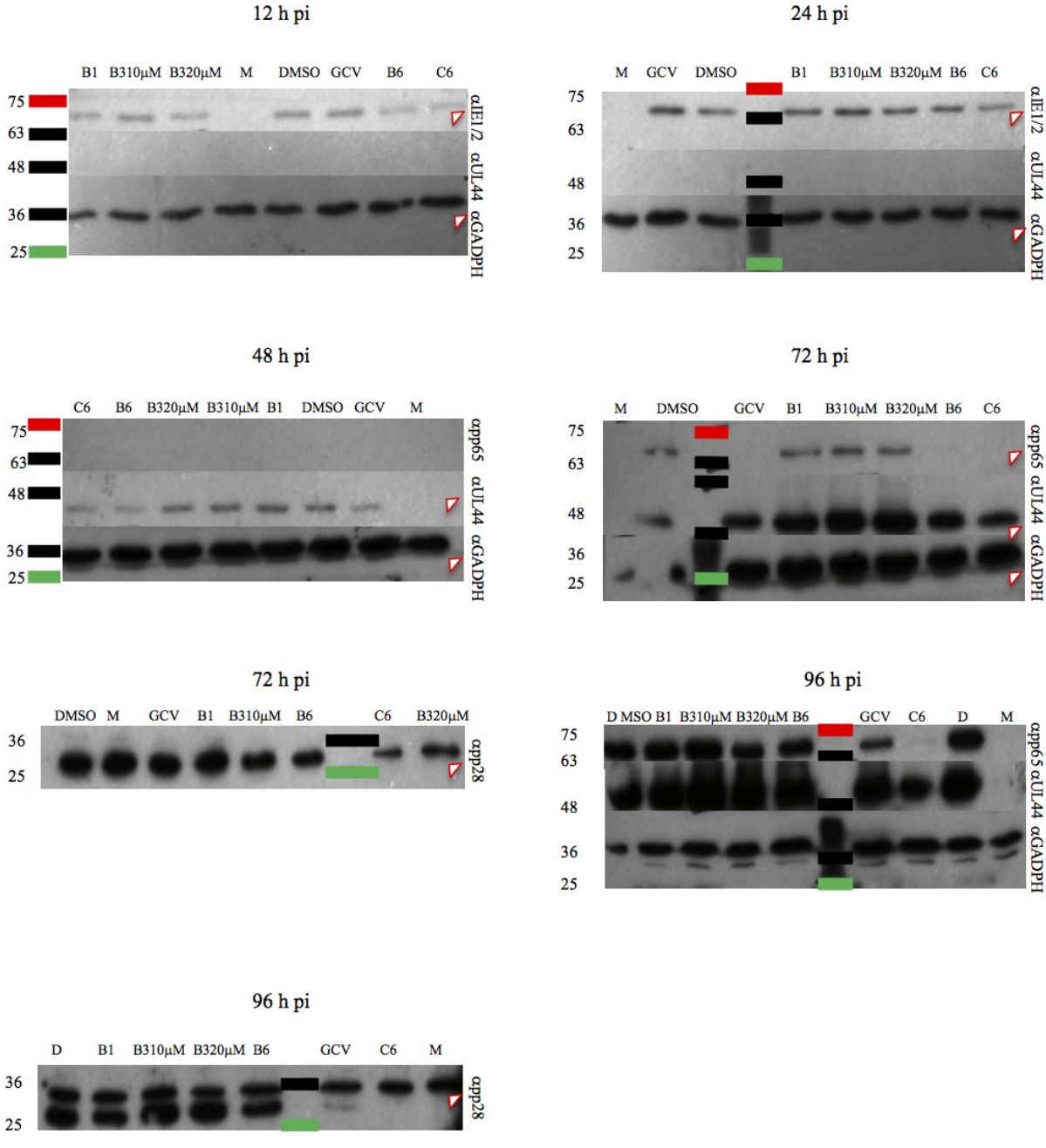
12 h pi
B1 B310µM B320µM M DMSO GCV B6 C6
75
63
48
36
25
αIE1/2 αUL44 αGADPH
24 h pi
M GCV DMSO B1 B310µM B320µM B6 C6
75
63
48
36
25
αIE1/2 αUL44 αGADPH
48 h pi
C6 B6 B320µM B310µM B1 DMSO GCV M
75
63
48
36
25
αpp65 αUL44 αGADPH
72 h pi
M DMSO GCV B1 B310µM B320µM B6 C6
75
63
48
36
25
αpp65 αUL44 αGADPH
72 h pi
DMSO M GCV B1 B310µM B6 C6 B320µM
36
25
αpp28
96 h pi
D MSO B1 B310µM B320µM B6 GCV C6 D M
75
63
48
36
25
αpp65 αUL44 αGADPH
96 h pi
D B1 B310µM B320µM B6 GCV C6 M
36
25
αpp28

Figure F1

Emission Filter :ROX Buffer: Citrate

Sypro 10x

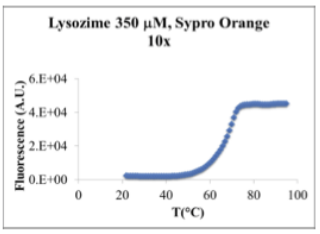

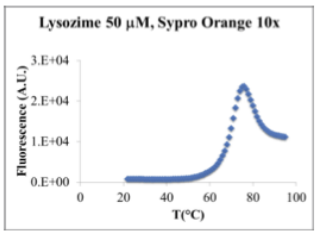

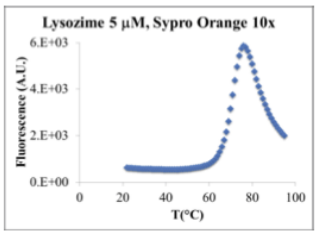

Tm = 73.1°C

Tm = 72.9°C

Tm = 72.2°C

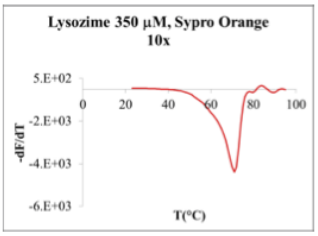

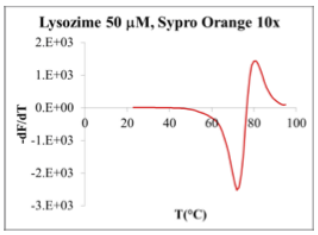

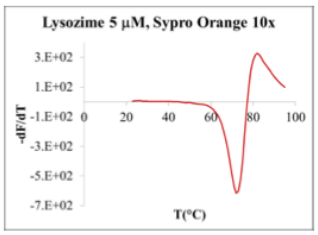

Sypro 2x

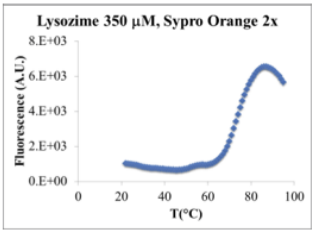

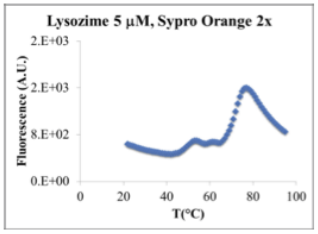

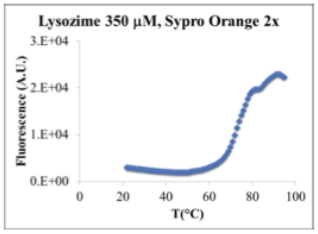

Tm = 73.2°C

Tm = 78.5 °C

Tm = NA

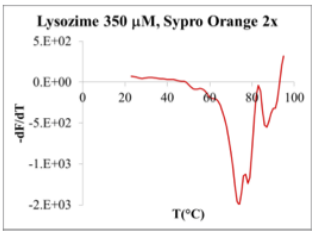

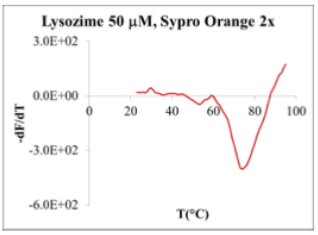

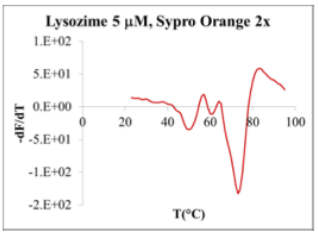

Figure F2

Emission Filter :ROX Buffer: KPO_4

Sypro 10x

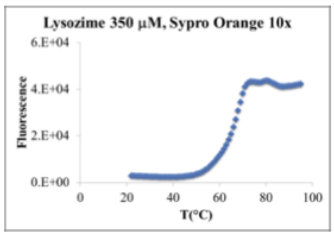

Tm = 65.7°C

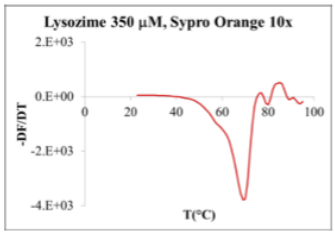

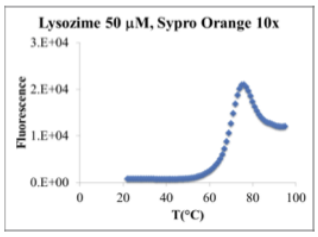

Tm = 70.4°C

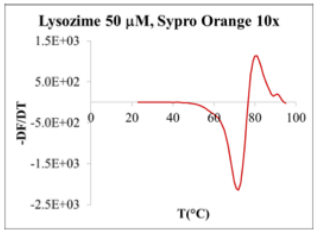

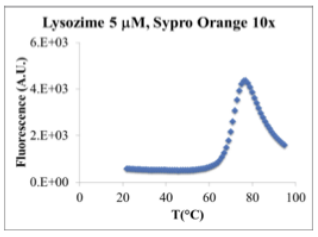

Tm = 71.6°C

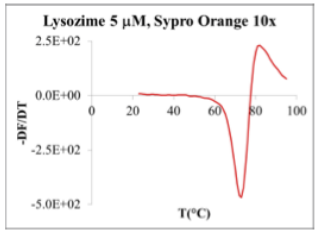

Sypro 2x

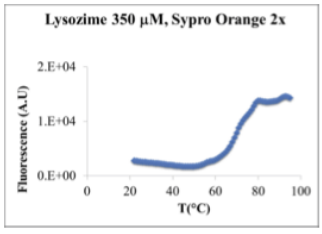

Tm = 70.4°C

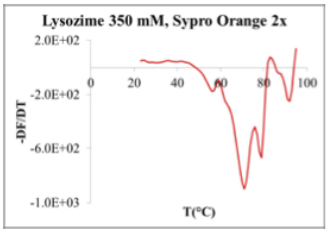

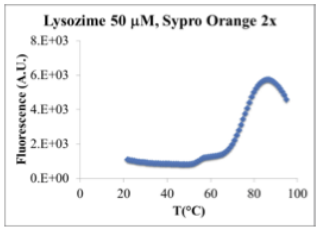

Tm = 75.8°C

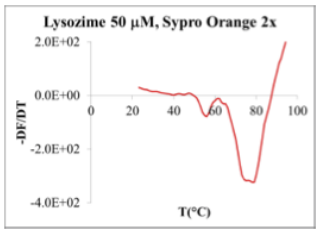

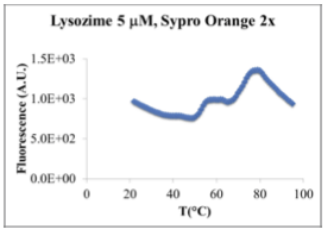

Tm = NA

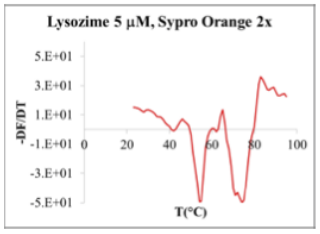

Figure F3

Emission Filter :SYBR Buffer: Citrate

Sypro 10x

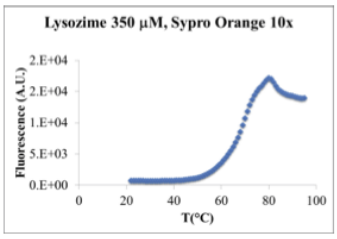

Tm = 73.1°C

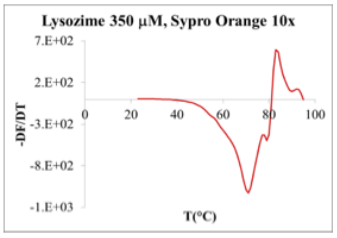

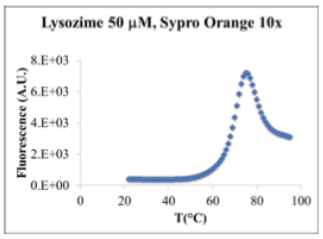

Tm = 72.9°C

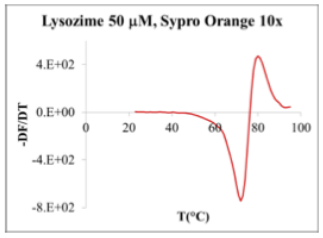

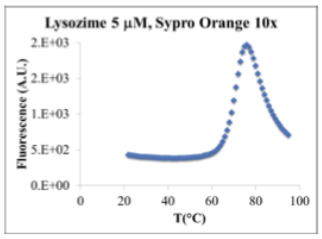

Tm = 72.2°C

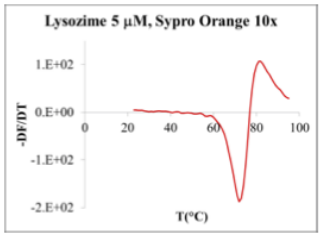

Sypro 2x

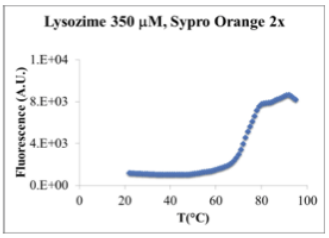

Tm = 73.2°C

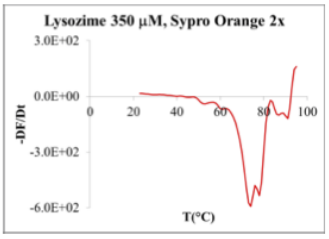

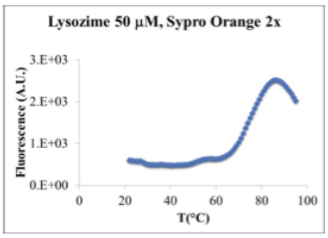

Tm = 78.8°C

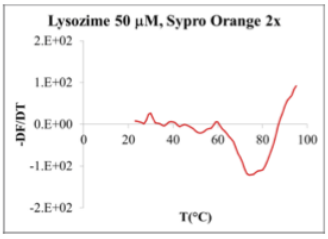

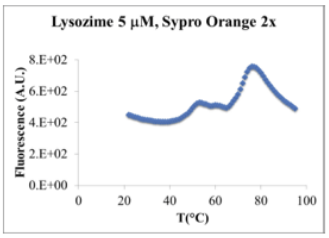

Tm = NA

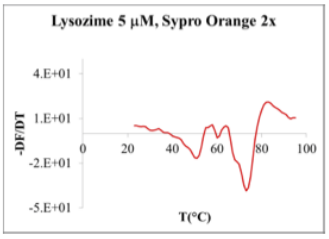

Figure F4

Emission Filter :SYBR Buffer: KPO_4

Sypro 10x

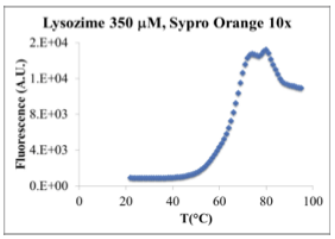

Tm = 65.6°C

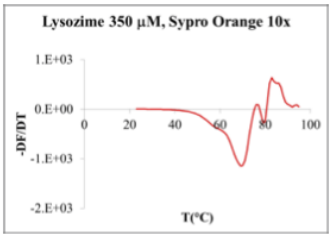

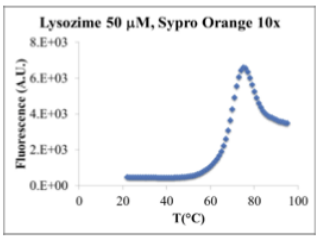

Tm = 71.1°C

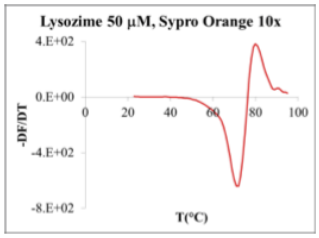

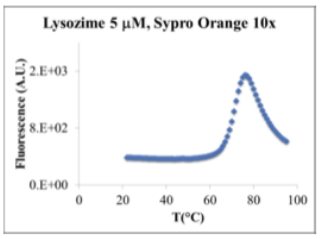

Tm = 71.4°C

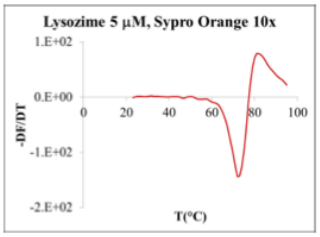

Sypro 2x

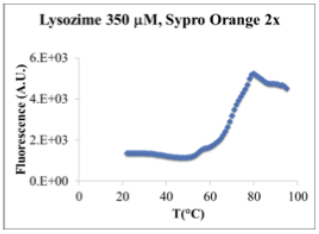

Tm = 71.7°C

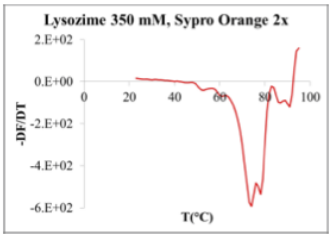

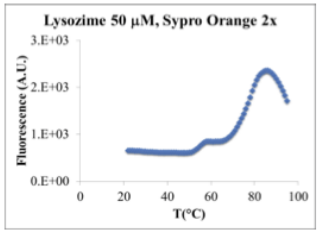

Tm = 77.5 °C

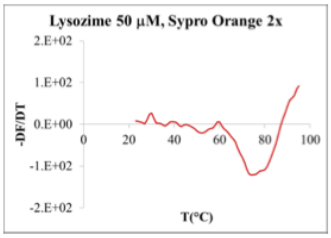

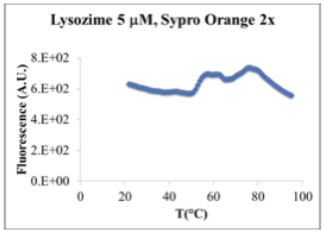

Tm = NA

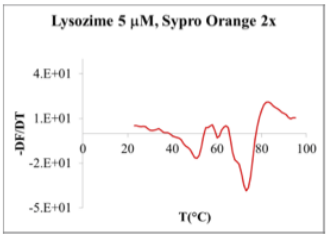

Appendix Figures Legends

Figure A1-4. Screening of 18 SMs by GST-pulldown assays. GST UL44(1-290) and 6His-UL44(1-290) were incubated in the presence (50 μM) or in the absence of the 18 SMs, in DMSO 0.25% and subjected to GST-pulldown assays and SDS page/Western blotting. Each elutions (E1, E2, E3, E4) or a mix containing the same portion of each elution were then analyzed by SDS-PAGE Western-Blotting. K- = control mixture incubated in the absence of SMs.

Figure B1-3. Evaluation of dose-response effects by GST-pulldown assays. GST-UL44(1-290) and 6His UL44(1-290) were incubated in the presence or in the absence of increasing concentrations (50, 12.5 and 3 μM) of the 5 selected SMs, in DMSO 0.25% and subjected to GST-pulldown assays and SDS page/Western blotting. K- = control mixture incubated in the absence of SMs, loaded in triplicate to allow estimation of lane to lane variations.

Figure C1-8. Calculation of CC50 values for 18 selected SMs by MTT assays. MRC5 cells were seeded into 96 well plates. 24 h later, cells were treated with increasing amounts of SMs (1.56 μM-100 μM). At the indicated times post treatment plates were processed for MTT assays. (1-2) Absorbance values at 620 nm were expressed as a percentage of those obtained for cells treated with DMEM/DMOSO1%, and plotted against the SM concentration. *x* data were transformed to logarithmic and fitted to a linear regression or 4 Parameter Logistic Equation to calculate cc50 values relative to each condition. (3-8) Data from panel (1-2) were used to generate individual plots relative to each time point. The CC50 values are shown in *red*.

Figure D1-2. Optimization of Fluorescence Reduction Assay (FRA) conditions.
Different number of MRC5 cells were seeded either in 96 well special optical plates or in 24-well plates and infected with TB4-IE2-EYFP and TB4-UL83-EYFP at different MOIs. At the indicated time points cells were processed for either microscopic analysis or fluorimetric quantification.
YFP signals relative to HCMV infected cells were quantified using a plate reader. Data were exported to excel and analyzed to calculate the mean fluorescence relative to each condition. To this end, the average signal relative to the mock infected samples was subtracted to the signal relative to every well. Data shown are mean $\pm$ standard deviation of the mean relative to a single experiment performed in triplicate, whereby the YFP mean fluorescence is plotted against the MOI (*top panels*) or the time post infection (*bottom panels*).

Figure E1-3. Analysis of HCMV gene expression by Western Blot assays. 30 μg of infected cell lysates were loaded on 8.5% bis polyacrylamide gels before being electrophoretically separated. Separated proteins were blotted on polyvinylidene fluoride membranes for 1 h in at 350 mV. Membranes were then saturated. The day after, membranes were washed and incubated 1 h with the appropriate secondary antibodies; then were incubated for 5 minutes with a made ECL substrate. Membranes were incubated for different times with an autoradiography film inside an autoradiography film cassette in the dark before being developed. Digital images were acquired with an imaging station (Gel Doc EZ System) and processed using Image J (NIH). Representative Western blot images of each experiment, relative to incubation with the indicated antibodies. Compounds were added at the following concentrations: B1 100 μM, B3 20 μM, B6 5 μM, C6 40 μM, GCV 5 μM.

Figure F1-4. Development of a TSA protein stability using ABI PRISM 7000. Lysozyme and SYPRO Orange were diluted to the indicated final concentrations, either in Potassium Phosphate (KPO_4) or in Citrate Phosphate (Citrate) buffers. Mixtures were loaded on 96-well white plates, before being loaded on a ABI PRISM7000 thermal cycler. Plates were heated from 22 to 95 °C at

approximately 1°C/min, and fluorescence data were acquired either with ROX or SYBR emission filters. Fluorescence data and -dF/dT ratios relative to the indicated conditions were plotted as a function of the temperature. Data were analyzed with GraphPad Prism to calculate the Tm after deletion of post-peak fluorescence using the Boltzman Sigmoidal Fit Function.

8. Appendix

8.1 Solutions

2YT Medium (pH 7). 16 g/L Tryptone, 10 g/L Yeast Extract, 5 g/L NaCl.

Buffer A. 50 mM Tris-HCl [pH 7.5], 5 mM EDTA, 2 mM DTT, 500 mM NaCl, and 20% glycerol.

Binding Buffer. 25mM HEPES pH 7.5, 12.5 mM MgCl2 , 20% glycerol, 0.1% NP-40, 150mM KCL, 0.15 mg/ml Bovine Serum Albumin (BSA), 1mM DTT.

NETN Buffer. 20mM Tris-HCL pH7.5, 100mM NaCl, 0.1mM EDTA, 0.5% NP-40.

cpt DMEM (GIBCO, 500ml). FBS 1:10, Pen-strep 1:100, L-Glutammina 1:100, Non-Essential Amino Acids Solution (1:100).

PBS 10x (1 litre). 2.4 g KH2PO4, 80 g NaCl, 11.45 g Na2HPO4, 2g KCL.

Freezing media (50 ml). 45 ml DMEM, 5 ml heath inactivated FBS (10 % v/v)**,** Solution stored at -20°C.

Luciferase lysis buffer. Triton 0,1%, Glycin-Glycine 25 mM, MgSO4 15 mM, EGTA 4 mM.

RIPA buffer. TrisHCl pH 7.4 50, NaCl 150 mM, Triton 1%, Sodium Deoxicolate 1%, SDS 0.1%, EDTA 1 mM

RIPA buffer plus protease inhibitors. TrisHCl pH 7.4 50, NaCl 150 mM, Triton 1%, Sodium Deoxicolate 1%, SDS 0.1%, EDTA 1 mM, Phenylmethylsulfonyl fluoride 17.4 ug/ml, Aprotinin 2 ug/ml, and Leupeptin 4 ug/ml

Protease inhibitors. Phenylmethylsulfonyl fluoride 1.74 mg/ml isopropanol; Aprotinin 500 ug/ml in MQ H_20; Leupeptin 1mg/ml in MQ H_20. Add fresh immediately before use.

Laemni loading buffer (5X). 0.25% Bromophenol blue, 0.5 M DTT (dithiothreitol), 50% Glycerol, 10% SDS (sodium dodecyl sulfate), 0.25 M Tris-Cl (pH 6.8).

Running buffer gel (8.5% - 8 %). H_2O, 30% acrylamide, 1.5M Tris pH 8.8, 10% SDS, 10% ammonium persulfate, TEMED.

Staking buffer gel (5%). H_2O, 30% acrylamide, 1M Tris pH 6.8, 10% SDS, 10% ammonium persulfate, TEMED.

Running buffer pH 8.3. 25mM Tris Base, 192mM glycine, 0.1% SDS.

Transfer buffer pH 8.3. 25mM Tris Base, 150mM glycine, 20% Methanol.

Protocol ECL (home made)
Stock A : 0.2 g 3- Aminophtalhydrazide(Luminol, Sigma A8511) in 4.5 ml DMSO
Stock B : 35 mg p Coumaric Acid (Sigma C9008) in 2.5 ml DMSO
1M Tris pH 9.35
Solution 1: Luminol 2.5 mM (3-Aminophtalhydrazide Luminol, Sigma Aldrich, A8511), p Coumaric Acid 1.5 mM (Sigma Aldrich C9008) in Tris pH 9.35 100 mM
Solution 2: H_20_2 0.0036% in Tris pH 9.35 100 mM
ECL home made substrate is composed by a mixture one to one of Solution 1 and Solution 2.

MTT. MTT (Applichem, A2231,0001) was diluited (5 mg/ml) in PBS in sterile conditions and in the dark. The solution was centrifuged at 1 minute x 700 rpm. Supernatant was aliquoted and stored in foil-covered eppendorfs (20 µl/vials) at -20°C until required.

Buffer Potassium Phosphate. K2HPO4 1M, KH2PO4 1M, NaCl 3M.

Citrate Phosphate Buffer (pH 7). Disodium phosphate 87 mM, Citric acid 6.4 mM, NaCl 50 mM.

Dilution Buffer: Na2HPO4 1M, NaH2PO4 1M, NaCl 3M.

TSA Buffers:

Buffer name	Buffer type
a) DNA polymerase stimulation buffer Tris HCl (PH8) 75 mM KCl 150 mM MgCl2 6,5 mM β-mercaptoetanolo 1,67 mM	**UL44 specific**
b) UL54 binding buffer Hepes (PH7.5) 50 mM EDTA 0,5 mM DTT 1 mM NaCl 150 mM Glycerol 4%	
c) DNA binding buffer Tris HCl (pH7.5) 20 mM NaCl 50 mM Glycerol 5% MgCl2 3 mM EDTA 0,1 mM DTT 0,1 mM	

Buffer name		Buffer type
d)Sodium Citrate pH4	50 mM	Sodium citrate (PH4-7)
NaCl	50 mM	
e) Sodium Citrate pH4	50 mM	
NaCl	250 mM	
f) Sodium Citrate pH5	50 mM	
NaCl	50 mM	
g) Sodium Citrate pH5	50 mM	
NaCl	250 mM	
h) Sodium Citrate pH6	50 mM	
NaCl	50 mM	
i) Sodium Citrate pH6	50 mM	
NaCl	250 mM	
l) Sodium Citrate pH7	50 mM	
NaCl	50 mM	
m) Sodium Citrate pH7	50 mM	
NaCl	250 mM	

Buffer name		Buffer type
n)Tris HCl pH7	50 mM	**Tris HCl (PH 7-9)**
NaCl	50 mM	
p)Tris HCl pH7	50 mM	
NaCl	250 mM	
q)Tris HCl pH8	50 mM	
NaCl	50 mM	
r)Tris HCl pH8	50 mM	
NaCl	250 mM	
s)Tris HCl pH9	50 mM	
NaCl	50 mM	
t)Tris HCl pH9	50 mM	
NaCl	250 mM	
n)Tris HCl pH7	50 mM	
NaCl	50 mM	
p)Tris HCl pH7	50 mM	
NaCl	250 mM	

Buffer name		Buffer type
u) Bicine pH8	50 mM	**Bicine (POH8-8.5)**
NaCl	50 mM	
v) Bicine pH8	50 mM	
NaCl	250 mM	
z) Bicine pH8.5	50 mM	
NaCl	50 mM	
z) Bicine pH8.5	50 mM	
NaCl	250 mM	

Table 8.2

Table 8.2.1 Layout of plates of Fluorescence Reduction assay with SMs 100 and 10 μM.

	1	2	3	4	5	6	7	8	9	10	11	12
A	PBS											
B	PBS	DMSO 0.5%		B1		B6		C3		MOCK		PBS
C		A1		DMSO 0.5%		B7		C4				
D		A2		B2		DMSO 0.5%		C6				
E		A3		B3		B8		DMSO 0.5%		DMEM		
F		A4		B4		C1		GCV		DMSO 0.5%		
G		A6		B5		C2						
H	PBS											

Table 8.2.2 VIKTOR X2 acquisition settings for Fluorometric detection of YFP signal in Fluorescence reduction assays

Protocol name ..... yfp x BRET
Protocol number ..... N/A
Name of the plate type ..... Generic 8x12 size plate
Number of repeats 1
Delay between repeats ..... 0 s
Measurement height ..... Default
Protocol notes .....

Shaking duration ..... 1.0 s
Shaking speed ..... Normal
Shaking diameter ..... 0.10 mm
Shaking type ..... Double orbit
Repeated operation ..... Yes

Name of the label ..... Fluorescein (1.0s)
Label technology ..... Prompt fluorometry
CW-lamp filter name F485
CW-lamp filter slot A5
Emission filter name F535
Emission filter slot A5
Measurement time ..... 1.0 s
Emission aperture ..... Small
CW-lamp energy 8704
Second measurement CW-lamp energy. 0
Emission side ..... Above
CW-Lamp Control ..... Stabilized Energy
Excitation Aperture ..... N/A

8.3 Instrument Set-up

8.3.1 Instrument set up for TSA assays with ABI PRISM 7000

Assay: Absolute Quantification
Detector: Sypro (ROX) – Passive Reference: None
Detector: Sypro (SYBER) – Passive Reference: None

Thermal Profile:
Stage 1 → Repetitions: 1 – Temperature: 20°C– Time 2:00
Stage 2 → Repetitions: 75
– Step1: Temperature: 23°C – Time 0:15
– Step2: Temperature: 22°C – Time 0:45

Data Collection: Stage 2, Step 2 at 0:45

Auto Increment:
Stage 1 → Repetitions: 1
Stage 2 → Repetitions: 75
– Step1: Temperature: 1°C – Time 0:00
– Step2: Temperature: 1°C – Time 0:00

8.3.2 Protocol TSA on a LightCycler 480 Real-Time PCR System

Program: Protein Melting Program

Thermal Profile:
First target → 20° C - Hold 15 seconds.
Second target →85 ° C - Acquisition Mode Continuous - 10 acquisitions per °C.
Third target → 20 ° C - Hold 15 seconds.

8.3.3 Protocol TSA on a ViiA 7 Real-Time PCR System [194]

Experiment Type: MELT CURVE
Ramp Speed: STANDARD
Target name: TARGET 1
Reporter: ROX
Quencher: NONE
Passive Reference: NONE
Run Method

Met Curve profile changes:
Delete Step 2 of the default cycle
Change the run method to "Step and Hold" with Time 1:00

Thermal Profile:
Temperature 25 °C - Time 2:00 hold
Ramping up in increments of 1 °C → Final Temperature of 95 °C - Time 2:00 hold

Select on all three cameras to activate fluorescence detection throughout the experiment.

Below the different combinations of excitation and emission filters that were used:

EXCITATION FILTERS	EMISSION FILTERS
x1: 470 nm +-15	m1: 520 nm+-15
x2: 520 nm +- 10	m3: 586 nm +- 10
x4: 580 nm +-10	m4: 623 nm +- 14
	m5 : 682 nm +-14

8.4 Markers

Protein marker. Prestained Protein SHARPMASS^{tm} VI (Euroclone).

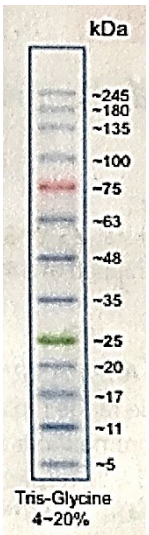

Bibliography.

1. Roizman, B., et al., *Herpesviridae. Definition, provisional nomenclature, and taxonomy. The Herpesvirus Study Group, the International Committee on Taxonomy of Viruses.* Intervirology, 1981. **16**(4): p. 201-17.
2. Kalejta, R.F., *Tegument proteins of human cytomegalovirus.* Microbiol Mol Biol Rev, 2008. **72**(2): p. 249-65, table of contents.
3. Pari, G.S., *Nuts and bolts of human cytomegalovirus lytic DNA replication.* Curr Top Microbiol Immunol, 2008. **325**: p. 153-66.
4. Gandhi, M.K. and R. Khanna, *Human cytomegalovirus: clinical aspects, immune regulation, and emerging treatments.* Lancet Infect Dis, 2004. **4**(12): p. 725-38.
5. Alford, C.A., et al., *Congenital and perinatal cytomegalovirus infections.* Rev Infect Dis, 1990. **12 Suppl 7**: p. S745-53.
6. Stagno, S. and R.J. Whitley, *Herpesvirus infections of pregnancy. Part I: Cytomegalovirus and Epstein-Barr virus infections.* N Engl J Med, 1985. **313**(20): p. 1270-4.
7. Stagno, S., et al., *Primary cytomegalovirus infection in pregnancy. Incidence, transmission to fetus, and clinical outcome.* JAMA, 1986. **256**(14): p. 1904-8.
8. Zaia, J.A., *Prevention and management of CMV-related problems after hematopoietic stem cell transplantation.* Bone Marrow Transplant, 2002. **29**(8): p. 633-8.
9. Roddie, C. and K.S. Peggs, *Immunotherapy for transplantation-associated viral infections.* J Clin Invest, 2017. **127**(7): p. 2513-2522.
10. van Rhee, F. and J. Barrett, *Adoptive transfer of Ag-specific T cells to prevent CMV disease after allogeneic stem-cell transplantation.* Cytotherapy, 2002. **4**(1): p. 3-10.
11. Mui, T.S., et al., *T-cell therapy for cytomegalovirus infection.* Curr Opin Organ Transplant, 2010. **15**(6): p. 744-50.
12. Kim, J., A.R. Kim, and E.C. Shin, *Cytomegalovirus Infection and Memory T Cell Inflation.* Immune Netw, 2015. **15**(4): p. 186-90.
13. Klenerman, P. and A. Oxenius, *T cell responses to cytomegalovirus.* Nat Rev Immunol, 2016. **16**(6): p. 367-77.
14. Camargo, J.F. and K.V. Komanduri, *Emerging concepts in cytomegalovirus infection following hematopoietic stem cell transplantation.* Hematol Oncol Stem Cell Ther, 2017. **10**(4): p. 233-238.
15. Cheung, T.W. and S.A. Teich, *Cytomegalovirus infection in patients with HIV infection.* Mt Sinai J Med, 1999. **66**(2): p. 113-24.
16. Cantoni, N., et al., *Evidence for a bidirectional relationship between cytomegalovirus replication and acute graft-versus-host disease.* Biol Blood Marrow Transplant, 2010. **16**(9): p. 1309-14.
17. Teira, P., et al., *Early cytomegalovirus reactivation remains associated with increased transplant-related mortality in the current era: a CIBMTR analysis.* Blood, 2016. **127**(20): p. 2427-38.
18. Schottstedt, V., et al., *Human Cytomegalovirus (HCMV) - Revised.* Transfus Med Hemother, 2010. **37**(6): p. 365-375.
19. Kalejta, R.F., *Functions of human cytomegalovirus tegument proteins prior to immediate early gene expression.* Curr Top Microbiol Immunol, 2008. **325**: p. 101-15.
20. Fields, B.N., D.M. Knipe, and P.M. Howley, , *Fields virology. 4th ed.* Fields virology., ed. D.M.K. editors-in-chief, Peter M. Howley, associate editors, Diane E. Griffin. 2001, Philadelphia: Lippincott Williams & Wilkins.
21. Baldanti, F., et al., *Use of the human cytomegalovirus (HCMV) antigenemia assay for diagnosis and monitoring of HCMV infections and detection of antiviral drug resistance in the immunocompromised.* J Clin Virol, 1998. **11**(1): p. 51-60.
22. Browne, E.P. and T. Shenk, *Human cytomegalovirus UL83-coded pp65 virion protein inhibits antiviral gene expression in infected cells.* Proc Natl Acad Sci U S A, 2003. **100**(20): p. 11439-44.
23. Chevillotte, M., et al., *Major tegument protein pp65 of human cytomegalovirus is required for the incorporation of pUL69 and pUL97 into the virus particle and for viral growth in macrophages.* J Virol, 2009. **83**(6): p. 2480-90.
24. Schmolke, S., et al., *The dominant phosphoprotein pp65 (UL83) of human cytomegalovirus is dispensable for growth in cell culture.* J Virol, 1995. **69**(10): p. 5959-68.
25. Kemble, G.W. and E.S. Mocarski, *A host cell protein binds to a highly conserved sequence element (pac-2) within the cytomegalovirus a sequence.* J Virol, 1989. **63**(11): p. 4715-28.
26. Van Damme, E. and M. Van Loock, *Functional annotation of human cytomegalovirus gene products: an update.* Front Microbiol, 2014. **5**: p. 218.
27. Pari, G.S. and D.G. Anders, *Eleven loci encoding trans-acting factors are required for transient complementation of human cytomegalovirus oriLyt-dependent DNA replication.* J Virol, 1993. **67**(12): p. 6979-88.
28. Karlin, S., E.S. Mocarski, and G.A. Schachtel, *Molecular evolution of herpesviruses: genomic and protein sequence comparisons.* J Virol, 1994. **68**(3): p. 1886-902.

29. Dunn, W., et al., *Functional profiling of a human cytomegalovirus genome.* Proc Natl Acad Sci U S A, 2003. **100**(24): p. 14223-8.
30. Sinzger, C., et al., *Modification of human cytomegalovirus tropism through propagation in vitro is associated with changes in the viral genome.* J Gen Virol, 1999. **80 (Pt 11)**: p. 2867-77.
31. MacCormac, L.P. and J.E. Grundy, *Two clinical isolates and the Toledo strain of cytomegalovirus contain endothelial cell tropic variants that are not present in the AD169, Towne, or Davis strains.* J Med Virol, 1999. **57**(3): p. 298-307.
32. Rowe, W.P., et al., *Cytopathogenic agent resembling human salivary gland virus recovered from tissue cultures of human adenoids.* Proc Soc Exp Biol Med, 1956. **92**(2): p. 418-24.
33. Craig, J.M., et al., *Isolation of intranuclear inclusion producing agents from infants with illnesses resembling cytomegalic inclusion disease.* Proc Soc Exp Biol Med, 1957. **94**(1): p. 4-12.
34. Plotkin, S.A., et al., *Protective effects of Towne cytomegalovirus vaccine against low-passage cytomegalovirus administered as a challenge.* J Infect Dis, 1989. **159**(5): p. 860-5.
35. Dargan, D.J., et al., *Sequential mutations associated with adaptation of human cytomegalovirus to growth in cell culture.* J Gen Virol, 2010. **91**(Pt 6): p. 1535-46.
36. Bissinger, A.L., et al., *Human cytomegalovirus as a direct pathogen: correlation of multiorgan involvement and cell distribution with clinical and pathological findings in a case of congenital inclusion disease.* J Med Virol, 2002. **67**(2): p. 200-6.
37. Soderberg-Naucler, C., K.N. Fish, and J.A. Nelson, *Reactivation of latent human cytomegalovirus by allogeneic stimulation of blood cells from healthy donors.* Cell, 1997. **91**(1): p. 119-26.
38. Sinzger, C., et al., *Fibroblasts, epithelial cells, endothelial cells and smooth muscle cells are major targets of human cytomegalovirus infection in lung and gastrointestinal tissues.* J Gen Virol, 1995. **76 (Pt 4)**: p. 741-50.
39. Plachter, B., C. Sinzger, and G. Jahn, *Cell types involved in replication and distribution of human cytomegalovirus.* Adv Virus Res, 1996. **46**: p. 195-261.
40. Vanarsdall, A.L. and D.C. Johnson, *Human cytomegalovirus entry into cells.* Curr Opin Virol, 2012. **2**(1): p. 37-42.
41. Soroceanu, L., A. Akhavan, and C.S. Cobbs, *Platelet-derived growth factor-alpha receptor activation is required for human cytomegalovirus infection.* Nature, 2008. **455**(7211): p. 391-5.
42. Feire, A.L., H. Koss, and T. Compton, *Cellular integrins function as entry receptors for human cytomegalovirus via a highly conserved disintegrin-like domain.* Proc Natl Acad Sci U S A, 2004. **101**(43): p. 15470-5.
43. Wang, X., et al., *Epidermal growth factor receptor is a cellular receptor for human cytomegalovirus.* Nature, 2003. **424**(6947): p. 456-61.
44. Compton, T., R.R. Nepomuceno, and D.M. Nowlin, *Human cytomegalovirus penetrates host cells by pH-independent fusion at the cell surface.* Virology, 1992. **191**(1): p. 387-95.
45. Ryckman, B.J., et al., *Human cytomegalovirus entry into epithelial and endothelial cells depends on genes UL128 to UL150 and occurs by endocytosis and low-pH fusion.* J Virol, 2006. **80**(2): p. 710-22.
46. Zhu, H., J.P. Cong, and T. Shenk, *Use of differential display analysis to assess the effect of human cytomegalovirus infection on the accumulation of cellular RNAs: induction of interferon-responsive RNAs.* Proc Natl Acad Sci U S A, 1997. **94**(25): p. 13985-90.
47. Zhu, H., et al., *Cellular gene expression altered by human cytomegalovirus: global monitoring with oligonucleotide arrays.* Proc Natl Acad Sci U S A, 1998. **95**(24): p. 14470-5.
48. Browne, E.P., et al., *Altered cellular mRNA levels in human cytomegalovirus-infected fibroblasts: viral block to the accumulation of antiviral mRNAs.* J Virol, 2001. **75**(24): p. 12319-30.
49. Boyle, K.A., R.L. Pietropaolo, and T. Compton, *Engagement of the cellular receptor for glycoprotein B of human cytomegalovirus activates the interferon-responsive pathway.* Mol Cell Biol, 1999. **19**(5): p. 3607-13.
50. Simmen, K.A., et al., *Global modulation of cellular transcription by human cytomegalovirus is initiated by viral glycoprotein B.* Proc Natl Acad Sci U S A, 2001. **98**(13): p. 7140-5.
51. Yurochko, A.D., et al., *Human cytomegalovirus upregulates NF-kappa B activity by transactivating the NF-kappa B p105/p50 and p65 promoters.* J Virol, 1995. **69**(9): p. 5391-400.
52. Fortunato, E.A. and D.H. Spector, *Regulation of human cytomegalovirus gene expression.* Adv Virus Res, 1999. **54**: p. 61-128.
53. Landolfo, S., et al., *The human cytomegalovirus.* Pharmacol Ther, 2003. **98**(3): p. 269-97.
54. Margolis, M.J., et al., *Interaction of the 72-kilodalton human cytomegalovirus IE1 gene product with E2F1 coincides with E2F-dependent activation of dihydrofolate reductase transcription.* J Virol, 1995. **69**(12): p. 7759-67.
55. Song, Y.J. and M.F. Stinski, *Effect of the human cytomegalovirus IE86 protein on expression of E2F-responsive genes: a DNA microarray analysis.* Proc Natl Acad Sci U S A, 2002. **99**(5): p. 2836-41.
56. Murphy, E.A., et al., *The human cytomegalovirus IE86 protein can block cell cycle progression after inducing transition into the S phase of permissive cells.* J Virol, 2000. **74**(15): p. 7108-18.

57. Fortunato, E.A., et al., *Exploitation of cellular signaling and regulatory pathways by human cytomegalovirus.* Trends Microbiol, 2000. **8**(3): p. 111-9.
58. Kalejta, R.F. and T. Shenk, *Manipulation of the cell cycle by human cytomegalovirus.* Front Biosci, 2002. **7**: p. d295-306.
59. Chambers, J., et al., *DNA microarrays of the complex human cytomegalovirus genome: profiling kinetic class with drug sensitivity of viral gene expression.* J Virol, 1999. **73**(7): p. 5757-66.
60. Ertl, P.F. and K.L. Powell, *Physical and functional interaction of human cytomegalovirus DNA polymerase and its accessory protein (ICP36) expressed in insect cells.* J Virol, 1992. **66**(7): p. 4126-33.
61. Tenney, D.J. and A.M. Colberg-Poley, *Human cytomegalovirus UL36-38 and US3 immediate-early genes: temporally regulated expression of nuclear, cytoplasmic, and polysome-associated transcripts during infection.* J Virol, 1991. **65**(12): p. 6724-34.
62. Skaletskaya, A., et al., *A cytomegalovirus-encoded inhibitor of apoptosis that suppresses caspase-8 activation.* Proc Natl Acad Sci U S A, 2001. **98**(14): p. 7829-34.
63. Goldmacher, V.S., et al., *A cytomegalovirus-encoded mitochondria-localized inhibitor of apoptosis structurally unrelated to Bcl-2.* Proc Natl Acad Sci U S A, 1999. **96**(22): p. 12536-41.
64. Terhune, S., et al., *Human cytomegalovirus UL38 protein blocks apoptosis.* J Virol, 2007. **81**(7): p. 3109-23.
65. Romanowski, M.J. and T. Shenk, *Characterization of the human cytomegalovirus irs1 and trs1 genes: a second immediate-early transcription unit within irs1 whose product antagonizes transcriptional activation.* J Virol, 1997. **71**(2): p. 1485-96.
66. Wright, D.A. and D.H. Spector, *Posttranscriptional regulation of a class of human cytomegalovirus phosphoproteins encoded by an early transcription unit.* J Virol, 1989. **63**(7): p. 3117-27.
67. Ahn, J.H., W.J. Jang, and G.S. Hayward, *The human cytomegalovirus IE2 and UL112-113 proteins accumulate in viral DNA replication compartments that initiate from the periphery of promyelocytic leukemia protein-associated nuclear bodies (PODs or ND10).* J Virol, 1999. **73**(12): p. 10458-71.
68. Park, M.Y., et al., *Interactions among four proteins encoded by the human cytomegalovirus UL112-113 region regulate their intranuclear targeting and the recruitment of UL44 to prereplication foci.* J Virol, 2006. **80**(6): p. 2718-27.
69. Tanner, N.K. and P. Linder, *DExD/H box RNA helicases: from generic motors to specific dissociation functions.* Mol Cell, 2001. **8**(2): p. 251-62.
70. Colletti, K.S., et al., *Human cytomegalovirus UL84 is a phosphoprotein that exhibits UTPase activity and is a putative member of the DExD/H box family of proteins.* J Biol Chem, 2005. **280**(12): p. 11955-60.
71. Gebert, S., et al., *The UL84 protein of human cytomegalovirus acts as a transdominant inhibitor of immediate-early-mediated transactivation that is able to prevent viral replication.* J Virol, 1997. **71**(9): p. 7048-60.
72. Lischka, P., et al., *Human cytomegalovirus UL84 protein contains two nuclear export signals and shuttles between the nucleus and the cytoplasm.* J Virol, 2006. **80**(20): p. 10274-80.
73. Xu, Y., et al., *Human cytomegalovirus UL84 insertion mutant defective for viral DNA synthesis and growth.* J Virol, 2004. **78**(19): p. 10360-9.
74. Gao, Y., K. Colletti, and G.S. Pari, *Identification of human cytomegalovirus UL84 virus- and cell-encoded binding partners by using proteomics analysis.* J Virol, 2008. **82**(1): p. 96-104.
75. Mettenleiter, T.C., *Herpesvirus assembly and egress.* J Virol, 2002. **76**(4): p. 1537-47.
76. Digard, P., et al., *Functional analysis of the herpes simplex virus UL42 protein.* J Virol, 1993. **67**(3): p. 1159-68.
77. Gallo, M.L., et al., *The essential 65-kilodalton DNA-binding protein of herpes simplex virus stimulates the virus-encoded DNA polymerase.* J Virol, 1989. **63**(12): p. 5023-9.
78. Davison, A.J. and J.E. Scott, *The complete DNA sequence of varicella-zoster virus.* J Gen Virol, 1986. **67 (Pt 9)**: p. 1759-816.
79. Agulnick, A.D., et al., *Identification of a DNA-binding protein of human herpesvirus 6, a putative DNA polymerase stimulatory factor.* J Gen Virol, 1993. **74 (Pt 6)**: p. 1003-9.
80. Nicholas, J., *Determination and analysis of the complete nucleotide sequence of human herpesvirus.* J Virol, 1996. **70**(9): p. 5975-89.
81. Lin, K., C.Y. Dai, and R.P. Ricciardi, *Cloning and functional analysis of Kaposi's sarcoma-associated herpesvirus DNA polymerase and its processivity factor.* J Virol, 1998. **72**(7): p. 6228-32.
82. Matthews, J.T., B.J. Terry, and A.K. Field, *The structure and function of the HSV DNA replication proteins: defining novel antiviral targets.* Antiviral Res, 1993. **20**(2): p. 89-114.
83. Larder, B.A., S.D. Kemp, and G. Darby, *Related functional domains in virus DNA polymerases.* EMBO J, 1987. **6**(1): p. 169-75.
84. Ye, L.B. and E.S. Huang, *In vitro expression of the human cytomegalovirus DNA polymerase gene: effects of sequence alterations on enzyme activity.* J Virol, 1993. **67**(11): p. 6339-47.
85. Nishiyama, Y., K. Maeno, and S. Yoshida, *Characterization of human cytomegalovirus-induced DNA polymerase and the associated 3'-to-5', exonuclease.* Virology, 1983. **124**(2): p. 221-31.

86. Alvisi, G., et al., *Human cytomegalovirus DNA polymerase catalytic subunit pUL54 possesses independently acting nuclear localization and ppUL44 binding motifs.* Traffic, 2006. **7**(10): p. 1322-32.
87. Loregian, A., et al., *The catalytic subunit of herpes simplex virus type 1 DNA polymerase contains a nuclear localization signal in the UL42-binding region.* Virology, 2000. **273**(1): p. 139-48.
88. Alvisi, G., et al., *Nuclear import of HSV-1 DNA polymerase processivity factor UL42 is mediated by a C-terminally located bipartite nuclear localization signal.* Biochemistry, 2008. **47**(52): p. 13764-77.
89. Ripalti, A., et al., *Cytomegalovirus-mediated induction of antisense mRNA expression to UL44 inhibits virus replication in an astrocytoma cell line: identification of an essential gene.* J Virol, 1995. **69**(4): p. 2047-57.
90. Weiland, K.L., et al., *Functional analysis of human cytomegalovirus polymerase accessory protein.* Virus Res, 1994. **34**(3): p. 191-206.
91. Alvisi, G., et al., *A protein kinase CK2 site flanking the nuclear targeting signal enhances nuclear transport of human cytomegalovirus ppUL44.* Traffic, 2005. **6**(11): p. 1002-1013.
92. Alvisi, G., et al., *Multiple phosphorylation sites at the C-terminus regulate nuclear import of HCMV DNA polymerase processivity factor ppUL44.* Virology, 2011. **417**(2): p. 259-267.
93. Sinigalia, E., et al., *The human cytomegalovirus DNA polymerase processivity factor UL44 is modified by SUMO in a DNA-dependent manner.* PLoS One, 2012. **7**(11): p. e49630.
94. Mattoscio, D., C.V. Segre, and S. Chiocca, *Viral manipulation of cellular protein conjugation pathways: The SUMO lesson.* World J Virol, 2013. **2**(2): p. 79-90.
95. Appleton, B.A., et al., *The cytomegalovirus DNA polymerase subunit UL44 forms a C clamp-shaped dimer.* Mol Cell, 2004. **15**(2): p. 233-44.
96. Gulbis, J.M., et al., *Structure of the C-terminal region of p21(WAF1/CIP1) complexed with human PCNA.* Cell, 1996. **87**(2): p. 297-306.
97. Zuccola, H.J., et al., *The crystal structure of an unusual processivity factor, herpes simplex virus UL42, bound to the C terminus of its cognate polymerase.* Mol Cell, 2000. **5**(2): p. 267-78.
98. Appleton, B.A., et al., *Crystal structure of the cytomegalovirus DNA polymerase subunit UL44 in complex with the C terminus from the catalytic subunit. Differences in structure and function relative to unliganded UL44.* J Biol Chem, 2006. **281**(8): p. 5224-32.
99. Komazin-Meredith, G., et al., *The human cytomegalovirus UL44 C clamp wraps around DNA.* Structure, 2008. **16**(8): p. 1214-25.
100. Sinigalia, E., et al., *Role of homodimerization of human cytomegalovirus DNA polymerase accessory protein UL44 in origin-dependent DNA replication in cells.* J Virol, 2008. **82**(24): p. 12574-9.
101. Alvisi, G., et al., *The tumor cell specific nuclear targeting signal of Apoptin*, in *Proteins Killing Tumour Cells*, C. Backendorf, M.H.M. Noteborn , and M. Tavassoli, Editors. 2009, Research-Signpost: Trivandrum. p. 11.
102. Snydman, D.R., et al., *Use of cytomegalovirus immune globulin to prevent cytomegalovirus disease in renal-transplant recipients.* N Engl J Med, 1987. **317**(17): p. 1049-54.
103. Ballow, M., *Mechanisms of action of intravenous immune serum globulin therapy.* Pediatr Infect Dis J, 1994. **13**(9): p. 806-11.
104. Clark, A.L., *Clinical uses of intravenous immunoglobulin in pregnancy.* Clin Obstet Gynecol, 1999. **42**(2): p. 368-80.
105. Keller, M.A. and E.R. Stiehm, *Passive immunity in prevention and treatment of infectious diseases.* Clin Microbiol Rev, 2000. **13**(4): p. 602-14.
106. Sawyer, L.A., *Antibodies for the prevention and treatment of viral diseases.* Antiviral Res, 2000. **47**(2): p. 57-77.
107. Nigro, G., et al., *Passive immunization during pregnancy for congenital cytomegalovirus infection.* N Engl J Med, 2005. **353**(13): p. 1350-62.
108. Revello, M.G., et al., *A randomized trial of hyperimmune globulin to prevent congenital cytomegalovirus.* N Engl J Med, 2014. **370**(14): p. 1316-26.
109. Limaye, A.P., et al., *Late-onset cytomegalovirus disease in liver transplant recipients despite antiviral prophylaxis.* Transplantation, 2004. **78**(9): p. 1390-6.
110. Razonable, R.R., V.C. Emery, and I. th Annual Meeting of the, *Management of CMV infection and disease in transplant patients. 27-29 February 2004.* Herpes, 2004. **11**(3): p. 77-86.
111. Biron, K.K., et al., *Metabolic activation of the nucleoside analog 9-[(2-hydroxy-1-(hydroxymethyl)ethoxy]methyl)guanine in human diploid fibroblasts infected with human cytomegalovirus.* Proc Natl Acad Sci U S A, 1985. **82**(8): p. 2473-7.
112. Biron, K.K., *Antiviral drugs for cytomegalovirus diseases.* Antiviral Res, 2006. **71**(2-3): p. 154-63.
113. Hamzeh, F.M., et al., *Identification of the lytic origin of DNA replication in human cytomegalovirus by a novel approach utilizing ganciclovir-induced chain termination.* J Virol, 1990. **64**(12): p. 6184-95.
114. Cheng, Y.C., et al., *Metabolism of 9-(1,3-dihydroxy-2-propoxymethyl)guanine, a new anti-herpes virus compound, in herpes simplex virus-infected cells.* J Biol Chem, 1983. **258**(20): p. 12460-4.
115. Crumpacker, C.S., *Ganciclovir.* N Engl J Med, 1996. **335**(10): p. 721-9.

116. De Clercq, E. and H.J. Field, *Antiviral prodrugs - the development of successful prodrug strategies for antiviral chemotherapy.* Br J Pharmacol, 2006. **147**(1): p. 1-11.
117. Boeckh, M., B. Fries, and W.G. Nichols, *Recent advances in the prevention of CMV infection and disease after hematopoietic stem cell transplantation.* Pediatr Transplant, 2004. **8 Suppl 5**: p. 19-27.
118. Hantz, S., et al., *Drug-resistant cytomegalovirus in transplant recipients: a French cohort study.* J Antimicrob Chemother, 2010. **65**(12): p. 2628-40.
119. Boivin, G., et al., *Cytomegalovirus resistance in solid organ transplant recipients treated with intravenous ganciclovir or oral valganciclovir.* Antivir Ther, 2009. **14**(5): p. 697-704.
120. Li, F., et al., *Incidence and clinical features of ganciclovir-resistant cytomegalovirus disease in heart transplant recipients.* Clin Infect Dis, 2007. **45**(4): p. 439-47.
121. Shmueli, E., et al., *High rate of cytomegalovirus drug resistance among patients receiving preemptive antiviral treatment after haploidentical stem cell transplantation.* J Infect Dis, 2014. **209**(4): p. 557-61.
122. Limaye, A.P., et al., *Emergence of ganciclovir-resistant cytomegalovirus disease among recipients of solid-organ transplants.* Lancet, 2000. **356**(9230): p. 645-9.
123. Boutolleau, D., et al., *Resistance pattern of cytomegalovirus (CMV) after oral valganciclovir therapy in transplant recipients at high-risk for CMV infection.* Antiviral Res, 2009. **81**(2): p. 174-9.
124. Lurain, N.S. and S. Chou, *Antiviral drug resistance of human cytomegalovirus.* Clin Microbiol Rev, 2010. **23**(4): p. 689-712.
125. Boeckh, M., et al., *Valganciclovir for the prevention of complications of late cytomegalovirus infection after allogeneic hematopoietic cell transplantation: a randomized trial.* Ann Intern Med, 2015. **162**(1): p. 1-10.
126. Schreiber, A., et al., *Antiviral treatment of cytomegalovirus infection and resistant strains.* Expert Opin Pharmacother, 2009. **10**(2): p. 191-209.
127. Ayala, E., et al., *Valganciclovir is safe and effective as pre-emptive therapy for CMV infection in allogeneic hematopoietic stem cell transplantation.* Bone Marrow Transplant, 2006. **37**(9): p. 851-6.
128. Cvetkovic, R.S. and K. Wellington, *Valganciclovir: a review of its use in the management of CMV infection and disease in immunocompromised patients.* Drugs, 2005. **65**(6): p. 859-78.
129. Chrisp, P. and S.P. Clissold, *Foscarnet. A review of its antiviral activity, pharmacokinetic properties and therapeutic use in immunocompromised patients with cytomegalovirus retinitis.* Drugs, 1991. **41**(1): p. 104-29.
130. Erice, A., *Resistance of human cytomegalovirus to antiviral drugs.* Clin Microbiol Rev, 1999. **12**(2): p. 286-97.
131. Ariza-Heredia, E.J., L. Nesher, and R.F. Chemaly, *Cytomegalovirus diseases after hematopoietic stem cell transplantation: a mini-review.* Cancer Lett, 2014. **342**(1): p. 1-8.
132. Hebart, H. and H. Einsele, *Clinical aspects of CMV infection after stem cell transplantation.* Hum Immunol, 2004. **65**(5): p. 432-6.
133. Ljungman, P., M. Hakki, and M. Boeckh, *Cytomegalovirus in hematopoietic stem cell transplant recipients.* Hematol Oncol Clin North Am, 2011. **25**(1): p. 151-69.
134. Lischka, P., et al., *In vitro and in vivo activities of the novel anticytomegalovirus compound AIC246.* Antimicrob Agents Chemother, 2010. **54**(3): p. 1290-7.
135. Verghese, P.S. and M.R. Schleiss, *Letermovir Treatment of Human Cytomegalovirus Infection Antiinfective Agent.* Drugs Future, 2013. **38**(5): p. 291-298.
136. Melendez, D.P. and R.R. Razonable, *Letermovir and inhibitors of the terminase complex: a promising new class of investigational antiviral drugs against human cytomegalovirus.* Infect Drug Resist, 2015. **8**: p. 269-77.
137. Marschall, M., et al., *In vitro evaluation of the activities of the novel anticytomegalovirus compound AIC246 (letermovir) against herpesviruses and other human pathogenic viruses.* Antimicrob Agents Chemother, 2012. **56**(2): p. 1135-7.
138. Goldner, T., et al., *Geno- and phenotypic characterization of human cytomegalovirus mutants selected in vitro after letermovir (AIC246) exposure.* Antimicrob Agents Chemother, 2014. **58**(1): p. 610-3.
139. Kropeit, D., et al., *Pharmacokinetics and Safety of Letermovir Coadministered With Cyclosporine A or Tacrolimus in Healthy Subjects.* Clin Pharmacol Drug Dev, 2018. **7**(1): p. 9-21.
140. Lischka, P., D. Michel, and H. Zimmermann, *Characterization of Cytomegalovirus Breakthrough Events in a Phase 2 Prophylaxis Trial of Letermovir (AIC246, MK 8228).* J Infect Dis, 2016. **213**(1): p. 23-30.
141. Lischka, P., et al., *Impact of glycoprotein B genotype and naturally occurring ORF UL56 polymorphisms upon susceptibility of clinical human cytomegalovirus isolates to letermovir.* Antiviral Res, 2016. **132**: p. 204-9.
142. Williams, S.L., et al., *In vitro activities of benzimidazole D- and L-ribonucleosides against herpesviruses.* Antimicrob Agents Chemother, 2003. **47**(7): p. 2186-92.
143. Drew, W.L., et al., *Maribavir sensitivity of cytomegalovirus isolates resistant to ganciclovir, cidofovir or foscarnet.* J Clin Virol, 2006. **37**(2): p. 124-7.
144. Chou, S., L.C. Wechel, and G.I. Marousek, *Cytomegalovirus UL97 kinase mutations that confer maribavir resistance.* J Infect Dis, 2007. **196**(1): p. 91-4.
145. Dropulic, L.K. and J.I. Cohen, *Update on new antivirals under development for the treatment of double-stranded DNA virus infections.* Clin Pharmacol Ther, 2010. **88**(5): p. 610-9.

146. Marty, F.M., et al., *Brincidofovir for Prevention of Cytomegalovirus (CMV) after Allogeneic Hematopoietic Cell Transplantation (HCT) in CMV-Seropositive Patients: A Randomized, Double-Blind, Placebo-Controlled, Parallel-Group Phase 3 Trial.* Biology of Blood and Marrow Transplantation, 2016. **22**(3): p. S23.
147. James, S.H., et al., *Selection and recombinant phenotyping of a novel CMX001 and cidofovir resistance mutation in human cytomegalovirus.* Antimicrob Agents Chemother, 2013. **57**(7): p. 3321-5.
148. Meesing, A. and R.R. Razonable, *New Developments in the Management of Cytomegalovirus Infection After Transplantation.* Drugs, 2018. **78**(11): p. 1085-1103.
149. Eid, A.J. and R.R. Razonable, *New developments in the management of cytomegalovirus infection after solid organ transplantation.* Drugs, 2010. **70**(8): p. 965-81.
150. Avery, R.K., et al., *Utility of leflunomide in the treatment of complex cytomegalovirus syndromes.* Transplantation, 2010. **90**(4): p. 419-26.
151. Ciszek, M., et al., *Leflunomide as a rescue treatment in ganciclovir-resistant cytomegalovirus infection in a seronegative renal transplant recipient--a case report.* Ann Transplant, 2014. **19**: p. 60-3.
152. Verkaik, N.J., et al., *Leflunomide as part of the treatment for multidrug-resistant cytomegalovirus disease after lung transplantation: case report and review of the literature.* Transpl Infect Dis, 2013. **15**(6): p. E243-9.
153. El Chaer, F., D.P. Shah, and R.F. Chemaly, *How I treat resistant cytomegalovirus infection in hematopoietic cell transplantation recipients.* Blood, 2016. **128**(23): p. 2624-2636.
154. Sellar, R.S., et al., *Evidence for clinical activity of artesunate in multidrug-resistant herpes simplex infection following HSCT.* Bone Marrow Transplant, 2012. **47**(11): p. 1482-3.
155. Wolf, D.G., et al., *Human cytomegalovirus kinetics following institution of artesunate after hematopoietic stem cell transplantation.* Antiviral Res, 2011. **90**(3): p. 183-6.
156. Shapira, M.Y., et al., *Artesunate as a potent antiviral agent in a patient with late drug-resistant cytomegalovirus infection after hematopoietic stem cell transplantation.* Clin Infect Dis, 2008. **46**(9): p. 1455-7.
157. Lau, P.K., et al., *Artesunate is ineffective in controlling valganciclovir-resistant cytomegalovirus infection.* Clin Infect Dis, 2011. **52**(2): p. 279.
158. Germi, R., et al., *Success and failure of artesunate treatment in five transplant recipients with disease caused by drug-resistant cytomegalovirus.* Antiviral Res, 2014. **101**: p. 57-61.
159. de Chassey, B., et al., *New horizons for antiviral drug discovery from virus-host protein interaction networks.* Curr Opin Virol, 2012. **2**(5): p. 606-13.
160. Pawson, T. and J.D. Scott, *Signaling through scaffold, anchoring, and adaptor proteins.* Science, 1997. **278**(5346): p. 2075-80.
161. Cohen, F.E. and S.B. Prusiner, *Pathologic conformations of prion proteins.* Annu Rev Biochem, 1998. **67**: p. 793-819.
162. Selkoe, D.J., *The cell biology of beta-amyloid precursor protein and presenilin in Alzheimer's disease.* Trends Cell Biol, 1998. **8**(11): p. 447-53.
163. Loregian, A., H.S. Marsden, and G. Palu, *Protein-protein interactions as targets for antiviral chemotherapy.* Rev Med Virol, 2002. **12**(4): p. 239-62.
164. Jaenicke, R., *Protein folding: local structures, domains, subunits, and assemblies.* Biochemistry, 1991. **30**(13): p. 3147-61.
165. Arkin, M.R. and J.A. Wells, *Small-molecule inhibitors of protein-protein interactions: progressing towards the dream.* Nat Rev Drug Discov, 2004. **3**(4): p. 301-17.
166. Venkatesan, K., et al., *An empirical framework for binary interactome mapping.* Nat Methods, 2009. **6**(1): p. 83-90.
167. Hwang, H., et al., *Protein-protein docking benchmark version 4.0.* Proteins, 2010. **78**(15): p. 3111-4.
168. Fuller, J.C., N.J. Burgoyne, and R.M. Jackson, *Predicting druggable binding sites at the protein-protein interface.* Drug Discov Today, 2009. **14**(3-4): p. 155-61.
169. Basse, M.J., et al., *2P2Idb: a structural database dedicated to orthosteric modulation of protein-protein interactions.* Nucleic Acids Res, 2013. **41**(Database issue): p. D824-7.
170. Higueruelo, A.P., et al., *Atomic interactions and profile of small molecules disrupting protein-protein interfaces: the TIMBAL database.* Chem Biol Drug Des, 2009. **74**(5): p. 457-67.
171. Labbe, C.M., et al., *iPPI-DB: a manually curated and interactive database of small non-peptide inhibitors of protein-protein interactions.* Drug Discov Today, 2013. **18**(19-20): p. 958-68.
172. Johnson, D.K. and J. Karanicolas, *Druggable protein interaction sites are more predisposed to surface pocket formation than the rest of the protein surface.* PLoS Comput Biol, 2013. **9**(3): p. e1002951.
173. Smith, M.C. and J.E. Gestwicki, *Features of protein-protein interactions that translate into potent inhibitors: topology, surface area and affinity.* Expert Rev Mol Med, 2012. **14**: p. e16.
174. Wells, J.A. and C.L. McClendon, *Reaching for high-hanging fruit in drug discovery at protein-protein interfaces.* Nature, 2007. **450**(7172): p. 1001-9.
175. Hajduk, P.J. and J. Greer, *A decade of fragment-based drug design: strategic advances and lessons learned.* Nat Rev Drug Discov, 2007. **6**(3): p. 211-9.

176. Kozakov, D., et al., *Structural conservation of druggable hot spots in protein-protein interfaces.* Proc Natl Acad Sci U S A, 2011. **108**(33): p. 13528-33.
177. Singh, S.K., et al., *Synthetic peptides as inactivators of multimeric enzymes: inhibition of Plasmodium falciparum triosephosphate isomerase by interface peptides.* FEBS Lett, 2001. **501**(1): p. 19-23.
178. Cochran, A.G., *Antagonists of protein-protein interactions.* Chem Biol, 2000. **7**(4): p. R85-94.
179. Cohen, E.A., et al., *Specific inhibition of herpesvirus ribonucleotide reductase by a nonapeptide derived from the carboxy terminus of subunit 2.* Nature, 1986. **321**(6068): p. 441-3.
180. Pilger, B.D., C. Cui, and D.M. Coen, *Identification of a small molecule that inhibits herpes simplex virus DNA Polymerase subunit interactions and viral replication.* Chem Biol, 2004. **11**(5): p. 647-54.
181. Shultz, M.D., et al., *Small-molecule dimerization inhibitors of wild-type and mutant HIV protease: a focused library approach.* J Am Chem Soc, 2004. **126**(32): p. 9886-7.
182. Divita, G., et al., *Inhibition of human immunodeficiency virus type 1 reverse transcriptase dimerization using synthetic peptides derived from the connection domain.* J Biol Chem, 1994. **269**(18): p. 13080-3.
183. Sourgen, F., et al., *A synthetic peptide from the human immunodeficiency virus type-1 integrase exhibits coiled-coil properties and interferes with the in vitro integration activity of the enzyme. Correlated biochemical and spectroscopic results.* Eur J Biochem, 1996. **240**(3): p. 765-73.
184. Li, C., et al., *Screening for Novel Small-Molecule Inhibitors Targeting the Assembly of Influenza Virus Polymerase Complex by a Bimolecular Luminescence Complementation-Based Reporter System.* J Virol, 2017. **91**(5).
185. Muratore, G., et al., *Small molecule inhibitors of influenza A and B viruses that act by disrupting subunit interactions of the viral polymerase.* Proc Natl Acad Sci U S A, 2012. **109**(16): p. 6247-52.
186. Loregian, A. and D.M. Coen, *Selective anti-cytomegalovirus compounds discovered by screening for inhibitors of subunit interactions of the viral polymerase.* Chem Biol, 2006. **13**(2): p. 191-200.
187. Pantoliano, M.W., et al., *High-density miniaturized thermal shift assays as a general strategy for drug discovery.* J Biomol Screen, 2001. **6**(6): p. 429-40.
188. Lo, M.C., et al., *Evaluation of fluorescence-based thermal shift assays for hit identification in drug discovery.* Anal Biochem, 2004. **332**(1): p. 153-9.
189. Loregian, A., et al., *Residues of human cytomegalovirus DNA polymerase catalytic subunit UL54 that are necessary and sufficient for interaction with the accessory protein UL44.* J Virol, 2004. **78**(1): p. 158-67.
190. Silva, N.L., et al., *The carboxyl-terminal region of the Na+/H+ exchanger interacts with mammalian heat shock protein.* Biochemistry, 1995. **34**(33): p. 10412-20.
191. Straschewski, S., et al., *Human cytomegaloviruses expressing yellow fluorescent fusion proteins--characterization and use in antiviral screening.* PLoS One, 2010. **5**(2): p. e9174.
192. Mercorelli, B., et al., *Sulfated derivatives of Escherichia coli K5 capsular polysaccharide are potent inhibitors of human cytomegalovirus.* Antimicrob Agents Chemother, 2010. **54**(11): p. 4561-7.
193. King, A.C., et al., *High-throughput measurement, correlation analysis, and machine-learning predictions for pH and thermal stabilities of Pfizer-generated antibodies.* Protein Sci, 2011. **20**(9): p. 1546-57.
194. Huynh, K. and C.L. Partch, *Analysis of protein stability and ligand interactions by thermal shift assay.* Curr Protoc Protein Sci, 2015. **79**: p. 28 9 1-14.
195. Tocci, M.J., et al., *Effects of the nucleoside analog 2'-nor-2'-deoxyguanosine on human cytomegalovirus replication.* Antimicrob Agents Chemother, 1984. **25**(2): p. 247-52.
196. West, P.G., et al., *Enhanced detection of cytomegalovirus in confluent MRC-5 cells treated with dexamethasone and dimethyl sulfoxide.* J Clin Microbiol, 1988. **26**(12): p. 2510-4.
197. Tanaka, J., et al., *Effect of dimethyl sulfoxide on interaction of human cytomegalovirus with host cell: conversion of a nonproductive state of cell to a productive state for virus replication.* Virology, 1985. **146**(2): p. 165-76.
198. Seetoh, W.G. and C. Abell, *Disrupting the Constitutive, Homodimeric Protein-Protein Interface in CK2beta Using a Biophysical Fragment-Based Approach.* J Am Chem Soc, 2016. **138**(43): p. 14303-14311.
199. Rayaprolu, V., et al., *Fluorometric Estimation of Viral Thermal Stability.* Bio Protoc, 2014. **4**(15).
200. Oliveira Silva, C., et al., *Lysozyme Photochemistry as a Function of Temperature. The Protective Effect of Nanoparticles on Lysozyme Photostability.* PLoS One, 2015. **10**(12): p. e0144454.
201. Loregian, A., et al., *Inhibition of human cytomegalovirus DNA polymerase by C-terminal peptides from the UL54 subunit.* J Virol, 2003. **77**(15): p. 8336-44.
202. Chen, H., et al., *A Small Covalent Allosteric Inhibitor of Human Cytomegalovirus DNA Polymerase Subunit Interactions.* ACS Infect Dis, 2017. **3**(2): p. 112-118.
203. Loregian, A., et al., *Binding parameters and thermodynamics of the interaction of the human cytomegalovirus DNA polymerase accessory protein, UL44, with DNA: implications for the processivity mechanism.* Nucleic Acids Res, 2007. **35**(14): p. 4779-91.